Paul Breiding, Kathlén Kohn and Bernd Sturmfels

Metric Algebraic Geometry

Springer Nature

Preface

This book grew out of the lecture notes we developed for the Oberwolfach seminar on metric algebraic geometry which was held in the week of May 29 to June 2, 2023. Each of the three lecturers presented five of the 15 chapters. The lectures were supplemented by intense working sessions and inspiring evening discussions.

In the early 19th century, there was no difference between algebraic and differential geometry. The two were part of the same subject. Geometers studied natural properties of curves and surfaces in 3-space, such as curvature, singularities, and defining equations. In the 20th century, the threads diverged. The standard mathematics curriculum now offers algebraic geometry and differential geometry in rather disconnected courses.

In the present days, the geometry of data requires us to rethink that schism. Many applied problems center around metric questions, such as optimization with respect to distances. These require tools from different areas in geometry, algebra and analysis.

Metric algebraic geometry offers a path towards integration. This term is a neologism which joins the names metric geometry and algebraic geometry. It first appeared in the title of Madeleine Weinstein's PhD dissertation (UC Berkeley 2021). Building on classical foundations, the field embarks towards a new paradigm that combines concepts from algebraic geometry and differential geometry, with the goal of developing practical tools for the 21st century.

Many problems in the sciences lead to solving polynomial equations over the real numbers. The solution sets are real algebraic varieties. Understanding distances, volumes and angles – in short, understanding metric properties – of varieties is important for modeling and analyzing data. Other metric problems in optimization and statistics involve, for instance, minimizing the Euclidean distance from a variety to a given data point. Furthermore, in topological data analysis, computing the homology of a submanifold depends on curvature and on bottlenecks. Related metric questions arise in machine learning, in the geometry of computer vision, in learning varieties from data, and in the study of Voronoi cells.

This book addresses a wide audience of researchers and students, who will find it useful for seminars or self-study. It can serve as the text for a one-semester course at the graduate level. The key prerequisite is a solid foundation in undergraduate mathematics, especially in algebra, geometry and numerics. Course work in statistics and computer science, as well as experience with mathematical software, are helpful.

We hope that you will enjoy this book, and we invite you to develop your own perspective, and to share your feedback.

Oberwolfach,
June 2023

Paul Breiding
Kathlén Kohn
Bernd Sturmfels

Acknowledgements

The authors of this book wish to wholeheartedly thank the following 21 enthusiastic and hard-working participants of the Oberwolfach workshop on Metric Algebraic Geometry:

Patience Ablett
Yueqi Cao
Nick Dewaele
Mirte van der Eyden
Luca Fiorindo
Sofia Garzon Mora
Sarah-Tanja Hess
Emil Horobet
Nidhi Kaihnsa
Elzbieta Polak
Hamid Rahkooy
Bernhard Reinke
Andrea Rosana
Felix Rydell
Pierpaola Santarsiero
Victoria Schleis
Svala Sverrisdóttir
Ettore Teixeira Turatti
Máté László Telek
Angelica Marcela Torres Bustos
Beihui Yuan

Their feedback was tremendously important for the development of this book. Without their input this work would not have been possible.

Contents

Chapter 1
Historical Snapshot

Throughout this book, we will encounter many classical instances of the interplay of metric concepts with algebraic objects. In classical texts such as Salmon [157], metric properties of algebraic varieties were essential. This includes the curvature of algebraic curves and computing their arc lengths and areas using integral calculus. Conversely, many curves of interest were defined in terms of distances or angular conditions. This chapter provides an introduction to algebraic curves of the latter kind.

Over the real numbers, the bilinear form

$$\langle \mathbf{p}, \mathbf{q} \rangle := \sum_{i=1}^{n} p_i q_i$$

is an inner product and induces the Euclidean norm

$$\|\mathbf{p}\| := \sqrt{\langle \mathbf{p}, \mathbf{p} \rangle}.$$

Throughout this volume, also when $\mathbf{p}, \mathbf{q} \in \mathbb{C}^n$ are complex points, we write $\langle \mathbf{p}, \mathbf{q} \rangle := \sum_{i=1}^{n} p_i q_i$ and $\|\mathbf{p}\|^2 := \langle \mathbf{p}, \mathbf{p} \rangle$. However, over the complex numbers, $\|\cdot\|$ is *not* a norm. For instance, $\|(1, i)\| = 0$.

1.1 Polars

For a fixed line L in the real plane with a distinguished point $\mathbf{o} \in L$, we can choose a positive and negative direction and define a signed Euclidean distance on L. More concretely, we fix a unit vector $\mathbf{v}$ through $\mathbf{o}$ spanning L and define

$$\overline{\mathbf{op}} := \lambda \in \mathbb{R}, \qquad \text{where } \mathbf{p} = \mathbf{o} + \lambda \mathbf{v} \in L.$$

In particular, this definition depends on the line L, the reference point $\mathbf{o}$, and the chosen direction given by the vector $\mathbf{v}$.

According to Salmon [157, §56], the following theorem was first proven by Roger Cotes (1682-1716) in his Harmonia Mensurarum:

Theorem 1.1 (Cotes [49]) *Consider an algebraic plane curve C of degree n and a fixed point $\mathbf{o}$ in the plane. For any line L through the point $\mathbf{o}$ intersecting the curve C in n points $\mathbf{r}_1, \ldots, \mathbf{r}_n$, we denote by $\mathbf{p}_L$ the point on L whose signed distance to $\mathbf{o}$ satisfies*

$$\frac{n}{\overline{\mathbf{op}_L}} = \frac{1}{\overline{\mathbf{or}_1}} + \frac{1}{\overline{\mathbf{or}_2}} + \ldots + \frac{1}{\overline{\mathbf{or}_n}}. \tag{1.1}$$

Then the locus of all points $\mathbf{p}_L$ (for all lines L through $\mathbf{o}$) is a straight line.

Salmon called this line the *polar line* of the curve C and the point $\mathbf{o}$. For instance, if the curve C is a conic and $\mathbf{o}$ a point outside of C, then the polar line is spanned by the two points on C whose tangent line contains $\mathbf{o}$; see Figure 1.1.

The relation (1.1) means that the signed distance from $\mathbf{o}$ to $\mathbf{p}_L$ is the harmonic mean of the signed distances from $\mathbf{o}$ to the intersection points $\mathbf{r}_i$. We rewrite this as

$$\sum_{i=1}^{n} \left(\frac{1}{\overline{\mathbf{op}_L}} - \frac{1}{\overline{\mathbf{or}_i}} \right) = 0. \tag{1.2}$$

In case the point $\mathbf{o}$ is at infinity, the point $\mathbf{p}_L$ becomes the average of the points $\mathbf{r}_1, \mathbf{r}_2, \ldots, \mathbf{r}_n$. This is proved in the next corollary.

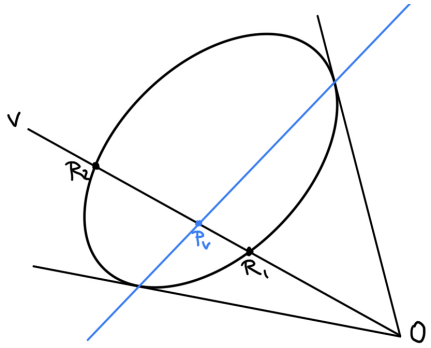

Fig. 1.1: A conic and its polar line (blue) with respect to the point O.

Corollary 1.2 *Let C be a plane curve of degree n and $\mathcal{L}$ a pencil of parallel lines. The locus of all points*

$$\mathbf{p}_L := \frac{1}{n}\sum_{i=1}^{n}\mathbf{r}_i, \qquad \textit{where} L \cap C = \{\mathbf{r}_1, \mathbf{r}_2, \ldots, \mathbf{r}_n\}, \tag{1.3}$$

that are the averages of the intersection points of $L \in \mathcal{L}$ with C, is a straight line.

Proof We start by fixing a line $L \in \mathcal{L}$. Since $\overline{\mathbf{o}\mathbf{r}_i} - \overline{\mathbf{o}\mathbf{p}_L} = \overline{\mathbf{o}\mathbf{r}_i} + \overline{\mathbf{p}_L\mathbf{o}} = \overline{\mathbf{p}_L\mathbf{r}_i}$, Equation (1.2) is equivalent to

$$\sum_{i=1}^{n}\frac{\overline{\mathbf{p}_L\mathbf{r}_i}}{\overline{\mathbf{o}\mathbf{r}_i}} = 0. \tag{1.4}$$

In the latter calculation, we kept the same choice of direction on the line L, but changed the reference point from $\mathbf{o}$ to $\mathbf{p}_L$. To investigate what happens in the limit when $\mathbf{o}$ goes to infinity, we fix a point $\mathbf{o}_0$ on the line L such that $\lambda_i := \overline{\mathbf{o}_0\mathbf{r}_i} > 0$. All the points on L beyond $\mathbf{o}_0$ we can express as $\mathbf{o}_t := \mathbf{o}_0 - t\mathbf{v}$, where $t \geq 0$ and $\mathbf{v}$ is the vector defining L and its direction. Then, we have $\overline{\mathbf{o}_t\mathbf{r}_i} = t + \lambda_i$. For every fixed $t \geq 0$, we write $\mathbf{p}_{L,t}$ for the point $\mathbf{p}_L$ that satisfies (1.4) for $\mathbf{o}_t$. Multiplying (1.4) with t, we obtain

$$\sum_{i=1}^{n}\frac{t}{t+\lambda_i}\cdot\overline{\mathbf{p}_{L,t}\mathbf{r}_i} = 0.$$

In the limit $t \to \infty$, the point $\mathbf{p}_{L,t}$ converges to a point $\mathbf{p}_L$ such that $\sum_{i=1}^{n}\overline{\mathbf{p}_L\mathbf{r}_i} = 0$, which means that $\mathbf{p}_L$ is the average of the points $\mathbf{r}_1, \mathbf{r}_2, \ldots, \mathbf{r}_n$. Hence, for $\mathbf{o}$ at infinity, Equation (1.1) describes the average point $\mathbf{p}_L$ in (1.3) and Theorem 1.1 specializes to Corollary 1.2. □

Salmon attributes Corollary 1.2 to Newton[1] who called the resulting straight line the *diameter* of the curve C corresponding to the parallel-lines pencil $\mathcal{L}$ [157, §51]. In contemporary applied mathematics, this result has been extended to higher-dimensional varieties and is known as the *trace test* in numerical algebraic geometry [162, Chapter 15.5].

Remark 1.3 Another theorem on distances of a point to intersection points between a curve and lines that was first given by Newton in his Enumeratio Linearum Tertii Ordinis is the following: For a plane curve C of degree n, a point $\mathbf{o}$ in the plane, and two distinct lines passing through $\mathbf{o}$, consider the ratio

[1] Cotes and Newton knew each other. In fact, Cotes edited the second edition of Newton's Principia before its publication.

$$\frac{\overline{\mathbf{or}_1} \cdot \overline{\mathbf{or}_2} \cdots \overline{\mathbf{or}_n}}{\overline{\mathbf{os}_1} \cdot \overline{\mathbf{os}_2} \cdots \overline{\mathbf{os}_n}}, \tag{1.5}$$

where $\mathbf{r}_1, \mathbf{r}_2, \ldots, \mathbf{r}_n$ and $\mathbf{s}_1, \mathbf{s}_2, \ldots, \mathbf{s}_n$ are the intersection points of the two lines with C. Then the ratio (1.5) is invariant under translations of the point $\mathbf{o}$ and the two intersecting lines [157, §46].

In [157, §57], Salmon generalizes the construction of polar lines to polar curves of higher order. Using the same notation as in Theorem 1.1, he shows that the locus of points $\mathbf{p}_L$ satisfying

$$\sum_{1 \le i < j \le n} \left(\frac{1}{\overline{\mathbf{op}_L}} - \frac{1}{\overline{\mathbf{or}_i}} \right) \left(\frac{1}{\overline{\mathbf{op}_L}} - \frac{1}{\overline{\mathbf{or}_j}} \right) = 0$$

instead of (1.1) is a conic, called the *polar conic* of the curve C and the point $\mathbf{o}$. If $\mathbf{o}$ is at infinity, the polar conic is also referred to as the *diametral conic*. More generally, the locus of points $\mathbf{p}_L$ satisfying

$$\sum_{i_i < \ldots < i_k} \left(\frac{1}{\overline{\mathbf{op}_L}} - \frac{1}{\overline{\mathbf{or}_{i_1}}} \right) \left(\frac{1}{\overline{\mathbf{op}_L}} - \frac{1}{\overline{\mathbf{or}_{i_2}}} \right) \cdots \left(\frac{1}{\overline{\mathbf{op}_L}} - \frac{1}{\overline{\mathbf{or}_{i_k}}} \right) = 0$$

is the *polar curve* of order k associated with the curve C and the point $\mathbf{o}$ [157, §58]. If $\mathbf{o}$ is at infinity, that polar curve is called the *curvilinear diameter* of order k.

The polar curves can be expressed without involving distances. We write $f(x, y, z) = 0$ for the defining equation of the curve C in homogeneous coordinates. For $\mathbf{o} = (a : b : c)$, we define the operator

$$\Delta_{\mathbf{o}} := a \frac{\partial}{\partial x} + b \frac{\partial}{\partial y} + c \frac{\partial}{\partial z}.$$

Then, letting $n := \deg C$, the polynomial $\Delta_{\mathbf{o}}^{n-k} f$ is the defining equation of the polar curve of order k [157, §63]. This metric-free approach is how polar curves are typically defined in more modern algebro-geometric literature; see Chapter 4.

By exploiting symmetry in Taylor series, Salmon also shows the following beautiful duality between polar curves that "may be written at pleasure" [157, §63]. Setting $\mathbf{p} = (x : y : z)$, Salmon's result states:

$$\frac{1}{(n-k)!} \Delta_{\mathbf{o}}^{n-k} f(x, y, z) \;=\; \frac{1}{k!} \Delta_{\mathbf{p}}^{k} f(a, b, c),$$

In particular, the polar curve of order k that is associated with the curve C and the point $\mathbf{o}$ is the locus of all points $\mathbf{p}$ such that the polar curve of order $n - k$ associated with C and $\mathbf{p}$ passes through $\mathbf{o}$.

1.2 Foci

"we believe that it will be found that every point which has any special relation to any curve will be found either to be a singular point of the curve, or a focus of it" [157, §125]

An ellipse is the locus of points in a plane whose sum of distances to two fixed points in the plane is constant. The two points are the *foci* of the ellipse. In 1832, Plücker generalized the definition of foci to arbitrary plane curves as follows. Consider a circle in the plane. If we embed the plane into two dimensional projective space $\mathbb{P}^2$ by sending $(x, y) \in \mathbb{C}^2$ to $(x : y : 1)$ every circle passes through the two *circular points at infinity* $(1 : i : 0)$ and $(1 : -i : 0)$. In fact, a quadric is a circle if and only if it passes through the two circular points.

Definition 1.4 ([148]) Consider a plane curve C. A point $\mathbf{f}$ in the plane is a *focus* of the curve C if both lines spanned by the point $\mathbf{f}$ and the circular points at infinity are tangent to the curve C.

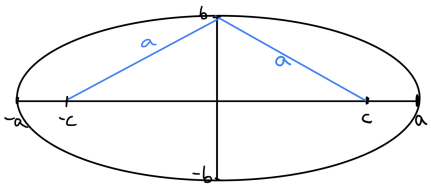

Fig. 1.2: The real foci of an ellipse with width $2a$ and height $2b$ ($a \geq b$) and its axes aligned with the $x-$ and $y-$axis of the real affine plane are $(\pm\sqrt{a^2-b^2}, 0)$.

Example 1.5 We determine the foci (in the sense of Plücker's Definition 1.4) of an ellipse. Since the condition that a line in $\mathbb{P}^2$ passes through the point $(1 : \pm i : 0)$ is invariant under translations and rotations of the real affine plane $\{z \neq 0\} \subseteq \mathbb{P}^2$, we may translate and rotate the ellipse such that its two defining foci (whose sum of distances is constant along the ellipse) become $(c, 0)$ and $(-c, 0)$ in the real affine plane (with $c \geq 0$). Now the ellipse is the locus of points satisfying

$$\sqrt{(x-c)^2+y^2} + \sqrt{(x+c)^2+y^2} = 2a,$$

for some constant $a > 0$. From this, we see that the two points $(\pm a, 0)$ lie on the ellipse. Moreover, the ellipse intersects the y-axis at $(0, \pm b)$ such that $b^2 = a^2 - c^2$; see Figure 1.2. Hence, the width and height of the ellipse are $2a$ and $2b$, respectively, (with $a \geq b > 0$) and its defining equation can alternatively be written as

$$\frac{x^2}{a^2} + \frac{y^2}{b^2} = 1.$$

If the ellipse is not a circle (i.e., $a > b$), then there are two tangent lines to the ellipse that pass through the circular point at infinity $(1 : i : 0)$, namely the tangent lines at $\mathbf{p}_+ := (a^2 : ib^2 : c)$ and $\mathbf{p}_- := (-a^2 : -ib^2 : c)$. The tangent lines at the complex conjugates $\bar{\mathbf{p}}_+$ and $\bar{\mathbf{p}}_-$ of the latter two points pass through the other circular point at infinity $(1 : -i : 0)$. The foci à la Plücker are the four points of intersection of the two tangent lines through $(1 : i : 0)$ with the two tangent lines lines through $(1 : -i : 0)$. Since the tangent lines at $\mathbf{p}_\pm$ and $\bar{\mathbf{p}}_\pm$ are a complex conjugated pair, they meet at a real point, namely $(\pm c : 0 : 1)$. This shows that the real foci we used to define the ellipse are indeed foci in the sense of Plücker's Definition 1.4. The other two foci are obtained by intersecting the tangent line at $\mathbf{p}_\pm$ with the tangent line at $\bar{\mathbf{p}}_\mp$. They are the imaginary points $(0 : \mp ic : 1)$.

If the ellipse is a circle (i.e., $a = b$), it passes through the circular points at infinity. The tangent lines at those points are the only ones that pass through the circular points at infinity. They are given by $x \pm iy = 0$ and intersect at the origin $(0 : 0 : 1)$. The four foci of a general ellipse come together to a single point, namely the center of the circle.

In general, the number of foci of an algebraic plane curve depends on its *class*, that is the degree of its dual curve. The *dual projective plane* is the set of lines in the original projective plane $\mathbb{P}^2$. The *dual curve* $C^\vee$ of a plane curve $C \subseteq \mathbb{P}^2$ is the Zariski closure in the dual projective plane of the set of tangent lines at regular points of C. Hence, the degree of the dual curve $C^\vee$ (equivalently, the class of C) is the number of tangent lines to C that pass through a generic point in the plane $\mathbb{P}^2$.

A curve C of class m has m^2 complex foci (counted with multiplicity). Indeed, through each of the two circular points at infinity, there are m tangent lines to the curve C. The foci are the m^2 intersection points of these two sets of m lines. When the curve C is real, exactly m foci are real (namely, the intersection points of conjugate pairs of tangent lines) [157, §125].

There are are several constructions that generalize ellipses in an obvious way. For instance, an *n-ellipse* is the locus of points in a plane whose sum of distances to n-fixed points in the plane is constant. n-ellipses were studied by Tschirnhaus in 1686 [171] and Maxwell in 1846 [129]. In general, n-ellipses are not algebraic, but semi-algebraic. In fact, they are special cases of spectrahedra [137].

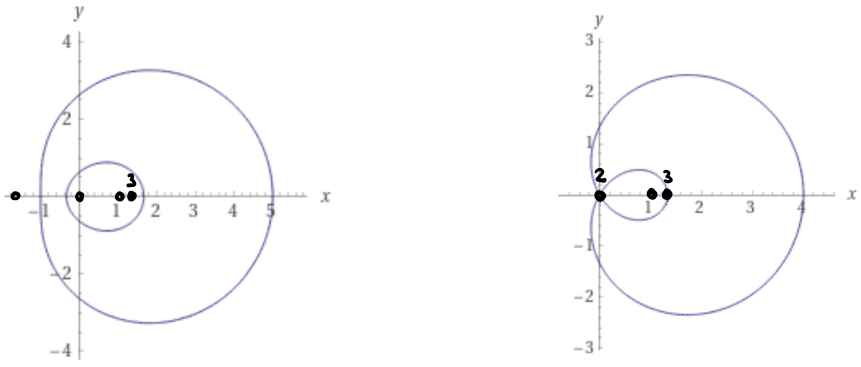

(a) $d = 3$ (b) $d = 2$

Fig. 1.3: Cartesian ovals with defining foci $\mathbf{f}_1 = (0,0), \mathbf{f}_2 = (1,0)$ and weight $s = 2$ are described by $(-3(x^2+y^2)+8x+d^2-4)^2-4d^2(x^2+y^2)=0$. All six real foci are marked.

In the following, we discuss the Cartesian and the Cassini ovals that replace the *sum* of the distances in the definition of an ellipse with a weighted sum or a product, respectively. A *Cartesian oval* (named after Descartes who first studied them in his 1637 *La Géométrie* for their application to optics) is the locus of points in a plane whose weighted sum of distances to two fixed points is constant, i.e., it is the locus of points $\mathbf{p}$ that satisfy

$$\|\mathbf{p}-\mathbf{f}_1\| + s\|\mathbf{p}-\mathbf{f}_2\| = d,$$

where $\mathbf{f}_1$ and $\mathbf{f}_2$ are fixed points in the plane and s, d are fixed constants. In general, that Cartesian oval is not an algebraic curve, but it does satisfy a quartic equation. In fact, the real vanishing locus of that quartic polynomial is two nested ovals; see Figure 1.3a. Among the four possible equations

$$\|\mathbf{p}-\mathbf{f}_1\| \pm s\|\mathbf{p}-\mathbf{f}_2\| = \pm d, \tag{1.6}$$

exactly two have real solutions and those describe the ovals. Salmon shows that a quartic curve is a Cartesian oval if and only if it has cusps at the two circular points at infinity [157, §129]. By Plücker's formula [157, §72], it follows that the class of such a quartic is six (except in degenerate cases). Salmon determines the six real foci of Cartesian oval quartic curves [157, §129] (see also Basset [10, §273]): Three of them form a triple focus which is located at the intersection of the cusps' tangent lines. The remaining three foci lie on a straight line. Two of them are the points $\mathbf{f}_1$ and $\mathbf{f}_2$ that define the curve in (1.6). It was already observed by Chasles that in fact any two of the three single foci can be used to define the Cartesian oval by an equation of the form (1.6) [43, Note XXI]. If two of the three single foci come

together, the Cartesian oval degenerates to a *Limaçon of Pascal*; see Figure 1.3b. Salmon further observes another interesting metric property of foci: Whenever a line meets a Cartesian oval in four points, the sum of their four distances from any of the three single foci is constant [157, §218].

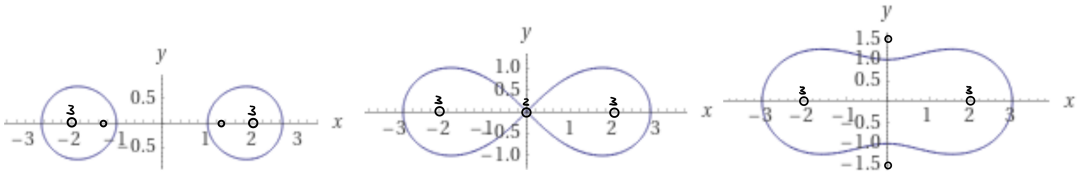

(a) $d = 3$ (b) $d = 4$ (c) $d = 5$

Fig. 1.4: Cassini ovals with defining foci $\mathbf{f}_1 = (-2, 0)$, $\mathbf{f}_2 = (2, 0)$ and their remaining foci.

A *Cassini oval* (named after Cassini who studied them in 1693 [39]) is the locus of points in a plane whose product of distances to two fixed points $\mathbf{f}_1$ and $\mathbf{f}_2$ is constant. This is an algebraic curve defined by the real quartic polynomial

$$\|\mathbf{p} - \mathbf{f}_1\|^2 \cdot \|\mathbf{p} - \mathbf{f}_2\|^2 = d^2$$

for some constant d. The circular points at infinity are double points on each Cassini oval, and since these are the only singularities (except in degenerate cases), the class of a Cassini oval is eight in general [157, §219]. Basset [10, §247] explains that the two pairs of complex conjugated tangent lines at the two nodes intersect at $\mathbf{f}_1$ and $\mathbf{f}_2$, respectively. Hence, those points are foci in the sense of Plücker's Definition 1.4. In fact, Basset shows that each of them is a triple focus (the reason being that the nodal tangents are stationary). To describe the remaining two real foci, we translate and rotate (as in Example 1.5) such that $\mathbf{f}_1 = (c, 0)$ and $\mathbf{f}_2 = (-c, 0)$. Then, the Cassini oval is defined by

$$\left((x-c)^2 + y^2\right)\left((x+c)^2 + y^2\right) = d^2.$$

If $d < c^2$, the real locus is two ovals. Otherwise, the real locus is connected, where the degenerate case $d = c^2$ is the *lemniscate of Bernoulli*; see Figure 1.4. In the case of two ovals, the remaining two real foci also lie on the x-axis; they are $(\pm\frac{1}{c}\sqrt{c^4 - d^2}, 0)$. If $d > c^2$, the two foci are $(0, \pm\frac{1}{c}\sqrt{d^2 - c^4})$ and lie on the y-axis. In the degenerate case $d = c^2$, they become a double focus at the origin.

1.3 Envelopes

Given a one-dimensional algebraic family of lines in the plane, its *envelope* is a curve such that each of the given lines is tangent to the curve. Equivalently, in the dual projective plane, the family of lines is an algebraic curve $\mathcal{L}$ and its dual curve $\mathcal{L}^\vee$ is the envelope.

Example 1.6 The diameters of a plane curve C form a one-dimensional family of lines. For a cubic curve C, the envelope of that family is the locus consisting of the centers of the diametral conics of C [157, §160]. For instance, for the cubic curve defined by $x^3 + y^3 + 5x^2 - 2xy + x - 1 = 0$, the diameter associated with the point $(a : b : 0)$ at infinity is the line given by $3a^2x + 3b^2y + 5a^2 - 2ab = 0$. The family of all diameters is the curve $\mathcal{L}$ in the dual plane that is defined by $25x^2 - 4xy - 30x + 9 = 0$. Its dual curve $\mathcal{L}^\vee$, that is the envelope of the diameters, is $9xy + 15y - 1 = 0$. The diametral conic associated with $(a : b : 0)$ is

Fig. 1.5: Cubic curve $x^3+5x^2+x-1-2xy+y^3=0$ (blue) and the envelope $9xy+15y-1=0$ (red) of its diameters. The diameter (green) and diametral conic (yellow) are associated with the point $(2:1:0)$ at infinity.

$3a\left(x+\frac{5a-b}{3a}\right)^2+3b\left(y-\frac{a}{3b}\right)^2+a-\frac{(5a-b)^2}{3a}-\frac{a^2}{3b}=0$ and so its center $\left(\frac{-5a+b}{3a},\frac{a}{3b}\right)$ lies on the envelope. In fact, the tangent line of the envelope at that point is the diameter associated with $(a:b:0)$; see Figure 1.5.

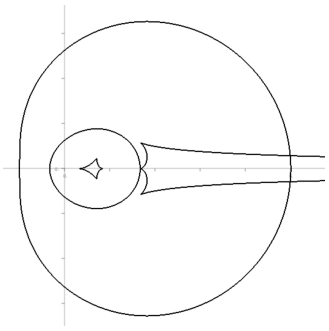

(a) The Cartesian oval from Figure 1.3a together with its evolute.

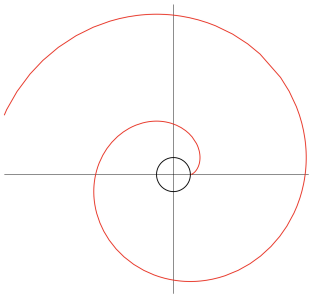

(b) A circle with one of its parallel involutes.

Fig. 1.6: Evolute and involute.

Special instances of envelopes that are defined by metric properties are evolutes and caustics, both of which we will discuss in the remainder of this chapter. The *evolute* of a plane curve C is the envelope of its normals (i.e., the lines orthogonal to its tangent lines). Equivalently, the evolute is the locus of the centers of curvature (see Proposition 6.2). The study of evolutes goes back to Apollonius (ca. 200 BC) [174]. A recent discussion of evolutes can be found in [145]. The degree and class of the evolute of a general smooth curve of degree n are $3n(n-1)$ (see Corollary 6.9) and n^2 [157, §116], respectively. Moreover, its evolute has $\frac{n}{2}(3n-5)(3n^2-n-6)$ double points, $3n(2n-3)$ cusps, and no other singularities. For instance, the evolute of the Cartesian oval in Figure 1.3a is illustrated in Figure 1.6a. Its defining equation is

$$
\begin{aligned}
&102036672x^{10}y^2 + 433655856x^8y^4 + 833407380x^6y^6 + 917059401x^4y^8 + 558336726x^2y^{10} + 143065521y^{12}\\
&-884317824x^9y^2 - 3106029888x^7y^4 - 4898885832x^5y^6 - 4008450240x^3y^8 - 1331276472xy^{10} + 3251316672x^8y^2\\
&+9515584512x^6y^4 + 12088352844x^4y^6 + 6432939486x^2y^8 + 620191890y^{10} - 40310784x^9 - 6758774784x^7y^2\\
&-16647933888x^5y^4 - 15962551632x^3y^6 - 4237194240xy^8 + 342641664x^8 + 9145229184x^6y^2 + 18728830368x^4y^4\\
&+11743648812x^2y^6 + 961612425y^8 - 1239556608x^7 - 9234062208x^5y^2 - 14497919136x^3y^4 - 4640798304xy^6\\
&+2495722752x^6 + 8064660672x^4y^2 + 8003654064x^2y^4 + 835700656y^6 - 3071831040x^5 - 6288399360x^3y^2\\
&-2974296960xy^4 + 2390342400x^4 + 3772699200x^2y^2 + 540271200y^4 - 1173312000x^3 - 1396800000xy^2\\
&+349920000x^2 + 228000000y^2 - 57600000x + 4000000 = 0.
\end{aligned}
$$

We will see in Proposition 6.5 that the finite cusps of the evolute correspond to the points of critical curvature of the original curve C. Salmon computes the length of an arc of the evolute as "the difference of the radii of curvature at its extremities" [157, §115]. The converse operation of computing the evolute is finding an *involute*, that is, for a given plane curve C, find any curve whose evolute is C. In contrast to evolutes, involutes of an algebraic curve are typically not unique (they are parallel curves / offset curves; see Section 7.2) and they might not be algebraic. For instance, the involute of a circle is a transcendental curve [157, §235] because it has infinitely many intersection points with any given line; see Figure 1.6b. Nevertheless, the foci of a plane curve are also foci of its evolute and involute [157, §127].

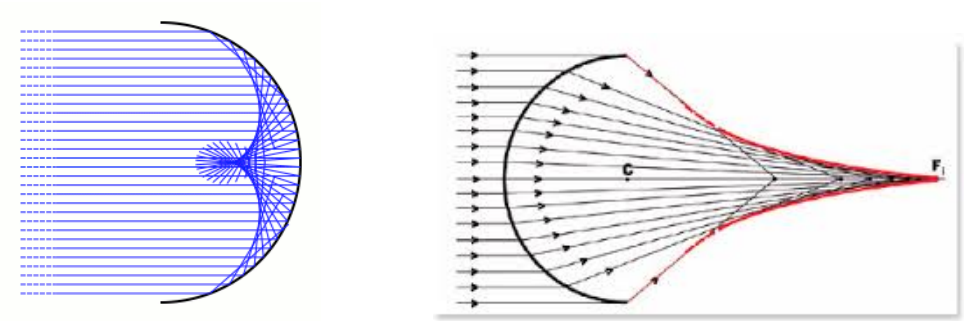

(a) by reflection (b) by refraction

Fig. 1.7: Caustics of a circle with light source at infinity.

Caustics of plane curves come in two flavors. Let us imagine that a fixed point in the plane emits light. The light rays get reflected at each point of a given plane curve. The *caustic by reflection* is the envelope of the family of reflected rays. Similarly, the *caustic by refraction* is the envelope of the family of refracted rays. Figure 1.7 shows caustics of a circle when the light source is at infinity. Those curves can be commonly observed in real life, e.g., when the sun shines on a round glass.

To appear: Example by Felix Rydell: The caustics by refractions of conics are the evolutes of Cartesian ovals (original result due to M. Quetelet). In the limit, when conics degenerate to double lines, one sees that caustics by refraction of lines are evolutes of conics.

Chapter 2
Critical Equations

We consider a model $X_{\mathbb{R}}$ that is given as the zero set in $\mathbb{R}^n$ of a collection $\{f_1, \ldots, f_k\}$ of nonlinear polynomials in n unknowns $x_1, \ldots, x_n$. Thus, $X_{\mathbb{R}}$ is a *real algebraic variety*. In order to apply algebraic methods, it is preferable to work with the complex algebraic variety $X \subset \mathbb{C}^n$ defined by the same polynomials. Thus $X_{\mathbb{R}}$ is the subset of real points in the complex variety X. We assume that X is irreducible, that $I_X = \langle f_1, \ldots, f_k \rangle$ is its prime ideal, and that the set of nonsingular real points is Zariski dense in X. The $k \times n$ Jacobian matrix $\mathcal{J} = (\partial f_i / \partial x_j)$ has rank at most c at any point $x \in X$, where $c = \operatorname{codim}(X)$. The point $\mathbf{x}$ is *nonsingular* on X if the rank is exactly c. The variety X is called *smooth* if all its points are nonsingular. Elaborations on these hypotheses are found in many text books, including [133, Chapter 2].

The following optimization problem arises in many applications. Given a data point $\mathbf{u} \in \mathbb{R}^n \backslash X$, compute the distance to the model $X_{\mathbb{R}}$. Thus, we seek a point $\mathbf{x}^*$ in $X_{\mathbb{R}}$ that is closest to $\mathbf{u}$. The answer depends on the chosen metric. We focus on the case when the metric is represented by a polynomial and $\mathbf{x}^*$ is a smooth point on X. The optimal point $\mathbf{x}^*$ is a solution to the *critical equations*. In optimization, these are also known as first-order conditions or KKT equations, and they arise from introducing Lagrange multipliers. We seek to compute all complex solutions to the critical equations. The set of these *critical points* is typically finite, and it includes all local maxima, all local minima and all saddle points.

2.1 Euclidean Distance Degree

We begin by discussing the *Euclidean distance (ED) problem*, which is as follows:

$$\text{minimize} \ \sum_{i=1}^{n} (x_i - u_i)^2 \ \text{subject to} \ \mathbf{x} \in X. \tag{2.1}$$

Our first step is to derive the critical equations for (2.1). The *augmented Jacobian matrix* $\mathcal{AJ}$ is the $(k+1) \times n$ matrix which is obtained by placing the row vector $(x_1 - u_1, \ldots, x_n - u_n)$ atop the Jacobian matrix $\mathcal{J}$. We form the ideal generated by its $(c+1) \times (c+1)$ minors, we add the ideal of the model I_X, and we then saturate that sum by the ideal of $c \times c$ minors of $\mathcal{J}$. See [60, Eqn. (2.1)]. The result is the *critical ideal* $C_{X,\mathbf{u}}$ of the model X with respect to the given data point $\mathbf{u}$.

Example 2.1 (Plane curves) Let X be the plane curve defined by a polynomial $f(x_1, x_2)$ in two unknowns. We wish to compute the Euclidean distance from X to a given point $\mathbf{u} = (u_1, u_2) \in \mathbb{R}^2$. To this end, we form the augmented Jabobian matrix. This matrix is square of size 2×2:

$$\mathcal{AJ} \ = \ \begin{pmatrix} x_1 - u_1 & x_2 - u_2 \\ \partial f / \partial x_1 & \partial f / \partial x_2 \end{pmatrix} \tag{2.2}$$

The critical ideal is obtained from f and the determinant of $\mathcal{AJ}$ by performing a saturation step:

$$C_{X,\mathbf{u}} \ = \ \langle \, f, \, \det(\mathcal{AJ}) \, \rangle \ : \ \langle \, \partial f / \partial x_1, \partial f / \partial x_2 \, \rangle^{\infty}. \tag{2.3}$$

The ideal $C_{X,\mathbf{u}}$ lives in $\mathbb{R}[x_1, x_2]$. Frequently, the coefficients of f and the coordinates of $\mathbf{u}$ are rational numbers, and in this case we can perform the computation purely symbolically in $\mathbb{Q}[x_1, x_2]$. The saturation step in (2.3) removes points that are singular on the curve $X = \mathcal{V}(f)$. If X is smooth then saturation is unnecessary, and we simply have $C_{X,\mathbf{u}} = \langle \, f, \, \det(\mathcal{AJ}) \, \rangle$.

In applications, we must expect singularities. For a concrete example take the cardioid

$$f \ = \ (x_1^2 + x_2^2 + x_2)^2 - (x_1^2 + x_2^2), \tag{2.4}$$

and fix a random point $\mathbf{u} = (u_1, u_2)$. See [60, Example 1.1]. The ideal $\langle f, \det(\mathcal{A}\mathcal{J}) \rangle$ is the intersection of $C_{X,\mathbf{u}}$ and an $\langle x_1, x_2 \rangle$-primary ideal of multiplicity 3. The critical ideal $C_{X,\mathbf{u}}$ has three distinct complex zeros. We can express their coordinates in radicals in the given numbers u_1, u_2.

The variety $\mathcal{V}(C_{X,\mathbf{u}})$ is the set of complex critical points of (2.1). For random data $\mathbf{u}$, this variety is a finite subset of $\mathbb{C}^n$, and it contains the optimal solution $\mathbf{x}^*$, provided the latter is attained at a smooth point of X. It was proved in [60] that the number of critical points, i.e. the cardinality of the variety $\mathcal{V}(C_{X,\mathbf{u}})$, is independent of $\mathbf{u}$, if we assume that the data point $\mathbf{u}$ is sufficiently general. This number is called the *ED degree* of the variety X. In Example 2.1 we examined a plane curve of degree 4 whose ED degree equals 3. The ED degree of a variety X measures the difficulty of solving the ED problem (2.1) using exact algebraic methods. The ED degree is an important complexity measure in metric algebraic geometry.

Example 2.2 (Space curves) Fix $n = 3$ and let X be the curve in $\mathbb{R}^3$ defined by two general polynomials f_1 and f_2 of degrees d_1 and d_2 in three unknowns x_1, x_2, x_3. The augmented Jacobian matrix is

$$\mathcal{A}\mathcal{J} \;=\; \begin{pmatrix} x_1 - u_1 & x_2 - u_2 & x_3 - u_3 \\ \partial f_1/\partial x_1 & \partial f_1/\partial x_2 & \partial f_1/\partial x_3 \\ \partial f_2/\partial x_1 & \partial f_2/\partial x_2 & \partial f_2/\partial x_3 \end{pmatrix}. \tag{2.5}$$

Fix a general data vector $\mathbf{u} \in \mathbb{R}^3$. Then the critical ideal equals $C_{X,\mathbf{u}} = \langle f_1, f_2, \det(\mathcal{A}\mathcal{J}) \rangle$. Hence the set of critical points is the intersection of three surfaces. These surfaces have degrees d_1, d_2 and $d_1 + d_2 - 1$. By Bézout's Theorem [133, Theorem 2.16], the expected number of solutions is the product of these degrees. Hence the ED degree of the curve X equals $d_1 d_2 (d_1 + d_2 - 1)$.

The same formula can be derived from a formula for general curves in terms of algebraic geometry data. Let X be a general smooth curve of degree d and genus g in any ambient space $\mathbb{R}^n$. By [60, Corollary 5.9], we have $\mathrm{EDdegree}(X) = 3d + 2g - 2$. The above curve in 3-space has degree $d = d_1 d_2$ and genus $g = d_1^2 d_2/2 + d_1 d_2^2/2 - 2 d_1 d_2 + 1$. We conclude that

$$\mathrm{EDdegree}(X) \;=\; 3d + 2g - 2 \;=\; d_1 d_2 (d_1 + d_2 - 1).$$

This formula also covers the case of plane curves (cf. Example 2.1). Namely, if we set $d_1 = d$ and $d_2 = 1$ then we see that a general plane curve X of degree d has $\mathrm{EDdegree}(X) = d^2$. In particular, a general plane quartic has ED degree 16. However, that number can drop a lot for curves that are special. For the cardiod in (2.4) the ED degree drops from 16 to 3.

Here is a general upper bound on the ED degree in terms of the given polynomials.

Proposition 2.3 *Let X be a variety of codimension c in $\mathbb{R}^n$ whose ideal I_X is generated by polynomials $f_1, f_2, \ldots, f_c, \ldots, f_k$ of degrees $d_1 \geq d_2 \geq \cdots \geq d_c \geq \cdots \geq d_k$. Then*

$$\mathit{EDdegree}(X) \;\leq\; d_1 d_2 \cdots d_c \cdot \sum_{i_1 + i_2 + \cdots + i_c \leq n-c} (d_1 - 1)^{i_1} (d_2 - 1)^{i_2} \cdots (d_c - 1)^{i_c}. \tag{2.6}$$

Equality holds when X is a generic complete intersection of codimension c (hence $c = k$).

Proof This appears in [60, Proposition 2.6]. We can derive it as follows. Bézout's Theorem ensures that the degree of the variety X is at most $d_1 d_2 \cdots d_c$. The entries in the ith row of the matrix $\mathcal{A}\mathcal{J}$ are polynomials of degrees $d_{i-1} - 1$. The degree of the variety of $(c+1) \times (c+1)$ minors of $\mathcal{A}\mathcal{J}$ is at most the sum in (2.6). This follows from the Giambelli–Thom–Porteous formula, which expresses the degree of a determinantal variety in terms of symmetric functions. The intersection of that determinantal variety with X is our set of critical points, and the cardinality of that set is bounded by the product of the two degrees. Generically, that intersection is a complete intersection and the inequality (2.6) is attained. □

Formulas or a priori bounds for the ED degree are important when studying exact solutions to the optimization problem (2.1). The paradigm is to compute all complex critical points, by either symbolic or numerical methods, and to then extract one's favorite real solutions among these. This leads, for instance, to all local minima in (2.1). The ED degree is an upper bound on the number of real critical points, but this bound is generally not tight.

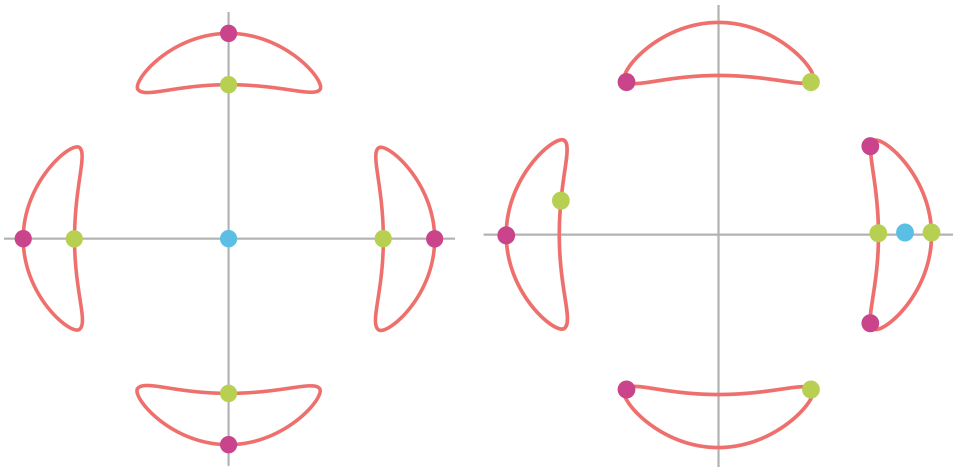

Fig. 2.1: ED problems on the Trott curve: configurations of eight (left) or ten (right) critical points. Data points are blue, local minimal are green, and local maxima are purple. The coordinates of the critical points are computed by solving the critical equations in (2.7).

Example 2.4 Consider the case $n = 2, c = 1, d_1 = 4$ in Proposition 2.3, where X is a generic quartic curve in the plane $\mathbb{R}^2$. The number of complex critical points is $\mathrm{EDdegree}(X) = 16$. But, they cannot be all real. For an illustration, consider the *Trott curve* $X = V(f)$, given by

$$f \;=\; 144(x_1^4 + x_2^4) \;-\; 225(x_1^2 + x_2^2) \;+\; 350x_1^2x_2^2 \;+\; 81.$$

This curve is shown in Figure 2.1. For general data $\mathbf{u} = (u_1, u_2)$ in $\mathbb{R}^2$, the critical equations

$$f \;=\; \frac{\partial f}{\partial x_2}(x_1 - u_1) - \frac{\partial f}{\partial x_1}(x_2 - u_2) \;=\; 0. \tag{2.7}$$

have distinct 16 complex solutions, and these are all critical points in X. Since the Trott curve is smooth, the saturation step in (2.3) is not needed when computing the ideal $C_{X,\mathbf{u}}$.

The ED degree 16 is an upper bound for the number of real critical points of the optimization problem (2.1) for any data point $\mathbf{u}$. The actual number of real critical points depends heavily on the specific location of $\mathbf{u}$. For data $\mathbf{u}$ near the origin, eight of the 16 points in $\mathcal{V}(C_{X,\mathbf{u}})$ are real. For $\mathbf{u} = (\frac{7}{8}, \frac{1}{100})$, which is inside the rightmost oval, there are 10 real critical points. The two scenarios are shown in Figure 2.1. Local minima are green, while local maxima are purple. Finally, consider $\mathbf{u} = (2, \frac{1}{100})$, which lies to the right of the rightmost oval. Here, the number of real critical points is 12.

In general, our task is to compute the complex zeros of the critical ideal $C_{X,\mathbf{u}}$. Algorithms for this computation can be either symbolic or numerical. Symbolic methods usually rest on the construction of a Gröbner basis, to be followed by a floating point computation to extract the solutions. In recent years, numerical methods have become popular. These are based on homotopy continuation. Two notable

packages are `Bertini` [13] and `HomotopyContinuation.jl` [31]. The ED degree is important here because it indicates how many paths need to be tracked to solve (2.1). We next illustrate current capabilities.

Example 2.5 Suppose X is defined by $c = k = 3$ random polynomials in $n = 7$ variables, for a range of degrees d_1, d_2, d_3. The table below lists the ED degree in each case, and the times used by `HomotopyContinuation.jl` to compute and certify all critical points in $\mathbb{C}^7$.

$d_1\, d_2\, d_3$	3 2 2	3 3 2	3 3 3	4 2 2	4 3 2	4 3 3	4 4 2	4 4 3
EDdegree	1188	3618	9477	4176	10152	23220	23392	49872
Solving (sec)	3.849	21.06	61.51	31.51	103.5	280.0	351.5	859.3
Certifying (sec)	0.390	1.549	4.653	2.762	7.591	17.16	21.65	50.07

Here we represent $C_{X,\mathbf{u}}$ by a system of 10 equations in 10 variables. In addition to the three equations $f_1 = f_2 = f_3 = 0$ in $x_1, \ldots, x_7$, we take the seven equations $(1, y_1, y_2, y_3) \cdot \mathcal{A}\mathcal{J} = 0$. Here y_1, y_2, y_3 are new variables. These additional equations ensure that the 4×7 matrix $\mathcal{A}\mathcal{J}$ has rank ≤ 3. This formulation avoids the listing of all $\binom{7}{4} = 35$ maximal minors. It is the preferred representation of determinantal varieties in the setting of numerical algebraic geometry.

The timings above refer to computing all complex solutions to the system of 10 equations in 10 variables. They include the certification step [30] that proves correctness and completeness. These computations were performed using `HomotopyContinuation.jl` v2.5.6 on a 16 GB MacBook Pro with an Intel Core i7 processor working at 2.6 GHz. They suggest that our critical equations can be solved fast and reliably, with proof of correctness, when the ED degree is less than 50000. When the ED degree exceeds 50000, success with numerical path tracking will depend on the specific structure of the family. A key player on the geometric side is the discriminant of the problem. If that is well-behaved, then even larger ED degrees are feasible. A successful application to a physics problem is reported in [168, Table 1].

2.2 Low Rank Matrix Approximation

When the ED problem (2.1) arises in an application, one often considers varieties of matrices of low rank that are constrained to have a special structure. Sometimes these matrices are flattenings of tensors. This version of the problem was studied in the article [141], which focuses on Hankel matrices, Sylvester matrices and generic subspaces of matrices, and which uses a weighted version of the Euclidean metric. In this section we offer a brief introduction to this special case of our general ED problem.

Our point of departure is the following low-rank approximation problem for rectangular matrices:

$$\text{minimize} \quad \| A - U \|_\Lambda^2 \;=\; \sum_{i=1}^{m} \sum_{j=1}^{n} \lambda_{ij} (a_{ij} - u_{ij})^2 \quad \text{subject to} \quad \text{rank}(A) \leq r. \tag{2.8}$$

In this problem, we are given a real *data matrix* $U = (u_{ij})$ of format $m \times n$, and we wish to find a real matrix $A = (a_{ij})$ of rank at most r that is closest to U in a weighted Frobenius norm. The entries of the *weight matrix* $\Lambda = (\lambda_{ij})$ are positive real numbers. If $m \leq n$ and the weight matrix Λ is the all-one matrix $\mathbf{1}$, then the solution to (2.8) is given by the *singular value decomposition*

$$U \;=\; T_1 \cdot \text{diag}(\sigma_1, \sigma_2, \ldots, \sigma_m) \cdot T_2.$$

Here T_1, T_2 are orthogonal matrices, and $\sigma_1 \geq \sigma_2 \geq \cdots \geq \sigma_m$ are the singular values of U. The following well-known theorem from numerical linear algebra concerns the variety X of $m \times n$ matrices of rank $\leq r$.

Theorem 2.6 (Eckart-Young) *The closest matrix of rank $\leq r$ to the given matrix U equals*

$$U^* \;=\; T_1 \cdot \mathrm{diag}(\sigma_1, \ldots, \sigma_r, 0, \ldots, 0) \cdot T_2. \tag{2.9}$$

This is the unique local minimum. All complex critical points are real. They are found by substituting zeros for $m - r$ of the entries of $\mathrm{diag}(\sigma_1, \ldots, \sigma_m)$. *Hence,* $\mathrm{EDdegree}(X) = \binom{m}{r}$.

For general weights Λ, the situation is more complicated. In particular, there can be complex critical points and multiple local minima. We discuss a small instance in Example 2.8.

First, let us define the problem of *structured low-rank approximation*. In this problem, we are given a linear subspace $\mathcal{L} \subset \mathbb{R}^{m\times n}$, and a data matrix $U \in \mathcal{L}$, and we wish to solve the restricted problem:

$$\text{minimize } ||\, A - U \,||^2 \;=\; \sum_{i=1}^{m}\sum_{j=1}^{n} \lambda_{ij}(a_{ij} - u_{ij})^2 \;\text{ subject to }\; A \in \mathcal{L} \text{ and } \mathrm{rank}(A) \leq r. \tag{2.10}$$

A best-case scenario for $\Lambda = \mathbf{1}$ would be the following: if U lies in $\mathcal{L}$ then so does the SVD solution U^* in (2.9). This happens for some linear subspaces $\mathcal{L}$, including symmetric and circulant matrices. However, most subspaces $\mathcal{L}$ of $\mathbb{R}^{m\times n}$ do not enjoy this property, and finding the global optimum in (2.10) can be quite difficult, even for $\Lambda = \mathbf{1}$. The article [141] studies this optimization problem for both generic and special subspaces $\mathcal{L}$. It rests on [60] and uses tools from algebraic geometry.

As before, our primary task is to compute the number of complex critical points of (2.10). Thus, we seek to find the Euclidean distance degree (ED degree) of the determinantal variety

$$\mathcal{L}_{\leq r} \quad := \quad \big\{\, A \in \mathcal{L} \,:\, \mathrm{rank}(A) \leq r \,\big\}.$$

This variety is always regarded as a subvariety of the matrix space $\mathbb{R}^{m\times n}$. We use the Λ-weighted Euclidean distance coming from $\mathbb{R}^{m\times n}$. We write $\mathrm{EDdegree}_\Lambda(\mathcal{L}_{\leq r})$ for the Λ-weighted Euclidean distance degree of the variety $\mathcal{L}_{\leq r}$. Thus $\mathrm{EDdegree}_\Lambda(\mathcal{L}_{\leq r})$ is the number of complex critical points of the problem (2.10) for data matrices U that are generic in $\mathcal{L}$. The importance of the weights Λ is highlighted in [60, Example 3.2], for the seemingly harmless situation when $\mathcal{L}$ is the space of all symmetric matrices in $\mathbb{R}^{n\times n}$.

Of special interest are the *unit ED degree*, when $\Lambda = \mathbf{1}$ is the all-one matrix, and the *generic ED degree*, denoted $\mathrm{EDdegree}_{\mathrm{gen}}(\mathcal{L}_{\leq r})$, when the weight matrix Λ is generic. The generic ED degree is given by a formula that rests on intersection theory. See [60, Theorem 7.7] and Theorem 2.9 below. Indeed, choosing the positive weights λ_{ij} to be generic ensures that the projective closure of $\mathcal{L}_{\leq r}$ has transversal intersection with the isotropic quadric

$$\Big\{\, A \in \mathbb{P}^{mn-1} \;:\; \sum_{i=1}^{m}\sum_{j=1}^{n} \lambda_{ij} a_{ij}^2 \;=\; 0 \,\Big\}.$$

We next present two examples that illustrate the concepts above. These can then also serve as examples for Theorem 2.9 below, as seen by the `Macaulay2` calculation in Example 2.15.

Example 2.7 Let $m = n = 3$ and $\mathcal{L} \subset \mathbb{R}^{3\times 3}$ the 5-dimensional space of Hankel matrices:

$$A \;=\; \begin{bmatrix} a_0 & a_1 & a_2 \\ a_1 & a_2 & a_3 \\ a_2 & a_3 & a_4 \end{bmatrix}, \quad U \;=\; \begin{bmatrix} u_0 & u_1 & u_2 \\ u_1 & u_2 & u_3 \\ u_2 & u_3 & u_4 \end{bmatrix} \quad \text{and} \quad \Lambda \;=\; \begin{bmatrix} \lambda_0 & \lambda_1 & \lambda_2 \\ \lambda_1 & \lambda_2 & \lambda_3 \\ \lambda_2 & \lambda_3 & \lambda_4 \end{bmatrix}.$$

Our goal in (2.10) is to solve the following constrained optimization problem for $r = 1, 2$:

$$\begin{array}{c} \text{minimize } \lambda_0(a_0 - u_0)^2 + 2\lambda_1(a_1 - u_1)^2 + 3\lambda_2(a_2 - u_2)^2 + 2\lambda_3(a_3 - u_3)^2 + \lambda_4(a_4 - u_4)^2 \\ \text{subject to } \mathrm{rank}(A) \leq r. \end{array}$$

This can be rephrased as an unconstrained optimization problem. For instance, for rank $r = 1$, we get a one-to-one parametrization of $\mathcal{L}_{\leq 1}$ by setting $a_i = st^i$. Our optimization problem is as follows:

$$\text{Minimize } \lambda_0(s-u_0)^2 + 2\lambda_1(st-u_1)^2 + 3\lambda_2(st^2-u_2)^2 + 2\lambda_3(st^3-u_3)^2 + \lambda_4(st^4-u_4)^2.$$

The ED degree is the number of critical points with $t \neq 0$. We consider three weight matrices:

$$\mathbf{1} = \begin{bmatrix} 1 & 1 & 1 \\ 1 & 1 & 1 \\ 1 & 1 & 1 \end{bmatrix}, \qquad \Omega = \begin{bmatrix} 1 & 1/2 & 1/3 \\ 1/2 & 1/3 & 1/2 \\ 1/3 & 1/2 & 1 \end{bmatrix}, \qquad \Theta = \begin{bmatrix} 1 & 2 & 2 \\ 2 & 2 & 2 \\ 2 & 2 & 1 \end{bmatrix}.$$

Here Ω gives the usual Euclidean metric when $\mathcal{L}$ is identified with $\mathbb{R}^5$. The last weight matrix Θ arises from identifying $\mathcal{L}$ with the space of symmetric $2 \times 2 \times 2 \times 2$-tensors. We compute

$$\begin{array}{lll} \text{EDdegree}_{\mathbf{1}}(\mathcal{L}_{\leq 1}) = 6, & \text{EDdegree}_{\Omega}(\mathcal{L}_{\leq 1}) = 10, & \text{EDdegree}_{\Theta}(\mathcal{L}_{\leq 1}) = 4, \\ \text{EDdegree}_{\mathbf{1}}(\mathcal{L}_{\leq 2}) = 9, & \text{EDdegree}_{\Omega}(\mathcal{L}_{\leq 2}) = 13, & \text{EDdegree}_{\Theta}(\mathcal{L}_{\leq 2}) = 7. \end{array}$$

In both cases, Ω exhibits the generic behavior, so we have $\text{EDdegree}_{\text{gen}}(\mathcal{L}_{\leq r}) = \text{EDdegree}_{\Omega}(\mathcal{L}_{\leq r})$. We refer to [141, Sections 3 and 4] for larger Hankel matrices and formulas for their ED degrees.

Example 2.8 Let $m = n = 3, r = 1$ but now take $\mathcal{L} = \mathbb{R}^{3\times 3}$. Thus, we are considering the weighted rank-one approximation problem for 3×3-matrices. We know from [60, Example 7.10] that $\text{EDdegree}_{\text{gen}}(\mathcal{L}_{\leq 1}) = 39$. We take a circulant data matrix and a circulant weight matrix:

$$U = \begin{bmatrix} -59 & 11 & 59 \\ 11 & 59 & -59 \\ 59 & -59 & 11 \end{bmatrix} \quad \text{and} \quad \Lambda = \begin{bmatrix} 9 & 6 & 1 \\ 6 & 1 & 9 \\ 1 & 9 & 6 \end{bmatrix}.$$

This instance has 39 complex critical points. Of these, 19 are real, and 7 are local minima:

$$\begin{bmatrix} 0.0826 & 2.7921 & -1.5452 \\ 2.7921 & 94.3235 & -52.2007 \\ -1.5452 & -52.2007 & 28.8890 \end{bmatrix}, \begin{bmatrix} -52.2007 & 28.8890 & -1.5452 \\ 2.7921 & -1.5452 & 0.0826 \\ 94.3235 & -52.2007 & 2.7921 \end{bmatrix}, \begin{bmatrix} -52.2007 & 2.7921 & 94.3235 \\ 28.8890 & -1.5452 & -52.2007 \\ -1.5452 & 0.0826 & 2.7921 \end{bmatrix},$$

$$\begin{bmatrix} -29.8794 & 36.2165 & -27.2599 \\ -32.7508 & 39.6968 & -29.8794 \\ 39.6968 & -48.1160 & 36.2165 \end{bmatrix}, \begin{bmatrix} -48.1160 & 36.2165 & 39.6968 \\ 36.2165 & -27.2599 & -29.8794 \\ 39.6968 & -29.8794 & -32.7508 \end{bmatrix}, \begin{bmatrix} -29.8794 & -32.7508 & 39.6968 \\ 36.2165 & 39.6968 & -48.1160 \\ -27.2599 & -29.8794 & 36.2165 \end{bmatrix},$$

$$\begin{bmatrix} -25.375 & -25.375 & -25.375 \\ -25.375 & -25.375 & -25.375 \\ -25.375 & -25.375 & -25.375 \end{bmatrix}.$$

The first three are the global minima in our ED distance problem. The last matrix is the local minimum where the objective function has the largest value: note that each entry equals $-203/8$. The entries of the first six matrices are algebraic numbers of degree 10 over $\mathbb{Q}$. For instance, the two upper left entries 0.0826 and −48.1160 are among the four real roots of the irreducible polynomial

$$\begin{aligned} &164466028468224x^{10} + 27858648335954688x^9 + 160220538668937667 2x^8 + 7285836260028875412x^7 \\ &-219872893604668041427 2x^6 - 14854532690380098143152x^5 + 26886730912283710957623 16x^4 \\ &+44612094455115888622678587x^3 - 41350080445712457319337106x^2 \\ &+27039129499043116889674775x - 19776324635637668787656 25. \end{aligned}$$

Here, the critical ideal in $\mathbb{Q}[x_{11}, x_{12}, \ldots, x_{33}]$ is not prime. It is the intersection of six maximal ideals. Their degrees over $\mathbb{Q}$ are $1, 2, 6, 10, 10, 10$. The sum of these numbers equals $39 = \text{EDdegree}_{\text{gen}}(\mathcal{L}_{\leq 1})$.

Explicit formulas are derived in [141, Section 3] for $\mathrm{EDdegree}_{\mathrm{gen}}(\mathcal{L}_{\leq r})$ when $\mathcal{L}$ is a generic subspace of $\mathbb{R}^{m\times n}$. This covers the four cases that arise by pairing affine subspaces or linear subspaces with either unit weights or generic weights. One important feature of determinantal varieties is they are not complete intersections. Their ED degrees are much smaller than suggested by the upper bound in Proposition 2.3.

2.3 Invitation to Polar Degrees

We have introduced the ED degree of an algebraic variety X as a complexity measure for the ED problem in (2.1). The number 39 in the previous example served as an illustration on how the ED degree controls the number of critical points. But a deeper understanding is needed. In this section, we develop the algebro-geometric roots of the ED degree, which will then yield more advanced algorithms for finding it.

Theorem 2.9 *If the given variety X meets both the hyperplane at infinity and the isotropic quadric transversally, then $\mathrm{EDdegree}(X)$ equals the sum of the polar degrees of the projective closure of X.*

We shall explain all the terms used in this theorem. First of all, the *projective closure* of our affine real variety $X \subset \mathbb{C}^n$ is its Zariski closure in complex projective space $\mathbb{P}^n$, which we also denote by X. Algebraically, $\mathbb{P}^n$ is obtained from $\mathbb{C}^n$ by adding one homogenizing coordinate x_0. We identify the affine space $\mathbb{C}^n$ with the open subset $\{\mathbf{x} \in \mathbb{P}^n : x_0 \neq 0\}$. Its set complement $\{\mathbf{x} \in \mathbb{P}^n : x_0 = 0\} \simeq \mathbb{P}^{n-1}$ is the *hyperplane at infinity* inside $\mathbb{P}^n$. The hypersurface $\{\mathbf{x} \in \mathbb{P}^{n-1} : \sum_{i=1}^n x_i^2 = 0\}$ is called the *isotropic quadric*. It lives in the hyperplane at infinity and it has no real points. The hypothesis in Theorem 2.9 means that the intersection of X with these two loci is reduced and has the expected dimension.

Theorem 2.9 appears in [60, Proposition 6.10]. The hypothesis is stated in precise terms in [60, equation (6.4)]. It holds for all varieties X after a general linear change of coordinates.

If we are given a real projective variety X in $\mathbb{P}^n$ from the start, then we also consider the ED problem for its affine cone in $\mathbb{R}^{n+1}$. The data vector now equals $\mathbf{u} = (u_0, u_1, \ldots, u_n)$, and the augmented Jacobian is redefined so as to respect the fact that all polynomials are homogeneous. The general formula for this matrix and the homogeneous critical ideal appears in [60, equation (2.7)].

For a curve $X \subset \mathbb{P}^2$ with defining polynomial $f(x_0, x_1, x_2)$, we use the modified augmented Jacobian

$$\mathcal{AJ} \;=\; \begin{pmatrix} u_0 & u_1 & u_2 \\ x_0 & x_1 & x_2 \\ \partial f/\partial x_0 & \partial f/\partial x_1 & \partial f/\partial x_2 \end{pmatrix}.$$

The homogeneous critical ideal in $\mathbb{R}[x_0, x_1, x_2]$ is computed as follows:

$$C_{X,\mathbf{u}} \;=\; \big\langle\, f,\, \det(\mathcal{AJ}) \,\big\rangle \;:\; \big(\, \langle \partial f/\partial x_0, \partial f/\partial x_1, \partial f/\partial x_2 \rangle \cdot (x_1^2 + x_2^2) \,\big)^{\infty}. \tag{2.11}$$

The critical points are given by the variety $\mathcal{V}(C_{X,\mathbf{u}})$ in $\mathbb{P}^2$, whose cardinality is $\mathrm{EDdegree}(X)$. The factor $(x_1^2 + x_2^2)$ in the saturation step (2.11) is the isotropic quadric. It is needed whenever the hypothesis of Theorem 2.9 is not satisfied. Namely, it removes any extraneous component that may arise from non-transversal intersection of the curve X with the isotropic quadric.

Example 2.10 (Cardioid) We consider the homogeneous version of the cardioid in Example 2.1:

$$f \;=\; (x_1^2 + x_2^2 + x_0 x_2)^2 \;-\; x_0^2 (x_1^2 + x_2^2). \tag{2.12}$$

The projective curve $X = \mathcal{V}(f)$ has three singular points, namely that at the origin $\mathcal{V}(x_1, x_2)$ in $\mathbb{C}^2 = \{x_0 \neq 0\}$ and the two points in the isotropic quadric $\mathcal{V}(x_1^2 + x_2^2)$ in $\mathbb{P}^1 = \{x_0 = 0\}$.

The homogeneous critical ideal $C_{X,\mathbf{u}}$ is generated by three cubics, and it defines seven points in $\mathbb{P}^2$. Hence the projective cardioid X has EDdegree$(X) = 7$. This is also the ED degree of the affine cardioid in (2.4) but only after a linear change of coordinates. Even a fairly modest change of coordinates can have dramatic impact. For instance, if we replace x_1 by $2x_1$ in (2.4) then the ED degree jumps from 3 to 7.

We now offer a first definition of the polar degrees of a projective variety $X \subset \mathbb{P}^n$. Recall that points $\mathbf{h}$ in the dual projective space $(\mathbb{P}^n)^\vee$ represent hyperplanes in the primal space $\mathbb{P}^n$. Namely, we identify $\mathbf{h}$ with the hyperplane $\{\mathbf{x} \in \mathbb{P}^n : h_0x_0 + \cdots + h_nx_n = 0\}$. We are interested in all pairs $(\mathbf{x}, \mathbf{h})$ in $\mathbb{P}^n \times (\mathbb{P}^n)^\vee$ such that $\mathbf{x}$ is a nonsingular point of X and $\mathbf{h}$ is tangent to X at $\mathbf{x}$. The Zariski closure of this set is the *conormal variety* $N_X \subset \mathbb{P}^n \times (\mathbb{P}^n)^\vee$. It is known that N_X has dimension $n-1$, and if X is irreducible then so is N_X. The image of N_X under projection onto the second factor is the dual variety $X^\vee$. The role of $x \in \mathbb{P}^n$ and $h \in (\mathbb{P}^n)^\vee$ can be swapped. The following biduality relations [74, §I.1.3] hold:

$$N_X = N_{X^\vee} \quad \text{and} \quad (X^\vee)^\vee = X.$$

The conormal variety is an object of algebraic geometry that offers the theoretical foundations for various aspects of duality in optimization, including primal-dual algorithms.

Example 2.11 For a plane curve $X = \mathcal{V}(f)$ in $\mathbb{P}^2$, the conormal variety N_X is a curve in $\mathbb{P}^2 \times (\mathbb{P}^2)^\vee$. Its ideal is derived from the ideal that is generated by f and the 2×2 minors of

$$\begin{pmatrix} h_0 & h_1 & h_2 \\ \partial f/\partial x_0 & \partial f/\partial x_1 & \partial f/\partial x_2 \end{pmatrix}$$

By saturation, we remove singularities and points on the isotropic quadric, to arrive at $C_{X,\mathbf{u}}$.

For instance, if f is the homogeneous cardioid in (2.12) then $X^\vee$ is the cubic defined by

$$16h_0^3 - 27h_0h_1^2 - 24h_0^2h_2 - 15h_0h_2^2 - 2h_2^3.$$

The ideal of N_X has ten minimal generators. In addition to the above generators of bidegrees $(4,0)$ and $(0,3)$, we find the quadric $x_0h_0 + x_1h_1 + x_2h_2$ of bidegree $(1,1)$, three cubics of bidegree $(2,1)$ like $x_1^2h_1 - 3x_2^2h_1 - x_0x_1h_2 + 4x_1x_2h_2$, and four cubics of bidegree $(1,2)$.

We now finally come to the polar degrees. The product of two projective spaces $\mathbb{P}^n \times (\mathbb{P}^n)^\vee$ serves as the ambient space for our primal-dual approach to the ED problem. We now consider its cohomology ring:

$$H^*(\mathbb{P}^n \times (\mathbb{P}^n)^\vee, \mathbb{Z}) \;=\; \mathbb{Z}[s,t]/\langle s^{n+1}, t^{n+1} \rangle.$$

The class of the conormal variety N_X in this cohomology ring is a binary form of degree $n+1 = \operatorname{codim}(N_X)$ whose coefficients are nonnegative integers:

$$[N_X] \;=\; \delta_1(X)s^nt \,+\, \delta_2(X)s^{n-1}t^2 \,+\, \delta_3(X)s^{n-2}t^3 \,+\, \cdots \,+\, \delta_n(X)st^n.$$

The coefficients $\delta_i(X)$ of this binary form are called the *polar degrees* of X.

Remark 2.12 The polar degrees satisfy $\delta_i(X) = \#(N_X \cap (L \times L'))$, where $L \subset \mathbb{P}^n$ and $L' \subset (\mathbb{P}^n)^\vee$ are general linear subspaces of dimensions $n+1-i$ and i respectively. This geometric interpretation implies that $\delta_i(X) = 0$ for $i < \operatorname{codim}(X^\vee)$ and for $i > \dim(X)+1$. Moreover, the first and last polar degree are the classical degrees for the dual pair of varieties:

$$\delta_i(X) = \text{degree}(X) \text{ for } i = \dim(X)+1 \text{ and } \delta_i(X) = \text{degree}(X^\vee) \text{ for } i = \operatorname{codim}(X^\vee). \tag{2.13}$$

Example 2.13 Let $X \subset \mathbb{P}^2$ be the cardioid in (2.12). The curve $N_X \subset \mathbb{P}^2 \times (\mathbb{P}^2)^\vee$ has the class

$$[N_X] \;=\; \text{degree}(X^\vee)\cdot s^2 t \;+\; \text{degree}(X)\cdot st^2 \;=\; 3\cdot s^2 t \,+\, 4\cdot st^2.$$

Thus the polar degrees of the cardiod are 3 and 4. Their sum 7 is the ED degree.

Example 2.14 Let X be a general surface of degree d in $\mathbb{P}^3$. Its dual $X^\vee$ is a surface of degree $d(d-1)^2$ in $(\mathbb{P}^3)^\vee$. The conormal variety N_X is a surface in $\mathbb{P}^3 \times (\mathbb{P}^3)^\vee$, with class

$$[N_X] \;=\; d(d-1)^2\, s^3 t \;+\; d(d-1)\, s^2 t^2 \;+\; d\, st^3.$$

The sum of the three polar degrees equals $\text{EDdegree}(X) = d^3 - d^2 + d$; see Proposition 2.3.

Theorem 2.9 allows us to compute the ED degree for many interesting varieties, e.g. using Chern classes [60, Theorem 5.8]. This is relevant for applications in machine learning [32] which rest on low-rank approximation of matrices and tensors with special structure [141].

Example 2.15 (Determinantal varieties) Let $X_r \subset \mathbb{P}^{m^2-1}$ be the variety of $m \times m$ matrices $x = (x_{ij})$ of rank $\leq r$. By [165], the conormal variety N_X is cut out by nice matrix equations:

$$N_X \;=\; \bigl\{(\mathbf{x},\mathbf{h}) \in \mathbb{P}^{m^2-1} \times \mathbb{P}^{m^2-1} \;:\; \text{rank}(\mathbf{x}) \leq r,\;\; \text{rank}(\mathbf{h}) \leq m-r,\;\; \mathbf{x}\cdot\mathbf{h} = 0 \text{ and } \mathbf{h}\cdot\mathbf{x} = 0\bigr\}.$$

In particular, the duality relation $(X_r)^\vee = X_{m-r}$ holds among determinantal varieties. Typing the above formula into `Macaulay2`, we compute the polar degrees for $r = 1$ and $m = 3$:

```
QQ[x11,x12,x13,x21,x22,x23,x31,x32,x33,h11,h12,h13,h21,h22,h23,h31,h32,h33,
   Degrees=> {{1,0},{1,0},{1,0},{1,0},{1,0},{1,0},{1,0},{1,0},{1,0},
              {0,1},{0,1},{0,1},{0,1},{0,1},{0,1},{0,1},{0,1},{0,1}}];
x = matrix {{x11,x12,x13},{x21,x22,x23},{x31,x32,x33}};
h = matrix {{h11,h12,h13},{h21,h22,h23},{h31,h32,h33}};
I = minors(2,x) + minors(3,h) + minors(1,x*h) + minors(1,h*x);
isPrime(I), codim(I), degree I
multidegree(I)
```

The code starts with the bigraded coordinate ring of $\mathbb{P}^8 \times \mathbb{P}^8$. It verifies that N_X has codimension 9 and that `I` is its prime ideal. The last command computes the polar degrees:

$$[N_X] \;=\; 3s^8 t \,+\, 6s^7 t^2 \,+\, 12 s^6 t^3 \,+\, 12 s^5 t^4 + 6 s^4 t^5. \tag{2.14}$$

After verifying (2.13), one concludes that $\text{EDdegree}(X_1) = 3+6+12+12+6 = 39$. Indeed, after changing coordinates, the EDdegree for 3×3-matrices of rank 1 equals 39. We saw this already in Example 2.8, where 39 critical points were found by a numerical computation.

The primal-dual set-up of conormal varieties allows for a very elegant formulation of the critical equations. This will be presented in the next theorem. We now assume that X is an irreducible variety defined by homogeneous polynomials in n variables. Thus X is an affine cone in $\mathbb{C}^n$. Its dual $Y = X^\vee$ is the affine cone over the dual of the projective variety given by X. Thus Y is also an affine cone in $\mathbb{C}^n$. In this setting, the conormal variety N_X is viewed as an affine variety of dimension n in $\mathbb{C}^{2n}$. The homogeneous ideals of these cones are precisely those discussed above.

Theorem 2.16 *The ED problems for X and Y coincide, and we have* $\text{EDdegree}(X) = \text{EDdegree}(Y)$. *Given a general data point $\mathbf{u} \in \mathbb{R}^n$, the critical equations for this ED problem are:*

$$(\mathbf{x},\mathbf{h}) \;\in\; N_X \quad \text{and} \quad \mathbf{x}+\mathbf{h} = \mathbf{u}. \tag{2.15}$$

Proof See [60, Theorem 5.2]. □

It is instructive to verify Theorem 2.16 for Example 2.15. For any data matrix $\mathbf{u}$ of size $m \times m$, the sum in (2.15) is a special decomposition of $\mathbf{u}$, namely $\mathbf{x}$ of rank r plus $\mathbf{h}$ of rank $m - r$. By the Eckhart-Young Theorem, it arises from zeroing out complementary singular values σ_i in the two matrices $\mathbf{x}$ and $\mathbf{h}$.

In general, there is no free lunch, even with a simple formulation like (2.15). The difficulty lies in computing the ideal of the conormal variety N_X. However, this should be thought of as a preprocessing step, to be carried out only once per model X. If an efficient presentation of N_X is available, our task is to solve the system $\mathbf{x} + \mathbf{h} = \mathbf{u}$ of n linear equations in $2n$ coordinates for the n-dimensional affine variety N_X.

The discussion so far was restricted to the Euclidean norm. But, we can measure distances in $\mathbb{R}^n$ with any other norm $|| \cdot ||$. Our optimization problem (2.1) extends naturally:

$$\text{minimize } ||\mathbf{x} - \mathbf{u}|| \text{ subject to } \mathbf{x} \in X. \tag{2.16}$$

The unit ball $B = \{\mathbf{x} \in \mathbb{R}^n : ||\mathbf{x}|| \leq 1\}$ is a centrally symmetric convex body. Conversely, every centrally symmetric convex body B defines a norm, and we can paraphrase the previous optimization problem as:

$$\text{minimize } \lambda \text{ subject to } \lambda \geq 0 \text{ and } (\mathbf{u} + \lambda B) \cap X \neq \emptyset. \tag{2.17}$$

If the boundary of the unit ball B is smooth and algebraic then we can express the critical equations for the corresponding norm as a polynomial system. This is derived as before, but we now replace the first row of the augmented Jacobian matrix $\mathcal{AJ}$ with the gradient of the map $\mathbb{R}^n \to \mathbb{R}$, $\mathbf{x} \mapsto ||\mathbf{x} - \mathbf{u}||$.

Chapter 3
Computations

In this chapter, we study two computational approaches to solve a system of polynomial equations. A system of m polynomial equations in n variables is a system of the form

$$F(\mathbf{x}) := \begin{pmatrix} f_1(\mathbf{x}) \\ \vdots \\ f_m(\mathbf{x}) \end{pmatrix} = 0,$$

where $f_1, \ldots, f_m \in \mathbb{C}[\mathbf{x}] := \mathbb{C}[x_1, \ldots, x_n]$. If $n = m$, we call $F(\mathbf{x})$ a *square system*. If $n > m$, we call $F(\mathbf{x})$ *underdetermined*. If $n < m$, we call $F(\mathbf{x})$ *overdetermined*. Here, we will mostly focus on square systems.

Example 3.1 In the previous chapter, we have considered constrained optimization problems of the form $\min_{\mathbf{x}\in\mathbb{R}^n : f(\mathbf{x})=0} g(\mathbf{x})$, where f and g are polynomials in n variables $\mathbf{x} = (x_1, \ldots, x_n)$. To solve this problem, one can compute the solutions of the critical equations $f(\mathbf{x}) = \frac{\partial f}{\partial x_1} - \lambda \frac{\partial g}{\partial x_1} = \cdots = \frac{\partial f}{\partial x_n} - \lambda \frac{\partial g}{\partial x_n} = 0$. This is a square system in the $n+1$ variables $(\mathbf{x}, \lambda)$, where λ is Lagrange multiplier. ◇

Solving the system $F(\mathbf{x}) = 0$ means that we compute *all* points $\mathbf{z} = (z_1, \ldots, z_n) \in \mathbb{C}^n$ such that $F(\mathbf{z}) = 0$. The first step is to find an appropriate *data structure* to represent a solution. In fact, $F(\mathbf{z}) = 0$ is already *implicitly* represented by its equation. Some information can be read off from this representation. For instance, if F has rational coefficients and we know that $F(\mathbf{z}) = \mathbf{0}$ has only finitely many complex solutions, then each coordinate z_i of $\mathbf{z}$ is an algebraic number. On the other hand, other information like whether or there is a real solution $\mathbf{z} \in \mathbb{R}^n$ is not directly accessible from this implicit representation.

The goal of this lecture is to discuss two data structures for representing solutions of systems of polynomial equations: the first is *Gröbner bases* and the second is *approximate zeros*.

3.1 Gröbner Bases

We use the notation $\mathbf{x}^\alpha := x_1^{\alpha_1} \cdots x_n^{\alpha_n}$ for the exponent vector $\alpha = (\alpha_1, \ldots, \alpha_n) \in \mathbb{N}^n$. In fact, we can identify monomials with their exponent vectors. A monomial ordering $>$ on $\mathbb{C}[\mathbf{x}]$ is then defined by a total order $>$ on $\mathbb{N}^n$ that satisfies (1) if $\alpha > \beta$, then $\alpha + \gamma > \beta + \gamma$ for every $\gamma \in \mathbb{N}^n$ and (2) every nonempty subset of $\mathbb{N}^n$ has a smallest element under $>$ (see, e.g., [50, Chapter 2 §2, Definition 1]).

Example 3.2 The Lex (Lexicographic) order is defined by setting $\alpha >_{\text{Lex}} \beta$, if $\alpha_j - \beta_j > 0$ for $\alpha, \beta \in \mathbb{N}^n$, where $j := \min\{i \mid \alpha_i \neq \beta_i\}$ is the first index where α and β are not equal. For instance, $x_1^2 x_2 > x_1 x_2 x_3^3$. Intuitively speaking, the Lex order views a polynomial $f \in \mathbb{C}[\mathbf{x}]$ as a polynomial in x_1 with coefficients that are polynomials in x_2, which has coefficients that are polynomials in x_3, and so on. ◇

Every monomial order induces the notion of *leading term* of a polynomial. Let $f = \sum_{i=1}^k c_i \mathbf{x}^{\alpha_i} \in \mathbb{C}[\mathbf{x}]$, where $\alpha_1 > \alpha_2 > \cdots > \alpha_k$ and $c_1 \neq 0$. Then, the leading term of f is $\mathrm{LT}(f) := c_1 \mathbf{x}^{\alpha_1}$. The *leading term ideal* of an ideal $I \subset \mathbb{C}[x_1, \ldots, x_n]$ is defined as

$$\mathrm{LT}(I) := \langle \{\mathrm{LT}(f) \mid f \in I \setminus \{0\}\} \rangle .$$

Next comes the definition of a Gröbner basis.

Definition 3.3 (Gröbner basis) Let $I \subset \mathbb{C}[x_1, \ldots, x_n]$ be an ideal and $>$ be a monomial order. A subset $G = \{g_1, \ldots, g_m\} \subset I$ is called a *Gröbner basis* for I with respect to $>$ if its leading terms generate the leading term ideal; i.e., if

$$\langle \mathrm{LT}(g_1), \ldots, \mathrm{LT}(g_m) \rangle = \mathrm{LT}(I).$$

Remark 3.4 If G is a Gröbner basis for an ideal I, then $I = \langle G \rangle$ (see [50, Chapter 2 §5, Corollary 6]), hence the name "basis". A Gröbner basis defines a notion of *normal form* of an ideal. More specifically, let $I \subset \mathbb{C}[\mathbf{x}]$ be an ideal and let $G = \{g_1, \ldots, g_m\}$ be a Gröbner basis for I. Then for every $f \in \mathbb{C}[\mathbf{x}]$ there is a unique $r \in \mathbb{C}[\mathbf{x}]$, such that $f = g + r$ with $g \in I$ and no term of r is divisible by any of $\mathrm{LT}(g_1), \ldots, \mathrm{LT}(g_m)$ (see [50, Chapter 2 §6, Proposition 1]). The *remainder* r can be computed using the division algorithm.

Our next example is [50, Chapter 2 §8, Example 2]. It illustrates how Gröbner bases can be used to solve systems of polynomial equations.

Example 3.5 Consider the following system of three polynomial equations in three variables:

$$F(x, y, z) = \begin{pmatrix} x^2 + y^2 + z^2 - 1 \\ x^2 + z^2 - y \\ x - z \end{pmatrix} = 0.$$

We compute a Gröbner basis of the ideal $I = \langle x^2 + y^2 + z^2 - 1, x^2 + z^2 - y, x - z \rangle$ relative to the Lex order with $x > y > z$ using `Macaulay2` [77].

```
R = QQ[x, y, z, MonomialOrder => Lex];
f = x^2 + y^2 + z^2 - 1;
g = x^2 + z^2 - y;
h = x - z;
I = ideal {f, g, h};
G = gb I
gens G
```

This computes the Gröbner basis $G = \{x - z,\ y - 2z^2,\ 4z^4 + 2z^2 - 1\}$. Because $I = \langle G \rangle$, we can solve $F(x, y, z) = 0$ by solving the system of equations given by G. Notice that the third polynomial in G only depends on z, the second only on y and z, and the third only on x and z. Thus, we can reduce solving $F(x, y, z) = 0$ to solving three univariate polynomial equations. This gives us the four solutions $(z, 2z^2, z)$, where z iterates through the four roots of $4z^4 + 2z^2 - 1$. ◇

The reason why using the Lex order in Example 3.5 works well is the *Elimination Theorem*. To state this, let $I \subset \mathbb{C}[\mathbf{x}]$ be an ideal. For every $0 \leq j < n$, the intersection $I_j := I \cap \mathbb{C}[x_{j+1}, \ldots, x_n]$ in an ideal in a polynomial subring. It consists of those polynomials in I that only contain the variables $x_{j+1}, \ldots, x_n$. We call I_j the j-th *elimination ideal* of I. For a proof of the next theorem see [50, Chapter 3, §1, Theorem 1].

Theorem 3.6 (The Elimination Theorem) *Let $I \subset \mathbb{C}[\mathbf{x}]$ be an ideal and G be a Gröbner basis for I with respect to the Lex order with $x_1 > \cdots > x_n$. Then*

$$G_j := G \cap \mathbb{C}[x_{j+1}, \ldots, x_n]$$

is a Gröbner basis of the j-th elimination ideal of I.

For us the most important consequence of the Elimination Theorem is that, if a system of polynomial equations $F(\mathbf{x}) = (f_1(\mathbf{x}), \ldots, f_n(\mathbf{x})) = 0$ has finitely many solutions, then the j-th elimination ideal will not be empty for $0 \leq j < n$. Consequently, we can solve $F(\mathbf{x}) = 0$ by computing a Gröbner basis for the Lex order and then sequentially solving univariate equations. We can compute zeros of univariate polynomials by computing eigenvalues λ of the associated *companion matrix*. If $f(x) = x^d + \sum_{i=0}^{d-1} c_i x^i$ is a univariate polynomial, we have $f(\lambda) = 0$ if and only if λ is an eigenvalue of the companion matrix

$$\begin{pmatrix} 0 & \cdots & 0 & -c_0 \\ 1 & \cdots & 0 & -c_1 \\ \vdots & \ddots & \vdots & \vdots \\ 0 & \cdots & 1 & -c_{d-1} \end{pmatrix}.$$

Sometimes we are not interested in the solutions of $F(\mathbf{x}) = 0$ per se, but only in the number of solutions. Gröbner bases naturally carry this information: Suppose $I \subset \mathbb{C}[\mathbf{x}]$ is an ideal and $>$ a monomial order. Recall that a monomial $\mathbf{x}^\alpha \notin \mathrm{LT}(I)$ is called a *standard monomial* of I relative to $>$. The next result shows how to get the number of solutions of $F(\mathbf{x}) = 0$ from a Gröbner basis; see [167, Proposition 2.1].

Proposition 3.7 *Let $I \subset \mathbb{C}[\mathbf{x}]$ be an ideal. Let $>$ be a term order and $\mathcal{B}$ be the set of standard monomials of I relative to $>$. Then, $\mathcal{B}$ is finite if and only if $V(I)$ is finite, and $\#\mathcal{B}$ equals the number of points in $V(I)$ counting multiplicities.*

Example 3.8 In Example 3.5, there are four standard monomials, namely, $1, z, z^2$ and z^3. That is why the system $F(x, y, z) = 0$ has four solutions. ⋄

We have now understood how to solve systems of polynomials with finitely many zeros using Gröbner bases. What about systems whose variety has positive dimensional components? In that case, the n-th elimination ideal is necessarily the zero ideal. To cope with that case, one can remove positive dimensional components using ideal saturation. Let $I, J \subset \mathbb{C}[\mathbf{x}]$ be two ideals. The *saturation* of I by J is the ideal

$$I : J^\infty \;:=\; \{f \in \mathbb{C}[\mathbf{x}] \mid \text{there is } \ell > 0 \text{ with } f \cdot g^\ell \in I \text{ for all } g \in J\}.$$

Saturation is the ideal analogue of removing components on the level of varieties. We have

$$V(I : J^\infty) \;=\; \overline{V(I) \setminus V(J)}; \tag{3.1}$$

see [50, Chapter 4 §4, Corollary 11].

Recall that a solution to a square system $F(\mathbf{x}) = (f_1(\mathbf{x}), \ldots, f_n(\mathbf{x})) = 0$ is called *regular* if the Jacobian determinant $\det\left(\frac{\partial f_i}{\partial x_j}\right)_{1 \le i,j \le n}$ does not vanish at that solution. There can only be finitely many regular zeros of a square system of polynomial equations, and a finite union of points is Zariski closed. Consequently, if we saturate $I = \langle f_1, \ldots, f_n \rangle$ by $J = \left\langle \det\left(\frac{\partial f_i}{\partial x_j}\right) \right\rangle$, we can use the strategy from above to solve $F(\mathbf{x}) = 0$.

Example 3.9 Consider the following system of two polynomials in two variables

$$F(x, y) = \begin{pmatrix} (x-1) \cdot (x-2) \cdot (x^2+y^2-1) \\ (y-1) \cdot (y-3) \cdot (x^2+y^2-1) \end{pmatrix} = 0.$$

It has 4 regular solutions $(1,1), (1,3), (2,1), (2,3)$ and the circle $x^2 + y^2 - 1$ as a positive dimensional component. We use `Macaulay2` [77] to saturate the ideal generated by F.

```
R = QQ[x, y, MonomialOrder => Lex];
f = (x-1) * (x-2) * (x^2+y^2-1);
g = (y-1) * (y-3) * (x^2+y^2-1);
I = ideal {f, g};
Jac = matrix{{diff(x, f), diff(x, g)}, {diff(y, f), diff(y, g)}};
J = ideal det(Jac)
K = saturate(I,J)
```

This returns the ideal $K = \langle y^2 - 4y + 3, x^2 - 3x + 2 \rangle$. These two generators form a Gröbner basis for K. ⋄

Next, we state two propositions related to elimination and saturation of ideals with parameters, and one lemma on Gröbner bases of parameterized ideals. For this, let $\mathbf{x} = (x_1, \ldots, x_n)$ and $\mathbf{p} = (p_1, \ldots, p_k)$ be two sets of variables, and $\mathbb{C}[\mathbf{x}, \mathbf{p}] := \mathbb{C}[x_1, \ldots, x_n, p_1, \ldots, p_k]$. We regard $\mathbf{p}$ as variables for *parameters*. For a fixed parameter $\mathbf{q} \in \mathbb{C}^k$, we consider the surjective ring homomorphism

$$\phi_{\mathbf{q}} : \mathbb{C}[\mathbf{x}, \mathbf{p}] \to \mathbb{C}[\mathbf{x}], \quad f(\mathbf{x}; \mathbf{p}) \mapsto f(\mathbf{x}; \mathbf{q}). \tag{3.2}$$

Proposition 3.10 *Consider an ideal $I \subset \mathbb{C}[\mathbf{x}, \mathbf{p}]$ and let $G = \{g_1, \ldots, g_m\}$ be a Gröbner basis for I relative to the Lex order $x_1 > \cdots > x_n > p_1 > \cdots > p_k$. For $1 \le i \le m$ with $g_i \notin \mathbb{C}[\mathbf{p}]$, write g_i in the form $g_i = c_i(\mathbf{p})\mathbf{x}^{\alpha_i} + h_i$, where all terms of h_i are strictly smaller than $\mathbf{x}^{\alpha_i}$. Let $\mathbf{q} \in V(I \cap \mathbb{C}[\mathbf{p}]) \subseteq \mathbb{C}^k$ such that $c_i(\mathbf{q}) \neq 0$ for all $g_i \notin \mathbb{C}[\mathbf{p}]$. Then,*

$$\phi_{\mathbf{q}}(G) = \{\phi_{\mathbf{q}}(g_i) \mid g_i \notin \mathbb{C}[\mathbf{p}]\}$$

is a Gröbner basis for the ideal $\phi_{\mathbf{q}}(I) \subset \mathbb{C}[\mathbf{x}]$.

Proof See, e.g., [50, Chapter 4 §7, Theorem 2]. □

Example 3.11 (Cardiod revisited) As an illustration, fix $n = m = 2$ and let I be the ideal generated by the cubic (2.4) and the determinant of (2.2), with u_1, u_2 replaced by p_1, p_2. The lexicographic Gröbner basis G has 15 elements. The 15 leading coefficients $c_i(\mathbf{p})$ are quite complicated. Three of them are

$$(4p_1^2 + 4p_2^2 + 4p_2 + 1)^2,\ 32p_2^2(4p_2+3)(3p_2+1)(3p_2+2)^3(2p_2+1)^3(4p_2^2+5p_2+2)^3(1+p_2)^5,$$
$$p_1p_2^2(4p_2+3)(8p_1^4+8p_1^2p_2^2-10p_1^2p_2-18p_2^3-7p_1^2-21p_2^2-8p_2-1)(p_1+p_2+1)^3(p_1-p_2-1)^3.$$

Suppose that we replace the unknowns p_1, p_2 by any complex numbers q_1, q_2 such that $c_i(q_1, q_2) \neq 0$ for all i. Then the specialization $\phi_{\mathbf{q}}(G)$ remains a Gröbner basis with the same leading terms. In particular, the number of zeros (x_1, x_2), which is six when counted with multiplicities, is independent of q_1, q_2.

In many applications, polynomial systems come with a non-degeneracy constraint. These are usually expressed in the form of a polynomial inequation $h \neq 0$. We now show how to incorporate such a constraint.

Proposition 3.12 *Let $I \subset \mathbb{C}[\mathbf{x}, \mathbf{p}]$ be an ideal and $J = \langle h \rangle$ a principal ideal in the same ring. Let u be an additional variable and $K := \langle 1 - u \cdot h \rangle$. Then,*

$$I : J^\infty = (I + K) \cap \mathbb{C}[\mathbf{x}, \mathbf{p}].$$

Furthermore, if G is a Gröbner basis of $I+K$ relative to the Lex order $u > x_1 > \cdots > x_n > p_1 > \cdots > p_k$, then $G \cap \mathbb{C}[\mathbf{x}, \mathbf{p}]$ is a Gröbner basis of $I : J^\infty$.

Proof See, e.g., [50, Chapter 4 §4, Theorem 14]. □

Example 3.13 Fix I from Example 3.11. Since the cardiod (2.4) is singular at the origin, we take $K = \langle 1 - u \cdot h \rangle$ where $h = x_1x_2$. The Gröbner basis G has 27 elements, but with friendlier leading coefficients:

$$p_1p_2^5(p_1+p_2+1)(p_1-p_2-1),\ p_2^5(p_2+1)^2,\ p_1p_2^3,\ p_2^2(9p_1^4+p_2^4+2p_2^3-9p_1^2+p_2^2),\ p_2^2(p_2+1), p_1(p_1^2-p_2-1), \ldots$$

Nonvanishing of these coefficients ensures that the system has three complex solutions, with multiplicities.

We now apply the technique above to identifying a discriminant Δ. The following is [21, Lemma 2.5].

Lemma 3.14 *Let $I \subset \mathbb{C}[\mathbf{x}, \mathbf{p}]$ be an ideal and $J = \langle h \rangle \subset \mathbb{C}[\mathbf{x}, \mathbf{p}]$ be a principal ideal such that $(I : J^\infty) \cap \mathbb{C}[\mathbf{p}] = \{0\}$. Let $G = \{g_1, \ldots, g_s\}$ be a Gröbner basis of $I : J^\infty$ with respect to the Lex order $x_1 > \cdots > x_n > p_1 > \cdots > p_k$. There is a proper subvariety $\Delta \subsetneq \mathbb{C}^k$ such that, for all $\mathbf{q} \notin \Delta$, the set $\{\phi_{\mathbf{q}}(g_1), \ldots, \phi_{\mathbf{q}}(g_s)\}$ is a Gröbner basis for $\phi_{\mathbf{q}}(I) : \phi_{\mathbf{q}}(J)^\infty$ and none of the leading terms of $g_1, \ldots, g_s$ vanish when evaluated at $\mathbf{q}$. In particular, $\phi_{\mathbf{q}}(I : J^\infty) = \phi_{\mathbf{q}}(I) : \phi_{\mathbf{q}}(J)^\infty$ for all $\mathbf{q} \notin \Delta$.*

Proof Let u be an additional variable and, as in Proposition 3.12, consider the ideal $K := \langle 1 - u \cdot h \rangle$. Then, we have $I : J^\infty = (I + K) \cap \mathbb{C}[\mathbf{x}, \mathbf{p}]$. Using our hypothesis $(I : J^\infty) \cap \mathbb{C}[\mathbf{p}] = \{0\}$, we conclude

$$V((I + K) \cap \mathbb{C}[\mathbf{p}]) \ = \ \mathbb{C}^k. \tag{3.3}$$

We may therefore apply Proposition 3.10 to $I + K$ without any restrictions on $\mathbf{q}$. As in Proposition 3.12, we augment the Lex order by letting u be the largest variable. Let $\overline{G} := \{g_1, \ldots, g_r\}$ be a Gröbner basis of $I + K$ relative to this order. By (3.3), we have $g_1, \ldots, g_r \notin \mathbb{C}[\mathbf{p}]$. We write each g_i in the form $g_i = c_i(\mathbf{p})u^\beta \mathbf{x}^{\alpha_i} + h_i$, where all terms of h_i are strictly smaller than $u^\beta \mathbf{x}^{\alpha_i}$, and define the hypersurface

$$\Delta \;:=\; \{\mathbf{q} \in \mathbb{C}^k \mid c_1(\mathbf{q}) \cdots c_r(\mathbf{q}) = 0\}. \tag{3.4}$$

Now let $\mathbf{q} \in \mathbb{C}^k \backslash \Delta$. By Proposition 3.10, the set $\phi_{\mathbf{q}}(\overline{G}) = \{\phi_{\mathbf{q}}(g_1), \ldots, \phi_{\mathbf{q}}(g_r)\}$ is a Gröbner basis for

$$\phi_{\mathbf{q}}(I + K) \;=\; \phi_{\mathbf{q}}(I) + \phi_{\mathbf{q}}(K) \;=\; \phi_{\mathbf{q}}(I) + (1 - u \cdot \phi_{\mathbf{q}}(h)).$$

Without loss of generality, suppose the first $s \le r$ elements in $\overline{G}$ do not depend on the variable u. We define $G := \{g_1, \ldots, g_s\} = \overline{G} \cap \mathbb{C}[\mathbf{x}, \mathbf{p}]$. It follows from Proposition 3.12 that G is a Gröbner basis of $I : J^\infty$. Because $\mathbf{q} \notin \Delta$, none of the leading terms in $\overline{G}$ when evaluated at $\mathbf{q}$ vanish. Consequently,

$$\phi_{\mathbf{q}}(G) \cap \mathbb{C}[\mathbf{x}] \;=\; \phi_{\mathbf{q}}(\overline{G}) \cap \mathbb{C}[\mathbf{x}].$$

Therefore, $\phi_{\mathbf{q}}(G) = \{\phi_{\mathbf{q}}(g_1), \ldots, \phi_{\mathbf{q}}(g_s)\}$ is a Gröbner basis of $\phi_{\mathbf{q}}(I) : \phi_{\mathbf{q}}(J)^\infty$, by Proposition 3.12. □

We refer to Δ as the *discriminant* of the pair (I, h). Equation (3.4) leads to the following corollary.

Corollary 3.15 *Fix an ideal $I = \langle f_1, \ldots, f_n \rangle \subset \mathbb{C}[\mathbf{x}, \mathbf{p}]$ and a principal ideal $J = \langle h \rangle \subset \mathbb{C}[\mathbf{x}, \mathbf{p}]$. The discriminant Δ in Lemma 3.14 is found by computing a Lex Gröbner basis G for $I + \langle 1 - u \cdot h \rangle$, where $u > x_1 > \cdots > x_n > p_1 > \cdots > p_k$. Namely, Δ is the product of the leading coefficients $c_i(\mathbf{p})$ in G.*

Example 3.16 (Hyperdeterminant) Let $m = 8, n = 2$ and consider a general pair of bilinear equations:

$$I \;=\; \langle f_1, f_2 \rangle, \quad \text{where } f_1 = p_1x_1x_2 + p_2x_1 + p_3x_2 + p_4 \text{ and } f_2 = p_5x_1x_2 + p_6x_1 + p_7x_2 + p_8.$$

Our nondegeneracy constraint is the Jacobian determinant $h = \partial f_1/\partial x_1 \cdot \partial f_2/\partial x_2 - \partial f_1/\partial x_2 \cdot \partial f_2/\partial x_1$. The Gröbner basis G in Corollary 3.15 has 11 elements. The most interesting Gröbner basis element is

$$\begin{aligned} & c_1(\mathbf{p}) \cdot u - 2p_1p_7x_2 + 2p_3p_5x_2 - p_1p_8 - p_2p_7 + p_3p_6 + p_4p_5, \\ \text{where} \quad & c_1(\mathbf{q}) \;=\; p_1^2p_8^2 - 2p_1p_2p_7p_8 - 2p_1p_3p_6p_8 - 2p_1p_4p_5p_8 + 4p_1p_4p_6p_7 + p_2^2p_7^2 \\ & \qquad + 4p_2p_3p_5p_8 - 2p_2p_3p_6p_7 - 2p_2p_4p_5p_7 + p_3^2p_6^2 - 2p_3p_4p_5p_6 + p_4^2p_5^2. \end{aligned}$$

This coefficient is the main factor in our discriminant Δ. It is the *hyperdeterminant* of a $2 \times 2 \times 2$ tensor.

3.2 The Parameter Continuation Theorem

The theorem to be proved in this section states that a square system of polynomial equations with parameters has a well-defined degree. This degree is the number of complex solutions for generic parameter choices. This result is the *Parameter Continuation Theorem* due to Morgan and Sommese [135]. We shall present a proof that rests on the results on Gröbner bases in the previous section. For this, we consider the polynomial ring $\mathbb{C}[\mathbf{x}, \mathbf{p}] := \mathbb{C}[x_1, \ldots, x_n, p_1, \ldots, p_k]$. We interpret $\mathbf{x}$ as variables and $\mathbf{p}$ as parameters.

Definition 3.17 Let $f_1(\mathbf{x}; \mathbf{p}), \ldots, f_n(\mathbf{x}; \mathbf{p}) \in \mathbb{C}[\mathbf{x}, \mathbf{p}]$. We consider the image of the polynomial map

$$\mathbb{C}^k \mapsto \mathbb{C}[\mathbf{x}]^n, \quad \mathbf{p}_0 \mapsto F(x; \mathbf{p}_0) = \begin{pmatrix} f_1(\mathbf{x}; \mathbf{p}_0) \\ \vdots \\ f_n(\mathbf{x}; \mathbf{p}_0) \end{pmatrix}.$$

This image is a *family* of square polynomial systems of size n. In other words, the above family $\mathcal{F} = \{F(\mathbf{x};\mathbf{p}) \mid \mathbf{p} \in \mathbb{C}^k\}$ consists of n polynomials in n variables that depend polynomially on k parameters.

In Examples 3.11, 3.13 and 3.16, we studied families of polynomials systems with $n = 2$, where the number m of parameters was 2, 2 and 8, respectively. The degrees of these families are 6, 3 and 2. These degrees count the numbers of complex zeros for generic parameters $\mathbf{p}$, which satisfy $c_i(\mathbf{p}) \neq 0$ for all i.

We now fix a family of polynomial systems $\mathcal{F}$ depending on k parameters $\mathbf{p} = (p_1, \ldots, p_k)$. Let $\mathbf{z} \in \mathbb{C}^n$ be a zero of $F(\mathbf{x};\mathbf{p}) = (f_1(\mathbf{x};\mathbf{p}), \ldots, f_n(\mathbf{x};\mathbf{p})) \in \mathcal{F}$, for some specific parameters $\mathbf{p} \in \mathbb{C}^{\mathbf{k}}$. We say that $\mathbf{z}$ is a *regular zero* if the Jacobian determinant $\det\left(\frac{\partial f_i}{\partial x_j}\right)_{1\leq i,j\leq n}$ does not vanish at $\mathbf{z}$. The next theorem is our main result. If shows that, for almost all parameters $\mathbf{p}$, the number of regular solutions is the same.

Theorem 3.18 (The Parameter Continuation Theorem) *Let $\mathcal{F}$ be a family of polynomial systems that consists of systems of n polynomials in n variables depending on k parameters. For $\mathbf{p} \in \mathbb{C}^k$, denote*

$$N(\mathbf{p}) := \#\{\mathbf{x} \in \mathbb{C}^n \mid x \text{ is a regular zero of } F(\mathbf{x};\mathbf{p})\}.$$

Let $N := \sup_{\mathbf{p}\in\mathbb{C}^k} N(\mathbf{p})$. Then, $N < \infty$, and there exists a proper algebraic subvariety $\Delta \subsetneq \mathbb{C}^k$, called the discriminant of the system $\mathcal{F}$, such that $N(\mathbf{p}) = N$ for $\mathbf{p} \notin \Delta$.

Proof We recall the proof from [21]. Another proof can also be found in the textbook [162].

Suppose $\mathcal{F} = \{F(\mathbf{x};\mathbf{p}) \mid \mathbf{p} \in \mathbb{C}^k\}$, where $F(\mathbf{x};\mathbf{p}) = (f_1(\mathbf{x};\mathbf{p}), \ldots, f_n(\mathbf{x};\mathbf{p})) \in \mathcal{F}$. Let

$$I = \langle f_1, \ldots, f_n\rangle \quad \text{and} \quad J := \langle \det\left(\tfrac{\partial f_i}{\partial x_j}\right)\rangle.$$

If $N = 0$, then no system in $\mathcal{F}$ has regular zeros. In this case, the statement is true. We now assume $N > 0$. By (3.1), the variety $V(I : J^\infty)$ consists of all pairs $(\mathbf{x},\mathbf{q}) \in \mathbb{C}^n \times \mathbb{C}^k$ such that $\mathbf{x}$ is a regular zero of $F(\mathbf{x};\mathbf{q})$. Since $N > 0$, we therefore have $V(I : J^\infty) \neq \emptyset$. Let $(\mathbf{x},\mathbf{q}) \in V(I : J^\infty)$. The Implicit Function Theorem ensures that there is a Euclidean open neighborhood U of $\mathbf{q}$ such that $F(\mathbf{x};\mathbf{q})$ has regular zeros for all $\mathbf{q} \in U$. Consequently, $(I : J^\infty) \cap \mathbb{C}[\mathbf{p}] = \{0\}$, so we can apply Lemma 3.14 in our situation.

Set $I_\mathbf{q} = \phi_\mathbf{q}(I)$ and $J_\mathbf{q} = \phi_\mathbf{q}(J)$. Let $G = \{g_1, \ldots, g_s\}$ be a Gröbner basis of $I : J^\infty$ for the Lex order $x_1 > \cdots > x_n > p_1 > \cdots > p_k$. By Lemma 3.14, there is a proper algebraic subvariety $\Delta \subsetneq \mathbb{C}^k$ such that $\phi_\mathbf{q}(G) = \{\phi_\mathbf{q}(g_1), \ldots, \phi_\mathbf{q}(g_s)\}$ is a Gröbner basis for $I_\mathbf{q} : J_\mathbf{q}^\infty$ and none of the leading terms of $g_1, \ldots, g_s$ vanish when evaluated at $\mathbf{q}$. This implies that the leading monomials of $I_\mathbf{q} : J_\mathbf{q}^\infty$ are constant on $\mathbb{C}^k \setminus \Delta$.

We consider the set of *standard monomials*, i.e. monomials not in the lexicographic initial ideal:

$$\mathcal{B}_\mathbf{q} := \left\{\text{standard monomials of } I_\mathbf{q} : J_\mathbf{q}^\infty\right\}.$$

We have shown is that $\mathcal{B}_\mathbf{q}$ is constant on $\mathbb{C}^k\backslash\Delta$. On the other hand, by (3.1) and since finite sets of points are Zariski closed, we have $V(I : J^\infty) = V(I)\backslash V(J)$. Proposition 3.7 and the fact that regular zeros have multiplicity one imply that the following holds for all parameters $\mathbf{q}$ that are not in the discriminant Δ:

$$N(\mathbf{q}) \;=\; \#\mathcal{B}_\mathbf{q}.$$

This shows that $N(\mathbf{q})$ is constant on $\mathbb{C}^k\backslash\Delta$. The Implicit Function Theorem implies that, for all $\mathbf{q} \in \mathbb{C}^k$, there exists a Euclidean neighborhood U of $\mathbf{q}$ such that $N(\mathbf{q}) \leq N(\mathbf{q}')$ for all $\mathbf{q}' \in U$. Since Δ is a proper subvariety of $\mathbb{C}^k$ and thus lower-dimensional, we have $N = N(\mathbf{q}) < \infty$ for $\mathbf{q} \in \mathbb{C}^k\backslash\Delta$. □

We can use the algorithm in Corollary 3.15 to compute the discriminant. Observe that this algorithm also returns the discriminant when $F(\mathbf{x};\mathbf{p}) = 0$ has non-regular solutions for *all* parameters $\mathbf{p}$. Resultant-based methods for computing the discriminant would fail in such cases because the resultant will be constant and equal to zero. Here is a simple example to illustrate this phenomenon.

Example 3.19 We slightly modify the system from Example 3.9 and consider

$$F(x,y;a) = \begin{pmatrix} (x-1)\cdot(x-2)\cdot(x^2+y^2-1) \\ (y-1)\cdot(y-a)\cdot(x^2+y^2-1) \end{pmatrix} = 0,$$

where $a \in \mathbb{C}$ is a parameter. If $a \notin \{0, 1, \pm\sqrt{-3}\}$, we have $N = 4$ regular solutions. Let us compute the discriminant using the algorithm in Corollary 3.15. We use the `Macaulay2` code from [21].

```
R = QQ[u, x, y, a, MonomialOrder => Lex];
f = (x-1) * (x-2) * (x^2+y^2-1);
g = (y-1) * (y-a) * (x^2+y^2-1);
I = ideal {f, g};
Jac = matrix{{diff(x, f), diff(x, g)}, {diff(y, f), diff(y, g)}};
K = ideal {1 - u * det(Jac)};
G = gens gb (I+K)
E = (entries(G))#0

P = QQ[a][u, x, y, MonomialOrder => Lex]
result = apply(E, t -> leadCoefficient(sub(t, P)))
factor(product result)
```

The result is the polynomial $a^6 \cdot (a-1)^4 \cdot (a^2+3)^2 \cdot g(a)$, where $g(a) = (a+1)\cdot(a^7 - 2a^6 + 8a^5 - 14a^4 + 23a^3 - 32a^2 + 32a - 32)$. Each zero of the additional factor $g(a)$ gives a system that also has four regular solutions. However, Theorem 3.18 only states that if a parameter is outside the discriminant, then it has the maximal number of regular zeros, but not the reverse implication. ◇

Example 3.20 The critical equations for the ED problem in (2.1) have parameters $\mathbf{u}$. In many situations, the critical equations form a square system, and Theorem 3.18 applies. The degree N is the Euclidean Distance Degree. For instance, in Example 2.2, we have a square system in $n = 3$ variables with $m = 3$ parameters, and the ED degree equals $N = d_1 d_2 (d_1 + d_2 + 1)$. What is the discriminant Δ in this case? ◇

Example 3.21 (Tact invariant) We consider the general system of two quadratic equations in $n = 2$ variables. Each of the two equations has six coefficients, so there are $m = 12$ parameters in total:

```
R = QQ[x,y,a20,a11,a02,a10,a01,a00,b20,b11,b02,b10,b01,b00];
f = a20*x^2 + a11*x*y + a02 * y^2 + a01*x + a10*y + a00;
g = b20*x^2 + b11*x*y + b02 * y^2 + b01*x + b10*y + b00;
```

For general parameter values $\mathbf{q}$, the set of lexicographic standard monomials is $B_{\mathbf{q}} = \{1, y, y^2, y^3\}$, so the number of solutions is $N = 4$. The main factor in the discriminant Δ is a polynomial in the 12 coefficients that is known as the *tact invariant*. This polynomial can be computed with following `Macaulay2` code:

```
I = ideal(f,g,diff(x,f)*diff(y,g)-diff(y,f)*diff(x,g));
tact = first first entries gens eliminate({x,y},I);
toString tact
degree tact, # terms tact
```

From the output we see that the tact invariant has degree 12, and that it is the sum of 3210 monomials.

3.3 Polynomial Homotopy Continuation

In Section 3.1, we have seen how to use Gröbner bases to reduce solving $F(\mathbf{x}) = 0$ to the problem of sequentially computing zeros of univariate polynomials. Another approach is *polynomial homotopy continuation* (PHC). This is a numerical method for computing the regular zeros of a square system of

polynomial equations. The textbook of Sommese and Wampler [162] provides a detailed introduction to the theory of polynomial homotopy continuation. We also refer to the overview article [12]. This subject area is known as *numerical algebraic geometry*, and the present section offers a lightning introduction.

The goal in polynomial homotopy continuation is to compute *approximate zeros*. The definition goes back to Smale (see [19, §8, Definition 1]). It rests on Newton's method from numerical analysis.

Definition 3.22 (Approximate Zeros) Let $F(\mathbf{x})$ be a square system of polynomial equations in n variables, and write $JF(\mathbf{x})$ for its (square) Jacobian matrix. A point $\mathbf{z} \in \mathbb{C}^n$ is called an *approximate zero* of F if the sequence of Newton iterates $\mathbf{z}_{k+1} := \mathbf{z}_k - JF(\mathbf{x}_k)^{-1}F(\mathbf{x}_k)$ starting at $\mathbf{z}_0 := \mathbf{z}$ converges to a zero of F.

An approximate zero $\mathbf{z}$ of a system F is in a precise sense close to an actual zero $\mathbf{x}$. Applying the Newton operator to $\mathbf{z}$, we can get as close to $\mathbf{x}$ as we want. We can approximate $\mathbf{x}$ to any desired accuracy.

Suppose now that $F(\mathbf{x}) = 0$ is a system of polynomial equations that we want to solve. The idea in homotopy continuation is to find a family $\mathcal{F}$ and parameters $\mathbf{p}, \mathbf{q} \in \mathbb{C}^k$ with the following properties:

- $F(\mathbf{x}) = F(\mathbf{x}; \mathbf{p})$;
- $G(\mathbf{x}) := F(\mathbf{x}; \mathbf{q})$ is a system whose solutions are known or can be computed by other means.

For a (piecewise) smooth path $\gamma(t)$ in $\mathbb{C}^k$ with $\gamma(0) = \mathbf{q}$ and $\gamma(1) = \mathbf{p}$, we define the *parameter homotopy*

$$H(\mathbf{x}, t) := F(\mathbf{x}; \gamma(t))$$

and *track* the solutions of $F(\mathbf{x}; \mathbf{q}) = 0$ to $F(\mathbf{x}; \mathbf{p})$ along the homotopy H. This tracking involves an ordinary differential equation (ODE). Namely, we use numerical algorithms to solve the *ODE initial value problem*

$$\left(\frac{\mathrm{d}}{\mathrm{d}\mathbf{x}} H(\mathbf{x}, t)\right) \frac{\mathrm{d}\mathbf{x}}{\mathrm{d}t} + \frac{\mathrm{d}}{\mathrm{d}t} H(\mathbf{x}, t) = 0, \quad \mathbf{x}(0) = \mathbf{z}. \tag{3.5}$$

Here the initial value $\mathbf{z}$ is a zero of $G(\mathbf{x})$. In this setting, $G(\mathbf{x}) = F(\mathbf{x}; \mathbf{q})$ is called *start system* and $F(\mathbf{x}) = F(\mathbf{x}; \mathbf{p})$ is called *target system*. The output of the numerical solver is then an approximate zero of $F(\mathbf{x})$. In implementations one often uses piecewise linear paths, such as that described below.

Remark 3.23 The left factor $\left(\frac{\mathrm{d}}{\mathrm{d}\mathbf{x}} H(\mathbf{x}, t)\right)$ in (3.5) is the $n \times n$ Jacobian matrix. Throughout the tracking process, it essential that this matrix is invertible. This means geometrically that our path must stay away from the discriminant Δ of the polynomial system. This is possible because Δ is a proper subvariety of the parameter space $\mathbb{C}^k$. The dimension of Δ over the real numbers $\mathbb{R}$ is an even number that is less than the real dimension $2k$ of the ambient space $\mathbb{R}^{2k} = \mathbb{C}^k$. This ensures that the space $\mathbb{C}^k \backslash \Delta$ is connected.

The next proposition explains why polynomial homotopy continuation works and when the initial value problem from (3.5) is well-posed. The proof of the proposition crucially relies on the Parameter Continuation Theorem (Theorem 3.18), and on the connectedness result in Remark 3.23.

Proposition 3.24 *Let $\mathcal{F}$ be a family of polynomial systems with parameters $\mathbf{p} \in \mathbb{C}^k$. Let N and Δ be as in Theorem 3.18, and assume that $N > 0$. Given $\mathbf{q} \in \mathbb{C}^k \setminus \Delta$ and $\mathbf{p} \in \mathbb{C}^k$, for almost all choices of $\mathbf{p}_{\mathrm{mid}} \in \mathbb{C}^k$, the piecewise linear path*

$$\gamma(t) = \begin{cases} (2t-1)\mathbf{q} + 2(1-t)\mathbf{p}_{\mathrm{mid}}, & \text{if } \frac{1}{2} \le t \le 1 \\ 2t\mathbf{p}_{\mathrm{mid}} + (1-2t)\mathbf{p}, & \text{if } 0 < t \le \frac{1}{2} \end{cases}$$

satisfies:

1. $\gamma((0, 1]) \cap \Delta = \emptyset$.

2. *The homotopy* $H(\mathbf{x}, t) := F(\mathbf{x}; \gamma(t))$ *defines* N *smooth curves* $\mathbf{x}(t)$ *with the property that* $H(\mathbf{x}(t), t) = 0$ *for* $0 < t \leq 1$. *These curves are called solution paths.*
3. *As* $t \to 0$, *the limits of the solution paths include all regular solutions of* $F(\mathbf{x}; \mathbf{p}) = 0$.
4. *If moreover* $\gamma(0) \notin \Delta$, *then every solution path* $\mathbf{x}(t)$ *converges for* $t \to 0$ *to a regular zero of* $F(\mathbf{x}; \mathbf{p})$.

Proof If $N > 0$, the discriminant $\Delta \subsetneq \mathbb{C}^k$ is a proper complex subvariety. Therefore, Δ is of complex codimension at least 1, hence of real codimension at least 2. This was a recap of Remark 3.23. It implies that for general $\mathbf{p}_{\text{mid}} \in \mathbb{C}^k$, the path $\gamma(t)$ does not intersect Δ for $t \in (0, 1]$. This proves the first item.

Since $\mathbf{q} = \gamma(0) \notin \Delta$, the implicit function theorem ensures that there exists a Euclidean neighborhood $\mathcal{U}_0 \subset \mathbb{C}^k$ of $\mathbf{q}$ and a smooth *solution map* $s_0 : \mathcal{U}_0 \to \mathbb{C}^n$ such that $F(s_0(\mathbf{p}), \mathbf{p}) = 0$ for all $\mathbf{p} \in \mathcal{U}_0$. Let

$$t_0 := \min \left\{ t \in [0, 1] \;\middle|\; \gamma(t) \in \overline{\mathcal{U}_0} \right\},$$

where $\overline{\mathcal{U}_0}$ is the Euclidean closure of $\mathcal{U}_0$. If $t_0 > 0$, then $\gamma(t_0) \notin \Delta$ and we can repeat the construction for the new start system $F(\mathbf{x}; \gamma(t_0))$. Eventually, we obtain an open cover

$$(0, 1] = \bigcup_{i \in \mathcal{I}} \mathcal{U}_i$$

for some index set $\mathcal{I}$, together with smooth solution maps $s_i : \mathcal{U}_i \to \mathbb{C}^n$. Taking a partition of unity $(\rho_i(t))_{i \in \mathcal{I}}$ relative to this cover (see [122, Chapter 2]), we set

$$\mathbf{x}(t) := \sum_{i \in \mathcal{I}} \rho_i(t) \cdot (s_i \circ \gamma)(t), \quad t \in (0, 1].$$

By construction, the path $\mathbf{x}(t)$ is smooth and has the property that $H(\mathbf{x}(t), t) = 0$. Furthermore, as $t \to 0$, the solution path $\mathbf{x}(t)$ either converges to a point $\mathbf{z}$ or diverges as $\|\mathbf{x}_i(t)\| \to \infty$. In the first situation, by continuity, $\mathbf{z}$ is a zero of $F(\mathbf{x}, \gamma(0)) = F(\mathbf{x}, \mathbf{p})$ (not necessarily regular).

By Theorem 3.18, $F(\mathbf{x}; \mathbf{q})$ has N regular zeros. The construction above yields N solution paths $\mathbf{x}_1(t), \ldots, \mathbf{x}_N(t)$. Smoothness implies that $\mathbf{x}_i(t) \neq \mathbf{x}_j(t)$ for $i \neq j$ and all $t \in (0, 1]$. This proves the second item. Furthermore, for every regular zero of $F(\mathbf{x}; \mathbf{q})$, we also find a (local) solution map, which connects to exactly one of the smooth paths $\mathbf{x}_1(t), \ldots, \mathbf{x}_N(t)$. This implies the third and fourth item. □

There are several software packages for solving polynomial systems that are based on homotopy continuation. In this book we use the software `HomotopyContinuation.jl` [26] that was developed by the first author together with Sascha Timme. In our view, this software is quite powerful and easy to use.

Example 3.25 We use to solve the system of polynomial equations from Example 3.5. The following are commands in the programming language `Julia` on which `HomotopyContinuation.jl` is based:

```
using HomotopyContinuation
@var x y z;
f = x^2 + y^2 + z^2 - 1;
g = x^2 + z^2 - y;
h = x - z;
F = System([f; g; h], variables = [x; y; z])
solve(F)
```

This code returns the four solutions (here displayed with only the 4 most significant digits):

$$
\begin{aligned}
&(0.556 + 0.0\sqrt{-1}\,,\ 0.618 - 0.0\sqrt{-1}\,,\ 0.556 + 0.0\sqrt{-1}\,),\\
&(-0.0 - 0.899\sqrt{-1}\,,\ -1.618 + 0.0\sqrt{-1}\,,\ -0.0 - 0.899\sqrt{-1}\,),\\
&(-0.556 - 0.0\sqrt{-1}\,,\ 0.618 + 0.0\sqrt{-1}\,,\ -0.556 + 0.0\sqrt{-1}\,),\\
&(0.0 + 0.899\sqrt{-1}\,,\ -1.618 + 0.0\sqrt{-1}\,,\ -0.0 + 0.899\sqrt{-1}\,).
\end{aligned}
$$

These are numerical approximations of the solutions found symbolically in Example 3.5. ◇

Remark 3.26 The capabilities of `HomotopyContinuation.jl` were already on display in Example 2.5. In that example we solved the critical equations for the ED problem on some complete intersections.

Remark 3.27 Numerical computations are not exact computations and therefore can produce errors. This is hence also true for polynomial homotopy continuation. It is possible, though, to *certify* the output of PHC. Certification means that we obtain a computer proof that we have indeed computed an approximate zero. There are various certification methods. Current implementations are [25, 85, 123].

Corollary 3.28 *A general system of polynomials $F(\mathbf{x}) = (f_1(\mathbf{x}), \ldots, f_n(\mathbf{x}))$ in n variables has*

$$N = d_1 \cdots d_n$$

isolated zeros in $\mathbb{C}^n$, where $d_i = \deg f_i$. (The number $d_1 \cdots d_n$ is also called the Bézout number of F.)

Proof We consider the family $\mathcal{F}_{\text{Bézout}}$ of polynomial systems $F(\mathbf{x}) = (f_1(\mathbf{x}), \ldots, f_n(\mathbf{x}))$ with $d_i = \deg f_i$. The parameters are the coefficients of the polynomials $f_1, \ldots, f_n$. Here, we can use the start system

$$G(\mathbf{x}) = \begin{pmatrix} x_1^{d_1} - 1 \\ \vdots \\ x_n^{d_n} - 1 \end{pmatrix}.$$

This system has the $d_1 \cdots d_n$ distinct complex zeros. Explictly, the zeros are $(\xi_1^{k_1}, \ldots, \xi_n^{k_n})$, where $\xi_i := \exp\left(2\pi\sqrt{-1}\,/d_i\right)$ is the d_i-th root of unity and k_i ranges from 1 to d_i. One calls $G(x)$ the *total degree start system*. All its zeros are regular, and it has no zeros at infinity. Together with Proposition 3.24 this implies that the system $G(\mathbf{x})$ has the maximal number $N = d_1 \cdots d_n$ of regular zeros in $\mathcal{F}_{\text{Bézout}}$. □

Remark 3.29 Corollary 3.28 only states that the number of solutions equals $d_1 \cdots d_n$ for systems outside the discriminant. The full version of Bézout's theorem also applies to systems $F \in \Delta$, where it states that the number of zeros counted with multiplicities is $d_1 \cdots d_n$. Corollary 3.28 does not prove this full version.

Corollary 3.28 implies that one can use the total degree start system for homotopy continuation in the family of system of polynomials with fixed degree pattern.

Example 3.30 The system $F(x, y, z) = (x^2 + y^2 + z^2 - 1,\ x^2 + z^2 - y,\ x - z)$ from Example 3.25 consists of three polynomials of degrees $d_1 = 2, d_2 = 2$ and $d_3 = 1$. We have shown that the number of zeros of F is the Bézout number $N = d_1 \cdot d_2 \cdot d_3 = 4$. In `HomotopyContinuation.jl` [26], we can use the total degree start system by setting the following flag:

```
solve(F; start_system = :total_degree)
```

The default option in `HomotopyContinuation.jl` is the *polyhedral homotopy*. Here the start system is constructed from Newton polytopes, and it respects the mixed volume, as described from Example 3.31. ◇

Example 3.31 Let $A \subset \mathbb{N}^n$ be a finite set and denote $\mathcal{F}_A := \{\sum_{\alpha\in A} c_\alpha \mathbf{x}^\alpha \mid c_\alpha \in \mathbb{C}\}$. An element in $\mathcal{F}_A$ is called a *sparse polynomial*, since only the monomials with exponent vector in A appear. For finite subsets $A_1, \ldots, A_n \subset \mathbb{N}^n$, we consider the family $\mathcal{F}_{\text{sparse}} := \mathcal{F}_{A_1} \times \cdots \times \mathcal{F}_{A_n}$. The parameters in this family are the coefficients of the n sparse polynomials of a system in $\mathcal{F}_{\text{sparse}}$. For $1 \le i \le n$, let P_i be the convex hull of A_i. The polytope P_i is called the *Newton polytope* of the polynomial F_{A_i}.

Let $\text{MV}(P_1, \ldots, P_n)$ denote the *mixed volume* of these n polytopes. The BKK Theorem [16,17] asserts that a general $F \in \mathcal{F}_{\text{sparse}}$ has $\text{MV}(P_1, \ldots, P_n)$ many zeros in the torus $(\mathbb{C}^*)^n$. Assuming that a general $F \in \mathcal{F}_{\text{sparse}}$ only has zeros with nonzero entries, the maximal number of regular zeros in $\mathcal{F}_{\text{sparse}}$ therefore is

$$N \;=\; \text{MV}(P_1, \ldots, P_n).$$

If the supports A_i are all the same, then there is only one Newton polytope $P = P_1 = \cdots = P_n$. In this situation, which occurs frequently in practise, the mixed volume $MV(P, \ldots, P)$ equals $n!$ times the volume of P. This product is a nonnegative integer, and it is referred to as the normalized volume of P. Thus the BKK bound for unmixed square systems is the normalized volume of the Newton polytope. ⋄

Remark 3.32 The article [101] provides an algorithm to compute an explicit start system for $\mathcal{F}_{\text{sparse}}$, called *polyhedral start system*. See also the summary in [12, Section 3]. The use of the polyhedral start system is the default option in `HomotopyContinuation.jl`.

We close this chapter with a brief discussion for two quadratic equations in two variables. The general system appeared in Example 3.21, where we computed the tact invariant, which serves as the discriminant. The nonvanishing of the tact invariant ensures that the two equations have four distinct complex solutions. Suppose we begin with the total degree start system $x_1^2 = x_2^2 = 1$, which has four solutions $(\pm 1, \pm 1)$. The homotopy in Proposition 3.24 is guaranteed to find the four solutions of the system we wish to solve.

By contrast, suppose now that our two quadratic equations are sparse, and the system has the form

$$F(x, y) \;=\; \begin{pmatrix} a + bx + cy + dxy \\ \alpha + \beta x + \gamma y + \delta xy \end{pmatrix} \;\in\; \mathcal{F}_{\text{sparse}},$$

where $\mathbf{p} = (a, b, c, d, \alpha, \beta, \gamma, \delta) \in \mathbb{C}^8$ are parameters. Both polynomials in F have the same Newton polytope P, namely the unit square. The normalized volume of the unit square equals $\text{MV}(P) = 2$. Therefore, the BKK Theorem tells us that $F(x, y) = 0$ has $N = 2$ solutions for general parameters $\mathbf{p} \in \mathbb{C}^8$.

The total degree start system $x_1^2 = x_2^2 = 1$ is not appropriate for the sparse family $F(x, y)$ because it has too many solutions. Indeed, two of the start solutions $(\pm 1, \pm 1)$ lead to paths that diverge when running the homotopy. Instead, one can use a polyhedral start system [101] that has precisely two solutions. A polyhedral start system is obtained by dividing the square P into two triangles, each of normalized area 1.

The two zeros of $F(x, y)$ are distinct when the discriminant does not vanish at $\mathbf{p}$. The discriminant of the system $F(x, y)$ is the hyperdeterminant of format $2 \times 2 \times 2$, which we computed in Example 3.16. In other words, the role of the tact invariant for two dense quadrics is now played by our hyperdeterminant. Hyperdeterminants of larger tensors, and the spectral theory of tensors, will be discussed in later chapters.

Chapter 4
Polar Degrees

We compare three definitions of *polar degrees*, in terms of non-transversal intersections, Schubert varieties and the Gauss map, and conormal varieties. The latter approach was used in Chapter 2.3. We discuss the key properties of polar degrees under projective duality and explain how polar degrees are related with Chern classes.

We work over an algebraically closed field of characteristic zero.

4.1 Polar Varieties

Example 4.1 Imagine that you look at an algebraic surface $X \subseteq \mathbb{P}^3$ from a point $V \in \mathbb{P}^3$. If you would want to sketch the surface from your point of view, you would draw its *contour curve* $P(X, V)$; see Figure 4.1. The contour curve consists of all points p on the surface X such that the line spanned by V and p is tangent at p. The *first polar degree* $\mu_1(X)$ of the surface X is the degree of the contour curve for a generic point V.

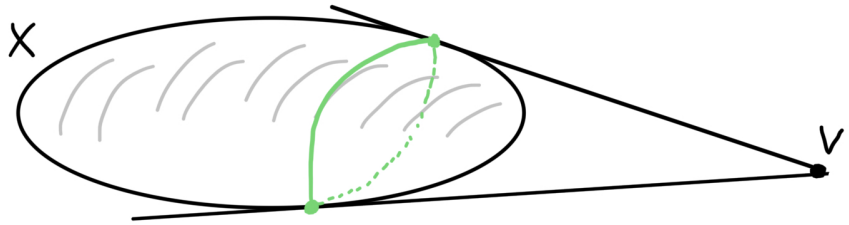

Fig. 4.1: Green contour curve when the ellipsoid X is viewed from the point V.

Now we change the setting slightly and imaging that our viewing of the surface X is not centered at a point but at a line $V \subseteq \mathbb{P}^3$. This time our contour set $P(X, V)$ consists of all point p on the surface X such that the plane spanned by the point p and the line V is tangent at p; see Figure 4.2. For a generic line V, the contour set $P(X, V)$ is finite, and the *second polar degree* is its cardinality. ◇

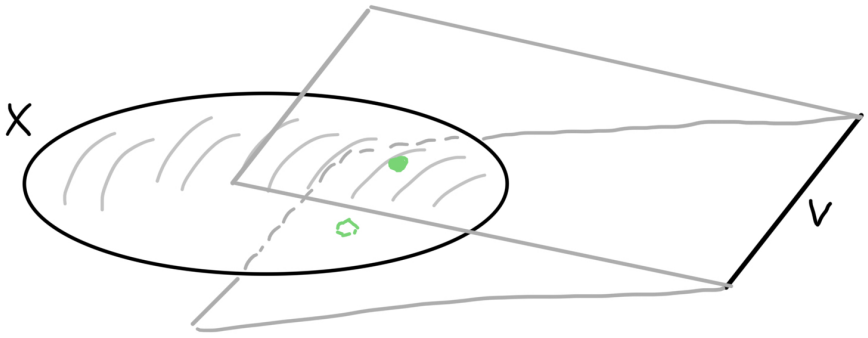

Fig. 4.2: The green contour set consists of two points when the ellipsoid X is viewed from the line V.

The contour sets described in the example above are also known as *polar varieties*. To define polar varieties in general, we need to fix some conventions and notations. For instance, the dimension of the empty set is considered to be -1. Given projective subspaces $V, W \subseteq \mathbb{P}^n$, their projective span (equivalently, their join) is denoted by $V + W \subseteq \mathbb{P}^n$. If V and W are disjoint in projective space then we have

$$\dim(V + W) \;=\; \dim(V) + \dim(W) + 1$$

.

Given a projective variety $X \subseteq \mathbb{P}^n$, we write $\mathrm{Reg}(X)$ for its regular locus. The *embedded tangent space* of X at $p \in \mathrm{Reg}(X)$ is

$$\mathbb{T}_p X := \left\{ v \in \mathbb{P}^n \mid \forall f \in I(X) : \sum_{i=0}^{n} \frac{\partial f}{\partial x_i}(p) \cdot v_i = 0 \right\}.$$

We recall that a projective subspace $W \subseteq \mathbb{P}^n$ is said to intersect X *non-transversely* at $p \in \mathrm{Reg}(X)$ if $p \in W$ and $\dim(W + \mathbb{T}_p X) < n$. For instance, if X is a smooth curve in $\mathbb{P}^3$, then every line that intersects it does so non-transversely, while the tangent planes of X are the only planes that meet X non-transversely.

Definition 4.2 Let $X \subseteq \mathbb{P}^n$ be an irreducible projective variety. The *polar variety* of X with respect to a projective subspace $V \subseteq \mathbb{P}^n$ is

$$P(X, V) \;:=\; \overline{\{p \in \mathrm{Reg}(X) \setminus V \;\mid\; V + p \text{ intersects } X \text{ at } p \text{ non-transversely}\}}.$$

For every $i \in \{0, \ldots, \dim X\}$, there is an integer $\mu_i(X)$ that is equal to the degree of $P(X, V)$ for almost all projective subspaces $V \subseteq \mathbb{P}^n$ with $\dim V = \mathrm{codim}\, X - 2 + i$. The nonnegative integer $\mu_i(X)$ is called the *i-th polar degree of X*.

Example 4.3 A surface $X \subseteq \mathbb{P}^3$ has three polar degrees. For $i = 0, 1, 2$, the generic subspace V in Definition 4.2 is empty, a point, or a line, respectively. We saw the latter two cases in Example 4.1. For the case $i = 0$, we observe that $P(X, \emptyset) = X$. So, the 0-th polar degree $\mu_0(X)$ is the degree of the surface X. $\diamond$

Example 4.4 The last observation that $\mu_0(X) = \deg(X)$ is true in general. If $i = 0$, the dimension of the generic subspace V in Definition 4.2 is $\mathrm{codim}\, X - 2$. Hence, we have for every $p \in \mathrm{Reg}(X)$ that

$$\begin{aligned} \dim\left((V + p) + \mathbb{T}_p X\right) = \dim\left(V + \mathbb{T}_p X\right) &= \dim V + \dim X - \dim(V \cap \mathbb{T}_p X) \\ &\leq (\mathrm{codim}\, X - 2) + \dim X + 1 = n - 1, \end{aligned}$$

which means that $V + p$ intersects X at p non-transversely. Therefore, we conclude that $P(X, V) = X$ and $\mu_0(X) = \deg(X)$. $\diamond$

We will now give a second definition of polar varieties in terms of the Gauss map and Schubert varieties. For that fix a projective subspace $V \subseteq \mathbb{P}^n$. We observe that $V + p$ intersects X at $p \in \mathrm{Reg}(X)$ non-transversely (i.e., $n > \dim((V + p) + \mathbb{T}_p X) = \dim V + \dim X - \dim(V \cap \mathbb{T}_p X)$) if and only if

$$\dim(V \cap \mathbb{T}_p X) > \dim V - \mathrm{codim}\, X. \tag{4.1}$$

Since $\dim V - \mathrm{codim}\, X$ is the expected dimension of the intersection of the two projective subspaces V and $\mathbb{T}_p X$, condition (4.1) means that the tangent space $\mathbb{T}_p X$ meets V in an unexpectedly large dimension. Such subspaces are collected in simple instances of *Schubert varieties*:

$$\Sigma_m(V) := \{T \in \mathrm{Gr}(m, \mathbb{P}^n) \mid \dim(V \cap T) > \dim V - n + m\}\,.$$

If $m = \dim X$, then condition (4.1) is equivalent to $\mathbb{T}_p X \in \Sigma_m(V)$. Hence, the *Gauss map*

$$\begin{aligned} \gamma_X : X &\dashrightarrow \mathrm{Gr}(m, \mathbb{P}^n), \\ p &\longmapsto \mathbb{T}_p X \end{aligned}$$

pulls the Schubert variety $\Sigma_m(V)$ back to the polar variety $P(X, V)$, i.e.,

$$P(X, V) = \overline{\gamma_X^{-1}\left(\Sigma_{\dim X}(V)\right)}.$$

4.2 Projective Duality

We recall that there is a one-to-one correspondence between hyperplanes H in the $\mathbb{P}^n$ and points $H^\vee$ in the dual projective space $(\mathbb{P}^n)^*$. The *dual variety* of a projective variety $X \subseteq \mathbb{P}^n$ consists of all tangent hyperplanes of X:

$$X^\vee := \overline{\left\{H^\vee \in (\mathbb{P}^n)^* \mid \exists p \in \mathrm{Reg}(X) : \mathbb{T}_p X \subseteq H\right\}}.$$

Theorem 4.5 (Biduality theorem, [75]) *Let $X \subseteq \mathbb{P}^n$ be a projective variety over an algebraically closed field of characteristic zero. Moreover, let $p \in \mathrm{Reg}(X)$ and $H^\vee \in \mathrm{Reg}(X^\vee)$. The hyperplane H is tangent to X at the point p if and only if the hyperplane $p^\vee$ is tangent to $X^\vee$ at the point $H^\vee$. In particular, $(X^\vee)^\vee = X$.*

Example 4.6 If X is a projective subspace of $\mathbb{P}^n$, then $X^\vee$ is a projective subspace of $(\mathbb{P}^n)^*$ with $\dim X^\vee = n - 1 - \dim X$. In particular, we have that $(\mathbb{P}^n)^\vee = \emptyset$.

Example 4.7 Let us revisit the example in Figure 4.2 that illustrates the polar variety $P(X, V)$ of a surface $X \subseteq \mathbb{P}^3$ and a generic line V. The tangent planes passing through the line V correspond in $(\mathbb{P}^3)^*$ to points on the dual variety $X^\vee$ that are contained in the line $V^\vee$; see Figure 4.3. Hence, if the dual variety is a surface as well, then its degree is given by the second polar degree of X, i.e., $\mu_2(X) = \deg(X^\vee)$. Otherwise, if the dual variety $X^\vee$ is of smaller dimension, the line $V^\vee$ misses it and $\mu_2(X) = 0$.

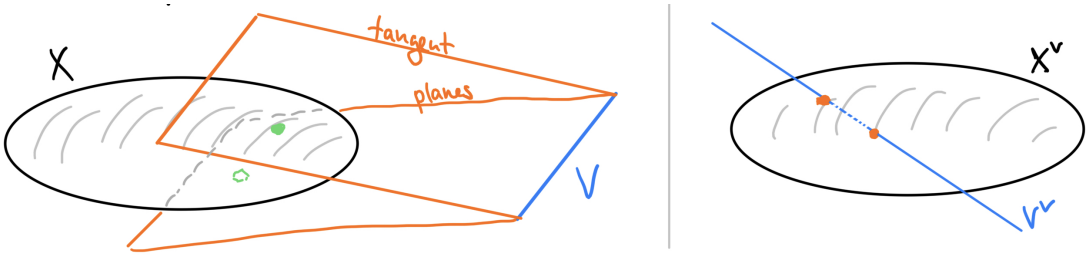

Fig. 4.3: $\mu_2(X) = \deg(X^\vee)$ holds for pairs of dual surfaces in projective 3-space ($q_i = (\mathbb{T}_{p_i} X)^\vee$).

In the setting of Figure 4.1, the polar variety $P(X, V)$ of a surface $X \subseteq \mathbb{P}^3$ and a generic point V is a curve. Thus, its degree ($= \mu_1(X)$) is computed by intersecting it with a generic plane H. The polar curve consists of all points on X whose tangent plane contains the point V, i.e., $P(X, V) = \overline{\left\{p \in \mathrm{Reg}(X) \mid V \in \mathbb{T}_p X\right\}}$. Hence, the first polar degree $\mu_1(X)$ counts all (regular) points $p \in X$ such that

$$p \in H \text{ and } V \in \mathbb{T}_p X. \tag{4.2}$$

The tangent planes at those points correspond to points $q := (\mathbb{T}_p X)^\vee$ in the dual projective space. By the biduality theorem, those points satisfy $\mathbb{T}_q X^\vee = p^\vee$ if the dual variety $X^\vee$ is a surface. Hence, in that case, the two conditions in (4.2) are equivalent to

$$H^\vee \in \mathbb{T}_q X^\vee \text{ and } q \in V^\vee. \tag{4.3}$$

Comparing now (4.3) with (4.2), we see that the point-plane pair $(H^\vee, V^\vee)$ imposes the same conditions on the points $q \in X^\vee$ as the point-plane pair (V, H) imposes on the points $p \in X$; see also Figure 4.4. Due to the genericity of (V, H), we conclude that $\mu_1(X) = \mu_1(X^\vee)$ if $X^\vee$ is a surface. If $X^\vee$ is a curve, then $\mathbb{T}_q X^\vee \subsetneq p^\vee$ and so the only conditions imposed by (4.2) on the points $q \in X^\vee$ is that they must lie in $V^\vee$, i.e., $\mu_1(X) = |X^\vee \cap V^\vee| = \deg(X^\vee) = \mu_0(X^\vee)$. Finally, if $X^\vee$ is a point (i.e., X is a plane), then $\mu_1(X) = 0$. ◊

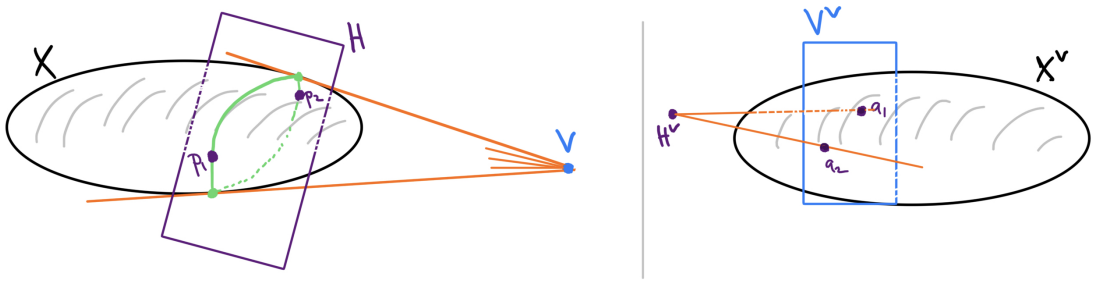

Fig. 4.4: $\mu_1(X) = \mu_1(X^\vee)$ holds for pairs of dual surfaces in projective 3-space.

The relations between the polar degrees of a variety and its dual that we observed in the previous example are true in more generality. More specifically, the list of polar degrees of a projective variety X is exactly the list of polar degrees of its dual variety $X^\vee$ in reversed order. As seen in Example 4.4, the first non-zero entry in that list is $\deg(X)$, and so its last non-zero entry is $\deg(X^\vee)$. We summarize these key properties of polar degrees:

Proposition 4.8 ([93]) *Let X be an irreducible projective variety, and let $\alpha(X) := \dim X - \operatorname{codim} X^\vee + 1$.*

(a) $\mu_i(X) > 0 \quad \Leftrightarrow \quad 0 \le i \le \alpha(X)$.
(b) $\mu_0(X) = \deg X$.
(c) $\mu_{\alpha(X)}(X) = \deg X^\vee$.
(d) $\mu_i(X) = \mu_{\alpha(X)-i}(X^\vee)$.

The ideas discussed in Example 4.7 can be turned into formal proofs for almost all assertions in Proposition 4.8 (only the direction "⇐" in (a) is rather tricky). Another strategy is to first establish the relation of the polar degrees with the *conormal variety* of the projective variety $X \subseteq \mathbb{P}^n$:

$$\mathcal{N}_X := \overline{\left\{(p, H^\vee) \in \mathbb{P}^n \times (\mathbb{P}^n)^* \;\middle|\; p \in \operatorname{Reg}(X), \mathbb{T}_p X \subseteq H\right\}}.$$

The projection of the conormal variety $\mathcal{N}_X$ onto the first resp. second factor is the variety X resp. its dual $X^\vee$. Moreover, by the biduality theorem, we have that

$$\mathcal{N}_{X^\vee} = \left\{(H^\vee, p) \;\mid\; (p, H^\vee) \in \mathcal{N}_X\right\}. \tag{4.4}$$

Independently of the dimension of X, the dimension of the conormal variety is always $n-1$. Hence, the *multidegree* of the conornomal variety is given by its intersections with $L_1 \times L_2$, where $L_1 \subseteq \mathbb{P}^n$ and $L_2 \subseteq (\mathbb{P}^n)^*$ are generic subspaces with $\dim L_1 + \dim L_2 = \operatorname{codim} \mathcal{N}_X = n+1$. We denote the entries of that multidegree by

$$\delta_j(X) := |\mathcal{N}_X \cap (L_1 \times L_2)|, \text{ for generic } L_1, L_2 \text{ with } \dim L_2 = j,\ \dim L_1 = n+1-j.$$

We saw in Section 2.3 that the multidegree is the cohomology class of the conormal variety N_X.

Proposition 4.9 ([109, Prop. (3) on page 187] or [73, Lem. (2.23) on page 169]) *The multidegree agrees with the polar degrees. More precisely, we have $\delta_j(X) = \mu_i(X)$, where $i := \dim X + 1 - j$.*

This proposition together with (4.4) implies immediately Proposition 4.8(d) and hence using Example 4.4 also (b) and (c). The direction "⇒" in Proposition 4.8(a) can also be deduced directly from the definition of the $\delta_j(X)$.

Before we present an idea of proof for Proposition 4.9, we revisit our running example.

Example 4.10 We see from Figure 4.4 and the conditions (4.2) and (4.3) that the first polar degree of a surface X in $\mathbb{P}^3$ is computed as $\mu_1(X) = |\mathcal{N}_X \cap (H \times V^\vee)| = \delta_2(X)$. In other words, Proposition 4.8 holds for surfaces X in $\mathbb{P}^3$.

Proof (Sketch for Proposition 4.9) Let $L_1 \subseteq \mathbb{P}^n$ and $L_2 \subseteq (\mathbb{P}^n)^*$ be generic subspace of dimensions $n+1-j$ and j, respectively. Setting $V := L_2^\vee$, we start by observing that V has the correct dimension to be used in the computation of the i-th polar degree (where $i = \dim X + 1 - j$), since $\dim V = n - j - 1 = \operatorname{codim} X - 2 + i$.

Now we consider a generic pair $(p, H^\vee) \in \mathcal{N}_X \cap (\mathbb{P}^n \times L_2)$. The point $p \in X$ is regular and both its tangent space $\mathbb{T}_p X$ and $V = L_2^\vee$ are contained in the hyperplane H. In particular, we have $\dim(V + \mathbb{T}_p X) < n$ and so p is in the polar variety $P(X, V)$. In fact, the projection $\mathcal{N}_X \cap (\mathbb{P}^n \times L_2) \to P(X, V)$ onto the first factor is birational. Hence, $\mu_i(X) = \deg P(X, V) = |P(X, V) \cap L_1| = |\mathcal{N}_X \cap (L_1 \times L_2)| = \delta_j(X)$. □

4.3 Chern Classes

Chern classes are topological invariants associated with vector bundles on smooth manifolds or varieties. For a smooth, irreducible projective variety X, its polar degrees can be computed from its Chern classes (see Proposition 4.11).

To a vector bundle $\mathcal{E}$ on X of rank r, we associate the Chern classes $c_0(\mathcal{E}), \ldots, c_r(\mathcal{E})$, which are formally elements in the *Chow ring* of X. Chern classes are easiest understood when the vector bundle $\mathcal{E}$ is globally generated. In that case, the Chern class $c_{r+1-j}(\mathcal{E})$ is the element in the Chow ring of X that is associated with the following degeneracy locus:

$$D(\sigma_1, \ldots, \sigma_j) := \left\{x \in X \mid \sigma_1(x), \ldots, \sigma_j(x) \text{ are linearly dependent}\right\},$$

where $\sigma_1, \ldots, \sigma_j : X \to \mathcal{E}$ are j general global sections. For the purpose of this section, it is not crucial to understand the Chow ring. It suffices for us to understand the *degree* of $c_{r+1-j}(\mathcal{E})$. This is defined to be the degree of the degeneracy locus $D(\sigma_1, \ldots, \sigma_j)$ for general σ_i. For instance, the degree of the *top Chern class* $c_r(\mathcal{E})$ is the degree of the vanishing locus of a single general global section.

There are some calculation rules that allow us to compute Chern classes of more complex vector bundles. Most notably, the *Whitney sum formula* states for a short exact sequence $0 \to \mathcal{E}' \to \mathcal{E} \to \mathcal{E}'' \to 0$ of

vector bundles that $c_k(\mathcal{E}) = \sum_{i+j=k} c_i(\mathcal{E}')c_j(\mathcal{E}'')$; see [72, Theorem 3.2]. The Chern class $c_k(X)$ of X is an abbreviation for the Chern class $c_k(\mathcal{T}X)$ of its tangent bundle $\mathcal{T}X$.

Proposition 4.11 ([93, eq. (3)]) *Let X be a smooth, irreducible projective variety, and let $m := \dim X$. Then,*

$$\mu_i(X) = \sum_{k=0}^{i} (-1)^k \binom{m-k+1}{m-i+1} \deg(c_k(X)).$$

This formula can also be reverted to express degrees of Chern classes in terms of polar degrees:

$$\deg(c_k(X)) = \sum_{i=0}^{k} (-1)^i \binom{m-i+1}{m-k+1} \mu_i(X). \tag{4.5}$$

Remark 4.12 Both formulas also hold for singular varieties, after replacing the classical Chern classes with Chern-Mather classes. That result is due to R. Piene (see [147, Theorem 3] or [146]).

An important difference between polar degrees and Chern classes is the following: Polar degrees are projective invariants of the embedded variety $X \subseteq \mathbb{P}^n$. This holds also more generally for the *polar classes*, i.e., the rational equivalence classes (in the Chow ring of X) of the polar varieties. Chern classes are even *intrinsic invariants* of the variety X, i.e., they do not depend on the embedding of X in projective space.

Example 4.13 Let X be a smooth, irreducible projective variety.

a) We see from (4.5) that $\deg(c_0(X)) = \mu_0(X) = \deg X$.
b) The top Chern class of X coincides with its topological Euler characteristic: $\deg(c_m(X)) = \chi(X)$, where $m = \dim X$.
c) If X is a curve, then $\chi(X) = 2 - 2g(X)$, where $g(X)$ denotes the genus. Moreover, we see from (4.5) that $\deg(c_1(X)) = 2\deg X - \mu_1(X)$. Hence, we conclude:

$$2\deg X - \mu_1(X) = 2 - 2g(X). \tag{4.6}$$

d) If $X \subseteq \mathbb{P}^n$ is a rational curve, we can easily verify the relation (4.6):

- If X is a line, its dual variety is never a hypersurface, and so $\mu_1(X) = 0$.
- If X is a conic (i.e., $\deg X = 2$), its dual variety is (a cone over) a conic, and so $\mu_1(X) = \deg X^\vee = 2$.
- If X is a twisted cubic (i.e., $\deg X = 3$), its dual variety is (a cone over) the discriminant hypersurface of a cubic polynomial, and so $\mu_1(X) = \deg X^\vee$ is the degree of that discriminant, which is 4.
- More generally, if X is a rational normal curve of degree d, its dual variety is (a cone over) the discriminant hypersurface of a degree-d polynomial, and so $\mu_1(X) = \deg X^\vee$ is the degree of that discriminant, which is $2d - 2$.

Chapter 5
Wasserstein Distance

A fundamental problem in metric algebraic geometry is distance minimization. We seek a point in a variety X in $\mathbb{R}^n$ that is closest to a given data point $\mathbf{u} \in \mathbb{R}^n$. Thus, we must solve the optimization problem

$$\text{minimize } ||\mathbf{x} - \mathbf{u}|| \text{ subject to } \mathbf{x} \in X. \tag{5.1}$$

In what follows, this minimum in (5.1) is always attained because X is non-empty and closed. Hence there exists at least one optimal solution. If that solution is unique then we denote it by $\mathbf{x}^*$.

In the previous chapter we discussed this problem for the Euclidean norm on $\mathbb{R}^n$. In what follows we study (5.1) in the case when the distance is given by a *polyhedral norm*. We will then focus on a particular class of polyhedral norms that arise from optimal transport theory. These are known as Wasserstein norms.

5.1 Polyhedral Norms

A norm $|| \cdot ||$ on the real vector space $\mathbb{R}^n$ is a *polyhedral norm* if its unit ball is polyhedral:

$$B = \{\mathbf{x} \in \mathbb{R}^n : ||\mathbf{x}|| \leq 1\}.$$

More precisely, B is a centrally symmetric convex polytope. Conversely, every centrally symmetric convex polytope B in $\mathbb{R}^n$ defines a polyhedral norm on $\mathbb{R}^n$. Using the unit ball, we can paraphrase (5.1) as follows:

$$\text{minimize } \lambda \text{ subject to } \lambda \geq 0 \text{ and } (\mathbf{u} + \lambda B) \cap X \neq \emptyset. \tag{5.2}$$

Familiar examples of polyhedral norms are $||\cdot||_\infty$ and $||\cdot||_1$. For these norms, the unit ball B is, respectively, the cube and the crosspolytope (a.k.a. generalized octahedron). Polyhedral norms are very important in optimal transport theory, where one uses a Wasserstein norm on the space of probability distributions. This will be our main application in this chapter, and it will be discussed in detail in the later sections.

We begin our discussion with a general polyhedral norm, that is, we allow B to be an arbitrary n-dimensional centrally symmetric polytope in $\mathbb{R}^n$. The boundary of B consists of faces whose dimensions range from 0 to $n-1$. We use the dot $\cdot$ for the standard inner product on $\mathbb{R}^n$. Recall that a subset F of the polytope B is a *face* if there exists a linear functional $\ell \in \mathbb{R}^n \backslash \{0\}$ such that

$$F = \{\mathbf{x} \in B : \ell \cdot \mathbf{x} \geq \ell \cdot \mathbf{y} \text{ for all } \mathbf{y} \in B\}. \tag{5.3}$$

The set of all faces, ordered by inclusion, is a partial ordered set, called the *face poset* of B. An important combinatorial invariant of our polytope B is its *f-vector* $f(B) = (f_0, f_1, \ldots, f_{n-1})$. By definition, the ith coordinate f_i of the f-vector is the number of i-dimensional faces of B.

The dual of the unit ball B is also a centrally symmetric polytope, namely it is the set

$$B^* = \{\ell \in \mathbb{R}^n : \ell \cdot \mathbf{x} \leq 1 \text{ for all } \mathbf{x} \in B\}.$$

The norm $|| \cdot ||_*$ defined by the dual polytope B^* is dual to the norm $|| \cdot ||$ given by B. The f-vector of B^* is the reverse of the f-vector of B. More precisely, we have $f_i(B^*) = f_{n-1-i}(B)$ for $i = 0, 1, \ldots, n-1$.

Example 5.1 Fix the unit cube $B = [-1, 1]^n$. Its dual is the crosspolytope

$$B^* = \text{conv}\{\pm\mathbf{e}_1, \pm\mathbf{e}_2, \ldots, \pm\mathbf{e}_n\} \subset \mathbb{R}^n.$$

Here $\mathbf{e}_j$ is the jth standard basis vector. The number of i-dimensional faces of the cube is

$$f_i(B) \;=\; \binom{n}{i} \cdot 2^{n-i}.$$

The 3-dimensional crosspolytope is the octahedron. The 3-cube and the octahedron satisfy

$$f(B) = (8, 12, 6) \quad \text{and} \quad f(B^*) = (6, 12, 8).$$

These numbers govern the combinatorial structure of the norms $||\cdot||_\infty$ and $||\cdot||_1$ on $\mathbb{R}^3$.

We now turn to the critical equations for the optimization problem given in (5.1) or (5.2). To derive these equations, a combinatorial stratification of the problem will be used. This is given by the face poset of the polytope B. Suppose that the variety X is in sufficiently general position in $\mathbb{R}^n$. This hypothesis implies that $(\mathbf{u} + \lambda^* B) \cap X = \{\mathbf{x}^*\}$ is a singleton for the optimal value λ^* in (5.2). The point $\frac{1}{\lambda^*}(\mathbf{x}^* - \mathbf{u})$ lies in boundary of the unit ball B. Hence it lies in the relative interior of a unique face F of the polytope B. Let L_F denote the linear span of F in $\mathbb{R}^n$. We have $\dim(L_F) = \dim(F) + 1$. Let ℓ be any linear functional on $\mathbb{R}^n$ that attains its maximum over the polytope B at the face F. This means that (5.3) holds.

Lemma 5.2 *The optimal point $\mathbf{x}^*$ in (5.1) is the unique solution to the optimization problem*

$$\textit{Minimize} \quad \ell(\mathbf{x}) \quad \textit{subject to } \mathbf{x} \in (\mathbf{u} + L_F) \cap X. \tag{5.4}$$

Proof The general position hypothesis ensures that the affine space $\mathbf{u} + L_F$ intersects the real variety X transversally, and $\mathbf{x}^*$ is a smooth point of that intersection. Moreover, $\mathbf{x}^*$ is a minimum of the restriction of ℓ to the variety $(\mathbf{u} + L_F) \cap X$. By our hypothesis, this linear function is generic relative to the variety, so the number of critical points is finite and the function values are distinct. □

Example 5.3 (Touching at a facet) Suppose that the face F is a facet of the unit ball B. Then $L_F = \mathbb{R}^n$, and ℓ is an outer normal vector to that facet, which is unique up to scaling. Here, the optimization problem (5.4) asks for the minimum of ℓ over X. This situation corresponds to the left diagram in Figure 5.1.

Example 5.4 (Touching at a vertex) Suppose F is a vertex of the unit ball B. This case arises when X is a hypersurface. It corresponds to the middle diagram in Figure 5.1. Here, the affine space $\mathbf{u} + L_F$ is the line that connects $\mathbf{u}$ and $\mathbf{x}^*$. That line intersects X in a finite set of cardinality degree(X). The optimal $\mathbf{x}^*$ is the real point in that finite set at which the value of the linear form ℓ is minimal.

Problem (5.4) amounts to linear programming over a real variety. We now determine the algebraic degree of this optimization task when F is a face of codimension i. To this end, we replace the affine variety $X \subset \mathbb{R}^n$ by its closure in complex projective space $\mathbb{P}^n$. We retain the same symbol X for that projective variety. Consider the affine space $L = u + L_F$ in $\mathbb{R}^n$, and also identify it with its closure in $\mathbb{P}^n$. If the face F has codimension i then the linear space L has codimension $i - 1$. The following result assumes that this space is in general position relative to the variety X and relative to the isotropic quadric.

Theorem 5.5 *Let L be a general affine-linear space of codimension $i - 1$ in $\mathbb{R}^n$ and let ℓ be a general linear form. The number of critical points of ℓ on $L \cap X$ is the polar degree $\delta_i(X)$.*

Proof This result appears in [42, Theorem 5.1]. The number of critical points of a linear form is the degree of the dual variety $(L \cap X)^\vee$. That degree coincides with the polar degree $\delta_i(X)$. □

Example 5.6 Examples 5.3 and 5.4 explain Theorem 5.5 in the two extreme cases $i = 1$ and $i = n$. Touching at a vertex ($i = n$) can only happen when X is a hypersurface, and here $\delta_n(X) = \text{degree}(X)$. Touching at a facet ($i = 1$) can happen for varieties of any dimension, as long as the dual variety $X^\vee$ is a hypersurface. In that case we have $\delta_1(X) = \text{degree}(X^\vee)$.

Theorem 5.5 offers a direct interpretation of each polar degree $\delta_i(X)$ in terms of optimization on X. This interpretation can be used as a definition of polar degrees. Some readers might prefer this.

Example 5.7 Consider the distance minimization problem in (5.1) and (5.2) where X is a general surface of degree d in $\mathbb{R}^3$. The optimal face F of the unit ball B depends on the location of the data point $\mathbf{u}$. The algebraic degree of the solution $\mathbf{x}^*$ equals $\delta_3(X) = d$ if $\dim(F) = 0$, it is $\delta_2(X) = d(d-1)$ if $\dim(F) = 1$, and it is $\delta_1(X) = d(d-1)^2$ if $\dim(F) = 2$. Here $\mathbf{x}^*$ is the unique point in $(\mathbf{u} + \lambda^* B) \cap X$, where λ^* is the optimal value in (5.2). Figure 5.1 visualizes this scenario for $d = 2$ and $||\cdot||_\infty$. The variety X is the green sphere, which is a surface of degree $d = 2$. The unit ball for the norm $||\cdot||_\infty$ is the cube $B = [-1, 1]^3$. The picture shows the smallest λ^* such that $\mathbf{u} + \lambda^* B$ touches the sphere X. The cross marks the point of contact. This is the point $\mathbf{x}^*$ in X which is closest in ∞-norm to the green point $\mathbf{u}$ in the center of the cube. Point of contact is either on a facet, or on an edge, or it is a vertex. The algebraic degree of $\mathbf{x}^*$ is two in all three cases, i.e. we can write the solution $\mathbf{x}^*$ in terms of the data $\mathbf{u}$ by solving the quadratic formula. If the green surface in Figure 5.1 were a cubic surface then these polar degrees would be 3, 6 and 12.

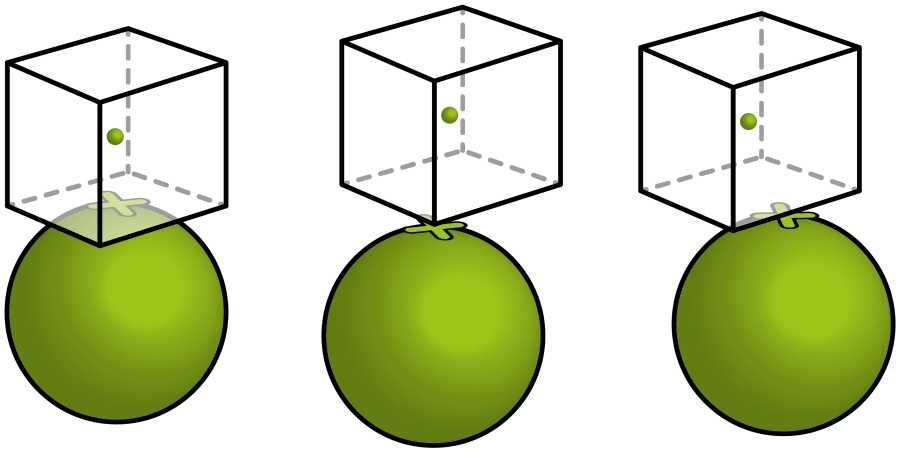

Fig. 5.1: The cube is an $||\cdot||_\infty$ ball around the green point u. The variety X is the sphere. The contact point x^* is marked with a cross. The optimal face F is a facet, vertex, or edge.

We have learned that the conormal variety N_X and its cohomology class $[N_X]$ are key players when it comes to reliably solving the distance minimization problem for a variety X. This applies not just to the Euclidean distance problem, but also to the analogous problem for polyhedral norms. The polar degrees $\delta_i(X)$ reveal precisely how many paths need to be tracked by numerical solvers like [13, 31] in order to find and certify [30] the optimal solution $\mathbf{x}^*$ in (5.1) or (5.4).

5.2 Optimal Transport and Independence Models

We now come to the main theme of this chapter, namely the Wasserstein distance to a given variety X. For us, X will be an independence model in a probability simplex, described algebraically by matrices or tensors of low rank, and we measure distances using Wasserstein metrics on that simplex. This is a class of polyhedral norms which are important in optimal transport theory. We now present the relevant definitions.

A probability distribution on the finite set $[n] = \{1, 2, \ldots, n\}$ is a point v in the simplex $\Delta_{n-1} = \{(v_1, \ldots, v_n) \in \mathbb{R}^n_{\geq 0} : \sum_{i=1}^n v_i = 1\}$. We metrize this simplex by the *Wasserstein distance*. To define this

notion, we first turn the state space $[n]$ into a finite metric space by fixing a symmetric $n \times n$ matrix $d = (d_{ij})$ with nonnegative entries. These entries satisfy $d_{ii} = 0$ and $d_{ik} \leq d_{ij} + d_{jk}$ for all i, j, k. Given two probability distributions μ and ν in Δ_{n-1}, we consider the following linear programming problem, where $\mathbf{z} = (z_1, \ldots, z_n)$ denotes the decision variables:

$$\text{Maximize} \ \sum_{i=1}^{n} (\mu_i - \nu_i)\, z_i \ \ \text{subject to} \ \ |z_i - z_j| \ \leq \ d_{ij} \ \ \text{for all} \ \ 1 \leq i < j \leq n. \tag{5.5}$$

The optimal value of (5.5), denoted $W_d(\mu, \nu)$, is the *Wasserstein distance* between μ and ν.

The optimal solution $\mathbf{z}^*$ to problem (5.5) is known as the *optimal discriminator* for the two probability distributions μ and ν. It satisfies $W_d(\mu, \nu) = \langle \mu - \nu, \mathbf{z}^* \rangle$, and its coordinates z_i^* are weights on the state space $[n]$ that tell μ and ν apart. Here $\langle \cdot\,, \cdot \rangle$ is the standard inner product on $\mathbb{R}^n$. The linear program (5.5) is the *Kantorovich dual* of the *optimal transport problem*.

The feasible region of the linear program (5.5) is unbounded because it is invariant under translation by $\mathbf{1} = (1, 1, \ldots, 1)$. It is compact after taking the quotient modulo the line $\mathbb{R}\mathbf{1}$:

$$P_d \ = \ \big\{ \mathbf{z} \in \mathbb{R}^n / \mathbb{R}\mathbf{1} \ : \ |z_i - z_j| \ \leq \ d_{ij} \ \ \text{for all} \ \ 1 \leq i < j \leq n \big\}. \tag{5.6}$$

This $(n-1)$-dimensional polytope is the *Lipschitz polytope* of the metric space $([n], d)$. In the field of tropical geometry, one calls P_d a *polytrope* because it is convex both classically and tropically.

The polytope P_d^* that is dual to P_d lies in the hyperplane perpendicular to the line $\mathbb{R}\mathbf{1}$. We call P_d^* the *root polytope* because its vertices are, up to scaling, the elements $\mathbf{e}_i - \mathbf{e}_j$ in the root system of Lie type A_{n-1}. More precisely, we have

$$P_d^* \ = \ \big\{ x \in \mathbb{R}^n \ : \ \max_{z \in P_d} \langle x, z \rangle \leq 1 \big\} \ = \ \text{conv} \big\{ \frac{1}{d_{ij}} (\mathbf{e}_i - \mathbf{e}_j) \ : \ \ 1 \leq i, j \leq n \big\}.$$

This is a centrally symmetric polytope since the finite metric space $([n], d)$ satisfies $d_{ij} = d_{ji}$.

Proposition 5.8 *The Wasserstein metric W_d on the probability simplex Δ_{n-1} is given by the polyhedral norm whose unit ball is the root polytope P_d^*.*

Proof Fix the polyhedral norm with unit ball P_d^*. The distance between μ and ν in this norm is the smallest real number λ such that $\mu \in \nu + \lambda P_d^*$, or, equivalently, $\frac{1}{\lambda}(\mu - \nu) \in P_d^*$. By definition of dual polytope, this minimal λ is the maximum inner product $\langle \mu - \nu, z \rangle$ over all points z in the dual $(P_d^*)^*$ of the unit ball. But this specifies the Lipschitz polytope, i.e. $(P_d^*)^* = P_d$. Hence the distance between μ and ν is equal to $W_d(\mu, \nu)$, which is the optimal value in (5.5). □

Example 5.9 Let $n = 4$ and fix the finite metric space graph distance on the 4-cycle

$$d \ = \ \begin{pmatrix} 0 & 1 & 1 & 2 \\ 1 & 0 & 2 & 1 \\ 1 & 2 & 0 & 1 \\ 2 & 1 & 1 & 0 \end{pmatrix}. \tag{5.7}$$

The induced metric on the tetrahedron Δ_3 is given by the Lipschitz polytope

$$\begin{aligned} P_d = \ & \big\{ (x_1, x_2, x_3, x_4) \in \mathbb{R}^4 / \mathbb{R}\mathbf{1} \ : \ |x_1 - x_2| \leq 1, |x_1 - x_3| \leq 1, |x_2 - x_4| \leq 1, |x_3 - x_4| \leq 1 \big\} \\ = \ & \text{conv} \big\{ (1,0,0,-1), (-1,0,0,1), (\tfrac{1}{2}, -\tfrac{1}{2}, -\tfrac{1}{2}, \tfrac{1}{2}), (-\tfrac{1}{2}, \tfrac{1}{2}, \tfrac{1}{2}, -\tfrac{1}{2}), (0,1,-1,0), (0,-1,1,0) \big\}. \end{aligned}$$

Note that this 3-dimensional polytope is an octahedron. Therefore, its dual is a cube:

$$\begin{aligned} P_d^* &= \{(y_1,y_2,y_3,y_4) \in (\mathbb{R}\mathbf{1})^\perp : |y_1-y_4| \le 1,\ |y_2-y_3| \le 1,\ |y_2+y_3| \le 1\} \\ &= \operatorname{conv}\{(1,-1,0,0),(1,0,-1,0),(0,1,0,-1),(0,0,1,-1) \\ &\qquad (-1,1,0,0),(-1,0,1,0),(0,-1,0,1),(0,0,-1,1)\}. \end{aligned}$$

This is the unit ball for the Wasserstein metric on the tetrahedron Δ_3 that is induced by d. Measuring the distance from a point to a surface with respect to this metric is illustrated in Figure 5.1.

We wish to compute the Wasserstein distance from a given distribution μ to a fixed *discrete statistical model* $\mathcal{M} \subset \Delta_{n-1}$. This is the problem studied in [41,42]. Our discussion serves as an introduction. As is customary in algebraic statistics, we assume that $\mathcal{M}$ is defined by polynomials in $\nu_1,\ldots,\nu_n$.

Our task is to solve the following optimization problem:

$$W_d(\mu,\mathcal{M}) \quad := \quad \min_{\nu\in\mathcal{M}} W_d(\mu,\nu) \quad = \quad \min_{\nu\in\mathcal{M}} \max_{x\in P_d} \langle \mu-\nu, x\rangle. \tag{5.8}$$

Computing this quantity means solving a non-convex optimization problem. Our aim is to study this problem and propose solution strategies, using methods from geometry, algebra and combinatorics. The analogous problem for the Euclidean metric was treated earlier.

We now present a detailed case study for the tetrahedron Δ_3 whose points are joint probability distributions of two binary random variables. The 2-*bit independence model* $\mathcal{M} \subset \Delta_3$ consists of all nonnegative 2×2 matrices of rank one whose entries sum to one:

$$\begin{pmatrix} \nu_1 & \nu_2 \\ \nu_3 & \nu_4 \end{pmatrix} = \begin{pmatrix} pq & p(1-q) \\ (1-p)q & (1-p)(1-q) \end{pmatrix}, \qquad (p,q) \in [0,1]^2. \tag{5.9}$$

Thus, $\mathcal{M}$ is the quadratic surface in the tetrahedron Δ_3 defined by the equation $\nu_1\nu_4 = \nu_2\nu_3$. The next theorem gives the optimal value function and the solution function for this independence model. We use the Wasserstein metric W_d that was defined in Example 5.9.

Theorem 5.10 *The Wasserstein distance from a distribution $\mu \in \Delta_3$ to the surface $\mathcal{M}$ equals*

$$W_d(\mu,\mathcal{M}) = \begin{cases} 2\sqrt{\mu_1}(1-\sqrt{\mu_1})-\mu_2-\mu_3 & \text{if } \mu_1 \ge \mu_4,\ \sqrt{\mu_1} \ge \mu_1+\mu_2,\ \sqrt{\mu_1} \ge \mu_1+\mu_3, \\ 2\sqrt{\mu_2}(1-\sqrt{\mu_2})-\mu_1-\mu_4 & \text{if } \mu_2 \ge \mu_3,\ \sqrt{\mu_2} \ge \mu_1+\mu_2,\ \sqrt{\mu_2} \ge \mu_2+\mu_4, \\ 2\sqrt{\mu_3}(1-\sqrt{\mu_3})-\mu_1-\mu_4 & \text{if } \mu_3 \ge \mu_2,\ \sqrt{\mu_3} \ge \mu_1+\mu_3,\ \sqrt{\mu_3} \ge \mu_3+\mu_4, \\ 2\sqrt{\mu_4}(1-\sqrt{\mu_4})-\mu_2-\mu_3 & \text{if } \mu_4 \ge \mu_1,\ \sqrt{\mu_4} \ge \mu_2+\mu_4,\ \sqrt{\mu_4} \ge \mu_3+\mu_4, \\ |\mu_1\mu_4-\mu_2\mu_3|/(\mu_1+\mu_2) & \text{if } \mu_1 \ge \mu_4,\ \mu_2 \ge \mu_3,\ \mu_1+\mu_2 \ge \sqrt{\mu_1},\ \mu_1+\mu_2 \ge \sqrt{\mu_2}, \\ |\mu_1\mu_4-\mu_2\mu_3|/(\mu_1+\mu_3) & \text{if } \mu_1 \ge \mu_4,\ \mu_3 \ge \mu_2,\ \mu_1+\mu_3 \ge \sqrt{\mu_1},\ \mu_1+\mu_3 \ge \sqrt{\mu_3}, \\ |\mu_1\mu_4-\mu_2\mu_3|/(\mu_2+\mu_4) & \text{if } \mu_4 \ge \mu_1,\ \mu_2 \ge \mu_3,\ \mu_2+\mu_4 \ge \sqrt{\mu_4},\ \mu_2+\mu_4 \ge \sqrt{\mu_2}, \\ |\mu_1\mu_4-\mu_2\mu_3|/(\mu_3+\mu_4) & \text{if } \mu_4 \ge \mu_1,\ \mu_3 \ge \mu_2,\ \mu_3+\mu_4 \ge \sqrt{\mu_4},\ \mu_3+\mu_4 \ge \sqrt{\mu_3}. \end{cases}$$

The solution function $\Delta_3 \to \mathcal{M},\ \mu \mapsto \nu^*(\mu)$ is given (with the same case distinction) by

$$\nu^*(\mu) = \begin{cases} (\mu_1,\ \sqrt{\mu_1}-\mu_1,\ \sqrt{\mu_1}-\mu_1,\ -2\sqrt{\mu_1}+\mu_1+1), \\ (\sqrt{\mu_2}-\mu_2,\ \mu_2,\ -2\sqrt{\mu_2}+\mu_2+1,\ \sqrt{\mu_2}-\mu_2), \\ (\sqrt{\mu_3}-\mu_3,\ -2\sqrt{\mu_3}+\mu_3+1,\ \mu_3,\ \sqrt{\mu_3}-\mu_3), \\ (-2\sqrt{\mu_4}+\mu_4+1,\ \sqrt{\mu_4}-\mu_4,\ \sqrt{\mu_4}-\mu_4,\ \mu_4), \\ (\mu_1,\ \mu_2,\ \mu_1(\mu_3+\mu_4)/(\mu_1+\mu_2),\ \mu_2(\mu_3+\mu_4)/(\mu_1+\mu_2)), \\ (\mu_1,\ \mu_1(\mu_2+\mu_4)/(\mu_1+\mu_3),\ \mu_3,\ \mu_3(\mu_2+\mu_4)/(\mu_1+\mu_3)), \\ (\mu_2(\mu_1+\mu_3)/(\mu_2+\mu_4),\ \mu_2,\ \mu_4(\mu_1+\mu_3)/(\mu_2+\mu_4),\ \mu_4), \\ (\mu_3(\mu_1+\mu_2)/(\mu_3+\mu_4),\ \mu_4(\mu_1+\mu_2)/(\mu_3+\mu_4),\ \mu_3,\ \mu_4). \end{cases}$$

The boundaries separating the various cases are given by the surfaces $\{\mu \in \Delta_3 : \mu_1 - \mu_4 = 0, \mu_1 + \mu_2 \geq \sqrt{\mu_1}, \mu_1 + \mu_3 \geq \sqrt{\mu_1}\}$ *and* $\{\mu \in \Delta_3 : \mu_2 - \mu_3 = 0, \mu_1 + \mu_2 \geq \sqrt{\mu_2}, \mu_2 + \mu_4 \geq \sqrt{\mu_2}\}$.

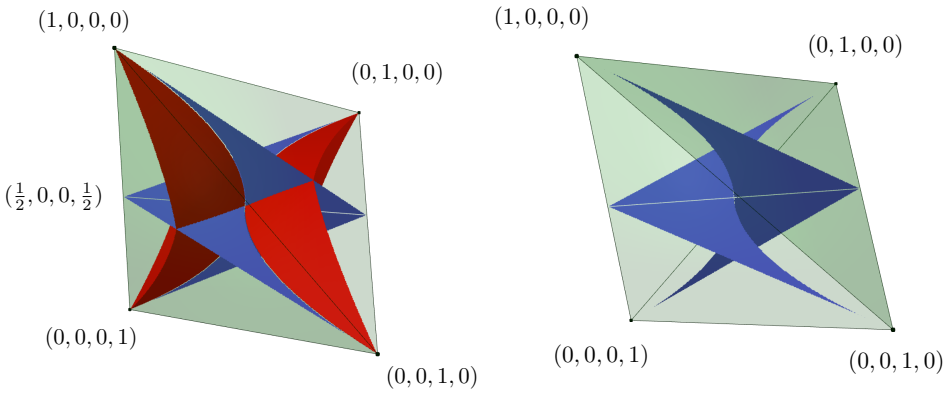

Fig. 5.2: The optimal value function of Theorem 5.10 subdivides the tetrahedron of probability distributions μ (left). The surfaces that separate the various cases are shown in blue (right).

Theorem 5.10 involves a distinction into eight cases. This division of Δ_3 is shown in Figure 5.2. Each of the last four cases breaks into two subcases, since the numerator in the formulas is the absolute value of $\mu_1\mu_4 - \mu_2\mu_3$. The sign of this 2×2 determinant matters for the pieces of our piecewise algebraic function. Thus, the tetrahedron Δ_3 is divided into 12 regions on which $\mu \mapsto W_d(\mu, \mathcal{M})$ is algebraic. We now explain how to visualize Figure 5.2. The red surface consists of eight pieces that, together with the blue surface, separate the eight cases (this surface is not the model). Four convex regions are enclosed between the red surfaces and the edges they meet. These regions represent the first four cases in Theorem 5.10. For instance, the region containing the points $(1, 0, 0, 0), (1/2, 0, 0, 1/2)$ corresponds to the first case. The remaining four regions are each bounded by two red and two blue pieces, and correspond to the last four cases. Each of these four regions is further split in two by the model. We do not depict this in our visualization. The two sides are determined by the sign of the determinant $\mu_1\mu_4 - \mu_2\mu_3$. The two blue surfaces in the right figure separate the various cases. These specify the points $\mu \in \Delta_3$ with more than one optimal solution. For the proof of Theorem 5.10 and a simpler example see [42]. For further details we refer to [41].

5.3 Wasserstein meets Segre-Veronese

Returning to the general case, let $\mathcal{M}$ be a smooth variety in $\Delta_{n-1} \subset \mathbb{R}^n$. For any $v \in \Delta_{n-1}$, we seek its distance to $\mathcal{M}$ under our polyhedral norm. As before, the optimal point v^* determines a unique face F of the unit ball $B = P_d^*$. Given that face F, we now characterize optimality as in Lemma 5.2. Let $\mathcal{F}$ be the set of all index pairs (i, j) such that the point $\frac{1}{d_{ij}}(\mathbf{e}_i - \mathbf{e}_j)$ is a vertex and it lies in F. Let ℓ_F be any linear functional on $\mathbb{R}^n$ that attains its maximum over B at F. We work in the linear space spanned by the face:

$$L_F \;=\; \Big\{ \sum_{(i,j)\in\mathcal{F}} \lambda_{ij}(\mathbf{e}_i - \mathbf{e}_j) \;:\; \lambda_{ij} \in \mathbb{R} \Big\}. \tag{5.10}$$

The point v^* on $\mathcal{M}$ that is closest to μ is the solution of the following optimization problem:

$$\text{Minimize } \ell_F = \ell_F(v) \text{ subject to } v \in (\mu + L_F) \cap \mathcal{M}. \tag{5.11}$$

This is an optimization problem in the linear subspace L_F. With the notation in (5.10), the decision variables are λ_{ij} for $(i,j) \in \mathcal{F}$. The algebraic complexity of this problem is given by the polar degree (Theorem 5.5). The combinatorial complexity is governed by the facial structure of the Wasserstein ball $B = P_d^*$ associated to a finite metric space $([n], d)$. We now focus on the polar dual, the $(n-1)$-dimensional Lipschitz polytope $B^* = P_d$. This polytope lives in $\mathbb{R}^n/\mathbb{R}\mathbf{1} \simeq \mathbb{R}^{n-1}$, and is defined in (5.6).

In the study of independence models $\mathcal{M} \subset \Delta_{n-1}$, the following metrics $([n], d)$ arise:

- The discrete metric on any finite set $[n]$ where $d_{ij} = 1$ for distinct i, j.
- The L_0-metric on the Cartesian product $[m_1] \times \cdots \times [m_k]$ where $d_{ij} = \#\{l : i_l \neq j_l\}$. Here $i = (i_1, \ldots, i_k)$ and $j = (j_1, \ldots, j_k)$ are elements in that Cartesian product.
- The L_1-metric on the Cartesian product $[m_1] \times \cdots \times [m_k]$ where $d_{ij} = \sum_{l=1}^k |i_l - j_l|$.

For the last two metrics, the number of states of the relevant independence models is $n = m_1 \cdots m_k$. To compute Wasserstein distances, we need to describe the Lipschitz polytope P_d as explicitly as possible. All three metrics above are *graph metrics*. This means that there exists an undirected simple graph G with vertex set $[n]$ such that d_{ij} is the length of the shortest path from i to j in G. The corresponding Wasserstein balls are called *symmetric edge polytopes*. They are investigated in [42, Section 4].

The following four independence models are used for the case studies in [42, Section 6]. We use the tuple $((m_1)_{d_1}, \ldots, (m_k)_{d_k})$ to denote the independence model with $n = \prod_{i=1}^k \binom{m_i+d_i-1}{d_i}$ states where the ith entry $(m_i)_{d_i}$ refers to a multinomial distribution with m_i possible outcomes and d_i trials, which can be interpreted as an unordered set of d_i identically distributed random variables on $[m_i] = \{1, 2, ..., m_i\}$. The subscript d_i is omitted if $d_i = 1$. For example, $(2_2, 2)$ is the independence model for three binary random variables where the first two are identically distributed. We list the $n = 6$ states in the order $00, 10, 20, 01, 11, 21$. These are the vertices of the associated graph G, which is the product of a 3-chain and a 2-chain. This model $\mathcal{M}$ is the image of the map from the square $[0,1]^2$ into the simplex Δ_5 given by

$$(p,q) \mapsto \big(p^2 q,\ 2p(1-p)q,\ (1-p)^2 q,\ p^2(1-q),\ 2p(1-p)(1-q),\ (1-p)^2(1-q)\big). \tag{5.12}$$

Example 5.11 We consider four models: the 3-bit model $(2,2,2)$ with the L_0-metric on $[2]^3$, the model $(3,3)$ for two ternary variables with the L_1-metric on $[3]^2$, the model (2_6) for six identically distributed binary variables with the discrete metric on $[7]$, and the model $(2_2, 2)$ in (5.12) with the L_1-metric on $[3] \times [2]$. In Table 5.1, we report the f-vectors of the Wasserstein balls for each of these models.

$\mathcal{M}$	n	$\dim(\mathcal{M})$	Metric d	f-vector of the $(n-1)$-polytope P_d^*
$(2,2,2)$	8	3	$L_0 = L_1$	(24, 192, 652, 1062, 848, 306, 38)
$(3,3)$	9	4	L_1	(24, 216, 960, 2298, 3048, 2172, 736, 82)
(2_6)	7	1	discrete	(42, 210, 490, 630, 434, 126)
$(2_2, 2)$	6	2	L_1	(14, 60, 102, 72, 18)

Table 5.1: f-vectors of the Wasserstein balls for the four models in Example 5.11.

Independence models correspond in algebraic geometry to *Segre-Veronese varieties*. They are of considerable current interest study of tensor decompositions. We here replace the model, which is a semialgebraic set inside a simplex, by its complex Zariski closure in a projective space. This allows us to compute the algebraic degrees of our optimization problem.

The Segre-Veronese variety $\mathcal{M} = ((m_1)_{d_1}, \ldots, (m_k)_{d_k})$ is the embedding of $\mathbb{P}^{m_1-1} \times \cdots \times \mathbb{P}^{m_k-1}$ in the projective space of partially symmetric tensors $\mathbb{P}(\mathrm{Sym}_{d_1}\mathbb{R}^{m_1} \otimes \cdots \otimes \mathrm{Sym}_{d_k}\mathbb{R}^{m_k})$. That projective space

equals $\mathbb{P}^{n-1}$ where $n = \prod_{i=1}^{k} \binom{m_i+d_i-1}{d_i}$. By definition, the Segre-Veronese variety $\mathcal{M}$ is the set of all tensors of rank one inside this projective space.

Example 5.12 Let $k = 2$. The Segre-Veronese variety $\mathcal{M}\big((2)_2, (2)_1\big)$ is an embedding of $\mathbb{P}^1 \times \mathbb{P}^1$ into $\mathbb{P}^5$, where it is a quartic surface. Its points are rank one tensors of format $2 \times 2 \times 2$ which are symmetric in the first two indices. This model appears in the last row of Table 5.3.

We identify the projective variety $\mathcal{M}$ with the intersection $\mathcal{M} \cap \Delta_{n-1}$. This is the set of real nonnegative points in $\mathcal{M}$. Thus, the independence model $\mathcal{M}$ consists of nonnegative rank one tensors whose entries sum to 1. The dimension of $\mathcal{M}$ is denoted $\mathbf{m} := (m_1 - 1) + \cdots + (m_k - 1)$. The computation of the polar degrees of $\mathcal{M}$ appears in the doctoral dissertation of Luca Sodomaco [161, Chapter 5]. We here state the result of this computation.

Theorem 5.13 (Sodomaco) *The polar degrees of the Segre-Veronese variety are*

$$\delta_{r-1}(\mathcal{M}) \;=\; \sum_{s=0}^{\mathbf{m}-n+1+r} (-1)^s \binom{\mathbf{m}-s+1}{n-r} (\mathbf{m}-s)! \left(\sum_{i_1+\cdots+i_k=s} \prod_{l=1}^{k} \frac{\binom{m_l}{i_l} d_l^{m_l-1-i_l}}{(m_l-1-i_l)!} \right). \tag{5.13}$$

Here r is any integer in the range $n - 1 - \dim(\mathcal{M}) \leq r \leq \dim(\mathcal{M}^*)$.

We next examine this formula for various special cases starting with the binary case.

Corollary 5.14 *Let $\mathcal{M}$ be the k-bit independence model. The formula (5.13) specializes to*

$$\delta_{r-1}(\mathcal{M}) \;=\; \sum_{s=0}^{k-2^k+1+r} (-1)^s \binom{k+1-s}{2^k-r} (k-s)!\, 2^s \binom{k}{s}. \tag{5.14}$$

In algebraic geometry language, our model $\mathcal{M}$ here is the Segre embedding of $(\mathbb{P}^1)^k$ into $\mathbb{P}^{2^k-1}$. This is the toric variety associated with the k-cube, so its degree is the normalized volume of the cube, which is $k!$. The polar degrees δ_{r-1} in (5.14) are shown for $k \leq 7$ in Table 5.2. The indices r with $\delta_{r-1} \neq 0$ range from $\operatorname{codim}(\mathcal{M}) = 2^k - 1 - k$ to $\dim(\mathcal{M}^*) = 2^k - 1$. For the sake of the table's layout, we shift the indices on each row so that the row labeled 0 contains $\delta_{\operatorname{codim}(\mathcal{M})-1} = \operatorname{degree}(\mathcal{M}) = k!$. The dual variety $\mathcal{M}^*$ is a hypersurface of degree δ_{2^k-2} known as the *hyperdeterminant* of format 2^k. For instance, for $k = 3$, this hypersurface in $\mathbb{P}^7$ is the $2 \times 2 \times 2$-hyperdeterminant which has degree four. The entries in the first column ($k = 2$) corresponds to the three scenarios in Figure 5.1, where the algebraic degree equals 2.

$r - \operatorname{codim}(\mathcal{M})$	$k=2$	$k=3$	$k=4$	$k=5$	$k=6$	$k=7$
0	2	6	24	120	720	5040
1	2	12	72	480	3600	30240
2	2	12	96	840	7920	80640
3		4	64	800	9840	124320
4			24	440	7440	120960
5				128	3408	75936
6					880	30016
7						6816

Table 5.2: The polar degrees $\delta_{r-1}(\mathcal{M})$ of the k-bit independence model for $k \leq 7$.

We briefly discuss the independence models (m_1, m_2) for two random variables. These are the classical contingency tables of format $m_1 \times m_2$. Here, $n = m_1 m_2$ and $\mathbf{m} = m_1 + m_2 - 2$. The Segre variety $\mathcal{M} = \mathbb{P}^{m_1-1} \times \mathbb{P}^{m_2-1} \subset \mathbb{P}^{n-1}$ consists of $m_1 \times m_2$ matrices of rank one.

Corollary 5.15 *The Segre variety of $m_1 \times m_2$ matrices of rank one has the polar degrees*

$$\delta_{r-1}(\mathcal{M}) \;=\; \sum_{s=0}^{\mathbf{m}-n+1+r} (-1)^s \binom{\mathbf{m}-s+1}{n-r} (\mathbf{m}-s)! \left(\sum_{i+j=s} \frac{\binom{m_1}{i}}{(m_1-1-i)!} \cdot \frac{\binom{m_2}{j}}{(m_2-1-j)!} \right).$$

The polar degrees above serve as upper bounds for any particular Wasserstein distance problem. For a fixed model $\mathcal{M}$, the equality in Theorem 5.5 holds only when the data (ℓ, L) is generic. However, for the optimization problem in (5.11), the linear space $L = L_F$ and the linear functional $\ell = \ell_F$ are very specific. They depend on the Lipschitz polytope P_d and the type F of the optimal solution ν^*. For such specific scenarios, we only get an inequality.

Proposition 5.16 *Consider the problem (5.11) for the independence model $((m_1)_{d_1}, \ldots, (m_k)_{d_k})$ with a given face F of the Wasserstein ball $B = P_d^*$. The degree of the optimal solution ν^* as an algebraic function of the data μ is bounded above by the polar degree δ_{r-1} in (5.13).*

Proof This follows from Theorem 5.5. The upper bound relies on general principles of algebraic geometry. Namely, the graph of the map $\mu \mapsto \nu^*(\mu)$ is an irreducible variety, and we seek its degree over μ. The map depends on the parameters (ℓ, L). When the coordinates of L and ℓ are independent transcendentals then the algebraic degree is the polar degree δ_{r-1}. That algebraic degree can only go down when these coordinates take on special values in the real numbers. That same semi-continuity argument holds for most polynomial optimization problems, including the Euclidean distance optimization in the last lecture. □

We now examine the drop in algebraic degree for the four models in Example 5.11. In the language of algebraic geometry, they are the Segre threefold $\mathbb{P}^1 \times \mathbb{P}^1 \times \mathbb{P}^1$ in $\mathbb{P}^7$, the variety $\mathbb{P}^2 \times \mathbb{P}^2$ of rank one 3×3 matrices in $\mathbb{P}^8$, the rational normal curve $\mathbb{P}^1$ in $\mathbb{P}^6 = \mathbb{P}(\mathrm{Sym}_6(\mathbb{R}^2))$, and the Segre-Veronese surface $\mathbb{P}^1 \times \mathbb{P}^1$ in $\mathbb{P}^5 = \mathbb{P}(\mathrm{Sym}_2(\mathbb{R}^2) \times \mathrm{Sym}_1(\mathbb{R}^2))$. The finite metrics d are specified in the fourth column of Table 5.1. The fifth column in Table 5.1 records the combinatorial complexity of our optimization problem, while the algebraic complexity is recorded in Table 5.3.

$\mathcal{M}$	Polar degrees	Maximal degree	Average degree
$(2, 2, 2)$	$(0, 0, 0, 6, 12, 12, 4)$	$(0, 0, 0, 4, 12, 6, 0)$	$(0, 0, 0, 2.138, 6.382, 3.8, 0)$
$(3, 3)$	$(0, 0, 0, 6, 12, 12, 6, 3)$	$(0, 0, 0, 2, 8, 6, 6, 0)$	$(0, 0, 0, 1.093, 3.100, 4.471, 6.0, 0)$
(2_6)	$(0, 0, 0, 0, 6, 10)$	$(0, 0, 0, 0, 6, 5)$	$(0, 0, 0, 0, 6, 5)$
$(2_2, 2)$	$(0, 0, 4, 6, 4)$	$(0, 0, 3, 5, 2)$	$(0, 0, 2.293, 3.822, 2.0)$

Table 5.3: The algebraic degrees of the problem (5.8) for the four models in Example 5.11.

The second column in Table 5.3 gives the vector $(\delta_0, \delta_1, \ldots, \delta_{n-2})$ of polar degrees. The third and fourth column are the results of a computational experiment. For each model, we take 1000 uniform samples μ with rational coordinates from Δ_{n-1}, and we solve the optimization problem (5.8). The output is an exact representation of the optimal solution ν^*. This includes the optimal face F that specifies ν^*, along with its maximal ideal over $\mathbb{Q}$. The algebraic degree of the optimal solution ν^* is computed as the number of complex zeros of that maximal ideal. This number is bounded above by the polar degree (cf. Proposition 5.16). The fourth column in Table 5.3 shows the average of the algebraic degrees we found. For example, for the 3-bit model $(2, 2, 2)$ we have $\delta_3 = 6$, corresponding to P_d^* touching $\mathcal{M}$ at a

3-face F. However, the maximum degree we saw in our computations was 4, with an average degree of 2.138. For 4-faces F, we have $\delta_4 = 12$, and this degree was attained in some runs. The average was 6.382.

Such computational experiments are organized naturally into three stages: (1) combinatorial preprocessing, (2) numerical optimization, and (3) algebraic postprocessing. Our object of interest is a model $\mathcal{M}$ in the simplex Δ_{n-1}, typically one of the independence models $((m_1)_{d_1}, \ldots, (m_k)_{d_k})$ where $n = \prod_{i=1}^{k} \binom{m_i+d_i-1}{d_i}$.

The state space $[n]$ is a metric space, with metric given by the matrix $d = (d_{ij})$. This matrix of pairwise distances is part of our input. It defines the Lipschitz polytope P_d and its dual, the Wasserstein ball P_d^*. Our first algorithm computes these combinatorial objects.

Algorithm 1: Combinatorial Preprocessing

Input: An $n \times n$ symmetric matrix $d = (d_{ij})$.
Output: A description of all facets F of the Wasserstein ball P_d^*.
From the inequality presentation in (5.6), find all vertices of the Lipschitz polytope P_d. These vertices are the inner normal vectors ℓ_F to the facets F of P_d^*. Store them.
Determine an inequality description of the cone C_F over each facet F.
return *the list of pairs* (ℓ_F, C_F)*, one for each vertex of the Lipschitz polytope* P_d.

In the original study [42], the software `Polymake` was used to run Algorithm 1. We next solve the optimization problem in (5.8), by examining each facet F of the Wasserstein ball. The problem is that in (5.11) but with the linear space L_F now replaced by the convex cone C_F that is spanned by F.

Algorithm 2: Numerical Optimization

Input: Model $\mathcal{M}$ and a point μ in the simplex Δ_{n-1}; complete output from Algorithm 1.
Output: The optimal solution ν^* in (5.8) along with its type G.
for *each facet* F *of the Wasserstein ball* P_d^* **do**
    Apply global optimization methods to identify a point $\nu^* \in \mathcal{M}$ that minimizes $\ell_F = \ell_F(\nu)$ subject to $\nu \in (\mu + C_F) \cap \mathcal{M}$.
    Identify the unique face G of F whose span contains ν^* in its relative interior.
    Identify a basis of vectors $\mathbf{e}_i - \mathbf{e}_j \in C_G$ for the linear space L_G spanned by G.
    Store the optimal solution ν^* and a basis for the linear subspace L_G of $\mathbb{R}^n$.
end
Among all candidate solutions, identify the solution ν^* for which the Wasserstein distance $W_d(\mu, \nu^*)$ to the given data point μ is smallest. Record its type G.
return *The optimal solution* ν^**, its associated linear space* L_G*, and the facet normal* ℓ_G.

In [42], the software `SCIP` was used to run Algorithm 2. `SCIP` employs sophisticated branch-and-cut strategies to solve constrained polynomial optimizaion problems via LP relaxation. Algorithm 1 is guaranteed to find the global optimum for our problem (5.8). Moreover, it furnishes an identification of the combinatorial type. This serves as the input to the symbolic computation in Algorithm 3 below.

Algorithm 3 can be carried out with a computer algebra system like`Macaulay2`. Steps 2 and 4 are the result of standard Gröbner basis calculations. The pipeline is illustrated with examples in [42, Section 6].

Algorithm 3: Algebraic Postprocessing

Input: The optimal solution (ν^*, G) to (5.8) in the form found by Algorithm 2.
Output: The maximal ideal in the polynomial ring $\mathbb{Q}[\nu_1, \ldots, \nu_n]$ which has the zero ν^*.
Use Lagrange multipliers to give polynomial equations that characterize the critical points of the linear function ℓ_F on the subvariety $(\mu + L_G) \cap \mathcal{M}$ in the affine space $\mathbb{R}^n$.
Eliminate all variables representing Lagrange multipliers from the ideal in the previous step. This ideal lives in $\mathbb{Q}[\nu_1, \ldots, \nu_n]$.
if *the ideal in step 4 is maximal* **then**
    Call the ideal M.
else
    Remove extraneous primary components to get the maximal ideal M of ν^*.
end
Determine the degree of ν^*, which is the dimension of $\mathbb{Q}[\nu_1, \ldots, \nu_n]/M$ over $\mathbb{Q}$.
return *the generators for the maximal ideal M along with the degree found in Step 10.*

Chapter 6
Curvature

6.1 Plane Curves

In this section, we consider a smooth algebraic curve $C \subset \mathbb{R}^2$ given as the zero set of an irreducible polynomial of degree $d \geq 1$:

$$f(x_1, x_2) \in \mathbb{R}[x_1, x_2]$$

Let $\mathbf{x} = (x_1, x_2)$. Geometrically, the *curvature* of C at a point $\mathbf{x} \in C$ is the rate of change at $\mathbf{x}$ of a unit normal vector traveling along C. To be precise, define

$$N(\mathbf{x}) := \frac{1}{\|\nabla f(\mathbf{x})\|} \nabla f(\mathbf{x}), \tag{6.1}$$

where $\nabla f(\mathbf{x}) = (\partial f/\partial x_1, \partial f/\partial x_2)$ is the gradient of f. Then, for all $\mathbf{x} \in C$, $N(\mathbf{x})$ returns a normal vector of C at $\mathbf{x}$; one calls $N(\mathbf{x})$ a *unit normal field*. Similarly, a *unit tangent field* is given by

$$T(\mathbf{x}) := (N(\mathbf{x})_2, -N(\mathbf{x})_1).$$

The curvature of C at $\mathbf{x}$ is defined as the (signed) magnitude of the derivative of $N(\mathbf{x})$ in tangent direction:

$$c(\mathbf{x}) := \left\langle T(\mathbf{x}),\ T(\mathbf{x})_1 \cdot \frac{\partial N}{\partial x_1}(\mathbf{x}) + T(\mathbf{x})_2 \cdot \frac{\partial N}{\partial x_2}(\mathbf{x}) \right\rangle. \tag{6.2}$$

Since the derivative of a unit normal field at a curve always points in tangent direction, (6.2) has the equivalent formulation $T(\mathbf{x})_1 \cdot \frac{\partial N}{\partial x_1}(\mathbf{x}) + T(\mathbf{x})_2 \cdot \frac{\partial N}{\partial x_2}(\mathbf{x}) = c(\mathbf{x}) \cdot T(\mathbf{x})$.

Example 6.1 Consider the ellipse $f(\mathbf{x}) = x_1^2 + \frac{1}{4}x_2^2 - 1$. The left picture in Figure 6.1 shows the ellipse in green and the normal field $N(\mathbf{x})$ in yellow. The right picture displays the curvature via $c(\mathbf{x}) \cdot T(\mathbf{x})$. The magnitude of a yellow vector attached to a point $\mathbf{x}$ in the right picture gives the curvature at $\mathbf{x}$. On the top and bottom, where the ellipse is rather flat, the normal vectors do not change much, hence the curvature is small. On the sides, normal vectors change more rapidly, so there the curvature is larger ◇

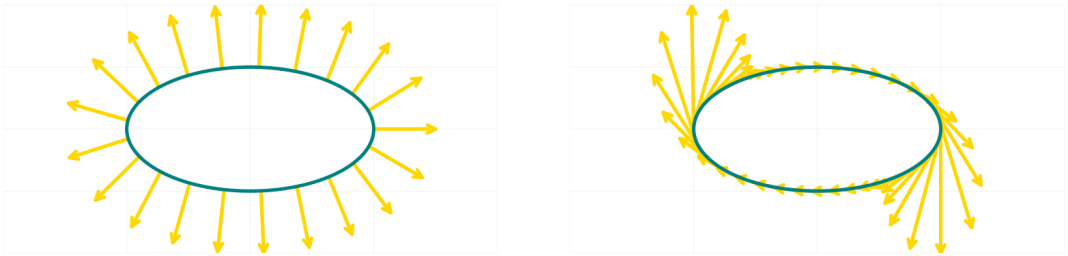

Fig. 6.1: The left picture shows a unit normal field of the ellipse $x_1^2 + \frac{1}{4}x_2^2 - 1 = 0$, and the right picture shows how the normal field changes when travelling along the ellipse.

The inverse of the signed curvature $r(\mathbf{x}) := c(\mathbf{x})^{-1}$ is called the (signed) *radius of curvature*. This is because C contains an infinitesimally small arc of a circle with radius $|r(\mathbf{x})|$ and center $\mathbf{x} - r(\mathbf{x}) \cdot N(\mathbf{x})$. This center is also called a *focal point* or *center of curvature* of C. The reason for the negative sign in this formula is that a normal vector pointing towards the focal point changes towards the direction that is opposite to $T(\mathbf{x})$; see Figure 6.2 for an illustration.

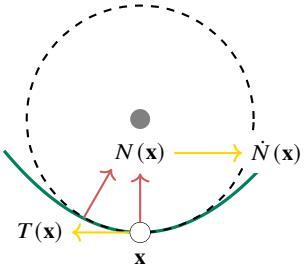

Fig. 6.2: The picture shows a green curve that contains an infinitesimally small arc of the dashed circle. The grey center of the circle is a focal point of the green curve. The red vertical normal vector $N(\mathbf{x})$ pointing towards the focal point changes into a normal vector that is slightly tilted in the direction opposite to $T(\mathbf{x})$. This means that $\dot{N}(\mathbf{x}) := T(\mathbf{x})_1 \frac{\partial N(\mathbf{x})}{\partial x_1} + T(\mathbf{x})_2 \frac{\partial N(\mathbf{x})}{\partial x_2}$ is a negative multiple of $T(\mathbf{x})$.

Proposition 6.2 *The Zariski closure of the set of all centers of curvature of a plane curve C is the evolute of C, as defined in Section 1.3.*

Proof We consider a local parametrization $\gamma(t)$ of C with $\gamma(0) = \mathbf{x}$ and $\dot{\gamma}(0) = T(\mathbf{x})$. Then, $\varepsilon(t) := \gamma(t) - r(\gamma(t)) \cdot N(\gamma(t))$ gives a local parametrization of the curve E that is traced by the centers of curvature of C. We have

$$\dot{\varepsilon}(0) = T(\mathbf{x}) - \big\langle \nabla r(\mathbf{x}), T(\mathbf{x}) \big\rangle \cdot N(\mathbf{x}) - r(\mathbf{x}) \cdot \big(T(\mathbf{x})_1 \cdot \tfrac{\partial N}{\partial x_1}(\mathbf{x}) + T(\mathbf{x})_2 \cdot \tfrac{\partial N}{\partial x_2}(\mathbf{x}) \big).$$

Since $T(\mathbf{x})_1 \cdot \frac{\partial N}{\partial x_1}(\mathbf{x}) + T(\mathbf{x})_2 \cdot \frac{\partial N}{\partial x_2}(\mathbf{x}) = c(\mathbf{x}) \cdot T(\mathbf{x}) = r(\mathbf{x})^{-1} \cdot T(\mathbf{x})$, we get

$$\dot{\varepsilon}(0) = -\big\langle \nabla r(\mathbf{x}), T(\mathbf{x}) \big\rangle \cdot N(\mathbf{x}). \tag{6.3}$$

This means that the tangent line of E at $\varepsilon(0) = \mathbf{x} - r(\mathbf{x}) \cdot N(\mathbf{x})$ is the normal line of C at $\mathbf{x}$. Hence, the curve E is the envelope of the normal lines of C; in other words, the evolute of C. □

The previous proof shows in particular that the absolute value of the curvature $|c(\mathbf{x})|$ at a point $\mathbf{x} \in C$ is the inverse distance from $\mathbf{x}$ to its corresponding point on the evolute. Indeed, the latter point is $\mathbf{x} - r(\mathbf{x}) \cdot N(\mathbf{x})$, and so its distance from $\mathbf{x}$ is $|r(\mathbf{x})| = |c(\mathbf{x})|^{-1}$.

In the remainder of this section, we will study two types of points: *inflection points* and *points of critical curvature*. These points exhibit special curvature of C. Inflection points are points where C is locally flat, and critical curvature points are points where the curvature has a local extremum.

Definition 6.3 Let $\mathbf{x} \in C$.

1. We call $\mathbf{x}$ an *inflection point* if $c(\mathbf{x}) = 0$.
2. We call $\mathbf{x}$ a *critical curvature point* if $\mathbf{x}$ is a critical point of the function $C \to \mathbb{R}$, $x \mapsto c(\mathbf{x})$.

Example 6.4 We consider the Trott curve $f(\mathbf{x}) = 144(x^4 + y^4) - 225(x^2 + y^2) + 350x^2y^2 + 81$ as we did in Figure 2.1. The Trott curve has degree $d = 4$. Figure 6.3 shows the curve in green. We first compute inflection points using `HomotopyContinuation.jl` [26] and the formulation in Lemma 6.7.

```
using HomotopyContinuation, LinearAlgebra
@var x y z
v = [x; y; z]
F = 144*(x^4 + y^4) - 225*(x^2 + y^2) + 350*x^2*y^2 + 81*z^4
dF = differentiate(F, v)
H0 = differentiate(dF, v)
```

```
f = subs(F, z=>1)
h = subs(-det(H0), z=>1)
inflection_points = solve([f; h])
```

By Theorem 6.8, there are $3d(d-2) = 24$ complex inflection points. Klein [110] proved that at most $d(d-2) = 8$ can be real and indeed, in this case, we find 8 real inflection points. They are the yellow points in Figure 6.3. Next, we compute critical curvature points using the equations in Lemma 6.10.

```
f1, f2 = dF[1:2]
f11, f12, f12, f22 = H0[1:2,1:2]
hx, hy = differentiate(h,[x; y])
g = f1 * f2 * (f11-f22) + f12 * (f2^2- f1^2)
c = subs(f2 * hy - f1 * hx - 3 * h * g, z=>1)
crit_curv = solve([f; c])
```

By Theorem 6.11, there are $2d(3d-5) = 56$ complex critical curvature points. We find that 24 of them are real; out of these 8 are close (but not equal to) to the 8 inflection points, which is why they are not visible in the picture. They are shown as red points in Figure 6.3. By Proposition 6.5, the critical curvature points correspond to the cusps on the evolute, which is illustrated in Figure 6.4. ◇

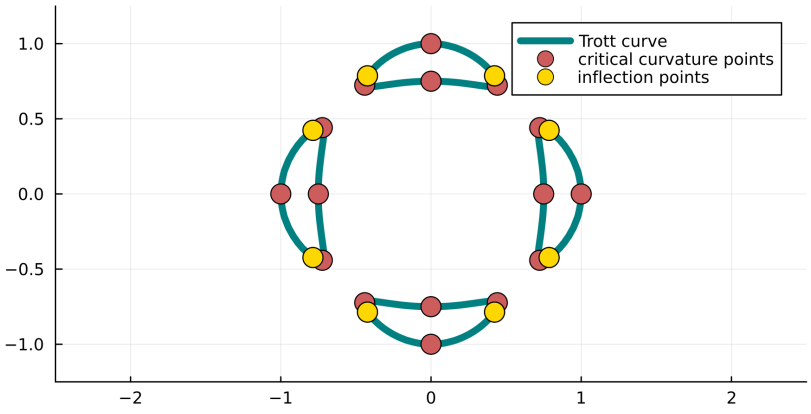

Fig. 6.3: The Trott curve $144(x^4+y^4) - 225(x^2+y^2) + 350x^2y^2 + 81 = 0$ in green together with its inflection points (yellow points) and critical curvature points (red points).

Proposition 6.5 *Let $C \subset \mathbb{R}^2$ be a smooth algebraic curve and $E \subset \mathbb{R}^2$ be its evolute. For $\mathbf{x} \in C$, let $r(\mathbf{x})$ be the radius of curvature and $\Gamma(\mathbf{x}) := \mathbf{x} - r(\mathbf{x}) \cdot N(\mathbf{x}) \in E$ be the corresponding point on the evolute.*

1. *$\mathbf{x}$ is an inflection point if and only if $\Gamma(\mathbf{x})$ is a point at infinity.*
2. *$\mathbf{x}$ is a point of critical curvature if and only if E has a cusp at $\Gamma(\mathbf{x})$.*

Proof Recall that $c(\mathbf{x}) = r(\mathbf{x})^{-1}$. The point $\Gamma(\mathbf{x})$ is at infinity if and only if $c(\mathbf{x}) = 0$, which means that $\mathbf{x}$ is an inflection point. This proves the first item. For the second item, we consider a local parametrization $\gamma(t)$ of C with $\gamma(0) = \mathbf{x}$ and $\dot{\gamma}(0) = T(\mathbf{x})$. As in the proof of Proposition 6.2, $\varepsilon(t) := \Gamma(\gamma(t))$ gives a

local parametrization of the evolute E. The evolute has a cusp at $\Gamma(\mathbf{x}) = \varepsilon(0)$ if and only if $\dot{\varepsilon}(0) = 0$. By (6.3),the latter is equivalent to $\langle \nabla r(\mathbf{x}), T(\mathbf{x}) \rangle = 0$. The latter equation holds exactly when the curvature $c(\mathbf{x})$ is critical at $\mathbf{x}$ since $\nabla c(\mathbf{x}) = \frac{-\nabla r(\mathbf{x})}{r(\mathbf{x})^2}$. □

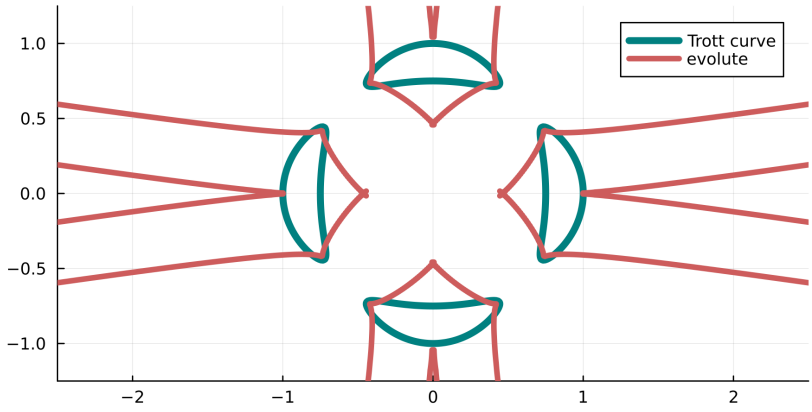

Fig. 6.4: The picture shows the Trott curve $144(x^4+y^4) - 225(x^2+y^2) + 350x^2y^2 + 81 = 0$ in green and its evolute in red. The cusps on the evolute correspond to the red critical curvature points in Figure 6.3. The Trott curve has 24 real critical curvature points. Out of those 8 have a radius of curvature which exceeds the boundary of this picture. This is why we only see 16 cusps. We thank Emil Horobet and Pierpaola Santarsiero for helping us computing the equation for the evolute.

We want to count the number of complex inflection and critical curvature points for a curve given by a general polynomial f. For this, let us first understand the curvature $c(\mathbf{x})$ better. In the following, we denote partial derivatives by $f_i := \frac{\partial f}{\partial x_i}$, $f_{i,j} := \frac{\partial^2 f}{\partial x_i x_j}$ and the *Hessian* by

$$H := \begin{pmatrix} f_{1,1} & f_{1,2} \\ f_{1,2} & f_{2,2} \end{pmatrix}.$$

Lemma 6.6 *The curvature equals* $c(\mathbf{x}) = \dfrac{1}{\|\nabla f(\mathbf{x})\|} \cdot T(\mathbf{x})^\top H(\mathbf{x})\, T(\mathbf{x})$

Proof Recall that $c(\mathbf{x}) = \left\langle T(\mathbf{x}),\ T(\mathbf{x})_1 \cdot \frac{\partial N}{\partial x_1}(\mathbf{x}) + T(\mathbf{x})_2 \cdot \frac{\partial N}{\partial x_2}(\mathbf{x}) \right\rangle$. By applying the product rule on (6.1), we obtain

$$T(\mathbf{x})_1 \cdot \tfrac{\partial N}{\partial x_1}(\mathbf{x}) + T(\mathbf{x})_2 \cdot \tfrac{\partial N}{\partial x_2}(\mathbf{x}) = \|\nabla f(\mathbf{x})\|^{-1} \cdot H(\mathbf{x})\, T(\mathbf{x}) + a(\mathbf{x}) \cdot \nabla f(\mathbf{x})$$

for some scalar function $a(\mathbf{x})$. Since $\langle T(\mathbf{x}), \nabla f(\mathbf{x}) \rangle = 0$, this gives the asserted formula. □

We can write the formula from Lemma 6.6 more explicitly as

$$c(\mathbf{x}) = \frac{f_{1,1} \cdot f_2^2 - 2 f_{1,2} \cdot f_1 \cdot f_2 + f_{2,2} \cdot f_1^2}{(f_1^2 + f_2^2)^{\frac{3}{2}}}(\mathbf{x}). \tag{6.4}$$

For what follows it will be helpful to embed C into complex projective space. We write

$$F(x_0, x_1, x_2) := x_0^d \, f\left(\frac{x_1}{x_0}, \frac{x_2}{x_0}\right)$$

for the homogenization of f. Moreover, let

$$H_0 = \begin{pmatrix} F_{0,0} & F_{0,1} & F_{0,2} \\ F_{0,1} & F_{1,1} & F_{1,2} \\ F_{0,2} & F_{1,2} & F_{2,2} \end{pmatrix}.$$

denote the Hessian of F viewed as polynomial in $\mathbf{x}$ by setting $x_0 = 1$. We can rewrite the curvature of C in terms of F. The next lemma goes back to Salmon [157].

Lemma 6.7 *The curvature at $\mathbf{x} \in C$ can be expressed as*

$$c(\mathbf{x}) = \frac{-\det H_0}{(d-1)^2 \cdot (f_1^2 + f_2^2)^{\frac{3}{2}}}(\mathbf{x}).$$

Proof Homogenizing polynomials in (6.4), we get $c = \frac{P}{Q}$, where $P = F_{1,1} \cdot F_2^2 - 2F_{1,2} \cdot F_1 \cdot F_2 + F_{2,2} \cdot F_1^2$ and $Q = (F_1^2 + F_2^2)^{\frac{3}{2}}$. By Euler's formula for homogeneous functions, we have

$$(d-1) \cdot F_j = x_0 F_{0,j} + x_1 F_{1,j} + x_2 F_{2,j}, \quad 0 \le j \le 2. \tag{6.5}$$

Substituting the F_j in P gives

$$\begin{aligned}(d-1)^2 \cdot P = (F_{1,1}F_{2,2} - F_{1,2}^2) \cdot (x_1^2 F_{1,1} + x_2^2 F_{2,2} + 2(x_0 x_1 F_{0,1} + x_0 x_2 F_{0,2} + x_1 x_2 F_{1,2})) \\ + x_0^2 (F_{0,1}^2 F_{2,2} - 2F_{1,2}F_{0,1}F_{0,2} + F_{1,1}F_{0,2}^2).\end{aligned}$$

Furthermore, we have $0 = dF = x_0 F_0 + x_1 F_1 + x_2 F_2$ on C. Substituting (6.5) into this equation, we have

$$0 = x_0^2 F_{0,0} + x_1^2 F_{1,1} + x_2 F_{2,2}^2 + 2(x_0 x_1 F_{0,1} + x_0 x_2 F_{0,2} + x_1 x_2 F_{1,2})$$

on C. We obtain

$$P = \frac{x_0^2}{(d-1)^2} \cdot (-(F_{1,1}F_{2,2} - F_{1,2}^2)F_{0,0} + F_{0,1}^2 F_{2,2} - 2F_{1,2}F_{0,1}F_{0,2} + F_{1,1}F_{0,2}^2) = \frac{-x_0^2 \cdot \det H_0}{(d-1)^2}.$$

Setting $x_0 = 1$ finishes the proof. □

We can now count the inflection points of a general curve.

Theorem 6.8 *The number of complex inflection points of a curve C defined by a general polynomial f of degree d is $3d(d-2)$.*

This theorem was first proved by Klein [110]. He also proved that the number of real inflection points is at most one third; i.e., $d(d-2)$. Here, we give a short proof for the complex count.

Proof By Lemma 6.7, inflection points on C are given as the zero set $f = \det H_0 = 0$, which is a system of two equations in two variables $\mathbf{x} = (x_1, x_2)$. The degree of f is d and the degree of $\det H_0$ is $3(d-2)$. Bézout's theorem implies that the number of inflection points is at most $3d(d-2)$. To show that the number is also at least $3d(d-2)$, we show that there exist polynomials with this number of inflection points.

Consider a univariate polynomial $g(x_1) \in \mathbb{R}[x_1]$ of degree d and let $G(x_0, x_1)$ be its homogenization. Let also $M := \begin{pmatrix} G_{0,0} & G_{0,1} \\ G_{0,1} & G_{1,1} \end{pmatrix}$ be the Hessian of G with respect to the variables x_0, x_1. We assume (1) that g has d regular zeros, (2) that $\det M = 0$ has only regular zeros, and (3) that $g = \det M = 0$ has no solutions. All three are Zariski open conditions, so almost all polynomials g satisfy this assumption. Define

$$f(x_1, x_2) := x_2^d - g(x_1).$$

Observe that in this case $\det H_0 = d(d-1) \cdot x_2^{d-2} \cdot \det M$. Consequently, $\det H_0 = 0$ if and only if either $x_2 = 0$, or x_1 is among the $2(d-2)$ zeros of $\det M$. This means that $\mathbf{x}$ is an inflection point if either $\mathbf{x} = (x_1, 0)$ and x_1 is a zero of g, or $\mathbf{x} = (x_1, x_2)$ where x_1 is a zero of $\det M$ and $x_2^d = g(x_1)$. In the first case, we find d inflection points and each has multiplicity $d-2$. In the second case, since $g(x_1) \neq 0$, we find $2d(d-2)$ many regular inflection points with multiplicity one. Now, if we perturb f slightly, the d points with multiplicity will split into $d(d-2)$ inflection points, while the other $2d(d-2)$ inflection points will remain distinct. In total, this gives $3d(d-2)$ inflection points. □

Corollary 6.9 *For a plane curve C defined by a general polynomial f of degree d, its evolute has degree $3d(d-1)$.*

Proof We compute the desired degree by intersecting the evolute with the line at infinity. For that, we consider the Zariski closure $\bar{C}$ of the curve C in the complex projective plane $\mathbb{P}^2_{\mathbb{C}}$. By Proposition 6.2, the evolute is the image of $\Gamma : \bar{C} \to \mathbb{P}^2_{\mathbb{C}}, \mathbf{x} \mapsto \mathbf{x} - r(\mathbf{x}) \cdot N(\mathbf{x})$. A point $\Gamma(\mathbf{x})$ on the evolute can be at infinity for two reasons: Either $\mathbf{x} \in \bar{C}$ is at infinity, or $\mathbf{x}$ is a finite point and a complex inflection point of the curve C by Proposition 6.5. Since C is a general curve of degree d, there are d points $\mathbf{x}$ of the first kind and $3d(d-2)$ points $\mathbf{x}$ of the second kind by Theorem 6.8. For each of the d points $\mathbf{x} \in \bar{C}$ at infinity, Salmon [157, §119] shows that $\Gamma(\mathbf{x})$ is a cusp whose tangent line is the line at infinity. Hence, when intersecting the evolute with the line at infinity, there are d cusps (that count with multiplicity three each) plus $3d(d-2)$ points that correspond to the complex inflection points of C. All in all, the degree of the evolute is $3d + 3d(d-2) = 3d(d-1)$. □

Let us now find polynomial equations for critical curvature.

Lemma 6.10 *Critical curvature points on the curve $C = \{f(\mathbf{x}) = 0\}$ are defined by the equation*

$$(f_1^2 + f_2^2) \cdot \left(f_2 \cdot \frac{\partial \det H_0}{\partial x_1} - f_1 \cdot \frac{\partial \det H_0}{\partial x_2} \right) - 3 \det H_0 \cdot g = 0,$$

where $g = f_1 f_2 \cdot (f_{1,1} - f_{2,2}) + f_{1,2}(f_2^2 - f_1^2)$.

Proof Critical curvature points on C are defined by the equations $f = 0$ and $f_2 \cdot \frac{\partial c(\mathbf{x})}{\partial x_1} - f_1 \cdot \frac{\partial c(\mathbf{x})}{\partial x_2} = 0$. By Lemma 6.7 and the product rule, we have

$$-(d-1)^2 (f_1^2 + f_2^2)^{\frac{5}{2}} \cdot \frac{\partial c(\mathbf{x})}{\partial x_i} = \frac{\partial \det H_0}{\partial x_i} \cdot (f_1^2 + f_2^2) - 3 \det H_0 \cdot (f_1 \cdot f_{1,i} + f_2 \cdot f_{2,i}).$$

This yields the stated polynomial equation. □

Theorem 6.11 *The number of complex critical curvature points of a curve C defined by a general polynomial f of degree d is $2d(3d-5)$.*

Proof Recall that critical curvature points correspond to finite cusps of the evolute by Proposition 6.5. Piene, Riener and Shapiro prove in [145, Proposition 3.3] that, counting in the complex projective plane, the number of cusps on the evolute for a general plane curve C of degree d is $6d^2 - 9d$. As explained in the proof of Corollary 6.9, Salmon [157, §119] shows that d of these cusps lie at infinity. Therefore, the curve C has $6d^2 - 9d - d = 2d(3d-5)$ complex critical curvature points. □

6.2 Algebraic Varieties

We study the curvature of smooth algebraic varieties in $\mathbb{R}^n$ of any dimension. This will lead us to the notions of *second fundamental form* and *Weingarten map*. These are fundamental concepts in Riemannian geometry, and in standard textbooks they are presented in much more general contexts; see, for instance, [57, 121, 138, 144]. Thus, our main goal in this section is to formulate the second fundamental form and Weingarten map in terms of the polynomial equations that define the variety.

Let $X \subset \mathbb{R}^n$ be a smooth algebraic variety of dimension $m := \dim(X)$. As in the case of plane curves, we consider a unit normal field $N(\mathbf{x})$ for X and differentiate it along a tangent field $T(\mathbf{x})$. The main difference to the case of curves in the plane is that there can be several tangent and normal directions. Nevertheless, similar to (6.2), we define the curvature of X at a point $\mathbf{x}$ in tangent direction $T(\mathbf{x})$ and in normal direction $N(\mathbf{x})$ to be $\langle T(\mathbf{x}),\ T(\mathbf{x})_1 \cdot \frac{\partial N}{\partial x_1}(\mathbf{x}) + \cdots + T(\mathbf{x})_n \cdot \frac{\partial N}{\partial x_n}(\mathbf{x})\rangle$. We will see that, as in the case of plane curves, this only depends on the values of $T(\mathbf{x})$ and $N(\mathbf{x})$ at a fixed point $\mathbf{x}$, but not on how those fields behave locally around $\mathbf{x}$. Let us work this out. Suppose that $I(X) = \langle f_1, \ldots, f_k\rangle$. We denote the gradients of the defining polynomials f_i by ∇f_i and their Hessians by H_i for $i = 1, \ldots, k$. Let also $J(\mathbf{x}) := (\ \nabla f_1\ \ldots\ \nabla f_k\ ) \in \mathbb{R}^{n\times k}$ be the (transpose of) the Jacobian of the f_i at $\mathbf{x}$. A (local) smooth unit normal field on X is given by

$$N(\mathbf{x}) = \frac{J(\mathbf{x})\, w(\mathbf{x})}{\|J(\mathbf{x})\, w(\mathbf{x})\|} = \frac{1}{\|J(\mathbf{x})\, w(\mathbf{x})\|} \sum_{i=1}^{k} w_i(\mathbf{x}) \cdot \nabla f_i(\mathbf{x}), \tag{6.6}$$

where $w : X \to \mathbb{R}^k$ is smooth with $w(\mathbf{x}) \notin \ker J(\mathbf{x})$ for all $\mathbf{x}$.

Differentiating (6.6) leads to

$$\frac{\mathrm{d}}{\mathrm{d}\mathbf{x}} N(\mathbf{x}) = \frac{1}{\|J(\mathbf{x})\, w(\mathbf{x})\|} \sum_{i=1}^{k} w_i(\mathbf{x}) \cdot H_i(\mathbf{x}) + J(\mathbf{x})\, R(\mathbf{x})$$

for some matrix valued function $R(\mathbf{x})$. Let us now fix a point $\mathbf{x} \in X$ and denote the tangent vector by $\mathbf{t} := T(\mathbf{x}) \in T_{\mathbf{x}}X$ and the normal vector by $\mathbf{v} := J(\mathbf{x})w(\mathbf{x}) \in N_{\mathbf{x}}X$. Since $\mathbf{t}^\top J(\mathbf{x}) = 0$, this implies

$$\Big\langle \mathbf{t},\ \mathbf{t}_1 \cdot \tfrac{\partial N}{\partial x_1} + \cdots + \mathbf{t}_n \cdot \tfrac{\partial N}{\partial x_n} \Big\rangle = \frac{1}{\|\mathbf{v}\|} \cdot \mathbf{t}^\top \Big(\sum_{i=1}^{k} \mathbf{w}_i H_i \Big) \mathbf{t}.$$

In particular, the right hand side only depends on the values of $T(\mathbf{x})$ and $N(\mathbf{x})$ at $\mathbf{x}$. This motivates the following definition.

Definition 6.12 Using the notation above, we define the curvature of X at $\mathbf{x}$ in tangent direction $\mathbf{t} \in T_{\mathbf{x}}X$ and in normal direction $\mathbf{v} \in N_{\mathbf{x}}X$ as

$$c(\mathbf{x}, \mathbf{t}, \mathbf{v}) := \frac{1}{\|\mathbf{v}\|} \mathbf{t}^T \Big(\sum_{i=1}^{k} \mathbf{w}_i \cdot H_i \Big) \mathbf{t},$$

where $\mathbf{v} = \sum_{i=1}^{k} \mathbf{w}_i \nabla f_i \in N_{\mathbf{x}}X$.

In fact, for $\mathbf{x} \in X$ and a fixed normal vector $\mathbf{v} \in N_{\mathbf{x}}X$, the curvature $c(\mathbf{x}, \mathbf{t}, \mathbf{v})$ is a quadratic form on $T_{\mathbf{x}}X$. This quadratic form is called the *second fundamental form* of X at $\mathbf{x}$ and $\mathbf{v}$. It is often denoted by

$$\mathrm{II}_{\mathbf{v}}(\mathbf{t}) := c(\mathbf{x}, \mathbf{t}, \mathbf{v}). \tag{6.7}$$

The associated linear map is called *Weingarten map*. We denote it by

$$L_{\mathbf{v}} : T_{\mathbf{x}}X \to T_{\mathbf{x}}X, \quad L_{\mathbf{v}}(\mathbf{t}) = P_{\mathbf{x}}\Big(\sum_{i=1}^{k} \mathbf{w}_i \cdot H_i \cdot \mathbf{t}\Big), \quad \text{where } \mathbf{v} = \sum_{i=1}^{k} \mathbf{w}_i \nabla f_i \tag{6.8}$$

and $P_{\mathbf{x}} : \mathbb{R}^n \to T_{\mathbf{x}}X$ is the orthgonal projection onto the tangent space of X at $\mathbf{x}$. Since $L_{\mathbf{v}}$ is a self-adjoint operator given by a real symmetric matrix, its eigenvalues are all real. If $\|\mathbf{v}\| = 1$, the eigenvalues of $L_{\mathbf{v}}$ are called the *principal curvatures* of X at $\mathbf{x}$ and in normal direction $\mathbf{v}$. The product of the principal curvatures is called the *Gauss curvature*; the arithmetic mean of the principal curvatures is called *mean curvature*. Since the principal curvatures are the critical points of the quadratic form $\mathrm{II}_{\mathbf{v}}(\mathbf{t})$, the *maximal curvature*

$$C(X) := \max_{\mathbf{x}\in X,\ \mathbf{t}\in T_{\mathbf{x}}X,\ \mathbf{v}\in N_{\mathbf{x}}X} c(\mathbf{x},\mathbf{t},\mathbf{v}) = \max_{\mathbf{x}\in X,\ \mathbf{v}\in N_{\mathbf{x}}X}\ \max_{\mathbf{t}\in T_{\mathbf{x}}X} c(\mathbf{x},\mathbf{t},\mathbf{v}) \tag{6.9}$$

is the maximum over all principal curvatures for varying $(\mathbf{x}, \mathbf{v})$.

Example 6.13 (Hypersurfaces) If X is defined by a single polynomial equation $f(\mathbf{x}) = 0$, we only have one normal direction (up to sign), and so the formula in Definition 6.12 can be written as

$$c(\mathbf{x},\mathbf{t}) := \frac{1}{\|\nabla f(\mathbf{x})\|}\, \mathbf{t}^T H\, \mathbf{t},$$

where H is the Hessian of f. This generalizes the formula in Lemma 6.6.

Let us now focus on surfaces in $\mathbb{R}^3$. Let $S \subset \mathbb{R}^3$ be a smooth algebraic surface and $\mathbf{x} \in S$. When the two principal curvatures of S at $\mathbf{x}$ are equal, the point $\mathbf{x}$ is called an *umbilic* or *umbilical point* of the surface S. Equivalently, the best second-order approximation of S at $\mathbf{x}$ is a 2-sphere. Umbilical points can be formulated as the zeros of a system of polynomial equations, whose complex zeros are called *complex umbilics* of the surface S. Salmon [158] computed the number of complex umbilics of a general surface.

Theorem 6.14 *A general surface in $\mathbb{R}^3$ defined by a polynomial of degree d has $10d^3 - 28d^2 + 22d$ umbilics.*

In the case of quadrics, we have results on the number of real umbilics and critical curvature points. Observe that rotations and translations do not affect the curvature, and that after a rotation and translation every quadric surface in $\mathbb{R}^3$ has the form $S = \{a_1x_1^2 + a_2x_2^2 + a_3x_3^2 = 1\}$. The next theorem is proved in [24].

Theorem 6.15 *Consider a quadric surface $S = \{a_1x_1^2 + a_2x_2^2 + a_3x_3^2 = 1\}$ with $a_1, a_2, a_3 \neq 0$ and $a_i \neq a_j$ for $i \neq j$. The number of real umbilics of S is*

- *4 if S is an ellipsoid (a_1, a_2, a_3 are positive) or a two-sheeted hyperboloid (one of the a_i is positive and two are negative);*
- *0 if S is a one-sheeted hyperboloid (two of the a_i are positive and one is negative).*

Similar to the case of plane curves, we call a point $\mathbf{x} \in S$ a *critical curvature point* if one of the two principal curvatures of S attains a critical value at $\mathbf{x}$. The first observation is that umbilics are always critical curvature points. This was shown in [24]. The following theorems, also proved in [24], cover the case of quadrics.

Theorem 6.16 *A general quadric surface $S \subset \mathbb{R}^3$ has 18 complex critical curvature points.*

Theorem 6.17 *Consider a quadric surface $S = \{a_1x_1^2 + a_2x_2^2 + a_3x_3^2 = 1\}$ with $a_1, a_2, a_3 \neq 0$ and $a_i \neq a_j$ for $i \neq j$. The number of real critical curvature points is*

- *10 if S is an ellipsoid (a_1, a_2, a_3 are positive);*
- *4 if S is a one-sheeted hyperboloid (two of the a_i are positive and one is negative);*
- *6 if S is a two-sheeted hyperboloid (one of the a_i is positive and two are negative).*

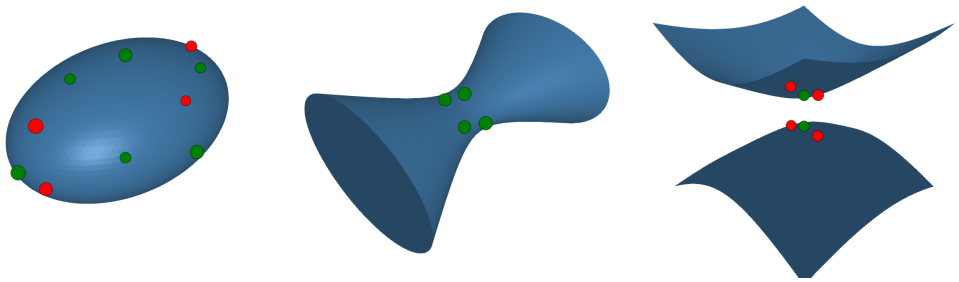

Fig. 6.5: The pictures illustrate Theorems 6.15 and 6.17. The figure on the left shows an ellipsoid with 4 red umbilics and 6 green critical curvature points. The umbilics are also critical curvature points, so that there are 10 in total. Similarly, the figure in the middle shows a one-sheeted hyperboloid with 4 green critical curvature points, and the figure on the left shows a two-sheeted hyperboloid with 4 red umbilics and 2 green critical curvature points (so 6 critical curvature points in total).

6.3 Volumes of Tubular Neighborhoods

We now turn to the problem of computing the volume of a *tubular neighborhood*. This is closely connected to curvature as we will see. We will discuss volumes of more general semialgebraic sets in Chapter 14. The tubular neighborhood of radius ε of a variety $X \subset \mathbb{R}^n$ is

$$\mathrm{Tube}(X, \varepsilon) := \{\mathbf{u} \in \mathbb{R}^n \mid d(\mathbf{u}, X) < \varepsilon\},$$

where $d(\mathbf{u}, X) = \min_{\mathbf{x} \in X} \|\mathbf{u} - \mathbf{x}\|$ is the Euclidean distance from $\mathbf{u}$ to X. There are several general formulas for upper bounds on the volume of $\mathrm{Tube}(X, \varepsilon)$ in the literature. For instance, Lotz [126] studied the case of a general complete intersection, and Bürgisser, Cucker and Lotz the case of a (possibly) singular hypersurface [34] of the sphere. The most general formula appeared in the paper by Basu and Lerario [11].

Theorem 6.18 *Let $X \subset \mathbb{R}^n$ be a real variety of dimension m. Let $I(X) = \langle f_1, \ldots, f_k \rangle$ be its ideal and let $d := \max \deg(f_i)$. Fix $\mathbf{u} \in \mathbb{R}^n$ and $r > 0$. Denoting the ball of radius r around $\mathbf{u}$ by $B_r(\mathbf{u})$, we have for every $0 < \varepsilon \leq r/(4dm + m)$ that*

$$\frac{\mathrm{vol}(\mathrm{Tube}(X, \varepsilon) \cap B_r(\mathbf{u}))}{\mathrm{vol}(B_r(\mathbf{u}))} \leq 4 \exp(1) \left(\frac{4nd\varepsilon}{r} \right)^{n-m}.$$

This theorem also holds for singular varieties. The proof of the theorem is based on approximating X in the Hausdorff topology by a sequence of smooth varieties $(X_n)_{n \in \mathbb{N}}$ and showing that the volume of the tubular neighborhood of X_n can be controlled as $n \to \infty$. The volume of tubular neighborhoods of smooth varieties (in fact, of smooth submanifolds of $\mathbb{R}^n$) is given by *Weyl's tube formula*. We derive this formula next. For a more detailed derivation and discussion, we refer to Weyl's original paper [177].

Let $X \subset \mathbb{R}^n$ be smooth and $\mathcal{N}X$ be the normal bundle of X. We denote the ε-normal bundle by

$$\mathcal{N}_\varepsilon X := \{(\mathbf{x}, \mathbf{v}) \in \mathcal{N}X \mid \|\mathbf{v}\| < \varepsilon\}.$$

Let us denote the *exponential map* by

$$\varphi_\varepsilon : \mathcal{N}_\varepsilon X \to \mathrm{Tube}(X, \varepsilon), \ (\mathbf{x}, \mathbf{v}) \mapsto \mathbf{x} + \mathbf{v}. \tag{6.10}$$

Definition 6.19 The *reach* of X or *injectivity radius* of X is defined as

$$\tau(X) := \sup\{\varepsilon > 0 \mid \varphi_\varepsilon \text{ is a diffeomorphism}\}. \tag{6.11}$$

For smooth X, the set in the right-hand side of (6.11) is non-empty and hence the reach $\tau(X)$ is always positive; see e.g. [122, Theorem 6.24]. We will discuss further properties and applications of the reach in Chapters 7 and 15.

We can assume that X is compact (if not, we replace X by $X \cap B$, where $B \subset \mathbb{R}^n$ is compact and full-dimensional). If $\varepsilon < \tau(X)$, the exponential map φ_ε is a diffeomorphism and we can pull back the integral over the tube to the normal bundle $\mathcal{N}_\varepsilon X$. More specifically, let A be the matrix representation of the derivative of φ_ε with respect to orthonormal bases on the tangent space of a local trivialization of $\mathcal{N}_\varepsilon X$ around $(\mathbf{x}, \mathbf{v})$ on the one side and $\mathbb{R}^n$ on the other side. Then, we have

$$\operatorname{vol}(\operatorname{Tube}(X, \varepsilon)) = \int_{\operatorname{Tube}(X,\varepsilon)} 1 \, \mathrm{d}\mathbf{u} = \int_{\mathbf{x}\in X} \int_{\mathbf{v}\in N_{\mathbf{x}}X : \|\mathbf{v}\|<\varepsilon} |\det(A(\mathbf{x}, \mathbf{v}))| \; \mathrm{d}\mathbf{v} \, \mathrm{d}\mathbf{x}. \tag{6.12}$$

We compute the matrix A. The derivative of φ_ε is given by $\frac{\mathrm{d}\varphi_\varepsilon}{\mathrm{d}(\mathbf{x},\mathbf{v})}(\dot{\mathbf{x}}, \dot{\mathbf{v}}) = \dot{\mathbf{x}} + \dot{\mathbf{v}}$. A local trivialization of $\mathcal{N}_\varepsilon X$ around $(\mathbf{x}, \mathbf{v})$ has tangent space $T_{\mathbf{x}}X \oplus N_{\mathbf{x}}X$. The derivative of the normal component $\dot{\mathbf{v}}$ splits into two components: one is due to movement in the normal space $N_{\mathbf{x}}X$, and one is due to curvature when moving in X. The derivative of φ_ε is thus given by the linear map $T_{\mathbf{x}}X \oplus N_{\mathbf{x}}X \to \mathbb{R}^n$, $(\mathbf{t}, \mathbf{z}) \mapsto \mathbf{t} + (\lambda \cdot L_{\mathbf{w}})\,\mathbf{t} + \mathbf{z}$, where $\mathbf{v} = \lambda \cdot \mathbf{w}$, $\lambda = \|\mathbf{v}\|$, and $L_{\mathbf{w}}$ is the Weingarten operator from (6.8). A matrix representation of the derivative of φ_ε with respect to orthonormal bases therefore is

$$A(\mathbf{x}, \mathbf{v}) = \begin{pmatrix} I_m + \lambda \cdot L_{\mathbf{w}} & 0 \\ 0 & I_{n-m} \end{pmatrix}, \qquad m = \dim X. \tag{6.13}$$

In fact, since $\lambda = \|\mathbf{v}\| < \tau(X)$, the eigenvalues of $\lambda \cdot L_{\mathbf{w}}$ are all of absolute value at most 1, so that $|\det(A(\mathbf{x}, \mathbf{v}))| = \det(I_m + \lambda \cdot L_{\mathbf{w}})$. The change of variables $\mathbf{v} \to (\mathbf{w}, \lambda)$ has Jacobian determinant λ^{n-m-1}. Plugging all this into equation (6.12), we finally arrive at

$$\operatorname{vol}(\operatorname{Tube}(X, \varepsilon)) = \int_{\mathbf{x}\in X} \int_0^\varepsilon \int_{\mathbf{w}\in N_{\mathbf{x}}X : \|\mathbf{w}\|=1} \lambda^{n-m-1} \cdot \det(I_m + \lambda \cdot L_{\mathbf{w}}) \, \mathrm{d}\mathbf{w} \, \mathrm{d}\lambda \, \mathrm{d}\mathbf{x}.$$

Expanding the characteristic polynomial in this expression, we see that $\operatorname{vol}(\operatorname{Tube}(X, \varepsilon))$ is given by a polynomial in ε of degree n whose coefficients are integrals of the principal minors of the Weingarten map $L_{\mathbf{v}}$ over X. Since $L_{-\mathbf{v}} = -L_{\mathbf{v}}$, the integrals over the odd-dimensional minors of $L_{\mathbf{v}}$ vanish. All this leads to the following theorem.

Theorem 6.20 (Weyl's tube formula [177]) *In the notation above, we have*

$$\operatorname{vol}(\operatorname{Tube}(X, \varepsilon)) = \sum_{0 \le 2i \le m} \kappa_{2i}(X) \cdot \varepsilon^{n-m+2i}.$$

The coefficients $\kappa_{2i}(X)$ of this polynomial are called curvature coefficients of X. Explicitly, we have

$$\kappa_{2i}(X) = \frac{1}{n-m+2i} \int_{\mathbf{x}\in X} \int_{\mathbf{w}\in N_{\mathbf{x}}X : \|\mathbf{w}\|=1} m_{2i}(L_{\mathbf{w}}) \, \mathrm{d}\mathbf{w} \, \mathrm{d}\mathbf{x},$$

where $m_i(\,\cdot\,)$ denotes the sum of the $2i$-principal minors.

In fact, the curvature coefficient $\kappa_0(X)$ is always equal to the m-dimensional volume of X times the volume of the unit ball $B^{n-m} = \{\mathbf{x} \in \mathbb{R}^{n-m} \mid \|\mathbf{x}\| \le 1\}$ This leads to the following corollary.

Corollary 6.21 *The volume of X can be obtained as the following limit:*

$$\mathrm{vol}(X) = \lim_{\varepsilon \to 0} \frac{\mathrm{vol}(\mathrm{Tube}(X, \varepsilon))}{\varepsilon^{n-m} \cdot \mathrm{vol}(B^{n-m})}.$$

We close this chapter by discussing Weyl's tube formula in two special cases.

Example 6.22 (Curves) If $X \subset \mathbb{R}^n$ is a smooth algebraic curve, then

$$\mathrm{vol}(\mathrm{Tube}(X, \varepsilon)) = \varepsilon^{n-1} \cdot \mathrm{vol}(B^{n-1}) \cdot \mathrm{length}(X).$$

For instance, the volume of the ε-tube around a plane curve C is $2\varepsilon \cdot \mathrm{length}(C)$.

Example 6.23 (Surfaces in 3-space) Let $S = \{f(\mathbf{x}) = 0\} \subset \mathbb{R}^3$ be a compact smooth algebraic surface. Let $\chi(S)$ be the Euler characteristic of S. Then, the volume of its ε-tube for $\varepsilon < \tau(S)$ is

$$2\varepsilon \,\mathrm{area}(S) + \varepsilon^3 \,\mathrm{vol}(B^3)\, \chi(S).$$

Let us prove this. Weyl's tube formula implies that

$$\mathrm{vol}(\mathrm{Tube}(S, \varepsilon)) = 2\varepsilon \,\mathrm{area}(S) + \varepsilon^3 \kappa_2(S).$$

The coefficient $\kappa_2(S)$ is the integral of the Gauss curvature:

$$\kappa_2(S) = \frac{2}{3} \int_{\mathbf{x} \in S} \det(L_{N(\mathbf{x})}) \, \mathrm{d}\mathbf{x},$$

where $N(\mathbf{x}) = \|\nabla f(\mathbf{x})\|^{-1} \cdot \nabla f(\mathbf{x})$ denotes the normal field of S at $\mathbf{x}$ given by the gradient of f. Notice that S is orientable – the orientation is given by the normal field $N(\mathbf{x})$. The Gauss-Bonnet theorem (see, e.g., [121, Theorem 9.3.]) implies that the integral over the Gauss curvature is $2\pi \cdot \chi(S)$, Moreover, the volume of the three-dimensional ball is $\mathrm{vol}(B^3) = 4\pi/3$.

Chapter 7
Medial Axis and Reach

The *medial axis* $\mathrm{Med}(X)$ of a subset $X \subset \mathbb{R}^n$ is the set of points $\mathbf{u} \in \mathbb{R}^n$ such that there exist at least two points on X minimizing the distance to $\mathbf{u}$. In this section, we consider the case when $X \subset \mathbb{R}^n$ is a real variety. Then, the medial axis is semialgebraic and we can study its complex Zariski closure

$$M_X := \overline{\mathrm{Med}(X)},$$

called the *algebraic medial axis* of X.

Example 7.1 Consider the parabola $X = V(x_2 - x_1^2)$. We compute the algebraic medial axis of X. If $\mathbf{x} = (x_1, x_2) \in X$ minimizes the distance to a point $\mathbf{u} = (u_1, u_2) \in \mathbb{R}^2$, we must have $\langle \mathbf{x} - \mathbf{u}, \mathbf{t} \rangle = 0$, where $\mathbf{t}$ spans the tangent space $T_{\mathbf{x}}X$. We use `Macaulay2` [77]:

```
R = QQ[x1, x2, y1, y2, u1, u2];
fx = x2 - x1^2; fy = y2 - y1^2;
Jx = matrix {{x1-u1, x2-u2}, {diff(x1, fx), diff(x2, fx)}};
Jy = matrix {{y1-u1, y2-u2}, {diff(y1, fy), diff(y2, fy)}};
distxu = (x1 - u1)^2 + (x2 - u2)^2;
distyu = (y1 - u1)^2 + (y2 - u2)^2;
I = ideal {fx, fy, det(Jx), det(Jy), distxu - distyu};
K = saturate(I, ideal {x1-y1, x2-y2});
eliminate({x1, x2, y1, y2}, K)
```

This returns the ideal $\langle u_1 \rangle$. Indeed, the medial axis is

$$\mathrm{Med}(X) = \left\{ (0, u_2) \;\middle|\; u_2 \geq \tfrac{1}{2} \right\},$$

so that the algebraic medial axis is $M_X = \{u_1 = 0\}$ (see also Figure 7.4 below). ◇

In Definition 6.19 we have introduced the reach of a smooth variety X. The next proposition shows that the reach is intimately linked with the medial axis. In fact, it can even be used as a definition for the reach of singular varieties. We provide yet another equivalent formulation of the reach in Theorem 7.6.

Proposition 7.2 *The distance from a real variety X to its medial axis* $\mathrm{Med}(X)$ *is the reach* $\tau(X)$.

Proof We study the exponential map $\varphi_\varepsilon : \mathcal{N}_\varepsilon X \to \mathrm{Tube}(X, \varepsilon)$, $(\mathbf{x}, \mathbf{v}) \mapsto \mathbf{x} + \mathbf{v}$ defined in (6.10). For all $\varepsilon < \tau(X)$, that map φ_ε is a diffeomorphism. In that case, the tubular neighborhood $\mathrm{Tube}(X, \varepsilon)$ cannot contain any point from the medial axis $\mathrm{Med}(X)$, because otherwise φ_ε could not be injective. Hence, the distance from X to its medial axis $\mathrm{Med}(X)$ is at least $\tau(X)$.

Now we show the reverse inequality. For that, let $\varepsilon > 0$ be less than the distance from X to its medial axis $\mathrm{Med}(X)$. We consider a point $\mathbf{u} \in \mathrm{Tube}(X, \varepsilon)$. In particular, $\mathbf{u}$ is outside the Euclidean closure of $\mathrm{Med}(X)$. Thus, in a Euclidean neighborhood $U \subset \mathrm{Tube}(X, \varepsilon)$ of $\mathbf{u}$, the points have a unique closest point on X. This defines a smooth map $U \to X, \mathbf{u} \mapsto \mathbf{x}(\mathbf{u})$. The map $\psi_{\mathbf{u}} : U \to \mathcal{N}_\varepsilon X, \mathbf{u} \mapsto (\mathbf{x}(\mathbf{u}), \mathbf{u} - \mathbf{x}(\mathbf{u}))$ is then smooth with smooth inverse $\psi_{\mathbf{u}}^{-1} = \varphi_\varepsilon|_{\psi_{\mathbf{u}}(U)}$. Via a partition of unity of $\mathrm{Tube}(X, \varepsilon)$ (see e.g. [122, Chapter 2]), we can obtain a global smooth inverse of φ_ε from the local inverses $\psi_{\mathbf{u}}$. Hence, φ_ε is a diffeomorphism and $\varepsilon < \tau(X)$. □

As the medial axis, the reach of a real variety is an algebraic notion. More concretely, if X is smooth and defined by rational polynomials, then its reach $\tau(X)$ is an algebraic number over $\mathbb{Q}$. This was shown in [95, Proposition 3.14]. An example comes next.

Example 7.3 The reach of the parabola X in Example 7.1 is $\tau(X) = \frac{1}{2}$. It is obtained as the distance between $(0, 0) \in X$ and $(0, \frac{1}{2})$, which is a point in the Euclidean closure of $\mathrm{Med}(X)$.

7.1 Bottlenecks

We can characterize the reach of a smooth variety $X \subset \mathbb{R}^n$ in terms of maximal curvature and bottlenecks. Curvature is discussed in details in the previous chapter. We now introduce bottlenecks. Let $\mathbf{x}, \mathbf{y} \in X$ be two distinct points. If $\mathbf{x} - \mathbf{y}$ is normal to $T_{\mathbf{x}}X$ (i.e., for all $\mathbf{t} \in T_{\mathbf{x}}X$ we have $\langle \mathbf{x} + \mathbf{t}, \mathbf{x} - \mathbf{y} \rangle = 0$) and also normal to $T_{\mathbf{y}}X$, then we call $(\mathbf{x}, \mathbf{y})$ a *bottleneck*. Complex solutions to the corresponding system of polynomial equations are called complex bottleneck. Di Rocco, Eklund and Weinstein [55] gave an algorithm for computing the number of complex bottlenecks of a variety in terms of polar classes. The following theorem is their result for planar curves.

Theorem 7.4 *If X is a general curve in the plane of degree d, it has $\frac{1}{2}(d^4 - 5d^2 + 4d)$ complex bottlenecks.*

Example 7.5 We compute bottlenecks of the Trott curve $144(x^4 + y^4) - 225(x^2 + y^2) + 350x^2y^2 + 81 = 0$ using `HomotopyContinuation.jl` [26].

```
@var x y u v
f = 144*(x^4 + y^4) - 225*(x^2 + y^2) + 350*x^2*y^2 + 81
g = subs(f, x=>u, y=>v)
df = differentiate(f, [x; y])
dg = differentiate(g, [u; v])
N = [x-u; y-v]
bottlenecks = solve([f; g; det([N df]); det([N dg])])
```

By Theorem 7.4 there are $\frac{1}{2}(d^4 - 5d^2 + 4d) = 96$ complex bottlenecks. We find that 36 of them are real. They are marked in Figure 7.1. We note here that one point can appear in more than one bottleneck. ◇

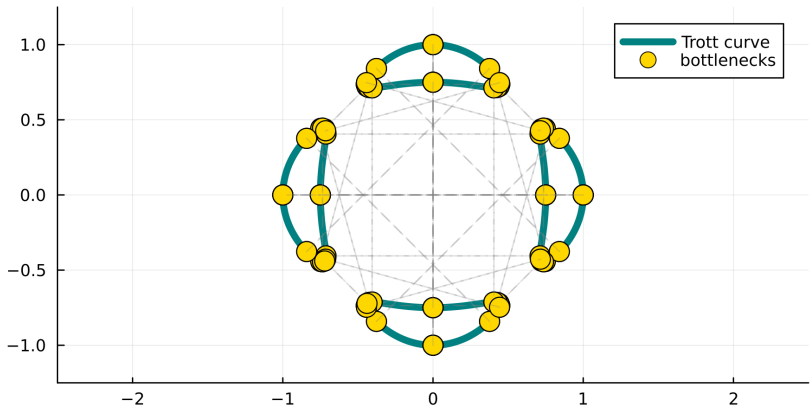

Fig. 7.1: Bottlenecks of the Trott curve $144(x^4 + y^4) - 225(x^2 + y^2) + 350x^2y^2 + 81 = 0$ are displayed as grey normal lines with yellow endpoints.

The *width* of a bottleneck is $b(\mathbf{x}, \mathbf{y}) := \frac{1}{2}\|\mathbf{x} - \mathbf{y}\|$. We denote the width of the smallest bottleneck of X by

$$B(X) := \min_{(\mathbf{x},\mathbf{y}) \text{ bottleneck of } X} b(\mathbf{x}, \mathbf{y}).$$

The next theorem links the reach of a smooth variety X to its bottlenecks and its maximal curvature $C(X)$ defined in (6.9).

Theorem 7.6 *If X is smooth, then*

$$\tau(X) = \min\left\{B(X),\ \frac{1}{C(X)}\right\}.$$

Proof Recall from (6.11) that the reach $\tau(X)$ is the supremum over all $\varepsilon > 0$ such that the exponential map $\varphi_\varepsilon : \mathcal{N}_\varepsilon X \to \mathrm{Tube}(X,\varepsilon)$, $(\mathbf{x},\mathbf{v}) \mapsto \mathbf{x}+\mathbf{v}$ is a diffeomorphism. Let

$$\varepsilon := \tau(X). \tag{7.1}$$

Then, for every $\varepsilon' > \varepsilon$, the exponential map $\varphi_{\varepsilon'}$ is not a diffeomorphism, which means that it is either not an immersion or it is not injective. Thus, there is a point $\mathbf{u} = \mathbf{x}+\mathbf{v} \in \mathbb{R}^n$, where $(\mathbf{x},\mathbf{v}) \in \mathcal{N}X$, at distance $\varepsilon = \|\mathbf{v}\|$ from X such that, for every $\varepsilon' > \varepsilon$, either the derivative of $\varphi_{\varepsilon'}$ at $(\mathbf{x},\mathbf{v})$ is not injective or $\varphi_{\varepsilon'}^{-1}(\mathbf{u})$ has at least two elements.

Suppose first that the derivative of each $\varphi_{\varepsilon'}$ at $(\mathbf{x},\mathbf{v})$ is not injective. Then it follows from (6.13) that ε^{-1} is a principal curvature at $\mathbf{x}$ in normal direction $-\varepsilon^{-1}\mathbf{v}$. Due to (7.1), ε is the smallest positive number with that property. Therefore, its inverse ε^{-1} must be the maximal curvature $C(X)$.

The remaining case to analyze is when each fiber $\varphi_{\varepsilon'}^{-1}(\mathbf{u})$ is larger one and the derivative of $\varphi_{\varepsilon'}$ at each point in that fiber is injective. We have two distinct points $\mathbf{x},\mathbf{y} \in X$ such that $\mathbf{u} = \mathbf{x}+\mathbf{v} = \mathbf{y}+\mathbf{w}$, where $(\mathbf{y},\mathbf{w}) \in \mathcal{N}X$ and $\delta := \|\mathbf{w}\| \le \varepsilon$. We distinguish two subcases. First, we assume that $\mathbf{u}$ lies on the line spanned by $\mathbf{x}$ and $\mathbf{y}$. Then, $(\mathbf{x},\mathbf{y})$ is a bottleneck. Moreover, $\mathbf{u}$ must be the midpoint between $\mathbf{x}$ and $\mathbf{y}$, since otherwise there would be a σ with $b(\mathbf{x},\mathbf{y}) < \sigma < \varepsilon$ and the fiber of the midpoint $\frac{1}{2}(\mathbf{x}+\mathbf{y})$ under φ_σ would contain at least two points, but the latter implies $\tau(X) \le \sigma < \varepsilon$; a contradiction to (7.1). Hence, $\varepsilon = b(\mathbf{x},\mathbf{y})$ and due to (7.1) there cannot be any smaller bottleneck, so that $\varepsilon = B(X)$ and we are done.

Second, we assume that $\mathbf{x},\mathbf{y},\mathbf{u}$ form a triangle. Since the derivative of $\varphi_{\varepsilon'}$ is injective at both $(\mathbf{x},\mathbf{v})$ and $(\mathbf{y},\mathbf{w})$, the inverse function theorem implies that existence of two locally defined and smooth maps $\mathbf{u} \mapsto \mathbf{x}(\mathbf{u})$ and $\mathbf{u} \mapsto \mathbf{y}(\mathbf{u})$ that project locally around $\mathbf{u}$ to X. These define two local smooth functions $d_\mathbf{x}(\mathbf{u}) := \|\mathbf{u}-\mathbf{x}(\mathbf{u})\|$ and $d_\mathbf{y}(\mathbf{u}) := \|\mathbf{u}-\mathbf{y}(\mathbf{u})\|$ that locally measure the distance to X. Their gradients are

$$\nabla d_\mathbf{x}(\mathbf{u}) = \varepsilon^{-1}(\mathbf{u}-\mathbf{x}) \quad \text{and} \quad \nabla d_\mathbf{y}(\mathbf{u}) = \delta^{-1}(\mathbf{u}-\mathbf{y});$$

see e.g. [76, Lemma 2.11] and also Remark 7.7. Let $\mathbf{a}$ be a unit norm vector that starts at $\mathbf{u}$, points inside the triangle with vertices $\mathbf{x},\mathbf{y},\mathbf{u}$ such that $\langle \mathbf{u}-\mathbf{x},\mathbf{a}\rangle < 0$ and $\langle \mathbf{u}-\mathbf{y},\mathbf{a}\rangle < 0$:

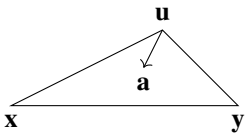

We get that the partial derivatives of $d_\mathbf{x}(\mathbf{u})$ and $d_\mathbf{y}(\mathbf{u})$ in direction $\mathbf{a}$ satisfy $\frac{\partial d_\mathbf{x}(\mathbf{u})}{\partial \mathbf{a}} < 0$ and $\frac{\partial d_\mathbf{y}(\mathbf{u})}{\partial \mathbf{a}} < 0$. This means that, when we move from $\mathbf{u}$ in direction $\mathbf{a}$, the local distances from $\mathbf{u}$ to X both decrease. Consequently, there is a $\sigma < \varepsilon$ such that φ_σ is not injective, hence $\tau(X) \le \sigma < \varepsilon$. This contradicts (7.1) and so $\mathbf{x},\mathbf{y},\mathbf{u}$ cannot form a triangle. □

Remark 7.7 As in the proof of Theorem 7.6 let d be a (locally) defined projection map to a variety X, such that $\mathbf{x} = d(\mathbf{u})$. An informal argument that shows $\nabla d(\mathbf{u}) = (\mathbf{u}-\mathbf{x})/\|\mathbf{u}-\mathbf{x}\|$ and that can be made rigorous goes as follows: Let us write $\mathbf{v} := (\mathbf{u}-\mathbf{x})/\|\mathbf{u}-\mathbf{x}\|$ for the unit normal direction. If we move from $\mathbf{u}$ infinitesimally in a direction that is perpendicular to $\mathbf{v}$, the distance $d(\mathbf{u})$ does not change. This means

that the derivative of $d(\mathbf{u})$ in a direction perpendicular to $\mathbf{v}$ is zero, hence the gradient of $d(\mathbf{u})$ must be a multiple of $\mathbf{v}$. On the other hand, $d(\mathbf{u} + t \cdot \mathbf{v}) = d(\mathbf{u}) + t$, which shows that the derivative of $d(\mathbf{u})$ in direction $\mathbf{v}$ is 1. Consequently, $\nabla d(\mathbf{u}) = \mathbf{v}$. In particular, the Weingarten map $L_{\mathbf{v}}$ can be obtained via the second derivative of $d(\mathbf{u})$. This is worked out in (7.4) below.

7.2 Offset Hypersurfaces

This section is based on the article [95]. We write $X_{\mathbb{C}}$ for the complex Zariski closure of X. We assume that X (and hence also $X_{\mathbb{C}}$) is irreducible.

The *ED correspondence* $\mathcal{E}_X$ of X is the Zariski closure of the set of tuples $(\mathbf{x}, \mathbf{u})$ with $\mathbf{x} \in X^{\mathrm{sm}}$ such that $\mathbf{x}$ is an ED-critical point for $\mathbf{u}$. We recall from Theorem 2.16 that

$$\mathcal{E}_X = \overline{\{(\mathbf{x}, \mathbf{x}+\mathbf{h}) \mid \mathbf{x} \in X^{\mathrm{sm}}, (\mathbf{x}, \mathbf{h}) \in N_X\}} \subseteq X_{\mathbb{C}} \times \mathbb{C}^n.$$

The branch locus of the projection $\mathcal{E}_X \to \mathbb{C}^n$ is called the *ED discriminant* or evolute. For planar curves, it coincides with the definition of the evolute above in Section 1.3. We denote it by $\Sigma_X \subset \mathbb{C}^n$.

For $\varepsilon \in \mathbb{C}$ and $\mathbf{u} \in \mathbb{C}^n$, the *$\varepsilon$-sphere around* $\mathbf{u}$ is the variety $S(\mathbf{u}, \varepsilon) := V(\|\mathbf{x} - \mathbf{u}\|^2 - \varepsilon^2)$.

Definition 7.8 The *offset correspondence* of X is

$$\mathrm{OC}_X = (\mathcal{E}_X \times \mathbb{C}) \cap \{(\mathbf{x}, \mathbf{u}, \varepsilon) \in \mathbb{C}^n \times \mathbb{C}^n \times \mathbb{C} \mid \mathbf{x} \in S(\mathbf{u}, \varepsilon)\}.$$

That is, OC_X is the complex Zariski closure of the set of tuples $(\mathbf{x}, \mathbf{u}, \varepsilon)$ such that $\mathbf{x}$ is an ED critical point for $\mathbf{u}$, and ε^2 is the squared Euclidean distance (over $\mathbb{R}$) between $\mathbf{x}$ and $\mathbf{u}$.

We consider the two coordinate projections $\pi_1 : \mathrm{OC}_X \to X_{\mathbb{C}}$ and $\pi_2 : \mathrm{OC}_X \to \mathbb{C}^n \times \mathbb{C}$. Clearly, π_1 is dominant, i.e., $\overline{\pi_1(\mathrm{OC}_X)} = X_{\mathbb{C}}$. However, the other projection is not:

Definition 7.9 We denote $\mathrm{Off}_X := \overline{\pi_2(\mathrm{OC}_X)} \subset \mathbb{C}^n \times \mathbb{C}$ and call it the *offset hypersurface* of X.

The next lemma justifies the name.

Lemma 7.10 $\operatorname{codim} \mathrm{Off}_X = 1$.

Proof The ED correspondence $\mathcal{E}_X$ is the Zariski closure of a vector bundle of rank $\operatorname{codim}(X)$ over X^{sm}, which shows that $\dim \mathcal{E}_X = n$. Since X is irreducible, $\mathcal{E}_X$ is irreducible. The offset correspondence OC_X is the intersection of $\mathcal{E}_X \times \mathbb{C}$, which is also irreducible, with a hypersurface. This implies $\dim \mathrm{OC}_X = n$. Because the Euclidean Distance Degree of X is finite, the projection π_2 has finite fibers generically, which implies $\dim \mathrm{Off}_X = n$. □

Remark 7.11 For a fixed radius $r > 0$, we can study the level set $\mathrm{Off}_{X,r} \subset \mathbb{C}^n$ that is the intersection of the offset hypersurface Off_X with the hypersurface $\varepsilon = r$. Figure 7.3 shows the level sets for $r = 0.5$ and $r = 1.25$, respectively, of the offset surface of a parabola.

The boundary of the tubular neighborhood $\mathrm{Tube}(X, r)$ is always contained in the real locus of $\mathrm{Off}_{X,r}$. In fact, the Euclidean boundary of $\mathrm{Tube}(X, r)$ is $\partial\mathrm{Tube}(X, r) = \{\mathbf{u} \in \mathbb{R}^n \mid d(\mathbf{u}, X) = r\}$. Thus, for any $\mathbf{u} \in \partial\mathrm{Tube}(X, r)$, there is a closest point $\mathbf{x} \in X$ with $\|\mathbf{x} - \mathbf{u}\| = r$. In particular, $\mathbf{x}$ is an ED critical point for $\mathbf{u}$ and $(\mathbf{x}, \mathbf{u}, r) \in \mathrm{OC}_X$, i.e., $\mathbf{u} \in \mathrm{Off}_{X,r}$.

For the parabola in Figure 7.3, the real locus of $\mathrm{Off}_{X,0.5}$ is equal to $\partial\mathrm{Tube}(X, 0.5)$, while $\partial\mathrm{Tube}(X, 1.25)$ is strictly contained in the real part of $\mathrm{Off}_{X,1.25}$. In this example, that change of behavior is governed by the reach $\tau(X) = 0.5$.

It follows from Lemma 7.10 that Off_X is the zero set of a polynomial that we denote by $g_X(\mathbf{u}, \varepsilon)$; i.e.,

$$\mathrm{Off}_X = V(g_X) \subset \mathbb{C}^n \times \mathbb{C}.$$

We call it the *offset polynomial*. It is also known as the *ED polynomial*. It is studied in detail in [139].

Example 7.12 Consider the parabola $X = V(x_2 - x_1^2)$. We compute the offset polynomial of the parabola in `Macaulay2` [77].

```
R = QQ[x1, x2, u1, u2, eps];
f = x2 - x1^2;  d = (x1-u1)^2 + (x2-u2)^2 - eps^2;
J = matrix {{x1-u1, x2-u2}, {diff(x1, f), diff(x2, f)}};
OC = ideal {f, det(J), d};
O = eliminate({x1, x2}, OC)
g = (gens O)_0_0
```

This gives $g_X(\mathbf{u}, \varepsilon) = g_0(\mathbf{u}) + g_1(\mathbf{u})\varepsilon^2 + g_2(\mathbf{u})\varepsilon^4 + g_3(\mathbf{u})\varepsilon^6$, where

$$\begin{aligned} g_0(\mathbf{u}) &= (u_1^2 - u_2)^2(16u_1^2 + 16u_2^2 - 8u_2 + 1), & g_2(\mathbf{u}) &= 48u_1^2 + 16u_2^2 + 32u_2 - 8, \\ g_1(\mathbf{u}) &= -48u_1^4 - 32u_1^2u_2^2 + 8u_1^2u_2 - 32u_2^3 - 20u_1^2 - 8u_2^2 + 8u_2 - 1, & g_3(\mathbf{u}) &= -16. \end{aligned}$$

Figure 7.2 shows the offset surface $g(\mathbf{u}, \varepsilon) = 0$. ◇

Fig. 7.2: The offset surface Off_X of the parabola. The surface is symmetric along the ε-axis, because only even powers of ε appear in the offset polynomial $g(\mathbf{u}, \varepsilon)$. The parabola itself is visible at level $\varepsilon = 0$. The image was created using `Surfer`.

Let us study some properties of the offset polynomial.

Proposition 7.13 *1. For a general $\mathbf{u} \in \mathbb{C}^n$, the zeros of $g_X(\mathbf{u}, \varepsilon)$ are precisely $\varepsilon = \pm\sqrt{\|\mathbf{u} - \mathbf{x}\|^2}$, where $\mathbf{x}$ ranges over all ED critical points for $\mathbf{u}$.*
2. The degree of the offset polynomial $g_X(\mathbf{u}, \varepsilon)$ in ε is two times the Euclidean distance degree of X.

Proof First, we observe that the projection $\mathrm{Off}_X \to \mathbb{C}^n$, $(\mathbf{u}, \varepsilon) \mapsto \mathbf{u}$ is dominant, because general points in $\mathbb{C}^n$ have ED-critical points on $X_{\mathbb{C}}$. Take a general $\mathbf{u} \in \mathbb{C}^n$. Then, $g_X(\mathbf{u}, \varepsilon) = 0$ if and only if there exists $\mathbf{x} \in X_{\mathbb{C}}$ with $(\mathbf{x}, \mathbf{u}) \in \mathcal{E}_X$ and $\varepsilon^2 = \|\mathbf{x} - \mathbf{u}\|^2$. Therefore, $\varepsilon = \pm\sqrt{\|\mathbf{u} - \mathbf{x}\|^2}$, where $\mathbf{x}$ ranges over all ED critical points for $\mathbf{u}$. In particular, this shows that $g_X(\mathbf{u}, \varepsilon)$ has $2 \cdot \mathrm{EDdeg}(X)$ many zeros for general $\mathbf{u}$. □

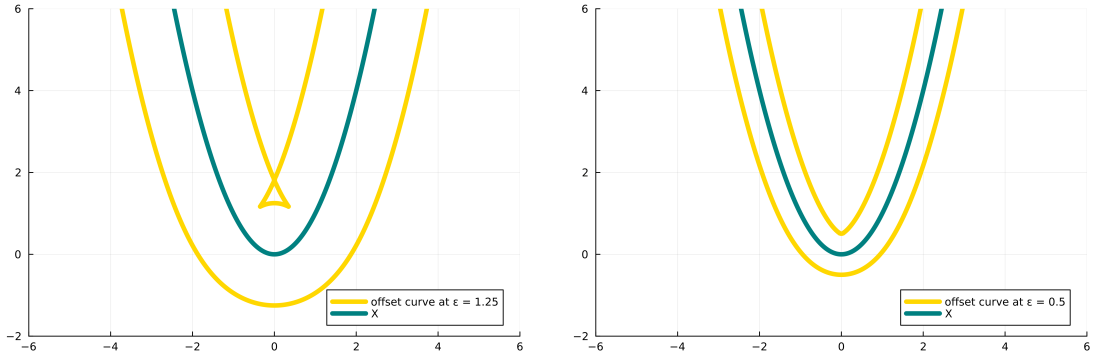

Fig. 7.3: The offset surface Off_X of the parabola intersected with the hypersurface $\varepsilon = 1.25$ and $\varepsilon = 0.5$.

Example 7.14 In Example 7.12, we see that $g_X(\mathbf{u}, \varepsilon)$ has degree six in ε. This corresponds to the fact that the Euclidean distance degree of the parabola is three. For instance, any point $\mathbf{u} \in \mathbb{R}^2$ in Figure 7.4 that is both above the green curve (the parabola) and the yellow curve (the evolute) has three real ED critical points on the parabola. ◇

The coefficients of the offset polynomial are studied in [139]. In particular, in that article one can find the following result.

Theorem 7.15 *If the variety X is general enough and $g_X(\mathbf{u}, \varepsilon) = c_0(\mathbf{u}) + c_1(\mathbf{u})\varepsilon + \cdots + c_k(\mathbf{u})\varepsilon^k$ is its offset polynomial, then $c_k(\mathbf{u})$ is constant.*

Proof See [139, Proposition 4.4]. □

We now understand that the offset polynomial $g_X(\mathbf{u}, \varepsilon)$ encodes for a fixed $\mathbf{u} \in \mathbb{R}^n$ the distances from $\mathbf{u}$ to its ED-critical points on X. We can combine this insight with Remark 7.7 to compute a unit normal field from the ED-polynomial. In fact, if $(\mathbf{u}, \varepsilon) \in \mathbb{R}^n \times \mathbb{R}$ is a real zero of g_X, then it follows from Remark 7.7 that the gradient $\frac{\mathrm{d}\varepsilon}{\mathrm{d}\mathbf{u}}(\mathbf{u}, \varepsilon)$ is a unit normal vector pointing from a real ED-critical point on X towards $\mathbf{u}$. Differentiating the equation $g_X(\mathbf{u}, \varepsilon) = 0$, we obtain

$$\nabla\varepsilon := \frac{\mathrm{d}\varepsilon}{\mathrm{d}\mathbf{u}}(\mathbf{u}, \varepsilon) = -\left(\frac{\partial g_X}{\partial \varepsilon}\right)^{-1} \cdot \frac{\partial g_X}{\partial \mathbf{u}} \in \mathbb{R}^n. \tag{7.2}$$

In a similar manner, we can compute the second fundamental form of X from the second derivatives of g_X. Namely, differentiating (7.2) we obtain the following formula for the Hessian matrix of ε:

$$\frac{\mathrm{d}^2\varepsilon}{\mathrm{d}\mathbf{u}^2} = -\left(\frac{\partial g_X}{\partial \varepsilon}\right)^{-1} \cdot \left(\frac{\partial^2 g_X}{\partial \mathbf{u}^2} + \frac{\partial^2 g_X}{\partial \varepsilon^2} \cdot \nabla\varepsilon\,(\nabla\varepsilon)^T + 2\nabla\varepsilon \left(\frac{\partial(\partial g_X/\partial\varepsilon)}{\partial \mathbf{u}}\right)^T\right) \in \mathbb{R}^{n\times n}. \tag{7.3}$$

If $\mathbf{x} \in X$ is the ED-critical point corresponding to $(\mathbf{u}, \varepsilon)$ and $\mathbf{t} \in T_{\mathbf{x}}X$ is a tangent vector, then by definition of the second fundamental form (6.7) we have that $\mathrm{II}_{\mathbf{u}-\mathbf{x}}(\mathbf{t})$ is the directional derivative of the unit normal field $\nabla\varepsilon = \frac{\mathrm{d}\varepsilon}{\mathrm{d}\mathbf{u}}$ in direction $\mathbf{t}$. That is, we have $\mathrm{II}_{\mathbf{u}-\mathbf{x}}(\mathbf{t}) = \mathbf{t}^T \left(\frac{\mathrm{d}}{\mathrm{d}\mathbf{x}} \frac{\mathrm{d}\varepsilon}{\mathrm{d}\mathbf{u}}(\mathbf{x}, 0)\right) \mathbf{t}$. We can rewrite this using the second derivative in (7.3) as

$$\mathrm{II}_{\mathbf{u}-\mathbf{x}}(\mathbf{t}) = \lim_{s\to 0} \mathbf{t}^T \left(\frac{\mathrm{d}^2\varepsilon}{\mathrm{d}\mathbf{u}^2}(\mathbf{x} + s(\mathbf{u} - \mathbf{x}),\ s\varepsilon)\right) \mathbf{t}, \tag{7.4}$$

which we can see as follows. We have shown in (6.13) that

$$\frac{\mathrm{d}\mathbf{u}}{\mathrm{d}\mathbf{x}} = I_n + \varepsilon \cdot \begin{pmatrix} L_{\nabla\varepsilon} & 0 \\ 0 & 0 \end{pmatrix},$$

where $L_{\nabla\varepsilon}$ is the Weingarten map. Hence, applying the chain rule yields

$$\frac{\mathrm{d}}{\mathrm{d}\mathbf{x}}\frac{\mathrm{d}\varepsilon}{\mathrm{d}\mathbf{u}} = \frac{\mathrm{d}^2\varepsilon}{\mathrm{d}\mathbf{u}^2} \cdot \frac{\mathrm{d}\mathbf{u}}{\mathrm{d}\mathbf{x}} = \frac{\mathrm{d}^2\varepsilon}{\mathrm{d}\mathbf{u}^2}\left(I_n + \varepsilon \cdot \begin{pmatrix} L_{\nabla\varepsilon} & 0 \\ 0 & 0 \end{pmatrix}\right).$$

Evaluating this equation at $(\mathbf{x} + s(\mathbf{u} - \mathbf{x}),\ s\varepsilon)$, we obtain

$$\frac{\mathrm{d}^2\varepsilon}{\mathrm{d}\mathbf{u}^2}(\mathbf{x} + s(\mathbf{u} - \mathbf{x}), s\varepsilon) = \frac{\mathrm{d}}{\mathrm{d}\mathbf{x}}\frac{\mathrm{d}\varepsilon}{\mathrm{d}\mathbf{u}}(\mathbf{x} + s(\mathbf{u} - \mathbf{x}), s\varepsilon) - s\varepsilon \cdot \left(\frac{\mathrm{d}^2\varepsilon}{\mathrm{d}\mathbf{u}^2} \cdot \begin{pmatrix} L_{\nabla\varepsilon} & 0 \\ 0 & 0 \end{pmatrix}\right)(\mathbf{x} + s(\mathbf{u} - \mathbf{x}), s\varepsilon).$$

In the limit $s \to 0$, the right-hand side becomes $\frac{\mathrm{d}}{\mathrm{d}\mathbf{x}}\frac{\mathrm{d}\varepsilon}{\mathrm{d}\mathbf{u}}(\mathbf{x}, 0)$, which shows (7.4).

Remark 7.16 The effect that curvature has on taking the derivative of $\mathbf{u}$ with respect to $\mathbf{x}$ can be observed in the case of the parabola in Figure 6.2.

Example 7.17 We compute the expression (7.2) for the parabola $X = V(x_2 - x_1^2)$ from Example 7.12. Namely, $\frac{\mathrm{d}\varepsilon}{\mathrm{d}\mathbf{u}}(\mathbf{u}, \varepsilon) = (h_1, h_2)$, where

$$h_1 = \frac{-96u_1\varepsilon^4 + \left(192u_1^3 + 64u_1u_2^2 - 16u_1u_2 + 40u_1\right)\varepsilon^2 - 4u_1\left(u_1^2 - u_2\right)\left(24\,u_1^2 + 16\,u_2^2 - 16\,u_2 + 1\right)}{-96\varepsilon^5 + \left(192u_1^2 + 64u_2^2 + 128u_2 - 32\right)\varepsilon^3 + \left(-96u_1^4 - 64u_1^2u_2^2 + 16u_1^2u_2 - 64u_2^3 - 40u_1^2 - 16u_2^2 + 16u_2 - 2\right)\varepsilon}$$

$$h_2 = \frac{\left(-32u_2 - 32\right)\varepsilon^4 + \left(64u_1^2u_2 - 8u_1^2 + 96u_2^2 + 16u_2 - 8\right)\varepsilon^2 - 2\left(u_1^2 - u_2\right)\left(16\,u_1^2u_22 - 20\,u_1^2 - 32\,u_2^2 + 12\,u_2 - 1\right)}{-96\varepsilon^5 + \left(192u_1^2 + 64u_2^2 + 128u_2 - 32\right)\varepsilon^3 + \left(-96u_1^4 - 64u_1^2u_2^2 + 16u_1^2u_2 - 64u_2^3 - 40u_1^2 - 16u_2^2 + 16u_2 - 2\right)\varepsilon}.$$

For instance, if we plug in $(u_1, u_2, \varepsilon) = (0, \frac{1}{4}, \frac{1}{4})$, we obtain $(h_1, h_2) = (0, 1)$, which is the unit normal vector on the parabola at $\mathbf{x} = (0, 0)$ pointing towards $\mathbf{u} = (0, \frac{1}{4})$. Now we compute the second derivative of ε using the formula in (7.3), evaluate it at $(u_1, u_2, \varepsilon) = (0, s, s)$ and let $s \to 0, s > 0$. This yields the matrix

$$A := \begin{pmatrix} -2 & 0 \\ 0 & 0 \end{pmatrix}.$$

By (7.4), the (signed) curvature of the parabola at $\mathbf{x} = (0, 0)$ is $\mathbf{t}^T A\mathbf{t} = -2$, where $\mathbf{t} = (1, 0)^T$ is the tangent direction of X at $\mathbf{x}$. We remark that in Example 7.3 we have shown that the reach of X is $\frac{1}{2}$. This is confirms Theorem 7.6, which states that the reach of the parabola is equal to the inverse of its maximal curvature $C(X)$ (a parabola has no real bottlenecks). Indeed, the curvature of a parabola is maximal at the apex. ⋄

7.3 Offset Discriminant

If $\mathbf{u}$ is on the medial axis, $g_X(\mathbf{u}, \varepsilon)$ must have a double root in ε. This motivates us to study the discriminant of the offset polynomial in ε.

Definition 7.18 The *offset discriminant* is the polynomial

$$\delta_X(\mathbf{u}) := \mathrm{Disc}_\varepsilon\, g_X(\mathbf{u}, \varepsilon).$$

Its zero set is denoted $\Delta_X^{\mathrm{Off}} := V(\delta_X) \subset \mathbb{C}^n$.

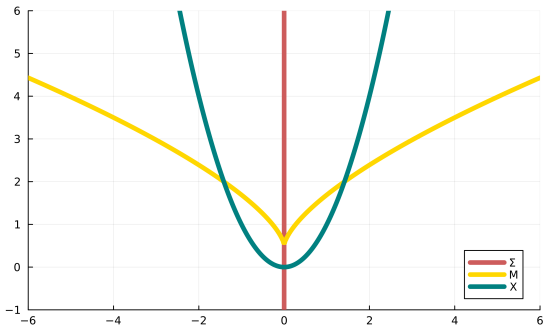

Fig. 7.4: The offset discriminant of the parabola $X = V(x_2 - x_1^2)$ has three real components: the parabola itself (green), the algebraic medial axis M_X (the red vertical line) and the ED-discriminant or evolute Σ_X (the yellow cubic curve).

Example 7.19 Using `Macaulay2` [77] we compute the discriminant of the offset polynomial of the parabola from Example 7.12. We get

$$\delta_X(\mathbf{u}) = u_1^4 \cdot (u_1^2 - u_2) \cdot \delta_1(\mathbf{u})^6 \cdot \delta_2(\mathbf{u}),$$

where

$$\delta_1(\mathbf{u}) = -27u_1^2 + 2(2u_2 - 1)^3 \quad \text{and} \quad \delta_2(\mathbf{u}) = 16u_1^2 + (4u_2 - 1)^2.$$

The factor $\delta_2(\mathbf{u})$ has no real zeros, and $u_1^2 - u_2$ is the polynomial of X. The real zero locus of the other factors u_1 and $\delta_1(\mathbf{u})$ are shown in Figure 7.4. The medial axis of the parabola is $\mathrm{Med}(X) = \{(0, u_2) \mid u_2 \geq \frac{1}{2}\}$ and $u_1 = 0$ is the Zariski closure of $\mathrm{Med}(X)$. The variety $\delta_1(\mathbf{u}) = 0$ is the ED-discriminant or evolute of the parabola, also known as the *semicubical parabola*. Above the evolute a point $\mathbf{u} \in \mathbb{R}^2$ has three real ED critical points on X, and below the evolute it has one real and two complex ED critical points. ⋄

The discriminant Δ_X^{Off} in the previous example we observed had three real components: the variety X, its algebraic medial axis and its evolute. We show that this is a general fact, following [95]. For that, we define the *bisector hypersurface* Bis_X of X: Writing $\mathrm{Bl}_X \subset \mathbb{C}^n \times \mathbb{C}$ for the branch locus of the projection $\pi_2 : \mathrm{OC}_X \to \mathbb{C}^n \times \mathbb{C}$, the bisector hypersurface is the union of the branch points u when varying over all ε:

$$\mathrm{Bis}_X := \bigcup_{(u,\varepsilon) \in \mathrm{Bl}_X} u.$$

Theorem 7.20 *The components of the offset discriminant are*

$$\Delta_X^{\mathrm{Off}} = \mathrm{Bis}_X \cup \Sigma_X \supseteq X_{\mathbb{C}} \cup M_X \cup \Sigma_X.$$

Its real components are the real parts of X, M_X, and Σ_X.

Proof By Proposition 7.13, the offset discriminant is the locus of those $\mathbf{u}$ such that $g_X(\mathbf{u}, \varepsilon)$ has less then $2 \times \mathrm{EDdeg}(X)$ distinct complex solutions. This can happen due to two reasons: $\mathbf{u}$ has either less than $\mathrm{EDdeg}(X)$ distinct ED critical points on X or two distinct ED critical points

$$\mathbf{x}_1 \neq \mathbf{x}_2 \text{ with } \|\mathbf{x}_1 - \mathbf{u}\|^2 = \|\mathbf{x}_2 - \mathbf{u}\|^2. \tag{7.5}$$

The first case is the ED discriminant Σ_X and second case the bisector hypersurface Bis_X. By definition, the medial axis $\mathrm{Med}(X)$ is contained in Bis_X, and thus we also have the inclusion $M_X \subseteq \mathrm{Bis}_X$. Since the ε that come from zeros of $g_X(\mathbf{u}, \varepsilon)$ come in signed pairs (cf. Proposition 7.13), we see that $X \times \{0\}$ is doubly covered by the projection π_2, meaning that $X \subseteq \mathrm{Bis}_X$. All other components of Bis_X besides $X \cup M_X$ consist of non-real points $\mathbf{u}$ that have ED critical points as in (7.5). □

Chapter 8
Voronoi Cells

Every real algebraic variety determines a Voronoi decomposition of its ambient Euclidean space. Each Voronoi cell is a convex semialgebraic set in the normal space of the variety at a point. In this chapter we study such Voronoi cells of algebraic varieties, with primary focus on their algebraic boundaries.

Metric algebraic geometry is concerned with properties of real algebraic varieties that depend on a distance metric. Key concepts include the Euclidean distance degree [60], distance function [140], bottlenecks [56, 68], reach, offset hypersurfaces, medial axis [94], and cut locus [47]. Voronoi cells are also an important topic in metric algebraic geometry. We here consider them only for the Euclidean metric, but it also makes much sense to study Voronoi cells with respect to Kullback-Leibler divergence [3] or Wasserstein distance [14].

8.1 Voronoi Basics

We begin with the familiar case when the given variety X is a finite subset of the Euclidean space $\mathbb{R}^n$. The *Voronoi cell* of a point $\mathbf{y} \in X$ consists of all points whose closest point in X is $\mathbf{y}$, i.e.

$$\mathrm{Vor}_X(\mathbf{y}) \;:=\; \bigl\{ \mathbf{u} \in \mathbb{R}^n : \mathbf{y} \in \arg\min_{\mathbf{x}\in X} \|\mathbf{x}-\mathbf{u}\|^2 \bigr\}. \tag{8.1}$$

This is a convex polyhedron with at most $|X|-1$ facets. The study of these cells, and how they depend on the configuration X, is ubiquitous in computational geometry and its numerous applications.

Proposition 8.1 *The Voronoi cell of a point* $\mathbf{y}$ *in the finite set* $X \subset \mathbb{R}^n$ *is the polyhedron*

$$\mathrm{Vor}_X(\mathbf{y}) \;=\; \bigl\{ \mathbf{u} \in \mathbb{R}^n \,:\, \mathbf{u}\cdot(\mathbf{x}-\mathbf{y}) \,\leq\, \frac{1}{2}\bigl(||\mathbf{x}||^2 - ||\mathbf{y}||^2\bigr) \;\textit{for all}\; \mathbf{x} \in X\backslash\{\mathbf{y}\} \bigr\}. \tag{8.2}$$

Proof By definition, $\mathrm{Vor}_X(\mathbf{y})$ consists of all points $\mathbf{u}$ such that $||\mathbf{x}-\mathbf{u}||^2 - ||\mathbf{y}-\mathbf{u}||^2$ is nonnegative for all $\mathbf{x} \in X\backslash\{\mathbf{y}\}$. But, this expression is equal to $||\mathbf{x}||^2 - ||\mathbf{y}^2|| - 2\,\mathbf{u}\cdot(\mathbf{x}-\mathbf{y})$. The main point is that the quadratic term drops out, so the expression is linear in $\mathbf{u}$. □

The collection of all Voronoi cells, as $\mathbf{y}$ ranges over the set X, is known as the *Voronoi diagram* of X. The Voronoi diagram is a polyhedral subdivision of $\mathbb{R}^n$ into finitely many convex cells.

We now shift gears, and we replace the finite set X by a real algebraic variety of positive dimension. As before, the ambient space is $\mathbb{R}^n$ with its standard Euclidean metric. We seek the Voronoi diagram $\{\mathrm{Vor}_X(\mathbf{y})\}_{\mathbf{y}\in X}$ in $\mathbb{R}^n$ where $\mathbf{y}$ runs over all (infinitely many) points in X.

One approach is to take a large but finite sample from X and to consider the Voronoi diagram of that sample. This is a finite approximation to the desired limit object. By taking finer and finer samples, the Voronoi diagram should converge nicely to a subdivision with infinitely many regions. The Voronoi cells in the limit are convex sets. However, for $n \geq 3$, they are generally not polyhedra. This process was studied by Brandt and Weinstein in [22] for the case when $n = 2$ and X is a curve. In [22, Figure 1] we see this for a quartic curve. The authors posted a delightful YouTube video, called *Mathemaddies' Ice Cream Map*. Please do watch that movie! Their curve X is the shoreline that separates the city of Berkeley from the San Francisco Bay. One hopes to find many ice cream shops at the shore.

Let X be a real algebraic variety of codimension c in $\mathbb{R}^n$, and consider a point $\mathbf{y} \in X$. The Voronoi cell $\mathrm{Vor}_X(\mathbf{y})$ is defined as before. It consists of all points $\mathbf{u}$ in $\mathbb{R}^n$ such that $\mathbf{y}$ is closer or equal to $\mathbf{u}$ than any other point $\mathbf{x} \in X$. The equation (8.2) still holds, and we conclude that $\mathrm{Vor}_X(\mathbf{y})$ is a convex set.

Proposition 8.2 *Suppose that* $\mathbf{y}$ *is a smooth point of the variety* X*. Then its Voronoi cell* $\mathrm{Vor}_X(\mathbf{y})$ *is a convex semialgebraic set of dimension* c*. This Voronoi cell is contained in the* normal space

$$N_X(\mathbf{y}) \;=\; \bigl\{\mathbf{u} \in \mathbb{R}^n \,:\, \mathbf{u}-\mathbf{y} \;\textit{is perpendicular to the tangent space of}\; X \;\textit{at}\; \mathbf{y}\bigr\} \;\simeq\; \mathbb{R}^c.$$

Proof Fix $\mathbf{u} \in \mathrm{Vor}_X(y)$. Consider any point $\mathbf{x}$ in X that is close to $\mathbf{y}$, and set $\mathbf{v} = \mathbf{x} - \mathbf{y}$. The inequality in (8.2) implies $\mathbf{u} \cdot \mathbf{v} \leq \frac{1}{2}(||\mathbf{y}+\mathbf{v}||^2 - ||\mathbf{y}||^2) = \mathbf{y} \cdot \mathbf{v} + \frac{1}{2}||\mathbf{v}||^2$. For any $\mathbf{w}$ in the tangent space of X at $\mathbf{y}$, there exists $\mathbf{v} = \epsilon\mathbf{w} + O(\epsilon^2)$ such that $\mathbf{x} = \mathbf{y} + \mathbf{v}$ is in X. The inequality above yields $\mathbf{u} \cdot \mathbf{w} \leq \mathbf{y} \cdot \mathbf{w}$, and the same with $-\mathbf{w}$ instead of $\mathbf{w}$. Then $(\mathbf{u} - \mathbf{y}) \cdot \mathbf{w} = 0$, and hence $\mathbf{u}$ is in the normal space $N_X(\mathbf{y})$. We already argued that $\mathrm{Vor}_X(\mathbf{y})$ is convex. It is semialgebraic, by Tarski's Theorem on Quantifier Elimination. This allows us to eliminate $\mathbf{x}$ from the formula (8.2). Finally, the Voronoi cell $\mathrm{Vor}_X(\mathbf{y})$ is full-dimensional in the c-dimensional space $N_X(\mathbf{y})$ because every point $\mathbf{u}$ in an ϵ-neighborhood of $\mathbf{y}$ has a unique closest point in X. Moreover, if $\mathbf{u} \in N_X(y)$ then that closest point must be $\mathbf{y}$, by the same inequality as above. □

The topological boundary of the Voronoi cell $\mathrm{Vor}_X(\mathbf{y})$ in the normal space $N_X(\mathbf{y})$ is denoted by $\partial\mathrm{Vor}_X(\mathbf{y})$. It consists of all points in $N_X(\mathbf{y})$ that have at least two closest points in X, including $\mathbf{y}$. We are interested in the *algebraic boundary* $\partial_{\mathrm{alg}}\mathrm{Vor}_X(\mathbf{y})$. This is the hypersurface in the complex affine space $N_X(\mathbf{y})_{\mathbb{C}} \simeq \mathbb{C}^c$ obtained as the Zariski closure of $\partial\mathrm{Vor}_X(\mathbf{y})$ over the field of definition of X. The degree of this hypersurface is denoted $\delta_X(\mathbf{y})$ and called the *Voronoi degree* of X at $\mathbf{y}$. If X is irreducible and $\mathbf{y}$ is a general point on X, then this degree does not depend on the choice of $\mathbf{y}$.

Example 8.3 (Surfaces in 3-space) Fix a general polynomial $f \in \mathbb{Q}[x_1, x_2, x_3]$ of degree $d \geq 2$ and let $X = V(f)$ be its surface in $\mathbb{R}^3$. The normal space at a general point $\mathbf{y} \in X$ is the line $N_X(\mathbf{y}) = \{\mathbf{y} + \lambda(\nabla f)(\mathbf{y}) : \lambda \in \mathbb{R}\}$. The Voronoi cell $\mathrm{Vor}_X(\mathbf{y})$ is a (possibly unbounded) line segment in $N_X(\mathbf{y})$ that contains $\mathbf{y}$. The boundary $\partial\mathrm{Vor}_X(\mathbf{y})$ consists of at most two points from among the zeros of an irreducible polynomial in $\mathbb{Q}[\lambda]$. We shall see that this univariate polynomial has degree $d^3 + d - 7$. Its complex zeros form the algebraic boundary $\partial_{\mathrm{alg}}\mathrm{Vor}_X(\mathbf{y})$. Thus, the Voronoi degree of the surface X is $d^3 + d - 7$.

Note that, in this example, our hypothesis "over the field of definition" becomes important. The $\mathbb{Q}$-Zariski closure of one boundary point is the collection of all $d^3 + d - 7$ points in $\partial_{\mathrm{alg}}\mathrm{Vor}_X(\mathbf{y})$.

For a numerical example, we take the degree to be $d = 2$ and we fix $\mathbf{y} = (0, 0, 0)$. Our quadric is $f = x_1^2 + x_2^2 + x_3^2 - 3x_1x_2 - 5x_1x_3 - 7x_2x_3 + x_1 + x_2 + x_3$. Let $r_0 \approx -0.209$, $r_1 \approx -0.107$, $r_2 \approx 0.122$ be the roots of the cubic polynomial $368\lambda^3 + 71\lambda^2 - 6\lambda - 1$. The Voronoi cell $\mathrm{Vor}_X(\mathbf{y})$ is the line segment connecting the points (r_1, r_1, r_1) and (r_2, r_2, r_2). The topological boundary $\partial\mathrm{Vor}_X(\mathbf{y})$ consists of the two points (r_1, r_1, r_1) and (r_2, r_2, r_2), whereas the algebraic boundary $\partial_{\mathrm{alg}}\mathrm{Vor}_X(\mathbf{y})$ also contains (r_0, r_0, r_0).

The cubic polynomial in the unknown λ was found with the algebraic method that is described in the next section. Namely, the Voronoi ideal in (8.3) equals $\mathrm{Vor}_I(0) = \langle u_1 - u_3,\ u_2 - u_3,\ 368u_3^3 + 71u_3^2 - 6u_3 - 1\rangle$. This is a maximal ideal in $\mathbb{Q}[u_1, u_2, u_3]$, and it defines a field extension of degree 3 over $\mathbb{Q}$.

Example 8.4 (Curves in 3-space) Let X be a general algebraic curve in $\mathbb{R}^3$. For $\mathbf{y} \in X$, the Voronoi cell $\mathrm{Vor}_X(\mathbf{y})$ is a convex set in the normal plane $N_X(\mathbf{y}) \simeq \mathbb{R}^2$. Its algebraic boundary $\partial_{\mathrm{alg}}\mathrm{Vor}_X(\mathbf{y})$ is a plane curve of degree $\delta_X(\mathbf{y})$. This Voronoi degree can be expressed in terms of the degree and genus of X. Specifically, this degree is 12 when X is the intersection of two general quadrics in $\mathbb{R}^3$. Figure 8.1 shows one such quartic space curve X together with the normal plane at a point $\mathbf{y} \in X$. The Voronoi cell $\mathrm{Vor}_X(\mathbf{y})$ is the planar convex region highlighted on the right. Its algebraic boundary $\partial_{\mathrm{alg}}\mathrm{Vor}_X(\mathbf{y})$ is a curve of degree $\delta_X(\mathbf{y}) = \mathbf{12}$. The topological boundary $\partial\mathrm{Vor}_X(\mathbf{y})$ is only a very small subset of that algebraic boundary.

8.2 Computing Algebraic Boundaries

We study the Voronoi decomposition to answer the question for any point in ambient space, "What point on the variety X am I closest to?" Another question one might ask is, "How far do we have to get away from X before there is more than one answer to the closest point question?" The union of the boundaries of the Voronoi cells is the locus of points in $\mathbb{R}^n$ that have more than one closest point on X. This set is called the *medial axis* (or *cut locus*) of the variety.

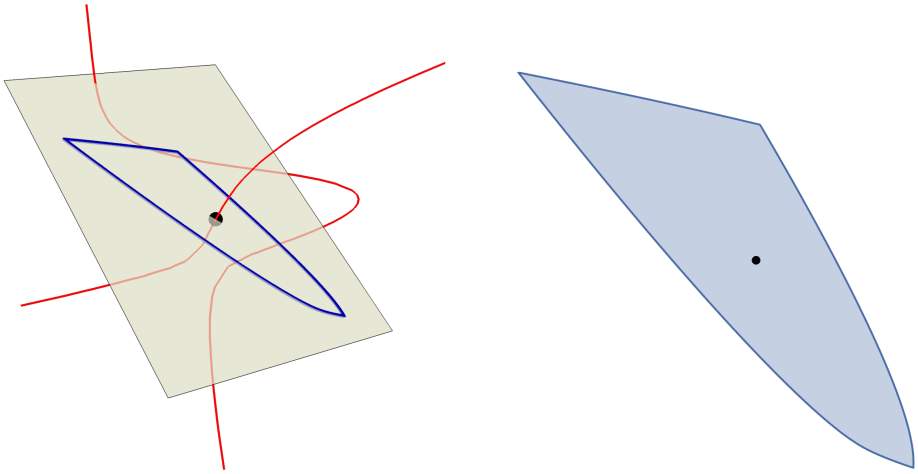

Fig. 8.1: A quartic space curve, shown with the Voronoi cell in one of its normal planes.

The distance from the variety to its medial axis, which is the answer to the "how far" question, is called the *reach* of X. This quantity is of interest, for example, in topological data analysis, as it is the main quantity determining the density of sample points needed to compute the persistent homology of X. We refer to [28, 66] for studies on sampling at the interface of topological data analysis with metric algebraic geometry. The distance from a point $\mathbf{y}$ on X to the variety's medial axis could be considered the *local reach* of X. Equivalently, this is the distance from $\mathbf{y}$ to the boundary of its Voronoi cell $\mathrm{Vor}_X(\mathbf{y})$.

The material that follows is based on the article [48]. We begin with the exact symbolic computation of the Voronoi boundary at $\mathbf{y}$ from the equations that define X. This uses a Gröbner-based algorithm whose input is $\mathbf{y}$ and the ideal of X and whose output is the ideal defining $\partial_{\mathrm{alg}}\mathrm{Vor}_X(\mathbf{y})$. In the next section we present formulas for the Voronoi degree $\delta_X(\mathbf{y})$ when X and $\mathbf{y}$ are sufficiently general and $\dim(X) \leq 2$. The proofs of these formulas require some intersection theory. Thereafter we study the case when $\mathbf{y}$ is a low rank matrix and X is the variety of these matrices. This relies on the *Eckart-Young Theorem*.

We now describe Gröbner basis methods for finding the Voronoi boundaries of a given variety. We start with an ideal $I = \langle f_1, f_2, \ldots, f_m \rangle$ in $\mathbb{Q}[x_1, \ldots, x_n]$ whose real variety $X = V(I) \subset \mathbb{R}^n$ is assumed to be nonempty. We assume that I is real radical and prime, so that $X_{\mathbb{C}}$ is an irreducible variety in $\mathbb{C}^n$ whose real points are Zariski dense. Our aim is to compute the Voronoi boundary of a given point $\mathbf{y} \in X$. In our examples, the coordinates of the point $\mathbf{y}$ and the coefficients of the polynomials f_i are rational numbers. Under these assumptions, the following computations can be done in polynomial rings over $\mathbb{Q}$.

Fix the polynomial ring $R = \mathbb{Q}[x_1, \ldots, x_n, u_1, \ldots, u_n]$ where $\mathbf{u} = (u_1, \ldots, u_n)$ is an auxiliary point with unknown coordinates. The *augmented Jacobian* of X at $\mathbf{x}$ is the following matrix of size $(m+1) \times n$ with entries in R. It contains the n partial derivatives of the m generators of I:

$$J_I(\mathbf{x}, \mathbf{u}) \quad := \quad \begin{bmatrix} \mathbf{u} - \mathbf{x} \\ (\nabla f_1)(\mathbf{x}) \\ \vdots \\ (\nabla f_m)(\mathbf{x}) \end{bmatrix}$$

Let N_I denote the ideal in R generated by I and the $(c+1) \times (c+1)$ minors of the augmented Jacobian $J_I(\mathbf{x}, \mathbf{u})$, where c is the codimension of the given variety $X \subset \mathbb{R}^n$. The ideal N_I in R defines a subvariety

of dimension n in $\mathbb{R}^{2n}$, namely the *Euclidean normal bundle* of X. Its points are pairs $(\mathbf{x}, \mathbf{u})$ where $\mathbf{x}$ is a point in the given variety X and $\mathbf{u}$ lies in the normal space of X at $\mathbf{x}$.

Example 8.5 (Cuspidal cubic) Let $n = 2$ and $I = \langle x_1^3 - x_2^2 \rangle$, so $X = V(I) \subset \mathbb{R}^2$ is a cubic curve with a cusp at the origin. The ideal of the Euclidean normal bundle of X is generated by two polynomials:

$$N_I \;=\; \left\langle x_1^3 - x_2^2 \,,\, \det\begin{pmatrix} u_1 - x_1 & u_2 - x_2 \\ 3x_1^2 & -2x_2 \end{pmatrix} \right\rangle \;\subset\; R \;=\; \mathbb{Q}[x_1, x_2, u_1, u_2]$$

For any $\mathbf{y} \in X$, let $N_I(\mathbf{y})$ denote the linear ideal that is obtained from N_I by replacing the unknown point $\mathbf{x}$ by the specific point $\mathbf{y}$. For instance, if that point is $\mathbf{y} = (4, 8)$ then $N_I(\mathbf{y}) = \langle u_1 + 3u_2 - 28 \rangle$.

Returning to the general setting, we define the *critical ideal* of the variety X at the point $\mathbf{y}$ as

$$C_I(\mathbf{y}) \quad = \quad N_I \,+\, N_I(\mathbf{y}) \,+\, \langle\, \|\mathbf{x} - \mathbf{u}\|^2 - \|\mathbf{y} - \mathbf{u}\|^2 \rangle \quad \subset \quad R.$$

The variety of the ideal $C_I(\mathbf{y})$ consists of pairs $(\mathbf{u}, \mathbf{x})$ such that $\mathbf{x}$ and $\mathbf{y}$ are equidistant from $\mathbf{u}$ and both are critical points of the distance function from $\mathbf{u}$ to X. The *Voronoi ideal* is the following ideal in $\mathbb{Q}[u_1, \ldots, u_n]$. It is obtained from the critical ideal by saturation and elimination:

$$\mathrm{Vor}_I(\mathbf{y}) \quad = \quad \big(C_I(\mathbf{y}) \,:\, \langle \mathbf{x} - \mathbf{y} \rangle^\infty \big) \,\cap\, \mathbb{Q}[u_1, \ldots, u_n]. \tag{8.3}$$

The geometric interpretation of each step in our construction implies the following result:

Proposition 8.6 *The affine variety in $\mathbb{C}^n$ defined by the Voronoi ideal $\mathrm{Vor}_I(\mathbf{y})$ contains the algebraic Voronoi boundary $\partial_{\mathrm{alg}}\mathrm{Vor}_X(\mathbf{y})$ of the given real variety X at its point $\mathbf{y}$.*

Remark 8.7 The verb "contains" sounds weak, but it is much stronger than it may seem. Indeed, in generic situations, the ideal $\mathrm{Vor}_I(\mathbf{y})$ will be prime, and it defines an irreducible hypersurface in the normal space $N_I(\mathbf{y})$. This hypersurface equals the algebraic Voronoi boundary, so containment is an equality. We saw this in Example 8.3. For special data, $\mathrm{Vor}_I(\mathbf{y})$ usually defines a hypersurface in $N_I(\mathbf{y})$, but it can have extraneous components, which are often easy to remove.

Example 8.8 For the point $\mathbf{y} = (4, 8)$ on the cuspidal cubic X in Example 8.5, we have $N_I(\mathbf{y}) = \langle u_1 + 3u_2 - 28 \rangle$. Going through the steps above, we find that the Voronoi ideal is

$$\mathrm{Vor}_I(\mathbf{y}) \;=\; \langle u_1 - 28, u_2 \rangle \;\cap\; \langle u_1 + 26, u_2 - 18 \rangle \;\cap\; \langle u_1 + 3u_2 - 28,\; 27u_2^2 - 486u_2 + 2197 \rangle.$$

The third component has no real roots and is hence extraneous. The Voronoi boundary consists of two points. Namely, we have $\partial\mathrm{Vor}_X(\mathbf{y}) = \{(28, 0), (-26, 18)\}$. The Voronoi cell $\mathrm{Vor}_X(\mathbf{y})$ is the line segment connecting these points. This segment is shown in green in Figure 8.2. Its right endpoint $(28, 0)$ is equidistant from $\mathbf{y}$ and the point $(4, -8)$. Its left endpoint $(-26, 18)$ is equidistant from $\mathbf{y}$ and the origin $(0, 0)$, whose Voronoi cell will be discussed in Remark 8.9.

The cuspidal cubic X is very special. If we replace X by a general cubic (defined over $\mathbb{Q}$) in the affine plane, then $\mathrm{Vor}_I(\mathbf{y})$ is generated modulo $N_I(\mathbf{y})$ by an irreducible polynomial of degree eight in $\mathbb{Q}[u_2]$. Thus, the expected Voronoi degree for general (affine) plane cubics is $\delta_X(\mathbf{y}) = 8$.

Remark 8.9 (Singularities) Voronoi cells at singular points can be computed with the same procedure as above. However, these Voronoi cells generally have higher dimensions. For an illustration, consider the cuspidal cubic, and let $\mathbf{y} = (0, 0)$ be the cusp. A Gröbner basis computation yields the Voronoi boundary $27u_2^4 + 128u_1^3 + 72u_1u_2^2 + 32u_1^2 + u_2^2 + 2u_1$. The Voronoi cell is the two-dimensional convex region bounded by this quartic, shown in blue in Figure 8.2. The Voronoi cell might also be empty at a singularity. This happens for instance for $V(x_1^3 + x_1^2 - x_2^2)$, which has an ordinary double point at $\mathbf{y} = (0, 0)$. In general, the cell dimension depends on both the embedding dimension and the branches of the singularity.

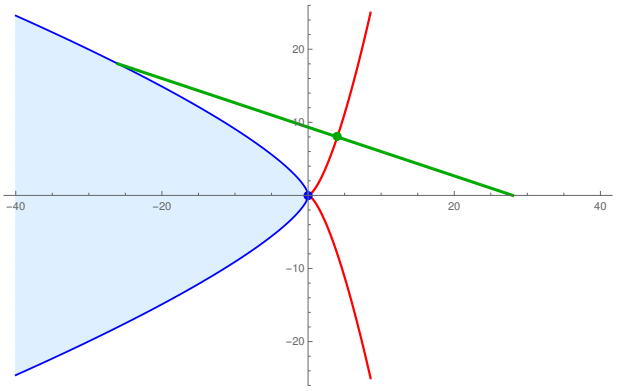

Fig. 8.2: The cuspidal cubic is shown in red. The Voronoi cell of a smooth point is a green line segment. The Voronoi cell of the cusp is the convex region bounded by the blue curve.

Proposition 8.6 gives an algorithm for computing the Voronoi ideal $\mathrm{Vor}_I(\mathbf{y})$ when $\mathbf{y}$ is a smooth point in $X = V(I)$. Experiments with `Macaulay2` [77] are reported in [48]. For small enough instances, the computation terminates and we obtain the defining polynomial of the Voronoi boundary $\partial_{\mathrm{alg}}\mathrm{Vor}_X(\mathbf{y})$. This polynomial is unique modulo the linear ideal of the normal space $N_I(\mathbf{y})$. For larger instances, we can only compute the degree of $\partial_{\mathrm{alg}}\mathrm{Vor}_X(\mathbf{y})$ but not its equation. This is done by working over a finite field and adding $c-1$ random linear equations in $u_1,\ldots,u_n$ in order to get a zero-dimensional polynomial system.

Computations are easiest to set up for the case of hypersurfaces ($c = 1$). One can explore random polynomials f of degree d in $\mathbb{Q}[x_1,\ldots,x_n]$, both inhomogeneous and homogeneous. These are chosen among those that vanish at a preselected point $\mathbf{y}$ in $\mathbb{Q}^n$. In each iteration, the Voronoi ideal $\mathrm{Vor}_I(\mathbf{y})$ from (8.3) was found to be zero-dimensional. In fact, $\mathrm{Vor}_I(\mathbf{y})$ is a maximal ideal in $\mathbb{Q}[u_1,\ldots,u_n]$, and the Voronoi deree $\delta_X(\mathbf{y})$ is the degree of the field extension of $\mathbb{Q}$ that is defined by that maximal ideal.

We summarize our results in Tables 8.1 and 8.2, and we extract conjectural formulas.

$n\backslash d$	2	3	4	5	6	7	8	$\delta_X(y) = \mathrm{degree}(\mathrm{Vor}_{\langle f\rangle}(y))$
1	1	2	3	4	5	6	7	$d-1$
2	2	8	16	26	38	52	68	d^2+d-4
3	3	23	61	123	215	343		d^3+d-7
4	4	56	202	520	1112			$d^4-d^3+d^2+d-10$
5	5	125	631					$d^5-2d^4+2d^3+d-13$
6	6	266	1924					$d^6-3d^5+4d^4-2d^3+d^2+d-16$
7	7	551						$d^7-4d^6+7d^5-6d^4+3d^3+d-19$

Table 8.1: The Voronoi degree of an inhomogeneous polynomial f of degree d in $\mathbb{R}^n$.

Conjecture 8.10 The Voronoi degree of a generic hypersurface of degree d in $\mathbb{R}^n$ equals

$$(d-1)^n + 3(d-1)^{n-1} + \tfrac{4}{d-2}((d-1)^{n-1}-1) - 3n.$$

The Voronoi degree of the cone of a generic homogeneous polynomial of degree d in $\mathbb{R}^n$ is

$$2(d-1)^{n-1} + \tfrac{4}{d-2}((d-1)^{n-1}-1) - 3n + 2.$$

$n\backslash d$	2	3	4	5	6	7	8	$\delta_X(y) = \text{degree}(\text{Vor}_{\langle f\rangle}(y))$
2	2	4	6	8	10	12	14	$2d-2$
3	3	13	27	45	67	93	123	$2d^2-5$
4	4	34	96	202				$2d^3-2d^2+2d-8$
5	5	79	309					$2d^4-4d^3+4d^2-11$
6	6	172						$2d^5-6d^4+8d^3-4d^2+2d-14$
7	7	361						$2d^6-8d^5+14d^4-12d^3+6d^2-17$

Table 8.2: The Voronoi degree of a homogeneous polynomial f of degree d in $\mathbb{R}^n$.

Both parts of this conjecture are proved for $n \leq 3$ in [48, Section 4], where the geometric theory of Voronoi degrees of low-dimensional varieties is developed. The case $d = 2$ was analyzed in [47, Proposition 5.8]. In general, for $n \geq 4$ and $d \geq 3$, the problem is open.

8.3 Formulas from Algebraic Geometry

To recap, the algebraic boundary of the Voronoi cell $\text{Vor}_X(\mathbf{y})$ is a hypersurface in the normal space to a variety $X \subset \mathbb{R}^n$ at a point $\mathbf{y} \in X$. We shall present formulas for the degree $\delta_X(\mathbf{y})$ of that hypersurface when X is a curve or a surface. All proofs appear in [48, Section 6]. We identify X and $\partial_{\text{alg}}\text{Vor}_X(\mathbf{y})$ with their Zariski closures in complex projective space $\mathbb{P}^n$, so there is a natural assigned hyperplane at infinity. We say that X is in *general position* in $\mathbb{P}^n$ if the hyperplane at infinity intersects X transversally, i.e. that the intersection is smooth.

Theorem 8.11 *Let $X \subset \mathbb{P}^n$ be a curve of degree d and geometric genus g with at most ordinary multiple points as singularities. The Voronoi degree at a general point $\mathbf{y} \in X$ equals*

$$\delta_X(\mathbf{y}) \;=\; 4d + 2g - 6,$$

provided X is in general position in $\mathbb{P}^n$.

Example 8.12 If X is a smooth curve of degree d in the plane, then $2g - 2 = d(d-3)$, so

$$\delta_X(y) \;=\; d^2 + d - 4.$$

This confirms our experimental results in the row $n = 2$ of Table 8.1.

Example 8.13 If X is a rational curve of degree d, then $g = 0$ and hence $\delta_X(\mathbf{y}) = 4d - 6$. If X is an elliptic curve, so the genus is $g = 1$, then we have $\delta_X(\mathbf{y}) = 4d - 4$. A space curve with $d = 4$ and $g = 1$ was studied in Example 8.4. Its Voronoi degree equals $\delta_X(\mathbf{y}) = 12$.

Theorem 8.11 is [48, Theorem 5.1]. The general position assumption is essential. For an example, let X be the twisted cubic curve in $\mathbb{P}^3$, with affine parameterization $t \mapsto (t, t^2, t^3)$. Here $g = 0$ and $d = 3$, so the expected Voronoi degree is 6. However, a computation shows that $\delta_X(\mathbf{y}) = 4$. This drop arises because the plane at infinity in $\mathbb{P}^3$ intersects the curve X in a triple point. After a general linear change of coordinates in $\mathbb{P}^3$, which amounts to a linear fractional transformation in $\mathbb{R}^3$, we correctly find $\delta_X(\mathbf{y}) = 6$.

We next present a formula for the Voronoi degree of a surface X which is smooth and irreducible in $\mathbb{P}^n$. Our formula is in terms of its degree d and two further invariants. The first, denoted $\chi(X)$, is the topological Euler characteristic. This equals the degree of the second Chern class of the tangent bundle. The second invariant, denoted $g(X)$, is the genus of the curve obtained by intersecting X with a general quadratic hypersurface in $\mathbb{P}^n$. Thus, $g(X)$ is the quadratic analogue to the sectional genus of the surface X.

Theorem 8.14 (Theorem 5.4 in [48]) *Let $X \subset \mathbb{P}^n$ be a smooth surface of degree d. Then*

$$\delta_X(y) \;=\; 3d + \chi(X) + 4g(X) - 11,$$

provided the surface X is in general position in $\mathbb{P}^n$ and y is a general point on X.

Example 8.15 If X is a smooth surface in $\mathbb{P}^3$ of degree d, then $\chi(X) = d(d^2-4d+6)$, by [71, Ex 3.2.12]. A smooth quadratic hypersurface section of X is an irreducible curve of degree (d,d) in $\mathbb{P}^1 \times \mathbb{P}^1$. The genus of such a curve is $g(X) = (d-1)^2$. We conclude that

$$\delta_X(y) \;=\; 3d + d(d^2-4d+6) + 4(d-1)^2 - 11 \;=\; d^3 + d - 7.$$

This confirms our experimental results in the row $n = 3$ of Table 8.1.

Example 8.16 Let X be the Veronese surface of order e in $\mathbb{P}^{\binom{e+1}{2}-1}$, taken after a general linear change of coordinates in that ambient space. The degree of X equals $d = e^2$. We have $\chi(X) = \chi(\mathbb{P}^2) = 3$, and the general quadratic hypersurface section of X is a curve of genus $g(X) = \binom{2e-1}{2}$. We conclude that the Voronoi degree of X at a general point $\mathbf{y}$ equals

$$\delta_X(y) \;=\; 3e^2 + 3 + 2(2e-1)(2e-2) - 11 \;=\; 11e^2 - 12e - 4.$$

For instance, for the quadratic Veronese surface in $\mathbb{P}^5$ we have $e = 2$ and hence $\delta_X(y) = 16$. This is smaller than the number 18 found in Example 8.22, since back then we were dealing with the cone over the Veronese surface in $\mathbb{R}^6$, and not with the Veronese surface in $\mathbb{R}^5 \subset \mathbb{P}^5$.

We finally consider affine surfaces defined by homogeneous polynomials. Namely, let $X \subset \mathbb{R}^n$ be the affine cone over a general smooth curve of degree d and genus g in $\mathbb{P}^{n-1}$.

Theorem 8.17 (Theorem 5.7 in [48]) *If $X \subset \mathbb{R}^n$ is the cone over a smooth curve in $\mathbb{P}^{n-1}$ then*

$$\delta_X(y) \;=\; 6d + 4g - 9,$$

provided that the curve is in general position and y is a general point.

Example 8.18 If $X \subset \mathbb{R}^3$ is the cone over a smooth curve of degree d in $\mathbb{P}^2$, then $2g - 2 = d(d-3)$, by the degree-genus formula for plane curves. We conclude that the Voronoi degree of X is equal to

$$\delta_X(y) \;=\; 2d^2 - 5.$$

This confirms our experimental results in the row $n = 3$ of Table 8.2.

Let us comment on the assumptions made in our theorems. We assumed that the variety X is in general position in $\mathbb{P}^n$. If this is not satisfied, then the Voronoi degree may drop. The point here is that the Voronoi ideal $\mathrm{Vor}_I(\mathbf{y})$ depends polynomially on the description of X, and the degree of this zero-dimensional ideal can only go down – and not up – when that description specializes. Making this statement precise would require a technical discussion of families in algebraic geometry, a topic best left to the experts on foundations. Nonetheless, the technique introduced in the next section can be adapted to determine the correct value. As an illustration, we consider the affine Veronese surface (Example 8.16).

Example 8.19 Let $X \subset \mathbb{P}^5$ be the Veronese surface with affine parametrization $(s,t) \mapsto (s,t,s^2,st,t^2)$. The hyperplane at infinity intersects X in a double conic, so X is not in general position. In the next section, we will show that the true Voronoi degree is $\delta_X(\mathbf{y}) = 10$. For the Frobenius norm, the Voronoi degree drops further. For this, we shall derive $\delta_X(\mathbf{y}) = 4$.

8.4 Voronoi meets Eckhart-Young

We now turn to the case of great interest in applications. Let X be the variety of real $m \times n$ matrices of rank $\leq r$. We consider two natural norms on the space $\mathbb{R}^{m\times n}$ of real $m \times n$ matrices. Our first matrix norm is the *Frobenius norm* $\|U\|_F := \sqrt{\sum_{ij} U_{ij}^2}$. Our second matrix norm is the *spectral norm* $\|U\|_2 := \max_i \sigma_i(U)$ which extracts the largest singular value of the matrix U.

Fix a rank r matrix V in X. This is a nonsingular point in X. We consider the Voronoi cell $\mathrm{Vor}_X(V)$ with respect to the Frobenius norm. This is consistent with our setting because the Frobenius norm agrees with the Euclidean norm on $\mathbb{R}^{m\times n}$. This identification will no longer be valid when we restrict to the subspace of symmetric matrices.

Fix $U \in \mathrm{Vor}_X(V)$. This means that the closest point to U in the rank r variety X is the matrix V. By the Eckart-Young Theorem, the matrix V is derived from U by computing the singular value decomposition $U = \Sigma_1 D \Sigma_2$. Here Σ_1 and Σ_2 are orthogonal matrices of size $m \times m$ and $n \times n$ respectively, and D is a nonnegative diagonal matrix whose entries are the singular values. Let $D^{[r]}$ be the matrix that is obtained from D by replacing all singular values except for the r largest ones by zero. Then, according to Eckart-Young, we have $V = \Sigma_1 \cdot D^{[r]} \cdot \Sigma_2$.

Remark 8.20 The Eckart-Young Theorem works for both the Frobenius norm and the spectral norm. This means that $\mathrm{Vor}_X(V)$ is also the Voronoi cell for the spectral norm.

The following theorem describes the Voronoi cells for low-rank matrix approximation.

Theorem 8.21 *Let V be an $m \times n$-matrix of rank r. The Voronoi cell $\mathrm{Vor}_X(V)$ is congruent up to scaling to the unit ball in the spectral norm on the space of $(m-r) \times (n-r)$-matrices.*

Before we present the proof, let us first see why the statement makes sense. The determinantal variety X has dimension $rm + rn - r^2$ in an ambient space of dimension mn. The dimension of the normal space at a point is the difference of these two numbers, so it equals $(m-r)(n-r)$. Every Voronoi cell is a full-dimensional convex body in the normal space. Next consider the case $m = n$ and restrict to the space of diagonal matrices. Now X is the set of vectors in $\mathbb{R}^n$ having at most r nonzero coordinates. This is a reducible variety with $\binom{n}{r}$ components, each a coordinate subspace. For a general point y in such a subspace, the Voronoi cell $\mathrm{Vor}_X(y)$ is a convex polytope. It is congruent to a regular cube of dimension $n - r$, which is the unit ball in the L^∞-norm on $\mathbb{R}^{n-r}$. Theorem 8.21 describes the orbit of this picture under the action of the two orthogonal groups on $\mathbb{R}^{m\times n}$.

For example, consider the special case where $n = 3$ and $r = 1$. In this case, X consists of the three coordinate axes in $\mathbb{R}^3$. The Voronoi decomposition of this reducible curve decomposes $\mathbb{R}^3$ into squares, each normal to a different point on the three lines. The image of this picture under orthogonal transformations is the Voronoi decomposition of $\mathbb{R}^{3\times 3}$ associated with the affine variety of rank 1 matrices. That variety has dimension 5, and each Voronoi cell is a 4-dimensional convex body in the normal space.

Proof (of Theorem 8.21) The Voronoi cell is invariant under orthogonal transformations. We may therefore assume that the matrix $V = (v_{ij})$ satisfies $v_{11} \geq v_{22} \geq \cdots \geq v_{rr} = u > 0$ and $v_{ij} = 0$ for all other entries. The Voronoi cell of the diagonal matrix V consists of matrices U whose block-decomposition into $r + (m-r)$ rows and $r + (n-r)$ columns satisfies

$$\begin{pmatrix} I & 0 \\ 0 & T_1 \end{pmatrix} \cdot \begin{pmatrix} U_{11} & U_{12} \\ U_{21} & U_{22} \end{pmatrix} \cdot \begin{pmatrix} I & 0 \\ 0 & T_2 \end{pmatrix} = \begin{pmatrix} V_{11} & 0 \\ 0 & V_{22} \end{pmatrix}.$$

Here $V_{11} = \mathrm{diag}(v_{11}, \ldots, v_{rr})$ agrees with the upper $r \times r$-block of V, and V_{22} is a diagonal matrix whose entries are bounded above by u in absolute value. This implies that $U_{11} = V_{11}$, $U_{12} = 0$ and $U_{21} = 0$,

Morevoer, U_{22} is an arbitrary $(m-r)\times(n-r)$ matrix with spectral norm at most u. Hence the Voronoi cell of the given diagonal matrix V is congruent to the set of all such matrices U_{22}. This convex body equals u times the unit ball in $\mathbb{R}^{(m-r)\times(n-r)}$ under the spectral norm. □

Our problem becomes even more interesting when we restrict to matrices in a linear subspace. To see this, let X denote the variety of symmetric $n\times n$ matrices of rank $\leq r$. We can regard X either as a variety in the ambient matrix space $\mathbb{R}^{n\times n}$, or in the space $\mathbb{R}^{\binom{n+1}{2}}$ whose coordinates are the upper triangular entries of a symmetric matrix. On the latter space we have both the *Euclidean norm* and the *Frobenius norm*. These are now different!

The Frobenius norm on $\mathbb{R}^{\binom{n+1}{2}}$ is the restriction of the Frobenius norm on $\mathbb{R}^{n\times n}$ to the subspace of symmetric matrices. For instance, if $n=2$, we identify the vector (a,b,c) with the symmetric matrix $\left(\begin{smallmatrix} a & b \\ b & c \end{smallmatrix}\right)$. The Frobenius norm of this matrix is $\sqrt{a^2+2b^2+c^2}$, whereas the Euclidean norm is $\sqrt{a^2+b^2+c^2}$. The two norms have dramatically different properties with respect to low rank approximation. The Eckart-Young Theorem remains valid for the Frobenius norm on $\mathbb{R}^{\binom{n+1}{2}}$, but it is not valid for the Euclidean norm. The implications of this are explained in [60, Example 3.2].

In what follows we elucidate this point by comparing the Voronoi cells with respect to the two norms.

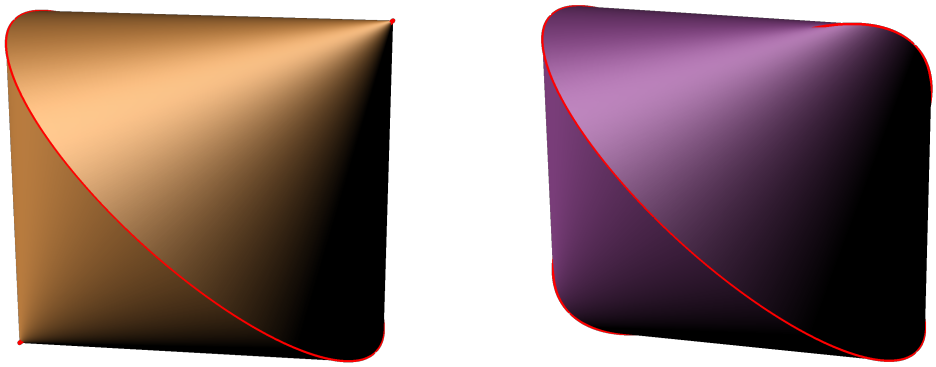

Fig. 8.3: The Voronoi cell of a symmetric 3×3 matrix of rank 1 is a convex body of dimension 3. It is shown for the Frobenius norm (left) and for the Euclidean norm (right).

Example 8.22 Let X be the variety of symmetric 3×3 matrices of rank ≤ 1. For the Euclidean metric, X lives in $\mathbb{R}^6$. For the Frobenius metric, X lives in a 6-dimensional subspace of $\mathbb{R}^{3\times 3}$. Let V be a smooth point in X, i.e. a symmetric 3×3 matrix of rank 1. The normal space to X at V has dimension 3. Hence, in either norm, the Voronoi cell $\mathrm{Vor}_X(V)$ is a 3-dimensional convex body. Figure 8.3 illustrates these two bodies.

For the Frobenius metric, the Voronoi cell is congruent to the set of matrices $\left(\begin{smallmatrix} a & b \\ b & c \end{smallmatrix}\right)$ with eigenvalues between -1 and 1. This semialgebraic set is bounded by the surfaces defined by the singular quadrics $\det\left(\begin{smallmatrix} a+1 & b \\ b & c+1 \end{smallmatrix}\right)$ and $\det\left(\begin{smallmatrix} a-1 & b \\ b & c-1 \end{smallmatrix}\right)$. The Voronoi ideal is of degree 4, defined by the product of these two determinants (modulo the normal space). The Voronoi cell is shown on the left in Figure 8.3. It is the intersection of two quadratic cones. The cell is the convex hull of the circle in which the two quadrics meet, together with the two vertices.

For the Euclidean metric, the Voronoi boundary at a generic point V in X is defined by an irreducible polynomial of degree 18 in a,b,c. In some cases, the Voronoi degree can drop. For instance, consider the special rank 1 matrix $V=\left(\begin{smallmatrix} 1 & 0 & 0 \\ 0 & 0 & 0 \\ 0 & 0 & 0 \end{smallmatrix}\right)$. For this point, the degree of the Voronoi boundary is only 12. This

particular Voronoi cell is shown on the right in Figure 8.3. This cell is the convex hull of two ellipses, which are shown in red in the diagram.

Chapter 9
Condition Numbers

The concept of a condition number has its origin in numerical analysis. It measures how much the output value of a function we wish to evaluate can change for a small change in the input argument. In this chapter we discuss condition numbers in the context of metric algebraic algebraic. In the first section we offer an introduction to the relevant notions for assessing errors in numerical computations.

Suppose the function to be evaluated is an algebraic function. For instance, we may wish to map the coefficients of a univariate polynomial to one of its roots. This function is well-defined locally, and it is well-behaved when the polynomial is far from the hypersurface defined by the discriminant. Indeed, the condition number stands in a reciprocal relationship to the distance to the variety of ill-posed instances.

This variety of ill-posed problems is often a discriminantal hypersurface, and thus we are naturally led to the ED problem for discriminants. This topic will be studied in the third and last section of this chapter. The classical discriminant is the dual variety to the Veronese variety, and other discriminants are dual to other toric varieties. We can apply ED duality (Theorem 2.16) to gain insights and computational speed.

A special case is the determinant of a square matrix, which arises when our function is matrix inversion. The relevant ED problem points us to the Eckhard-Young Theorem (Theorem 2.6) and this is why we include the proof of Eckhard-Young in the second section, about the condition number of matrix inversion.

9.1 Errors in Numerical Computations

Input data for numerical algorithms can have errors, caused, for instance, by measurements errors. Hence, the output of the computation also has errors. We wish to compare the output error with the input error.

Example 9.1 (Exact algorithm) Given a matrix $A \in \mathbb{R}^{2\times 2}$ with $\det(A) \neq 0$, we want to compute its inverse. We consider two instances of this problem. The errors are measured by the Euclidean norm.

1. First, let $A = \left(\begin{smallmatrix} 1 & 1 \\ -1 & 1 \end{smallmatrix}\right)$. We consider this matrix to be the true input data. A small measurement error gives the new input data $\tilde{A} = \left(\begin{smallmatrix} 1 & 1 \\ -1+\varepsilon & 1 \end{smallmatrix}\right)$, where $0 < \varepsilon \ll 1$. The *exact* solutions A^{-1} and $\tilde{A}^{-1}$ are then
$$A^{-1} \;=\; \frac{1}{2}\begin{pmatrix} 1 & -1 \\ 1 & 1 \end{pmatrix}, \quad \text{and} \quad \tilde{A}^{-1} \;=\; \frac{1}{2-\varepsilon}\begin{pmatrix} 1 & -1 \\ 1-\varepsilon & 1 \end{pmatrix} \;=\; A^{-1} + \frac{\varepsilon}{2(2-\varepsilon)}\begin{pmatrix} 1 & -1 \\ -1 & 1 \end{pmatrix}.$$
Comparing the errors, we find that $\|A^{-1} - \tilde{A}^{-1}\| \approx \|A - \tilde{A}\|$. In words, the error in the input $\|A - \tilde{A}\|$ and the error in the output $\|A^{-1} - \tilde{A}^{-1}\|$ are roughly the same. They both are of the order $O(\varepsilon)$.
2. The true input in the second example is the matrix $B = \left(\begin{smallmatrix} 1 & 1 \\ 1 & 1+\delta \end{smallmatrix}\right)$, where $|\delta| \neq 0$ is small. We perturb the input by adding ε to the lower left entry. The perturbed input is $\tilde{B} = \left(\begin{smallmatrix} 1 & 1 \\ 1+\varepsilon & 1+\delta \end{smallmatrix}\right)$. The matrix inverses are
$$B^{-1} = \frac{1}{\delta}\begin{pmatrix} 1+\delta & -1 \\ -1 & 1 \end{pmatrix} \quad \text{and} \quad \tilde{B}^{-1} = \frac{1}{\delta-\varepsilon}\begin{pmatrix} 1+\delta & -1 \\ -1-\varepsilon & 1 \end{pmatrix} = B^{-1} + \frac{\varepsilon}{\delta(\varepsilon-\delta)}\begin{pmatrix} 1+\delta & -1 \\ -(1+\delta) & 1 \end{pmatrix}.$$
This implies $\|B^{-1} - \tilde{B}^{-1}\| \approx \frac{1}{\delta(\varepsilon-\delta)} \cdot \|B - \tilde{B}\|$. If $\varepsilon < \delta$, then we have an amplification of the error by a factor of roughly δ^{-2}, which is large. The behavior here is different from that before.

We applied an exact algorithm to the problem, but we observed considerable differences in the output. In the first example, the output for the perturbed data $\tilde{A}^{-1}$ was close the true output A^{-1}. On the other hand, in the second example the output for the perturbed data $\tilde{B}^{-1}$ was far from the true output B^{-1}. ⋄

The previous example shows that, even if we can compute the *exact* solution of a problem, small errors in the data may be amplified tremendously in the output. The theory of *condition numbers* helps us to understand when and why this happens. In simple terms, a condition number is a quantity associated to a *computational problem*, and it measures the sensitivity of the output to small errors in the input data.

Definition 9.2 A *computational problem* is a function $f : M \to N$ from a space M of inputs to a space N of outputs. For us, each space is a subset of a Euclidean space, and it carries the induced Euclidean metric.

Example 9.3 In Example 9.1 the input space and the output space is $M = N = \{A \in \mathbb{R}^{2\times 2} \mid \det(A) \neq 0\}$. The computational problem is matrix inversion, so the relevant function is $f(A) = A^{-1}$. ◇

We regard (M, d_N) and (N, d_N) as metric spaces. The following definition is due to Rice [152].

Definition 9.4 The *(absolute) condition number* of $f : M \to N$ at the input datum $\mathbf{x} \in M$ is

$$\kappa[f](\mathbf{x}) \;:=\; \lim_{\varepsilon\to 0} \sup_{\mathbf{y}\in M:\; d_M(\mathbf{x},\mathbf{y})\le\varepsilon} \frac{d_N(f(\mathbf{x}), f(\mathbf{y}))}{d_M(\mathbf{x},\mathbf{y})}.$$

The motivation for this definition of a condition number is as follows: For small $d_M(\mathbf{x}, \mathbf{y})$ we have

$$d_N(f(\mathbf{x}), f(\mathbf{y})) \;\le\; \kappa[f](\mathbf{x}) \cdot d_M(\mathbf{x}, \mathbf{y}) \;+\; o(d_M(\mathbf{x}, \mathbf{y})).$$

In words, a small error $\varepsilon = d_M(\mathbf{x}, \mathbf{y})$ in the input data causes an error of roughly $\kappa[f](\mathbf{x}) \cdot \varepsilon$ in the output data. This is entirely independent of the algorithm which is used to evaluate $f(\mathbf{x})$. At this stage, given the lim-sup definition, it is unclear how condition numbers can be computed. As we shall see, this is where the geometric perspective of Bürgisser and Cucker [33] comes in. But, let's first discuss an important variant.

Remark 9.5 Fix the Euclidean spaces $M = \mathbb{R}^n$ and $N = \mathbb{R}^m$. What does "small error" mean in this case? If $\|\mathbf{x}\| = 10^4$, is an error of size $\|\mathbf{x} - \mathbf{y}\| = 10^2$ small or large? To address a question like this, there is a notion of relative error in numerical analysis. By definition, the *relative error* is

$$\mathrm{RelError}(\mathbf{x}, \mathbf{y}) \;=\; \frac{\|\mathbf{x} - \mathbf{y}\|_1}{\|\mathbf{x}\|_2} \quad \text{for } \mathbf{x}, \mathbf{y} \in M.$$

With this, we define the *relative condition number* of the function f at the input datum $\mathbf{x} \in M$ as follows:

$$\kappa_{\mathrm{REL}}[f](\mathbf{x}) \;:=\; \lim_{\varepsilon\to 0} \sup_{\mathrm{RelError}(\mathbf{x},\mathbf{y})\le\varepsilon} \frac{\mathrm{RelError}(f(\mathbf{x}), f(\mathbf{y}))}{\mathrm{RelError}(\mathbf{x}, \mathbf{y})} \;=\; \kappa[f](\mathbf{x}) \cdot \frac{\|\mathbf{x}\|_M}{\|f(\mathbf{x})\|_N}.$$

In numerical analysis, relative errors are more significant than absolute errors, because *floating point* arithmetic introduces relative errors (see, e.g., [91] or [175, p. 91]). Modern architecture is optimized for computing with floating point numbers. A floating point number system $\mathcal{F}$ is a subset of the real numbers $\mathbb{R}$ that is specified by four integers $\beta, t, e_{\min}, e_{\max}$, where β is called *base*, t is called *precision*, and $[e_{\min}, e_{\max}]$ is called *exponential range*. Then, $\mathcal{F} = \{\pm\beta^e \sum_{i=1}^{t} \frac{d_i}{\beta} \mid 0 \le d_i \le \beta - 1,\ e_{\min} \le e \le e_{\max}\}$. The quantity $u = \frac{1}{2}\beta^{1-t}$ is referred to as the *relative precision* of floating point number system $\mathcal{F}$.

The *range* of $\mathcal{F}$ is the set $\mathcal{G} := \{x \in \mathbb{R} \mid \beta^{e_{\min}-1} \le |x| \le \beta^{e_{\max}}(1 - \beta^{-1})\}$. Note that $\mathcal{F} \subset \mathcal{G}$. Consider the *rounding function* $\mathrm{fl} : \mathbb{R} \to \mathcal{F}, x \mapsto \mathrm{argmin}_{y\in\mathcal{F}} |x - y|$. One can show that every $x \in \mathcal{G}$ satisfies $\mathrm{fl}(x) = x(1 + \delta) \in \mathcal{F}$ for some δ with $|\delta| \le u$. This is a crucial property. It tells us that every number in $\mathcal{G}$ can be approximated by a number of $\mathcal{F}$ with relative precision u. Namely, the following inequality holds:

$$\mathrm{RelError}\,(x, \mathrm{fl}(x)) \;=\; \|\delta\| \;\le\; u \quad \text{for all } \; x \in \mathcal{G}. \tag{9.1}$$

Many hardware floating-point units use the IEEE 754 standard. This is a system $\mathcal{F}$ with the specifications

	β	t	$e_{\min}$	$e_{\max}$	u
half (16 bit)	2	11	−14	$16 = 2^4$	$\approx 5 \cdot 10^{-4}$
single (32 bit)	2	24	−125	$128 = 2^7$	$\approx 6 \cdot 10^{-8}$
double (64 bit)	2	53	−1021	$1024 = 2^{10}$	$\approx 10^{-16}$

This is designed so that the arithmetic operations $\circ \in \{+, -, \times, /, \sqrt{\cdot}\}$ satisfy $\mathrm{fl}(x \circ y) = (x \circ y)(1+\delta)$ for some $|\delta| \leq u$. For instance, the 64-bit floating point number system, specified in the third row of the table, can approximate any real number within its range with a relative error of at most $u \approx 10^{-16}$.

After this digression to the practical aspects of numerical computing, we now return to the mathematical theory. The next theorem is also due to Rice [152]. In his article, M and N are arbitrary Riemannian manifolds. We here specialize to the algebraic setting. For us, each of M and N is a submanifold in a Euclidean space, described by a finite Boolean combination of polynomial equations and inequalities.

Theorem 9.6 *Fix differentiable function $f : M \to N$. The condition number of this computational problem at $\mathbf{x} \in M$ is the maximal norm of the derivative over the unit sphere in the tangent space at $\mathbf{x}$, i.e.*

$$\kappa[f](\mathbf{x}) \;=\; \max_{\mathbf{t} \in T_{\mathbf{x}}M:\ \|\mathbf{t}\|=1} \|D_{\mathbf{x}} f(\mathbf{t})\|.$$

We obtain the relative condition number $\kappa_{\mathrm{REL}}[f](\mathbf{x})$ by multiplying this quantity with $||\mathbf{x}||/||f(\mathbf{x})||$.

A key step in computing the condition number with Rice' formula is to find an epression for the Jacobian $D_{\mathbf{x}} f$. For problems of interest to us, this step uses implicit differentiation or geometric arguments.

Example 9.7 (Roots of univariate polynomials) Following [33, Section 14.1.1], we examine the computational problem of finding one real root of a polynomial g in one variable z of degree d. We write

$$g(z) \;=\; g_0 + g_1 z + g_2 z^2 + \cdots + g_d z^d.$$

The coefficient vector $g = (g_0, g_1, \ldots, g_d)$ now serves as the input $\mathbf{x}$, and the output is a particular a real number a which satisfies $g(a) = 0$. The function $g \mapsto a(g)$ is well defined in a small open subset of the coefficient space $\mathbb{R}^{d+1}$. This must be small enough so that one root can be identified for each polynomial.

To find the derivative $D_g a$ of our root-finding function $g \mapsto a(g)$, we assume that the coefficients are differentiable functions $g_i(t)$ of a parameter t, and we set $\dot{g}_i = g_i'(0)$ and $\dot{g} = \sum_{i=0}^d \dot{g}_i z^i$. By differentiating the identity $g(a(g)) = 0$ with respect to t, we find the following formula for the desired derivative:

$$D_g a \;=\; -\frac{\dot{g}(a)}{g'(a)}.$$

We now think of a as a fixed root of a fixed polynomial $g(z)$. Theorem 9.6 implies that the condition number $\kappa[a](g)$ equals $|g'(a)|^{-1}$ times the maximal value $|\dot{g}(a)|$, where $\dot{g}$ runs over all points $(\dot{g}_0, \dot{g}_1, \ldots \dot{g}_d)$ on the unit d-sphere. A computation shows that this maximum equals $|\dot{g}(a)| = \sqrt{\sum_{i=0}^d a^{2i}}$, and therefore

$$\kappa[a](g) \;=\; \frac{\sqrt{\sum_{i=0}^d a^{2i}}}{g'(a)}.$$

This quantity is $+\infty$ when a is a double zero of f. The further away from being a double zero, the smaller the condition number. The relative condition number for the univariate root finding problem equals

$$\kappa_{\mathrm{REL}}[a](g) \;=\; \frac{\sqrt{(\sum_{i=0}^d g_i^2)(\sum_{i=0}^d a^{2i})}}{|a|\,|g'(a)|}. \tag{9.2}$$

We emphasize that this formula involves not just the polynomial $g(z)$ but also the zero a we seek to find.

Example 9.8 (The condition number of the ED minimization problem) We view the ED minimization problem for a smooth algebraic variety $X \subset \mathbb{R}^n$ from the point of view of condition numbers. Recall from

Chapter 7 the definition of the medial axis $\mathrm{Med}(X)$. Every point outside the medial axis has a unique closest point on X. Formulating this as a computational problem we have the input space $M = \mathbb{R}^n \, \mathrm{Med}(X)$, the output space $N = X$ and $f : (\mathbb{R}^n \backslash \mathrm{Med}(X)) \to X$ is the function that projects $\mathbf{u}$ to the closest point $f(\mathbf{u}) = \mathrm{argmin}_{\mathbf{x} \in X} \|\mathbf{x} - \mathbf{u}\|$ on X. We can apply Theorem 9.6 to compute the associated condition number $\kappa[f](\mathbf{u})$. This was carried out in detail in [27]. Suppose $\mathbf{x} = f(\mathbf{u})$. By [27, Theorem 4.3], we have

$$\kappa[f](\mathbf{u}) \;=\; \max_{\mathbf{t} \in T_{\mathbf{x}} X:\ \|\mathbf{t}\| = 1} \left\| (I_m - \lambda \cdot L_{\mathbf{v}})^{-1} \, \mathbf{t} \right\|.$$

In this formula, $\lambda = \|\mathbf{u} - \mathbf{x}\|$ is the distance from $\mathbf{u}$ to X, $\mathbf{v} = \lambda^{-1}(\mathbf{u} - \mathbf{x})$ is the normal vector at $\mathbf{x}$ pointing towards $\mathbf{u}$, and $L_{\mathbf{v}}$ is the Weingarten map of X at $\mathbf{x}$ in normal direction $\mathbf{v}$; see (6.8).

9.2 Matrix Inversion and Eckhart-Young

In this section we study the condition number of the problem of matrix inversion. This will lead us back to the Eckhart-Young theorem, for which we here present a proof. We begin by reviewing some norms on the space of real $m \times n$ matrices. The usual Euclidean norm, or Frobenius norm, of a matrix $A \in \mathbb{R}^{m \times n}$ is

$$\|A\| \;=\; \sqrt{\sum_{i,j} a_{ij}^2} \;=\; \sqrt{\mathrm{trace}(AA^T)}.$$

By contrast, in Theorem 9.6 we used the operator norm, or nuclear norm. This is defined as follows:

$$\|A\|_{\mathrm{op}} \;:=\; \max_{\|\mathbf{x}\| = 1} \|A\mathbf{x}\|.$$

If U and V are orthogonal matrices, then $\|UAV^T\|_{\mathrm{op}} = \|A\|_{\mathrm{op}}$ and $\|UAV^T\| = \|A\|$. In words, *orthogonal invariance* holds for both norms. Suppose $n \leq m$. Let $A = U\Sigma V^T$ be the singular value decomposition of A, where $U \in R^{m \times m}$ and $V \in \mathbb{R}^{n \times n}$ are orthogonal matrices and $\Sigma = \mathrm{diag}(\sigma_1, \ldots, \sigma_n)$ with $\sigma \geq \cdots \geq \sigma_n \geq 0$ is the $m \times n$ diagonal matrix of singular values. Orthogonal invariance implies $\|A\|_{\mathrm{op}} = \sigma_1$ and $\|A\| = \sqrt{\sigma_1^2 + \cdots + \sigma_n^2}$. If $n = m$ and $\sigma_1 \neq 0$, we have $A^{-1} = V\Sigma^{-1}U^T$ and hence $\|A^{-1}\|_{\mathrm{op}} = \sigma_n^{-1}$.

We now focus on the case of square matrices ($m = n$). Matrix inversion corresponds to the map

$$\mathrm{inv} : \mathcal{D} \to \mathcal{D}, \;\; A \mapsto A^{-1},$$

where $\mathcal{D} = \{A \in \mathbb{R}^{n \times n} \mid \det(A) \neq 0\}$. We shall prove the following characterization of the condition number of matrix inversion. For any $A \in \mathcal{D}$, the smallest singular value σ_n is a positive real number.

Theorem 9.9 *The condition number of matrix inversion at $A \in \mathcal{D}$ is*

$$\kappa[\mathrm{inv}](A) \;=\; \|A^{-1}\|_{\mathrm{op}}^2 \;=\; \sigma_n^{-2}.$$

Before we prove this theorem, let us briefly bring it in context with Remark 9.5. In numerical analysis, a popular choice for measuring the relative error is using the operator norm. In this case, by Theorem 9.9 the relative condition number can be expressed as the ratio of the largest and smallest singular value of A:

$$\kappa_{\mathrm{REL}}[\mathrm{inv}](A) \;=\; \kappa[\mathrm{inv}](A) \cdot \frac{\|A\|_{\mathrm{op}}}{\|A^{-1}\|_{\mathrm{op}}} \;=\; \frac{\sigma_1}{\sigma_n}$$

This ratio is known as *Turing's condition number* and goes back to the work of Turing [176].

Proof (of Theorem 9.9) Let $\mathrm{adj}(A)$ denote the adjoint matrix of A. Since $\mathrm{inv}(A) = A^{-1} = \frac{1}{\det(A)} \cdot \mathrm{adj}(A)$, the map inv is a polynomial function on $\mathcal{D}$. In particular, inv is differentiable on $\mathcal{D}$. By Theorem 9.6 the condition number is $\kappa[\mathrm{inv}](A) = \|D_A\mathrm{inv}\|_{\mathrm{op}}$. We compute the derivarive of inv. Taking the derivative of $AB = \mathbf{I}_n$ we have $\dot{A}B + A\dot{B} = 0$. Since $B = A^{-1}$, we conclude $\dot{B} = -A^{-1}\dot{A}A^{-1}$. For a tangent vector $\dot{A} = R \in \mathbb{R}^{n\times n}$ we therefore have $D_A\mathrm{inv}(R) = A^{-1}RA^{-1}$. Let $A = U\Sigma V^T$ be the singular value decomposition of A. Then, $A^{-1} = V\Sigma^{-1}U^T$. By orthogonal invariance of the Euclidean norm, we find

$$\max_{\|R\|=1} \|A^{-1}RA^{-1}\|^2 \;=\; \max_{\|R\|=1} \|\Sigma^{-1}R\Sigma^{-1}\|^2 \;=\; \max_{\sum_{i,j} r_{i,j}^2 = 1} \sum_{i,j} \frac{r_{i,j}^2}{\sigma_i^2\sigma_j^2}.$$

The last expression is maximized when $r_{n,n} = 1$ and all other $r_{i,j}$ are zero. We conclude that the condition number of matrix inversion at A is equal to $\kappa[\mathrm{inv}](A) = \max_{\|R\|=1} \|D_A\mathrm{inv}(R)\|_{\mathrm{op}} = \frac{1}{\sigma_n^2} = \|A^{-1}\|_{\mathrm{op}}^2$. □

Example 9.10 We revisit Example 9.1. The two matrices were $A = \left(\begin{smallmatrix} 1 & 1 \\ -1 & 1 \end{smallmatrix}\right)$ and $B = \left(\begin{smallmatrix} 1 & 1 \\ 1 & 1+\delta \end{smallmatrix}\right)$. To be concrete, we set $\delta = 10^{-8}$. Since $A^TA = 2 \cdot 1_2$, we have $\|A^{-1}\mathbf{x}\| = \frac{1}{2}\|\mathbf{x}\|$ for all $\mathbf{x} \in \mathbb{R}^2$. By Theorem 9.9,

$$\kappa[\mathrm{inv}](A) = \|A^{-1}\|_{\mathrm{op}}^2 = \frac{1}{4}.$$

On the other hand, and $\|B^{-1}\|_{\mathrm{op}} \geq \|B^{-1}\mathbf{e}_1\| \geq 10^8$, so that

$$\kappa[\mathrm{inv}](B) = \|B^{-1}\|_{\mathrm{op}}^2 \geq 10^{16}.$$

This explains the different behaviors of the outputs with respect to errors in the input in Example 9.1. ⋄

The Eckhart-Young Theorem (Theorem 2.6) yields a metric interpretation of Turing's condition number $\kappa[\mathrm{inv}](A)$ from Theorem 9.9. The smallest singular value σ_n of a square matrix A equals the Euclidean distance of A to the variety of singular matrices. This is the hypersurface defined by the determinant:

$$\Sigma := \{A \in \mathbb{R}^{n\times n} \mid \det(A) = 0\}.$$

Thus, Turing's condition number of the matrix A is the inverse distance (squared) to the hypersurface Σ:

$$\kappa[\mathrm{inv}](A) = \frac{1}{\mathrm{dist}(A,\Sigma)^2} \quad \text{and} \quad \kappa_{\mathrm{REL}}[\mathrm{inv}](A) = \frac{\|A\|_{\mathrm{op}}}{\mathrm{dist}(A,\Sigma)}; \tag{9.3}$$

Such a relation is called a *condition number theorem* in the literature. To a numerical analysist, the elements of a set like Σ are the *ill-posed inputs* of the computational problem. Condition number theorems give us the metric geometric interpretation that the numerical difficulty of an input to a problem is directly related to the distance of this input to the locus of ill-posed inputs. Condition number theorems were, for instance, also derived for computing zeros of polynomials [96] or computing eigenvalues of matrices [178]. See also [54]. To an algebraic geometer, the determinant of a square matrix is a special case of a discriminant, and Σ will generally be a discriminantal hypersurface. We will make this precise in the next section.

Example 9.11 Consider the determinant hypersurface for 2×2-matrices $\Sigma = V(\det) \subset \mathbb{R}^{2\times 2}$. Following the discussion above, the Zariski closure of those matrices $A \in \mathbb{R}^{2\times 2}$, for which $\kappa[\mathrm{inv}](A) = \varepsilon^{-1}$, is given by the offset hypersurface of Σ at level $\sqrt{\varepsilon}$. We can compute the offset hypersurface as in Example 7.12. In this example let us instead consider the surface defined by $\kappa_{\mathrm{REL}}[\mathrm{inv}](A) = \varepsilon^{-1}$ for $\varepsilon > 0$. To make the formula in (9.3) more convenient, we replace $\|A\|_{\mathrm{op}}$ by $\|A\|$. We proceed as in Section 7.2 to compute

a polynomial equation for $\operatorname{dist}(A,\Sigma) = \varepsilon \cdot \|A\|$ in terms of A and ε, but for $B \in \Sigma$ we replace the affine sphere $\|A-B\| = \varepsilon$ by the homogeneous sphere $\|A-B\| = \varepsilon \cdot \|A\|$. We use `Macaulay2` [77]:

```
R = QQ[a_0..a_3, b_0..b_3, eps];
f = b_0*b_3 - b_1*b_2;
normAsq = a_0^2 + a_1^2 + a_2^2 + a_3^2
d = (a_0-b_0)^2 + (a_1-b_1)^2 + (a_2-b_2)^2 + (a_3-b_3)^2 - eps^2 * normAsq;
J1 = {diff(b_0, f), diff(b_1, f), diff(b_2, f), diff(b_3, f)};
J2 = {diff(b_0, d), diff(b_1, d), diff(b_2, d), diff(b_3, d)};
J = matrix {J1, J2};
OC = ideal {f, minors(2, J), d};
O = eliminate({b_0, b_1, b_2, b_3}, OC)
g = (gens O)_0_0
```

The result is the polynomial $g(\mathbf{a},\varepsilon) = (a_0^2+a_1^2+a_2^2+a_3^2)^2 \cdot (g_0(\mathbf{a})+g_1(\mathbf{a})\varepsilon^2+g_2(\mathbf{a})\varepsilon^4+g_3(\mathbf{a})\varepsilon^6+g_4(\mathbf{a})\varepsilon^8)$, where the coefficients of the second factor are

$$
\begin{aligned}
g_4(\mathbf{a}) &= (a_0^2+a_1^2+a_2^2+a_3^2)^2 \\
g_3(\mathbf{a}) &= -3(a_0^2+a_1^2+a_2^2+a_3^2)^2 \\
g_2(\mathbf{a}) &= 3\,a_0^4+6\,a_0^2a_1^2+3\,a_1^4+6\,a_0^2a_2^2+7\,a_1^2a_2^2+3\,a_2^4-2\,a_0a_1a_2a_3+7\,a_0^2a_3^2+6\,a_1^2a_3^2+6\,a_2^2a_3^2+3\,a_3^4 \\
g_1(\mathbf{a}) &= -(a_0^4+2\,a_0^2a_1^2+a_1^4+2\,a_0^2a_2^2+4\,a_1^2a_2^2+a_2^4-4\,a_0a_1a_2a_3+4\,a_0^2a_3^2+2\,a_1^2a_3^2+2\,a_2^2a_3^2+a_3^4) \\
g_0(\mathbf{a}) &= (a_1a_2-a_0a_3)^2.
\end{aligned}
$$

Figure 9.1 shows the zero set of $g(\mathbf{a},\varepsilon)$ at level $\varepsilon = 0.5$ in the affine patch $a_0 = 1$. We remark that, if $\operatorname{dist}(A,\Sigma) = \varepsilon \cdot \|A\|$, then $\varepsilon = \sin\alpha$, where α is the minimal angle between the line $\mathbb{R}\cdot A$ and a line $\mathbb{R}\cdot B$ with $B \in \Sigma$. In this case, ε^{-1} is also called a *conic condition number* (see [33, Chapters 20 & 21]). ⋄

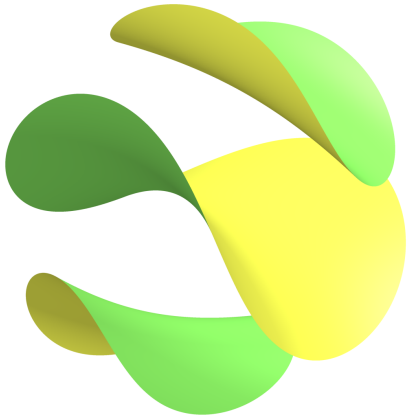

Fig. 9.1: The picture shows the determinantal hypersurface $\Sigma = \{\det(A) = 0\} \subset \mathbb{R}^{2\times 2}$ (the surface in the middle) together with the hypersurface defined by $\operatorname{dist}(A,\Sigma) = \varepsilon \cdot \|A\|$ with $\varepsilon = 0.5$ (the union of the two surfaces on the outside) in the affine patch where the upper left entry of A is fixed to be one. The image was created using `Surfer`.

In the remainder of this section we give a proof of the Eckart-Young theorem. For this we return now to rectangular matrices and denote by $X_r := \{A \in \mathbb{R}^{m\times n} \mid \operatorname{rank}(A) \le r\}$ the variety of real matrices of rank at most r. Recall that $\operatorname{Sing}(X_r) = X_{r-1}$. We first compute the normal space of X_r at a smooth point. Lemma 9.12 can be viewed as a variant of Example 2.15, but presented in a more down-to-earth manner.

Lemma 9.12 *Let $A \in X_r$ be a smooth point (i.e.,* $\operatorname{rank}(A) = r$*). Suppose that $A = RS^T$, where $R \in \mathbb{R}^{m\times r}$ and $S \in \mathbb{R}^{n\times r}$ have rank r. The normal space of X_r at A has dimension $(m-r)(n-r)$ and it equals*

$$N_A X_r \;=\; \operatorname{span}\left\{ \mathbf{u}\mathbf{v}^T \mid \mathbf{u}^T R = 0 \text{ and } S^T\mathbf{v} = 0 \right\}.$$

Proof Let $R(t) \in \mathbb{R}^{m\times r}$ and $S(t) \in \mathbb{R}^{n\times r}$ be smooth curves with $R(0) = R$ and $S(0) = S$. Then, $\gamma(t) := R(t)S(t)^T$ is a smooth curve with $\gamma(0) = A$. The product rule from calculus gives

$$\frac{\partial}{\partial t}\gamma(t)\Big|_{t=0} = R\left(\frac{\partial}{\partial t}S(t)\Big|_{t=0}\right)^T + \left(\frac{\partial}{\partial t}R(t)\Big|_{t=0}\right)S^T. \tag{9.4}$$

Let $\mathcal{V} := \{RP^T \mid P \in \mathbb{R}^{n\times r}\}$ and $\mathcal{W} := \{QS^T \mid Q \in \mathbb{R}^{m\times r}\}$. The equation (9.4) shows that the tangent space of X_r at A is the sum $T_A X_r = \mathcal{V} + \mathcal{W}$. (Aside for students: what is the intersection $\mathcal{V} \cap \mathcal{W}$?)

We note that $\mathcal{V}$ consists of all matrices $L \in \mathbb{R}^{m\times n}$ such that $\mathbf{u}^T L\mathbf{x} = 0$ for all $\mathbf{u}$ with $\mathbf{u}^T R = 0$ and $\mathbf{x} \in \mathbb{R}^n$ arbitrary. Since $\mathbf{u}^T L\mathbf{x} = \operatorname{Trace}(L^T\mathbf{u}\mathbf{x}^T)$, this shows that the normal space of $\mathcal{V}$ is spanned by matrices of the form $\mathbf{u}\mathbf{x}^T$. Similarly, the normal space of $\mathcal{W}$ is spanned by $\mathbf{y}\mathbf{v}^T$, where $S^T\mathbf{v} = 0$ and $\mathbf{y} \in \mathbb{R}^m$ arbitrary. Therefore, the normal space of $T_A X_r = \mathcal{V} + \mathcal{W}$ is spanned by all $\mathbf{u}\mathbf{v}^T$ with $\mathbf{u}$ and $\mathbf{v}$ as above. □

Corollary 9.13 $\dim X_r = nm - (m-r)(n-r) = r(m+n-r)$.

We use Lemma 9.12 to prove the Eckart-Young Theorem.

Proof (of Theorem 2.6) Let $B \in X_r$ be a matrix of rank r. We consider a singular value decomposition $B = U\Sigma V^T$. The matrices $U \in \mathbb{R}^{m\times r}$ and $V \in \mathbb{R}^{r\times n}$ have orthonormal columns, and $\Sigma = \operatorname{diag}(\sigma_1, \ldots, \sigma_r)$ with $\sigma_1, \ldots, \sigma_r > 0$ (not necessarily ordered). To derive Theorem 2.6, we shall prove a claim that is reminiscent of Theorem 8.21. Namely, the singular value decomposition of all matrices $A \in \mathbb{R}^{m\times n}$, such that B is an ED-critical point for A, has the form $A = [U\ U']\left(\begin{smallmatrix}\Sigma & 0\\ 0 & \Sigma'\end{smallmatrix}\right)[V\ V']^T$, where $\Sigma' = \operatorname{diag}(\sigma_{r+1}, \ldots, \sigma_n)$.

By orthogonal invariance, we can assume that $B = \left(\begin{smallmatrix}\Sigma & 0\\ 0 & 0\end{smallmatrix}\right)$. Let $A \in B + N_B X_r$ be a matrix in the normal space of B. By Lemma 9.12, we have $A = B + \sum_{i=r+1}^{m}\sum_{j=r+1}^{n} a_{ij}\,\mathbf{e}_i\mathbf{e}_j^T$ for some coefficients $a_{ij} \in \mathbb{R}$, i.e.

$$A \;=\; \begin{pmatrix}\Sigma & 0\\ 0 & A'\end{pmatrix}, \qquad \text{where } A' = (a_{ij}) \in \mathbb{R}^{(m-r)\times(n-r)}.$$

Let now $A' = U'\Sigma'V'$ be the singular value decomposition of A'. Then,

$$A \;=\; [1_r\ U']\begin{pmatrix}\Sigma & 0\\ 0 & \Sigma'\end{pmatrix}[1_r\ V']^T. \tag{9.5}$$

This must be the desired singular value decomposition of the $m \times n$ matrix A, because the singular value decomposition of any rectangular matrix is unique up to ordering the singular values. □

Remark 9.14 Our proof of the Eckart-Young Theorem also works for symmetric $n \times n$ matrices. It implies that the rank r matrix B which minimizes the distance to a symmetric matrix A is also symmetric.

9.3 Distance to the Discriminant

Let $\mathcal{H}_d$ be the vector space of homogeneous polynomials in $n+1$ many variables $\mathbf{x} = (x_0, \ldots, x_n)$ of degree d. For $m \le n$ and a tuple $\mathbf{d} = (d_1, \ldots, d_m)$ we write $\mathcal{H}_\mathbf{d} := \mathcal{H}_{d_1} \times \cdots \times \mathcal{H}_{d_m}$.

The goal of this section is to use the Eckart-Young theorem for computing the distance of a polynomial system $F \in \mathcal{H}_\mathbf{d}$ to the real polynomial discriminant

$$\Omega := \{F \in \mathcal{H}_{\mathbf{d}} \mid \text{ there is } \mathbf{x} \in \mathbb{P}^n_{\mathbb{R}} \text{ s.t. } F(\mathbf{x}) = 0 \text{ and } \operatorname{rank} JF(\mathbf{x}) < m\}, \tag{9.6}$$

where $JF(\mathbf{x}) = \left(\frac{\partial f_i}{\partial x_j}(\mathbf{x})\right) \in \mathbb{R}^{m\times(n+1)}$ is the Jacobian matrix of F at $\mathbf{x}$. For this, we first need to introduce a distance on $\mathcal{H}_d$. We use the so-called *Bombieri-Weyl distance*.

Write $I := \{\alpha \in \mathbb{N}^{n+1} \mid \alpha_0 + \cdots \alpha_n = d\}$. The *Bombieri-Weyl inner product* between two polynomials $f = \sum_{\alpha\in I} f_\alpha \mathbf{x}^\alpha \in \mathcal{H}_d$ and $g = \sum_{\alpha\in I} g_\alpha \mathbf{x}^\alpha \in \mathcal{H}_d$ is defined by

$$\langle f, g\rangle_{\mathrm{BW}} := \sum_{\alpha\in I} \frac{\alpha_0!\cdots\alpha_n!}{d!} f_\alpha \cdot g_\alpha.$$

Notice that for $d = 1$ this is the usual Euclidean inner product in $\mathbb{R}^{n+1}$. The motivation for the multinomial coefficients in the definition of $\langle\ ,\ \rangle_{\mathrm{BW}}$ is that the Bombieri-Weyl inner product – like the Euclidean inner product in $\mathbb{R}^{n+1}$ – is invariant under orthogonal change of variables. More specifically, if $U \in O(n+1)$ is an orthogonal matrix, then

$$\langle f \circ U, g \circ U\rangle_{\mathrm{BW}} = \langle f, g\rangle_{\mathrm{BW}}.$$

As before, we call this property *orthogonal invariance*. Kostlan [113, 114] classified all orthogonally invariant inner products on $\mathcal{H}_d$ and he showed that the Bombieri-Weyl inner product is the unique orthogonally invariant inner product (up to scaling) such that monomials are pairwise orthogonal.

The Bombieri-Weyl inner product extends to $\mathcal{H}_{\mathbf{d}}$. For $F = (f_1, \ldots, f_m)$ and $G = (f_1, \ldots, f_m)$ we have

$$\langle F, G\rangle_{\mathrm{BW}} := \langle f_1, g_1\rangle_{\mathrm{BW}} + \cdots + \langle f_m, g_m\rangle_{\mathrm{BW}}.$$

The Bombieri-Weyl norm is $\|F\|_{\mathrm{BW}} := \sqrt{\langle F, F\rangle_{\mathrm{BW}}}$ and the distance corresponding to this norm is given by $\operatorname{dist}_{\mathrm{BW}}(F, G) := \|F - G\|_{\mathrm{BW}}$ for $F, G \in \mathcal{H}_{\mathbf{d}}$.

Example 9.15 Let $n = 1, d = 2$. Consider two quadrics in two variables $f(x_0, x_1) = ax_0^2 + bx_0x_1 + cx_1^2$ and $g(x_0, x_1) = \alpha x_0^2 + \beta x_0x_1 + \gamma x_1^2$. The inner product between them is

$$\langle f, g\rangle_{\mathrm{BW}} = \frac{2!\cdot 0!}{2!} a\alpha + \frac{1!\cdot 1!}{2!} b\beta + \frac{2!\cdot 0!}{2!} c\gamma = a\alpha + \frac{1}{2} b\beta + c\gamma.$$

We can also write $f(\mathbf{x}) = \mathbf{x}^T A\mathbf{x}$ and $g(\mathbf{x}) = \mathbf{x}^T B\mathbf{x}$, where $\mathbf{x} = (x_0, x_1)^T$, with

$$A = \begin{pmatrix} a & b/2 \\ b/2 & c \end{pmatrix}, \quad B = \begin{pmatrix} \alpha & \beta/2 \\ \beta/2 & \gamma \end{pmatrix}.$$

Then, $\langle f, g\rangle_{\mathrm{BW}} = a\alpha + \frac{1}{2}b\beta + c\gamma = \operatorname{Trace}(A^T B)$. The same holds true for quadrics in more than 2 variables, so the Bombieri-Weyl products for quadrics is the usual Euclidean inner products for matrices. In this sense, the Bombieri-Weyl product is a generaliztion of the trace inner product for symmetric matrices to homogeneous polynomials of any degree. ⋄

The next theorem was proved by Rafalli [151] for the case $m = 1$. The book by Bürgisser and Cucker [33] covers the case $m = n$.

Theorem 9.16 *Let $m \le n$ and $\mathbf{d} = (d_1, \ldots, d_m)$ be a tuple of degrees. Let $F \in \mathcal{H}_{\mathbf{d}}$. Then,*

$$\operatorname{dist}_{\mathrm{BW}}(F, \Omega) = \min_{\mathbf{x}\in\mathbb{S}^n} \sqrt{\|F(\mathbf{x})\|^2 + \sigma_m(D^{-1/2}\, JF(\mathbf{x})\, P_{\mathbf{x}})^2}\,,$$

where $D = \operatorname{diag}(d_1, \ldots, d_m)$ and $P_{\mathbf{x}} := 1_{n+1} - \mathbf{x}\mathbf{x}^T$ is the projection onto the tangent space $T_{\mathbf{x}}\mathbb{S}^n$.

Proof Since we are considering homogeneous polynomials, we can replace real projective space $\mathbb{P}^n_{\mathbb{R}}$ by the sphere $\mathbb{S}^n$ in the definition of Ω from (9.6). For $\mathbf{x} \in \mathbb{S}^n$ let

$$\Omega(\mathbf{x}) := \{F \in \mathcal{H}_{\mathbf{d}} \mid F(\mathbf{x}) = 0 \text{ and } \operatorname{rank} JF(\mathbf{x}) < m\}.$$

By definition, we have $\Omega = \bigcup_{\mathbf{x}\in\mathbb{S}^n} \Omega(\mathbf{x})$, so that

$$\operatorname{dist}_{\mathrm{BW}}(F, \Omega) = \min_{\mathbf{x}\in\mathbb{S}^n} \operatorname{dist}_{\mathrm{BW}}(F, \Omega(\mathbf{x})) \tag{9.7}$$

(the minimum is obtained, because $\mathbb{S}^n$ is compact). Fix $\mathbf{x} \in \mathbb{S}^n$, let $U \in O(n+1)$ be an orthogonal matrix with $U\mathbf{e}_1 = \mathbf{x}$ and denote $F_0 := F \circ U$. By orthogonal invariance $\operatorname{dist}_{\mathrm{BW}}(F, \Omega(\mathbf{x})) = \operatorname{dist}_{\mathrm{BW}}(F_0, \Omega(\mathbf{e}_1))$. We compute the latter.

Let us write

$$F_0(\mathbf{x}) = x_0^d \cdot a + x_0^{d-1} \cdot A\,(x_1, \ldots, x_n)^T + h(\mathbf{x}),$$

where $a \in \mathbb{R}^m$, $A \in \mathbb{R}^{m\times n}$ and h involves only powers of x_0 of degree less than $d-1$. Then,

$$a = F_0(\mathbf{e}_1) = F(\mathbf{x}) \quad \text{and} \quad A = JF_0(\mathbf{e}_1)\, P_{\mathbf{e}_1} = JF(\mathbf{x})\, P_{\mathbf{x}}\, U^T.$$

Recall that $G = (g_1, \ldots, g_m) \in \Omega(\mathbf{e}_1)$, if and only if $G(\mathbf{e}_1) = 0$ and the Jacobian $JG(\mathbf{x})$ has rank at most $m-1$. This means that the distance from $\Omega(\mathbf{e}_1)$ to F_0 is minimized at a polynomial of the form $G_0(\mathbf{x}) = x_0^{d-1} \cdot B\,(x_1, \ldots, x_n)^T \in \Omega(\mathbf{e}_1)$, where B has rank at most $m-1$. We have

$$\|F_0 - G_0\|^2_{\mathrm{BW}} = \|a\|^2 + \|D^{-1/2}\,(A - B)\|^2.$$

The Eckhart-Young theorem implies that the distance of $D^{-1}A$ to the variety of matrices of rank at most $m-1$ is precisely $\sigma_m(D^{-1/2}A)$. Since the singular values of a matrix are invariant under multiplication with orthogonal matrices, we have $\sigma_m(D^{-1/2}A) = \sigma_m(D^{-1/2}\, JF(\mathbf{x})\, P_{\mathbf{x}})$. Consequently,

$$\operatorname{dist}_{\mathrm{BW}}(F, \Omega(\mathbf{x})) = \sqrt{\|a\|^2 + \sigma_m(D^{-1}A)^2} = \sqrt{\|F(\mathbf{x})\|^2 + \sigma_m(D^{-1/2}\, JF(\mathbf{x})\, P_{\mathbf{x}})^2}.$$

Combining this with (9.7) proves the statement. □

Remark 9.17 The statement of Theorem 9.16 can be generalized as follows. Fix $1 \le k < m$. The distance of $F \in \mathcal{H}_{\mathbf{d}}$ to the space of systems of polynomials $F \in \mathcal{H}_{\mathbf{d}}$, such that there exists $\mathbf{x} \in \mathbb{P}^n_{\mathbb{R}}$ with $F(\mathbf{x}) = 0$ and $\operatorname{rank} JF(\mathbf{x}) < k$ is given by

$$\min_{\mathbf{x}\in\mathbb{S}^n} \sqrt{\|F(\mathbf{x})\|^2 + \sum_{i=k}^{m} \sigma_i(D^{-1}\, JF(\mathbf{x})\, P_{\mathbf{x}})^2},$$

where $\sigma_k(\cdot), \ldots, \sigma_m(\cdot)$ are the $m-k+1$ smallest singular values. This is because the distance of a matrix $A \in \mathbb{R}^{m\times n}$ to the nearest matrix of rank at most $k-1$ is $\sqrt{\sum_{i=k}^m \sigma_i(A)^2}$, by the Eckart-Young Theorem.

Remark 9.18 In the case $m = 1$, where we have only one polynomial $f \in \mathcal{H}_d$, Theorem 9.16 yields $\operatorname{dist}_{\mathrm{BW}}(f, \Omega) = \min_{\mathbf{x}\in\mathbb{S}^n} \sqrt{f(\mathbf{x})^2 + \frac{1}{d}\|P_{\mathbf{x}}\nabla f(\mathbf{x})\|^2}$, where $\nabla f(\mathbf{x}) = \left(\frac{\partial f}{\partial x_1}(\mathbf{x}), \ldots, \frac{\partial f}{\partial x_1}(\mathbf{x})\right)^T$ is the gradient of f at $\mathbf{x}$ (the gradient is a column vector, so we have to multiply it by $P_{\mathbf{x}}$ from the left). By Euler's formula for homogeneous functions, $\mathbf{x}^T\nabla f(\mathbf{x}) = d \cdot f(\mathbf{x})$, so $P_{\mathbf{x}}\nabla f(\mathbf{x}) = \nabla f(\mathbf{x}) - (d \cdot f(\mathbf{x}))\,\mathbf{x}$. We get

$$\operatorname{dist}_{\mathrm{BW}}(f, \Omega) = \min_{\mathbf{x}\in\mathbb{S}^n} \sqrt{f(\mathbf{x})^2 + \tfrac{1}{d}\|\nabla f(\mathbf{x}) - (d \cdot f(\mathbf{x}))\,\mathbf{x}\|^2}\,. \tag{9.8}$$

Example 9.19 We use the formula (9.8) for computing the distance of the Fermat cubic $f(\mathbf{x}) = x_0^3+x_1^3+x_2^3$ to the real polynomial discriminant Ω. Let $h(\mathbf{x}) = (x_0^3 + x_1^3 + x_2^3)^2 + 3\sum_{i=0}^2 \left(x_i^2 - (x_0^3 + x_1^3 + x_2^3)\, x_i\right)^2$. Then $\mathrm{dist}_{\mathrm{BW}}(f, \Omega) = \min_{\mathbf{x}\in\mathbb{S}^n} \sqrt{h(\mathbf{x})}$. The polynomial function $h : \mathbb{S}^2 \to \mathbb{R}$ is minimized at the point $\mathbf{x}_0 = \frac{1}{\sqrt{3}}(1, 1, 1)$, which gives

$$\mathrm{dist}_{\mathrm{BW}}(f, \Omega) = \sqrt{h(\mathbf{x}_0)} = \frac{1}{\sqrt{3}}.$$

The norm of the Fermat Cubic is $\|f\|_{\mathrm{BW}} = \sqrt{3}$. Since Ω is a cone, the minimal angle (measured in the Bombieri-Weyl metric) between f and a polynomial in Ω therefore is $\arcsin(1/3) \approx 0.21635 \cdot \frac{\pi}{2}$. ⋄

We interpret Theorem 9.16 from the perspective of condition numbers. Consider the problem of computing the regular zeros of a square system of polynomial equations $F \in \mathcal{H}_{\mathbf{d}}$, where $\mathbf{d} = (d_1, \ldots, d_n)$, in n variables $\mathbf{x} = (x_1, \ldots, x_n)$. We can compute the zeros in projective space $\mathbb{P}^n_{\mathbb{R}}$ or in the sphere $\mathbb{S}^n$. We use the metric structure of the latter to establish a condition number for this problem.

Suppose that $\mathbf{x} \in \mathbb{S}^n$ is a regular zero of $F \in \mathcal{H}_{\mathbf{d}}$. The implicit function theorem implies that there exists a neighborhood $\mathcal{U} \subset \mathcal{H}_{\mathbf{d}}$ of F and a smooth map $s : \mathcal{U} \to \mathbb{S}^n$ such that $F(s(F)) = 0$ for all $F \in \mathcal{U}$. One can show that the operator norm of $D_F s$ is the operator norm of $(JF(\mathbf{x})\, P_{\mathbf{x}})^{-1}$. By Rice's theorem (Theorem 9.6), the condition number of solving $F(\mathbf{x}) = 0$ therefore is

$$\kappa[s](F) = \|JF(\mathbf{x})^{-1}\|_{\mathrm{op}} = \frac{1}{\sigma_n(JF(\mathbf{x})\, P_{\mathbf{x}})}.$$

By contrast, in the proof of Theorem 9.16 we have shown that $\sigma_n(D^{-1/2}JF(\mathbf{x})\, P_{\mathbf{x}}) = \mathrm{dist}_{\mathrm{BW}}(f, \Omega(\mathbf{x}))$. This means that for the problem of solving systems of polynomial equations we have an "almost" condition number theorem (up to the additional factor $D^{-1/2}$).

Chapter 10
Machine Learning

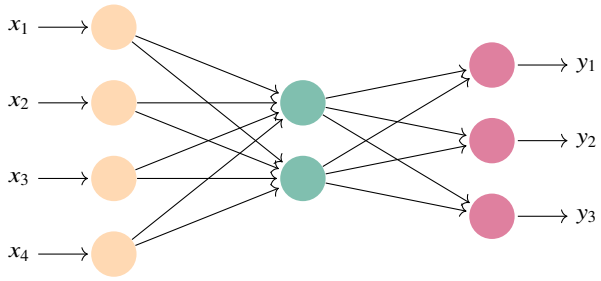

Fig. 10.1: A fully-connected feedforward neural network with two layers $f_{1,\theta} : \mathbb{R}^4 \to \mathbb{R}^2$ and $f_{2,\theta} : \mathbb{R}^2 \to \mathbb{R}^3$.

A *feedforward neural network* is a family of functions that is given by the network's parametrization map

$$\begin{aligned} \mu : \mathbb{R}^N &\longrightarrow \mathcal{M}, \\ \theta &\longmapsto f_{L,\theta} \circ \cdots \circ f_{2,\theta} \circ f_{1,\theta}; \end{aligned} \tag{10.1}$$

see Figure 10.1. Each parameter tuple θ determines a function $f_{i,\theta}$ in each layer of the network whose composition is the end-to-end function $\mu(\theta)$. The map μ depends on the network's architecture, including the number L of layers, the width of each layer (i.e., the dimension of the domain of each $f_{i,\theta}$), and the type of each layer function $f_{i,\theta}$. Most commonly, the layer functions are compositions

$$f_{i,\theta} = \sigma_i \circ \alpha_{i,\theta} \tag{10.2}$$

of an affine map $\alpha_{i,\theta} : \mathbb{R}^{k_{i-1}} \to \mathbb{R}^{k_i}$ with a (typically non-linear) map $\sigma_i : \mathbb{R}^{k_i} \to \mathbb{R}^{k_i}$ that applies the same *activation function* $\tilde{\sigma}_i : \mathbb{R} \to \mathbb{R}$ to each component, i.e., $\sigma_i(x) = \big(\tilde{\sigma}_i(x_1), \ldots, \tilde{\sigma}_i(x_{k_i})\big)$. The image $\mathcal{M}$ of the network's parametrization map μ is called the *function space* or *neuromanifold* of the neural network architecture (although $\mathcal{M}$ is typically not a smooth manifold).

A neural network is typically trained by minimizing a loss function of the form

$$\mathcal{L} : \mathbb{R}^N \xrightarrow{\mu} \mathcal{M} \xrightarrow{\ell_{\mathcal{D}}} \mathbb{R}, \tag{10.3}$$

where the functional $\ell_{\mathcal{D}}$ depends on training data $\mathcal{D}$. Many geometric questions arise in the theoretical study of this optimization problem, e.g.,

1. How does the network architecture affect the geometry of the function space $\mathcal{M}$?
2. How does the geometry of the function space impact the training of the network?

We discuss these questions in the following two sections for network architectures that can be studied with techniques from nonlinear algebra, i.e., where the activation function is the identity, polynomial, or ReLU. In Section 10.3, we give a brief account of the practical usage of machine learning for algebro-geometric computations. This chapter is not intended as a complete survey of the mathematical theory of machine learning with neural networks. We refer the interested reader to the book *Mathematical Aspects of Deep Learning* [79] and the references therein. In the following, we only highlight some algebro-geometric concepts in neural-network theory.

10.1 Expressivity

The study of which functions a given neural network can express or approximate is commonly referred to as expressivity.

Linear and Fully Connected.

The simplest class of networks are *linear fully-connected neural networks* where the activation function $\tilde{\sigma}_i$ in each layer i is the identity and the layer functions $f_{i,\theta}$ are arbitrary linear maps. In that case, the parameters θ are the entries of the matrices representing the linear layer functions. In other words, the network parametrization map (10.1) specializes to

$$\begin{aligned} \mu : \mathbb{R}^{k_1 \times k_0} \times \mathbb{R}^{k_2 \times k_1} \times \ldots \times \mathbb{R}^{k_L \times k_{L-1}} &\longrightarrow \mathbb{R}^{k_L \times k_0}, \\ (W_1, W_2, \ldots, W_L) &\longmapsto W_L \cdots W_2 W_1. \end{aligned} \tag{10.4}$$

Its image is the determinantal variety $\mathcal{M} = \{W \in \mathbb{R}^{k_L \times k_0} \mid \operatorname{rank}(W) \leq \min(k_0, k_1, \ldots, k_L)\}$. If the input or output dimension is one of the minimal widths (i.e., $\min(k_0, k_1, \ldots, k_L) = \min(k_0, k_L)$), the function space is the whole ambient vector space: $\mathcal{M} = \mathbb{R}^{k_L \times k_0}$. Otherwise, the function space $\mathcal{M}$ is a lower-dimensional Zariski closed subset whose singular locus is parametrized by a smaller network architecture: $\operatorname{Sing}(\mathcal{M}) = \{W \in \mathbb{R}^{k_L \times k_0} \mid \operatorname{rank}(W) \leq \min(k_0, k_1, \ldots, k_L) - 1\}$.

Linear and Convolutional.

Many neural networks that are used in practice have *convolutional layers* (instead of fully-connected ones) where the affine map $\alpha_{i,\theta}$ in (10.2) is a convolution. A convolution on one-dimensional signals depends on a *filter* $w \in \mathbb{R}^r$ and a stride $s \in \mathbb{N}$. It computes the inner product of the filter w with parts of a given input vector v, and traverses the whole vector v by moving the filter w through it with stride s; in formulas,

$$\begin{aligned} \alpha_{w,s} : \mathbb{R}^{s(k-1)+r} &\longrightarrow \mathbb{R}^k, \\ v &\longmapsto \left(\sum_{j=0}^{r-1} w_j \cdot v_{is+j} \right)_{i=0}^{k-1}. \end{aligned}$$

A *linear convolutional neural network* is the composition of L such convolutions with filter sizes $(r_1, r_2, \ldots, r_L)$ and strides $(s_1, s_2, \ldots, s_L)$. The resulting end-to-end function is also a convolution with filter size $r := \sum_{i=1}^{L} (r_i - 1) S_i + 1$, where $S_i := \prod_{j=1}^{i-1} s_j$ (and $S_1 := 1$), and stride S_{L+1}. Hence, the network parametrization map (10.1) becomes

$$\mu : \mathbb{R}^{r_1} \times \mathbb{R}^{r_2} \times \ldots \times \mathbb{R}^{r_L} \longrightarrow \mathbb{R}^r,$$

sending the filters of each layer to the filter of the end-to-end convolution. Equivalently, the end-to-end filter can be computed via polynomial multiplication as follows: For positive integers S and r, we write $\mathbb{R}[x^S, y^S]_{r-1}$ for the vector space of all polynomials that are homogeneous of degree $r - 1$ in the pair (x^S, y^S). We then identify any filter of size r with the coefficient vector of such a polynomial via

$$\pi_{S,r} : \mathbb{R}^r \longrightarrow \mathbb{R}[x^S, y^S]_{r-1},$$
$$w \longmapsto w_0 x^{S(r-1)} + w_1 x^{S(r-2)} y^S + \ldots + w_{r-2} x^S y^{S(r-2)} + w_{r-1} y^{S(r-1)}.$$

Then, the end-to-end filter corresponds to a polynomial with a sparse factorization given by the filters in the L layers:

$$\pi_{1,r}(\mu(w_1, \ldots, w_L)) = \pi_{S_L,r_L}(w_L) \cdots \pi_{S_2,r_2}(w_2) \cdot \pi_{S_1,r_1}(w_1).$$

In other words, we can reinterpret the network parametrization map as polynomial multiplication:

$$\begin{aligned} \mu : \mathbb{R}[x^{S_1}, y^{S_1}]_{r_1-1} \times \mathbb{R}[x^{S_2}, y^{S_2}]_{r_2-1} \times \ldots \times \mathbb{R}[x^{S_L}, y^{S_L}]_{r_L-1} &\longrightarrow \mathbb{R}[x, y]_{r-1}, \\ (P_1, P_2, \ldots, P_L) &\longmapsto P_L \cdots P_2 P_1. \end{aligned} \tag{10.5}$$

Hence, the function space $\mathcal{M}_{\boldsymbol{r},\boldsymbol{s}} = \mathrm{im}(\mu)$ of a linear convolutional network is a semialgebraic set of polynomials with a sparse factorization given by the network's filter sizes $\boldsymbol{r} = (r_1, \ldots, r_L)$ and strides $\boldsymbol{s} = (s_1, \ldots, s_L)$. It is closed in the Euclidean topology, and describing its Euclidean relative boundary is a challenging problem [112]. As in the case of fully-connected linear networks, its singular locus is parametrized by smaller network architectures. To see this, we successively merge all neighboring layers $i-1$ and i in (10.5) with $S_{i-1} = S_i$ to eventually obtain a *reduced architecture* $(\tilde{\boldsymbol{r}}, \tilde{\boldsymbol{s}})$ such that $1 = \tilde{S}_1 < \tilde{S}_2 < \tilde{S}_3 < \ldots$ (where $\tilde{S}_i := \prod_{j=1}^{i-1} \tilde{s}_j$). This process can enlarge the function space, i.e., $\mathcal{M}_{\boldsymbol{r},\boldsymbol{s}} \subseteq \mathcal{M}_{\tilde{\boldsymbol{r}},\tilde{\boldsymbol{s}}}$, but does not change its Zariski closure in $\mathbb{R}[x, y]_{r-1}$, i.e., $\overline{\mathcal{M}}_{\boldsymbol{r},\boldsymbol{s}} = \overline{\mathcal{M}}_{\tilde{\boldsymbol{r}},\tilde{\boldsymbol{s}}}$ [112, Lemma 3.5]. Hence, to determine the singular locus of the Zariski closure of the function space, it is sufficient to assume that its architecture is reduced. If the reduced architecture has a single layer, the Zariski closure of the function space is the whole ambient vector space: $\overline{\mathcal{M}}_{\boldsymbol{r},\boldsymbol{s}} = \mathbb{R}[x, y]_{r-1}$. Otherwise, it is a lower-dimensional subvariety whose singular locus is a union of lower-dimensional function spaces with the same reduced stride sequence:

Theorem 10.1 ([112, Theorem 2.8]) *Let $(\boldsymbol{r}, \boldsymbol{s})$ be a reduced architecture with $L > 1$ layers of a linear convolutional network. Then,*

$$\mathrm{Sing}(\overline{\mathcal{M}}_{\boldsymbol{r},\boldsymbol{s}}) = \{0\} \cup \bigcup_{\boldsymbol{r}' \in R} \overline{\mathcal{M}}_{\boldsymbol{r}',\boldsymbol{s}} = \{0\} \cup \bigcup_{\boldsymbol{r}' \in R} \mathcal{M}_{\boldsymbol{r}',\boldsymbol{s}},$$

where $R := \{\boldsymbol{r}' \in \mathbb{Z}^L_{\geq 0} \mid \overline{\mathcal{M}}_{\boldsymbol{r}',\boldsymbol{s}} \subsetneq \overline{\mathcal{M}}_{\boldsymbol{r},\boldsymbol{s}}\}$.

Remark 10.2 The discussion above is restricted to convolutions on one-dimensional signals. Many practical neural networks use convolutions on two-dimensional signals, e.g., when the input data is pictures. Higher-dimensional convolutions move a *filter tensor* w through an *input tensor* v of the same dimension. The composition of such convolutions corresponds to the multiplication of multivariate polynomials (cf. [111, Section 4.3]).

Non-Linear.

The theoretical study of neural networks becomes a lot more challenging if the activation function is non-linear. A first algebro-geometric study for polynomial activation functions is pursued in [108]. For fully-connected neural networks with an activation function that takes the n-th power (i.e., $\tilde{\sigma}_i : x \mapsto x^n$), the authors provide bounds on the dimension of the semi-algebraic function space, with equality in some cases, and conditions for when the (Zariski closure) of the function space is a vector space.

A common activation function in practice is *rectified linear unit (ReLU)*, i.e., $\tilde{\sigma}_i : x \mapsto \max(0, x)$. The end-to-end function of a ReLU neural network is piecewise affine-linear. In fact, every piecewise linear functions with finitely many pieces can be obtained from a fully-connected ReLU network [5]. Although ReLU end-to-end functions are not algebraic, it was explained in [183] that they can be interpreted as tropical rational functions. That perspective was developed further in [134] to provide sharp bounds on the number of linear regions of the end-to-end functions. The local dimension of ReLU function spaces was investigated in [78].

10.2 Optimization

The theoretical works on the optimization problem of training neural networks can be roughly grouped into *static* and *dynamic* studies. Static investigations concern the loss landscape [125] and the critical points of (10.3), while dynamic studies depend on the choice of a training algorithm, e.g., investigating its convergence.

10.2.1 Static Properties

One of the big mysteries in machine learning theory is why training neural networks (i.e., minimizing the loss function (14.5)) results in "nice" minima. The concrete meaning of the adjective nice varies in the literature (see also the algebro-geometric article [130] clarifying the various uses of "flat" minima).

Training a neural network minimizes the loss function $\mathcal{L} = \ell_{\mathcal{D}} \circ \mu$ in (10.3) on the parameter space. The meaningful critical points of that minimization problem are those that actually come from critical points of $\ell_{\mathcal{D}}$ on the function space. Formally, such *pure critical points* θ of $\mathcal{L}$ satisfy that $\mu(\theta)$ is a smooth point of the function space $\mathcal{M}$ and a critical point of the functional $\ell_{\mathcal{D}}$ restricted to smooth locus $\mathrm{Reg}(\mathcal{M})$. The network parametrization map μ can induce additional *spurious critical points* of $\mathcal{L}$.

Linear and Fully-Connected.

For linear fully-connected networks, the pure and spurious critical points were characterized in [32]. Recall that in that case the function space $\mathcal{M}$ is the determinantal variety consisting of all matrices whose rank is bounded from above by a constant determined by the network's architecture. The critical points θ of $\mathcal{L}$ such that $\mu(\theta)$ is a matrix of maximal possible rank are pure [32, Proposition 6]. In other words, all spurious critical points θ correspond to lower-rank matrices $\mu(\theta)$ (i.e., they map to the singular locus of the function space $\mathcal{M}$ if the latter is a proper subvariety of the ambient vector space). Moreover, spurious critical points are essentially always saddles [32, Proposition 9]. More concretely, if $\ell_{\mathcal{D}}$ is a smooth and convex function, then all non-global local minima of $\mathcal{L}$ (often called "bad" minima in the literature) are pure critical points [32, Proposition 10]. It is a common, but false, belief that linear fully-connected networks generally do not have "bad" minima. In fact, the previous cited result implies the following:

Theorem 10.3 ([32, Proposition 10]) *Consider a linear fully-connected network and a smooth and convex function $\ell_{\mathcal{D}}$. Then, $\mathcal{L} = \ell_{\mathcal{D}} \circ \mu$ has non-global local minima if and only if $\ell_{\mathcal{D}}|_{\mathrm{Reg}(\mathcal{M})}$ has non-global local minima.*

Two well-known results from machine learning theory are immediate consequences of this theorem. First, if $\mathcal{M}$ is equal to the ambient vector space (i.e., the input or output dimension of the network is one of

its minimal widths), then any convex function $\ell_{\mathcal{D}}$ has exactly one minimum on $\mathcal{M}$ (namely, its global minimum), and hence $\mathcal{L}$ does not have any non-global minima. This is the main result from [120]. The second well-known result applies to the squared-error loss $\ell_{\mathcal{D}}$

$$\begin{aligned} \ell_{\mathcal{D}} : \mathbb{R}^{k_L \times k_0} &\longrightarrow \mathbb{R}, \\ W &\longmapsto \sum_{i=1}^{d} \|Wx_i - y_i\|^2, \end{aligned} \tag{10.6}$$

where the training data $\mathcal{D}$ consists of pairs of input and output vectors $(x_i, y_i) \in \mathbb{R}^{k_0} \times \mathbb{R}^{k_L}$. Writing $X \in \mathbb{R}^{k_0 \times d}$ and $Y \in \mathbb{R}^{k_L \times d}$ for the data matrices whose i-th columns are x_i and y_i, respectively, the squared-error loss becomes the squared Frobenius norm $\ell_{\mathcal{D}}(W) = \|WX - Y\|^2$. If $XX^\top$ is a full-rank matrix, minimizing this squared Frobenius norm over all $W \in \mathrm{Reg}(\mathcal{M})$ is equivalent to minimizing the squared Euclidean distance

$$\|W - U\|^2, \qquad \text{where } U := YX^\top((XX^\top)^{\frac{1}{2}})^{-1}, \tag{10.7}$$

over all $W \in \mathrm{Reg}(\mathcal{M})$; see [32, Section 3.3]. Now, the Eckart-Young Theorem tells us that the latter optimization problem has a unique local and global minimum if the singular values of U are pairwise distinct and positive. Hence, if there are sufficiently many and sufficiently generic data pairs (x_i, y_i), the squared-error loss $\ell_{\mathcal{D}}$ has no non-global minima on $\mathrm{Reg}(M)$ and so Theorem 10.3 shows that the squared-error loss $\mathcal{L}$ on the parameter space has no "bad" minima. The latter is a celebrated result in the machine learning community, often attributed to [8] or [106]. However, the settings where the function space $\mathcal{M}$ is a vector space or the loss function is the squared-error loss, are rather special, and Theorem 10.3 suggests that we should expect the existence of non-global local minima for other loss functions and architectures where $\mathcal{M}$ is a proper determinantal variety; see also [32, Example 13].

Linear and Convolutional.

For linear convolutional networks where are all strides are one, the associated reduced network architecture has a single layer and so the function space $\mathcal{M}$ is a Euclidean closed, full-dimensional semialgebraic subset of the ambient vector space $\mathbb{R}[x, y]_{r-1}$. Therefore, critical points of the loss $\mathcal{L}$often correspond to points $\mu(\theta)$ on the Euclidean boundary of $\mathcal{M}$, and in particular have to be critical points of the network parametrization map μ. This is in sharp contrast to linear convolutional networks where all strides are strictly larger one (i.e., reduced architectures):

Theorem 10.4 ([112, Theorem 2.11]) *Let $(\boldsymbol{r}, \boldsymbol{s})$ be a reduced architecture with L layers of a linear convolutional network. Moreover, let $d \geq r := \sum_{i=1}^{L}(r_i - 1)S_i + 1$, where $S_i := \prod_{j=1}^{i-1} s_j$. For almost all d-tuples $\mathcal{D}$ of training data, every critical point θ of the the squared-error loss $\mathcal{L} = \ell_{\mathcal{D}} \circ \mu$ satisfies one of the following:*

1. *θ is a regular point of μ and $\mu(\theta)$ is a smooth point in the Euclidean relative interior of $\mathcal{M}$ (in particular, θ is a pure critical point), or*
2. *$\mu(\theta) = 0$.*

Here, the squared-error loss is the same as in (10.6) where the W are the matrices representing the end-to-end convolutions.

We summarize the discussion so far for training linear networks with the squared-error loss. For fully-connected networks, the function space $\mathcal{M}$ is a determinantal variety. In particular, its Euclidean relative boundary is empty. Nevertheless, spurious critical points commonly appear; namely, they correspond to

singular points of $\mathcal{M}$. For convolutional networks of stride one, the function space is a semialgebraic, Euclidean closed, full-dimensional subset. So its singular locus (formally, the singular locus of its Zariski closure) is empty, but often critical points are on its Euclidean boundary and are thus critical points of μ. Finally, for convolutional networks with all strides strictly larger one, the function space $\mathcal{M}$ is a semialgebraic, Euclidean closed, lower-dimensional subset. Hence, it typically has a non-trivial Euclidean relative boundary and a non-trivial singular locus (of its Zariski closure). Nevertheless, these loci are not relevant for training the network when using a sufficient amount of generic data, because all critical points – except those where a filter in one of the layers is zero – are pure (even stronger, regular points of μ) and correspond to interior smooth points of $\mathcal{M}$.

10.2.2 Dynamic Properties

The most common optimization algorithms in the training of neural networks are variations of gradient descent. After picking initial parameters θ, gradient descent adapts the parameters successively with the goal to minimize the loss $\mathcal{L}(\theta)$.

Linear and Fully-Connected.

When training linear fully-connected networks using the squared-error loss such that the data matrix $XX^\top$ in (10.7) has full rank, gradient descent converges for almost all initializations (under reasonable assumptions on its step sizes) to a critical point θ of the loss $\mathcal{L}$ [136, Theorem 2.4]. Moreover, the matrix $\mu(\theta) \in \mathcal{M}$ is a global minimum of ℓ_D restricted to the smooth manifold of all matrices of the same format and same rank [136, Theorem 2.6]. The authors of [136] conjecture that the matrix $\mu(\theta)$ has in fact the maximal possible rank in $\mathcal{M}$ (in other words, that $\mu(\theta)$ is a smooth point of the function space $\mathcal{M}$), but their proof techniques cannot exclude that the critical point θ computed by gradient descent is a *non-strict saddle point* of the loss $\mathcal{L}$ and those saddle points may correspond to lower-rank matrices $\mu(\theta)$.

An essential ingredient in the convergence analysis of [136] are the *algebraic invariants* of gradient flow. The curve in parameter space traced by gradient flow is typically transcendental, but it does satisfy some algebraic relations. In other words, its Zariski closure is not the whole ambient parameter space.

Proposition 10.5 ([6]) *Consider a linear fully-connected neural network with parametrization map* (10.4). *Let* $\theta(t) = (W_1(t), W_2(t), \ldots, W_L(t))$ *for* $t \geq 0$ *be the curve traced by gradient flow initialized at* $t = 0$. *Then the quantities*

$$W_i^\top(t)W_i(t) - W_{i-1}(t)W_{i-1}^\top(t) \quad \text{for } i = 2, 3, \ldots, L$$

remain constant for all $t \geq 0$.

This result also has practical consequences: A parameter tuple $\theta = (W_1, \ldots, W_L)$ is called *balanced* if $W_i^\top W_i = W_{i-1}W_{i-1}^\top$ for all $i \in \{2, \ldots, L\}$. In particular, all matrices in a balanced tuple need to have the same Frobenius norm, i.e., $\|W_i\| = \|W_1\|$ for all $i \in \{2, \ldots, L\}$. If a linear network is initialized at a balanced parameter tuple $\theta(0)$, then it follows from Proposition 10.5 that every parameter tuple $\theta(t)$ along the gradient flow curve is balanced. Since all matrices in the balanced tuple $\theta(t)$ need to have the same Frobenius norm, it can in particular not happen that one of the matrices converges to zero while another matrix in the tuple has entries that converge to infinity. In fact, if one matrix in a balanced tuple converges to zero, the whole tuple converges to zero.

Algebraic invariants of gradient flow have also been computed for linear convolutional networks [111, Proposition 5.13] and ReLU networks [179, Lemma 3]; see also [62, Theorems 2.1–2.2].

Nonlinear Autoencoders.

Invariants also play a crucial role in the study of attractors of autoencoders. An *autoencoder* is a composition of two feedforward neural networks: an encoder and a decoder network, such that the input dimension of the encoder equals the output dimension of the decoder. It is typically trained using the *autoencoding loss*

$$\arg\min_{f\in\mathcal{M}} \sum_{i=1}^{d} \|f(x_i) - x_i\|^2,$$

where $\mathcal{M}$ is the function space of the composed autoencoder network and the $x_1, \ldots, x_d$ are training data. It is shown in [150] that an autoencoder trained with gradient descent on a single training example x (i.e., $d = 1$) memorizes that example x as an attractor (under suitable assumptions on the activation function and initialization). An *attractor* x of the learned function $f \in \mathcal{M}$ is a fixed point such that in an open neighborhood O of x, for any $y \in O$, the sequence $\left(f^i(y)\right)_{i\in\mathbb{N}}$ converges to x as $i \to \infty$.

10.3 Machine Learning in Algebraic Geometry

Several works have explored how machine learning can be helpful in algebraic geometry research, some of which we outline shortly below. However, it is not clear yet what type of information can be learned and which type of tasks can be solved by training neural networks. Despite its massive success for classification tasks (e.g., "is there a cat on this pircture?"), machine learning with neural networks has not improved explicitly geometric tasks such as solving systems of polynomial equations. For instance, the structure-from-motion problem in computer vision (see Chapter 13) is essentially equivalent to solving certain polynomial equation systems. The attempts to solve that problem with machine learning methods have not been as successful as traditional computer vision techniques that are based on symbolic computations with Gröbner bases or resultants [159, 184].

The works that have used machine learning techniques to answer questions in algebraic geometry come roughly in two flavors. On the one hand, several machine learning techniques have been implemented to directly compute geometric properties, e.g. of Hilbert series [9], of irreducible representations [45], or numerical Calabi-Yau (Ricci flat Kähler) metrics [59]. Those approaches trade off the reliability of the computed solutions with performance, which can yield insights into problem instances that lie outside of the scope of traditional computation techniques.

On the other hand, many algebro-geometric algorithms depend on a heuristic that has to be chosen by the user and that might heavily influence their performance. For instance, to obtain a Gröbner basis of a polynomial equation system, we need to choose a monomial ordering. Machine learning has been successful at predicting such a heuristic for a given problem instance which then speeds up the computation using traditional algorithms. In that way the performance can be enhanced without compromising the reliability of the final output. This approach has been used to speed up both Buchberger's algorithm by learning S-pair selection strategies [143] and Cylindrical Algebraic Decomposition by learning a variable ordering and whether Gröbner basis preconditioning is beneficial [100]. In a similar spirit, the authors of [87] improve the computation of periods of hypersurfaces. Their strategy considers pencils of hypersurfaces and uses neural networks to predict the complexity of the Gauss-Manin connection which governs the change of the period matrix along the pencil. Based on that prediction, they explore the space of smooth squartic surface in $\mathbb{P}^3$ that are defined by a sum of five monomials and guess for which of those their periods are computable by non-learning algorithms. This leads them to determine the periods of 96% of those surfaces.

Although neural networks have not shown a great potential for explicitly solving systems of polynomial equations, they can be trained to predict their number of real solutions [15, 29]. Such a prediction can be potentially used by real homotopy methods that only track real solutions instead of all complex solutions if one has pre-computed a starting system for each possible number of real solutions (in the best case, even for each chamber in the complement of the real discriminant). That would yield a reliable numerical computation that requires less computation time since it tracks fewer paths. A more drastic approach has been taken in [98] where the authors learn a *single* starting solution for a real homotopy that has good chances to reach a good solution of the desired target system. That way of computing produces a less reliable solution, but since they propose their method as part of a random sample consensus (RANSAC) scheme, bad solutions can be detected and disregarded. Since tracking a single solution can be very fast, they can simply repeat their approach for each bad solution.

Chapter 11
Maximum Likelihood

This book started out with the problem of minimizing the Euclidean distance from a data point $\mathbf{u}$ to a model X that is given by polynomial equations. We studied the analogous problem in the setting of algebraic statistics [170], where the model X represents a family of probability distributions, and we used the Wasserstein metric to measure the distances from $\mathbf{u}$ to X. In this chapter we stay with statistical models but we now use Kullback-Leibler divergence and likelihood inference instead of Wasserstein distance.

11.1 Kullback-Leibler Divergence

The two scenarios of most interest for statisticians are Gaussian models and discrete models. We start with discrete models, where we take the state space is the finite set $\{0, 1, \ldots, n\}$. The simplex of all probability distributions on this state space equals

$$\Delta_n \;=\; \bigl\{ \mathbf{p} = (p_0, p_1, \ldots, p_n) \in \mathbb{R}^{n+1} \;:\; p_0 + p_1 + \cdots + p_n = 1 \text{ and } p_0, p_1, \ldots, p_n > 0 \bigr\}. \tag{11.1}$$

Given two probability distributions $\mathbf{q}$ and $\mathbf{p}$ in Δ_n, their *Kullback-Leibler (KL) divergence* is defined as

$$D_{\mathrm{KL}}(\,\mathbf{q}\,||\,\mathbf{p}\,) \;=\; \sum_{i=0}^{n} q_i \cdot \log(q_i/p_i). \tag{11.2}$$

This function is not symmetric in its two arguments, i.e. we have $D_{\mathrm{KL}}(\,\mathbf{q}\,||\,\mathbf{p}\,) \neq D_{\mathrm{KL}}(\,\mathbf{p}\,||\,\mathbf{q}\,)$ in general. Nevertheless, we interpret KL divergence as a kind of metric on the open simplex Δ_n.

Lemma 11.1 *The KL divergence is nonnegative and it is zero if and only if the two distributions agree. In symbols,* $D_{\mathrm{KL}}(\,\mathbf{q}\,||\,\mathbf{p}\,) \;\geq\; 0$ *for all* $\mathbf{p}, \mathbf{q} \in \Delta_n$*, and equality holds if and only if* $\mathbf{p} = \mathbf{q}$.

Proof We use the calculus fact that the function $x \mapsto (x-1) - \log(x)$ is nonnegative for $x \in \mathbb{R}_{>0}$ and its only zero occurs at $x = 1$. Hence the sum in (11.2) is bounded below as follows:

$$D_{\mathrm{KL}}(\,\mathbf{q}\,||\,\mathbf{p}\,) \;=\; -\sum_{i=0}^{n} q_i \cdot \log(p_i/q_i) \;\geq\; -\sum_{i=0}^{n} q_i \cdot \bigl(p_i/q_i - 1\bigr) \;=\; \sum_{i=0}^{n} p_i \;-\; \sum_{i=0}^{n} q_i \;=\; 1 - 1 \;=\; 0.$$

Moreover, equality holds if and only if $p_i/q_i = 1$ for all indices i. □

Our model is a subset X of Δ_n defined by homogeneous polynomial equations. As before, for venturing beyond linear algebra, we identify X with its Zariski closure in complex projective space $\mathbb{P}^n$.

We shall present the algebraic approach to maximum likelihood estimation (MLE). Our sources include [40, 63, 92, 103, 104, 170] and references therein. Suppose we are given N i.i.d. samples. These are summarized in the *data vector* $\mathbf{u} = (u_0, u_1, \ldots, u_n)$ where u_i is the number of samples that were in state i. Thus the sample size is $N = u_0 + u_1 + \cdots + u_n$. The associated log-likelihood function equals

$$\ell_{\mathbf{u}} : \Delta_n \to \mathbb{R}, \;\; \mathbf{p} \mapsto u_0 \cdot \log(p_0) \;+\; u_1 \cdot \log(p_1) \;+\; \cdots + \; u_n \cdot \log(p_n).$$

Performing MLE for the model X means solving the following optimization problem:

$$\text{Maximize } \; \ell_{\mathbf{u}}(\mathbf{p}) \;\; \text{subject to } \; \mathbf{p} \in X. \tag{11.3}$$

Viewed through the lens of metric algebraic geometry, this problem amounts to minimizing a certain distance, namely KL divergence, to the variety X. Namely, given a data vector $\mathbf{u}$ with $u_i > 0$ for all i, we write $\mathbf{q} = \frac{1}{N}\mathbf{u}$ for the corresponding empirical distribution in Δ_n.

Remark 11.2 The maximum likelihood estimation problem (11.3) is equivalent to:

$$\text{Minimize } \; D_{\mathrm{KL}}(\,\mathbf{q}\,||\,\mathbf{p}\,) \;\text{ subject to }\; \mathbf{p} \in X. \tag{11.4}$$

This holds because the KL divergence can be rewritten as the entropy of the empirical distribution $\mathbf{q}$ minus the log-likelihood function: $D_{\mathrm{KL}}(\,\mathbf{q}\,||\,\mathbf{p}\,) \;=\; \sum_{i=0}^{n} q_i \log(q_i) \;-\; \frac{1}{N}\,\ell_{\mathbf{u}}(\mathbf{p})$.

As before, we identify the model X with a projective variety in $\mathbb{P}^n$. The objective function in the optimization problem (11.3) involves logarithms and it is not an algebraic function. However, each of its partial derivatives is a rational function, and therefore we can study this problem using algebraic geometry.

11.2 Maximum Likelihood Degree

We fix a real projective variety X in $\mathbb{P}^n$, and we consider the the optimization problem in (11.3) or (11.4) The *maximum likelihood degree (ML degree)* of X is defined to be the number of complex critical points of this optimization problem for generic data $\mathbf{u}$. For arbitrary fixed data $\mathbf{u}$, the optimal solution is denoted $\hat{\mathbf{p}}$ and called the *maximum likelihood estimate* of the model X for the data $\mathbf{u}$. Thus ML degree is the analogue to ED degree, when now KL divergence replaces Euclidean distance.

The critical equations for (11.3) are similar to those of ED problem. Let $I_X = \langle f_1, \ldots, f_k \rangle$ be the homogeneous ideal of the model X. In addition, we consider the inhomogeneous linear polynomial $f_0 := p_0 + p_1 + \cdots + p_n - 1$. Let $\mathcal{J} = \left(\partial f_i / \partial p_j\right)$ denote the Jacobian matrix of size $(k+1) \times (n+1)$ for these polynomials, and set $c = \mathrm{codim}(X)$. The *augmented Jacobian* $\mathcal{A}\mathcal{J}$ is obtained from $\mathcal{J}$ by prepending one more row, namely the gradient of the objective function

$$\nabla \ell_{\mathbf{u}} \;=\; \left(\, u_0/p_0,\, u_1/p_1,\, \ldots\,,\, u_n/p_n \,\right).$$

To obtain the critical equations, enlarge I_X by the $(c+2) \times (c+2)$ minors of the $(k+2) \times (n+1)$ matrix $\mathcal{A}\mathcal{J}$, then clear denominators, and remove extraneous components by saturation.

Example 11.3 (Space curves) Let $n = 3$ and X the curve in Δ_3 defined by two general polynomials f_1 and f_2 of degrees d_1 and d_2 in p_0, p_1, p_2, p_3. The augmented Jacobian matrix is

$$\mathcal{A}\mathcal{J} \;=\; \begin{pmatrix} u_0/p_0 & u_1/p_1 & u_2/p_2 & u_3/p_3 \\ 1 & 1 & 1 & 1 \\ \partial f_1/\partial p_0 & \partial f_1/\partial p_1 & \partial f_1/\partial p_2 & \partial f_1/\partial p_3 \\ \partial f_2/\partial p_0 & \partial f_2/\partial p_1 & \partial f_2/\partial p_2 & \partial f_2/\partial p_3 \end{pmatrix}. \tag{11.5}$$

Clearing denominators amounts to multiplying the ith column by p_i, so the determinant contributes a polynomial of degree $d_1 + d_2 + 1$ to the critical equations. Since the codimension of X equals $c = 2$, we need to take the 4×4 minors of $\mathcal{A}\mathcal{J}$. The generators of I_X have degrees d_1 and d_2 respectively. We therefore conclude that the ML degree of X equals $d_1 d_2 (d_1 + d_2 + 1)$.

The following general upper bound on the ML degree is established in [92, Theorem 5].

Proposition 11.4 *Let X be a model of codimension c in the probability simplex Δ_n whose ideal I_X is generated by polynomials $f_1, f_2, \ldots, f_c, \ldots, f_k$ of degrees $d_1 \geq d_2 \geq \cdots \geq d_c \geq \cdots \geq d_k$. Then*

$$\mathit{MLdegree}(X) \;\;\leq\;\; d_1 d_2 \cdots d_c \cdot \sum_{i_1+i_2+\cdots+i_c \leq n-c} d_1^{i_1} d_2^{i_2} \cdots d_c^{i_c}. \tag{11.6}$$

Equality holds when X is a generic complete intersection of codimension c (hence $c = k$).

We next present a more precise formula. For the ED degree, the polar degrees in $\mathbb{P}^n$ were used to give such a formula. For the ML degree, we shall use the Euler characteristic instead.

Given our variety X in the complex projective space $\mathbb{P}^n$, and let X^o be the open subset of X that is obtained by removing the hyperplane arrangement $\{p_0 p_1 \cdots p_n (\sum_{i=0}^n p_i) = 0\}$. We recall from [102, 103] that a *very affine variety* is a closed subvariety of an algebraic torus $(\mathbb{C}^*)^r$. In our setting, the open set X^o is a very affine variety, with $r = n + 2$. The following formula works for any very affine variety.

Theorem 11.5 *Suppose that the very affine variety X^o is non-singular. The ML degree of the model X equals the signed Euler characteristic $(-1)^{dim(X)} \cdot \chi(X^o)$ of the manifold X^o.*

Proof (and Discussion) This was proved under additional assumptions in [40, Theorem 19], and in full generality in [102, Theorem 1]. If the very affine variety X^o is singular, then the Euler characteristic can be replaced by the Chern-Schwartz-MacPherson class, as shown in [102, Theorem'2]. □

The optimal solution to our optimization problem (11.3)-(11.4) in the statistical model $X^o \cap \Delta_n = X \cap \Delta_n$ is denoted $\hat{\mathbf{p}}$. This point is called the *maximum likelihood estimate (MLE)* for the given data $\mathbf{u}$ and the model X. The ML degree measures the algebraic complexity of the MLE. Theorem 11.5 says that the ML degree is a topological invariant. Varieties X for which the ML degree is equal to one are of special interest, both statistically and geometrically. For a model X to have ML degree one means that the MLE $\hat{\mathbf{p}}$ is a rational function of the data $\mathbf{u}$. Here are two natural examples where this happens.

Example 11.6 ($n = 3$) The independence model for two binary random variables is a quadratic surface X in the tetrahedron Δ_3. This model is described by the constraints

$$\det \begin{bmatrix} p_0 & p_1 \\ p_2 & p_3 \end{bmatrix} = 0 \quad \text{and} \quad p_0 + p_1 + p_2 + p_3 = 1 \quad \text{and} \quad p_0, p_1, p_2, p_3 > 0.$$

Consider data $\mathbf{u} = \begin{bmatrix} u_0 & u_1 \\ u_2 & u_3 \end{bmatrix}$ of *sample size* $|u| = u_0+u_1+u_2+u_3$. The ML degree of the surface X equals one because the MLE $\hat{\mathbf{p}}$ is a rational function of the data. To be precise, the coordinates of the MLE $\hat{\mathbf{p}}$ are

$$\begin{aligned} \hat{p}_0 &= |u|^{-2}(u_0+u_1)(u_0+u_2), \quad & \hat{p}_1 &= |u|^{-2}(u_0+u_1)(u_1+u_3), \\ \hat{p}_2 &= |u|^{-2}(u_2+u_3)(u_0+u_2), \quad & \hat{p}_3 &= |u|^{-2}(u_2+u_3)(u_1+u_3). \end{aligned} \tag{11.7}$$

In words, we multiply the row sums with the column sums in the empirical distribution $\frac{1}{|\mathbf{u}|}\mathbf{u}$.

Here is another simple model where the MLE is a rational function in the data.

Example 11.7 ($n = 2$) Given a biased coin, we perform the following experiment: *Flip a biased coin. If it shows heads, flip it again*. The outcome of this experiment is the number of heads: 0, 1 or 2.

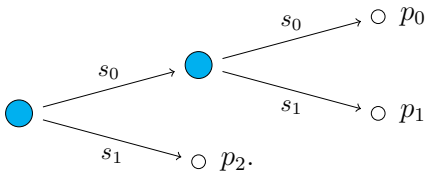

Fig. 11.1: Probability tree that describes the coin toss model in Example 11.7.

If s denotes the bias of our coin, then the model is the parametric curve X given by

$$(0,1) \to X \subset \Delta_2\,, \;\; s \mapsto \big(s^2, s(1-s), 1-s\big).$$

This model is the conic $X = V(p_0p_2 - (p_0 + p_1)p_1) \subset \mathbb{P}^2$. Its MLE is given by the formula

$$(\hat{p}_0, \hat{p}_1, \hat{p}_2) \;=\; \left(\frac{(2u_0 + u_1)^2}{(2u_0+2u_1+u_2)^2} \,,\, \frac{(2u_0+u_1)(u_1+u_2)}{(2u_0 + 2u_1 + u_2)^2} \,,\, \frac{u_1 + u_2}{2u_0+2u_1+u_2} \right). \tag{11.8}$$

Since the coordinates of $\hat{p}$ are rational functions, the ML degree of X is equal to one.

The following theorem explains what we saw in equations (11.7) and (11.8):

Theorem 11.8 *If $X \subset \Delta_n$ is a model of ML degree one, so that $\hat{\mathbf{p}}$ is a rational function of $\mathbf{u}$, then each coordinate $\hat{p}_i$ is an alternating product of linear forms with positive coefficients.*

Proof (and Discussion) This was proved in the setting of arbitrary complex very affine varieties by Huh in [103]. It was adapted to real algebraic geometry and hence to statistical models in [63]. These two articles offer precise statements via Horn uniformization for A-discriminants [74], i.e. hypersurfaces dual to toric varieties. For additional information we refer to [104, Corollary 3.12]. □

Models given by rank constraints on matrices and tensors are particularly important in applications, since these represent conditional independence. Consider two random variables, having n_1 and n_2 states respectively, which are conditionally independent, given a hidden random variable with r states. In algebraic geometry, this model is the variety X_r in $\mathbb{P}^{n_1n_2-1}$ that is defined by the $(r+1) \times (r+1)$ minors of an $n_1 \times n_2$ matrix (p_{ij}). The ML degree of this rank r model was first studied by Hauenstein, Rodriguez and Sturmfels in [86], who obtained the following results using methods from numerical algebraic geometry.

Proposition 11.9 *For small values of n_1 and n_2, the ML degrees of low rank models X_r are*

$(n_1, n_2) =$	$(3,3)$	$(3,4)$	$(3,5)$	$(4,4)$	$(4,5)$	$(4,6)$	$(5,5)$
$r = 1$	1	1	1	1	1	1	1
$r = 2$	10	26	58	191	843	3119	6776
$r = 3$	1	1	1	191	843	3119	61326
$r = 4$				1	1	1	6776
$r = 5$							1

(11.9)

Every entry in the $r = 1$ row is 1 because the MLE for the independence model is a rational function in the data (u_{ij}). One finds $\hat{\mathbf{p}} = (\hat{p}_{ij})$ by multiplying the column vector of row sums of $\mathbf{u}$ with the row vector of column sums of $\mathbf{u}$, and then dividing by $|\mathbf{u}|^2$, as shown in (11.7). The other entries are more interesting, and they give precise information on the algebraic complexity of minimizing the Kullback-Leibler distance from a given data matrix $\mathbf{u}$ to the conditional independence model X_r. Here is an example taken from [86].

Example 11.10 ($n_1 = n_2 = 5$) Following [86, Example 7], we consider the data

$$\mathbf{u} \;=\; \begin{pmatrix} 2864 & 6 & 6 & 3 & 3 \\ 2 & 7577 & 2 & 2 & 5 \\ 4 & 1 & 7543 & 2 & 4 \\ 5 & 1 & 2 & 3809 & 4 \\ 6 & 2 & 6 & 3 & 5685 \end{pmatrix}.$$

For $r = 2$ and $r = 4$, this instance of our MLE problem has the expected number of 6776 distinct complex critical points. In both cases, 1774 of these are real and 90 of these are real and positive. This illustrates the last statement in Theorem 11.11 below. The number of local maxima for $r = 2$ equals 15, and the number of local maxima for $r = 4$ equals 6. For $r = 3$, we have 61326 critical points, of which 15450 are real. Of these, 362 are positive and 25 are local maxima. We invite our readers to critically check these claims, by running software for solving polynomial equations, such as `HomotopyContinuation.jl`.

The columns of the table in (11.9) exhibit an obvious symmetry. This was conjectured in [86], and it was proved by Draisma and Rodriguez in their article [61] on maximum likelihood duality. We now state their result. Given an $n_1 \times n_2$ matrix $\mathbf{u}$, we write $\Omega_{\mathbf{u}}$ for the matrix whose (i, j) entry equals

$$\frac{u_{ij} u_{i+} u_{+j}}{(u_{++})^3}.$$

In the following theorem, the symbol $\star$ denotes the Hadamard product (or entrywise product) of two matrices. All matrices $\mathbf{p}_i$ and $\mathbf{q}_i$ have format $n_1 \times n_2$ and they have complex entries.

Theorem 11.11 *Fix $n_1 \leq n_2$ and $\mathbf{u}$ an $n_1 \times n_2$-matrix with strictly positive integer entries. There exists a bijection between the complex critical points $\mathbf{p}_1, \mathbf{p}_2, \ldots, \mathbf{p}_s$ of the likelihood function for $\mathbf{u}$ on X_r and the complex critical points $\mathbf{q}_1, \mathbf{q}_2, \ldots, \mathbf{q}_s$ on X_{n_1-r+1} such that*

$$\mathbf{p}_1 \star \mathbf{q}_1 \;=\; \mathbf{p}_2 \star \mathbf{q}_2 \;=\; \cdots \;=\; \mathbf{p}_s \star \mathbf{q}_s \;=\; \Omega_{\mathbf{u}}. \tag{11.10}$$

In particular, this bijection preserves reality, positivity, and rationality of the critical points.

This result represents a multiplicative version of the duality we encountered in our study of ED degrees. Recall that the ED degree of any projective variety X, when viewed as a cone in affine space, equals that of its dual variety $X^\vee$. Under some genericity assumption, this common ED degree is the sum of the polar degrees, which arises from the conormal variety $N_X = N_{X^\vee}$. By "multiplicative" we mean that $\mathbf{u}_i / \mathbf{p}_i$ instead of $\mathbf{u}_i - \mathbf{p}_i$ appears in the first row of the augmented Jacobian matrix.

It is a challenge in intersection theory and singularity theory to find general formulas for the ML degrees in Proposition 11.9. This problem was solved for $r = 2$ by Rodriguez and Wang in [155]. They give a recursive formula in [155, Theorem 4.1], and they present impressive values in [155, Table 1]. They unravel the recursion, and they obtain the explicit formulas for the ML degree of conditional independence in many cases. In particular, they obtain the following result which had been stated as a conjecture in [86].

Theorem 11.12 (Rodriguez-Wang [155]) *Consider the variety $X_2 \subset \mathbb{P}^{3n-1}$ whose points are the $3 \times n$ matrices of rank ≤ 2. The ML degree of this variety equals $2^{n+1} - 6$.*

11.3 Scattering Equations

We now turn to a connection between algebraic statistics and particle physics that was developed in [168]. The context is scattering amplitudes, where the critical equations for (11.3)-(11.4) are known as *scattering equations*. We consider the *CEGM model*, due to Cachazo and his collaborators [36, 37]. The role of the data vector $\mathbf{u}$ is played in physics by the *Mandelstam invariants*. This theory rests on the space X^o of m labeled points in general position in $\mathbb{P}^{k-1}$, up to projective transformations. Consider the Grassmannian $\mathrm{Gr}(k, m)$ in its Plücker embedding into $\mathbb{P}^{\binom{m}{k}-1}$. The torus $(\mathbb{C}^*)^m$ acts on $\mathrm{Gr}(k, m)$ by scaling the columns of $k \times m$ matrices representing subspaces. Let $\mathrm{Gr}(k, m)^o$ be the open Grassmannian where all Plücker coordinates are nonzero. The CEGM model is the $(k-1)(m-k-1)$-dimensional manifold

$$X^o \quad = \quad \mathrm{Gr}(k, m)^o / (\mathbb{C}^*)^m. \tag{11.11}$$

Example 11.13 ($k = 2$) For $k = 2$, the very affine variety in (11.11) has dimension $m - 3$, and it is the moduli space of m distinct labeled points on the complex projective line $\mathbb{P}^1$. This space is ubiquitous in algebraic geometry where it is known as $\mathcal{M}_{0,m}$. The punchline of our discussion here is that we interpret the moduli space $\mathcal{M}_{0,m}$ as a statistical model. And, we then argue that its ML degree is equal to $(m-3)!$.

For instance, if $m = 4$ then $X^o = \mathcal{M}_{0,4}$ is the Riemann sphere $\mathbb{P}^1$ with three points removed. The signed Euler characteristic of this surface is one, and Theorem 11.8 applies.

Proposition 11.14 *The configuration space X^o in (11.11) is a very affine variety, with coordinates given by the $k\times k$ minors of the following $k \times m$ matrix, which we denote by $M_{k,m}$:*

$$\begin{bmatrix} 0 & 0 & 0 & \cdots & 0 & (-1)^k & 1 & 1 & 1 & \cdots & 1 \\ 0 & 0 & 0 & \cdots & (-1)^{k-1} & 0 & 1 & x_{1,1} & x_{1,2} & \cdots & x_{1,m-k-1} \\ \vdots & \vdots & \vdots & \ddots & \vdots & \vdots & \vdots & \vdots & \vdots & \ddots & \vdots \\ 0 & 0 & -1 & \cdots & 0 & 0 & 1 & x_{k-3,1} & x_{k-3,2} & \cdots & x_{k-3,m-k-1} \\ 0 & 1 & 0 & \cdots & 0 & 0 & 1 & x_{k-2,1} & x_{k-2,2} & \cdots & x_{k-2,m-k-1} \\ -1 & 0 & 0 & \cdots & 0 & 0 & 1 & x_{k-1,1} & x_{k-1,2} & \cdots & x_{k-1,m-k-1} \end{bmatrix}.$$

To be precise, the coordinates on $X^o \subset (\mathbb{C}^*)^{\binom{m}{k}}$ are the non-constant minors $p_{i_1 i_2 \cdots i_k}$ of the matrix M_k.

Following [2, equation (4)], the antidiagonal matrix in the left $k \times k$ block of $M_{k,m}$ is chosen so that each unknown $x_{i,j}$ is precisely equal to $p_{i_1 i_2 \cdots i_k}$ for some $i_1 < i_2 < \cdots < i_k$. No signs are needed. The *scattering potential* for the CEGM model is the following multivalued function on X^o:

$$\ell_u \quad = \quad \sum_{i_1 i_2 \cdots i_k} u_{i_1 i_2 \cdots i_k} \cdot \log(p_{i_1 i_2 \cdots i_k}). \tag{11.12}$$

The critical point equations, known as *scattering equations* [2, equation (7)], are given by

$$\frac{\partial \ell_u}{\partial x_{i,j}} = 0 \qquad \text{for } 1 \le i \le k-1 \text{ and } 1 \le j \le m-k-1. \tag{11.13}$$

These are equations of rational functions. Solving these equations is the agenda in [36, 37, 168].

Corollary 11.15 *The number of complex solutions to (11.13) is the ML degree of the CEGM model X^o. This number equals the signed Euler characteristic $(-1)^{(k-1)(m-k-1)} \cdot \chi(X^o)$.*

Example 11.16 ($k = 2, m = 6$) The very affine threefold $X^o = \mathcal{M}_{0,6}$ is embedded in $(\mathbb{C}^*)^9$ via

$$p_{24} = x_1,\ p_{25} = x_2,\ p_{26} = x_3,\ p_{34} = x_1 - 1,\ p_{35} = x_2 - 1,$$
$$p_{36} = x_3 - 1,\ p_{45} = x_2 - x_1,\ p_{46} = x_3 - x_1,\ p_{56} = x_3 - x_2.$$

These nine coordinates on $X^o \subset (\mathbb{C}^*)^9$ are the non-constant 2×2 minors of our matrix

$$M_{2,6} \quad = \quad \begin{bmatrix} 0 & 1 & 1 & 1 & 1 & 1 \\ -1 & 0 & 1 & x_1 & x_2 & x_3 \end{bmatrix}.$$

The scattering potential is the analogue to the log-likelihood function in statistics:

$$\ell_u \quad = \quad u_{24} \log(p_{24}) + u_{25} \log(p_{25}) + \cdots + u_{56} \log(p_{56}).$$

This function has six critical points in X^o. Hence $\text{MLdegree}(X^o) = -\chi(X^o) = 6$.

We now examine the number of critical points of the scattering potential (11.12).

Theorem 11.17 *The known values of the ML degree for the CEGM model (11.11) are as follows. For $k = 2$, the ML degree equals $(m-3)!$ for all $m \ge 4$. For $k = 3$, the ML degree equals $2, 26, 1272, 188112, 74570400$ when the number of points is $m = 5, 6, 7, 8, 9$. For $k = 4, m = 8$, the ML degree equals 5211816.*

Proof We refer to [2, Example 2.2], [2, Theorem 5.1] and [2, Theorem 6.1] for $k = 2, 3, 4$. □

Knowing these ML degrees helps in solving the scattering equations reliably. It was demonstrated in [2, 168] how this can be done in practice, namely with the software `HomotopyContinuation.jl` [30, 31]. For instance, we see in [168, Table 1] that the $10! = 3628800$ critical points for $k = 2, m = 13$ are found in under one hour. See [2, Section 6] for the solution in the challenging case $k = 4, m = 8$.

11.4 Gaussian Models

We now change topic by turning to models for Gaussian random variables. Let PD_n denote the set of positive-definite symmetric $n \times n$ matrices, i.e. matrices all of whose eigenvalues are positive. This is an open convex cone in a real vector space in the matrix space $\mathrm{Sym}_2(\mathbb{R}^n)$, which has dimension $\binom{n+1}{2}$. This cone now plays the role which was played by the simplex Δ_n when we discussed discrete models.

Given a mean vector $\mu \in \mathbb{R}^n$ and a covariance matrix $\Sigma \in \mathrm{PD}_n$, the associated *Gaussian distribution* is supported on $\mathbb{R}^n$. Its density has the familiar "bell shape"; it is the function

$$f_{\mu,\Sigma}(x) \;:=\; \frac{1}{\sqrt{(2\pi)^n \det \Sigma}} \cdot \exp\left(-\frac{1}{2}(x-\mu)^T \Sigma^{-1}(x-\mu)\right).$$

We fix a model $Y \subset \mathbb{R}^n \times \mathrm{PD}_n$ that is defined by polynomial equations in (μ, Σ). Suppose we are given N samples $U^{(1)}, \ldots, U^{(N)}$. These samples are vectors in $\mathbb{R}^n$. They are summarized in the *sample mean* $\bar{U} = \frac{1}{N}\sum_{i=1}^N U^{(i)}$ and in the *sample covariance matrix* $S = \frac{1}{N}\sum_{i=1}^N (U^{(i)} - \bar{U})(U^{(i)} - \bar{U})^T$. Given this representation of the data, the log-likelihood is the following function in the unknowns (μ, Σ):

$$\ell(\mu, \Sigma) \;=\; -\frac{N}{2} \cdot \left[\log\det\Sigma \;+\; \mathrm{trace}(S\Sigma^{-1}) \;+\; (\bar{U}-\mu)^T \Sigma^{-1}(\bar{U}-\mu) \right]. \tag{11.14}$$

The task of likelihood inference is to minimize this function subject to $(\mu, \Sigma) \in Y$.

There are two extreme cases. First, consider a model where Σ is fixed to be the identity matrix Id_n. Then $Y = X \times \{\mathrm{Id}_n\}$ and we are supposed to minimize the Euclidean distance from the sample mean $\bar{U}$ to the variety X in $\mathbb{R}^n$. This is precisely the earlier ED problem.

We instead focus on the second case, the family of *centered Gaussians*, where the mean vector μ is fixed to be zero. The model has the form $\{0\} \times X$, where X is a variety in the space $\mathrm{Sym}_2(\mathbb{R}^n)$ of symmetric $n \times n$ matrices. Following [170, Proposition 7.1.10], our task is now as follows:

$$\text{Minimize the function } \;\Sigma \;\mapsto\; \log\det\Sigma \;+\; \mathrm{trace}(S\,\Sigma^{-1}) \quad \text{subject to } \Sigma \in X. \tag{11.15}$$

Using the concentration matrix $K = \Sigma^{-1}$, we can write this equivalently as follows:

$$\text{Maximize the function } \;K \;\mapsto\; \log\det K \;-\; \mathrm{trace}(S\,K) \quad \text{subject to } K \in X^{-1}. \tag{11.16}$$

Here the variety X^{-1} is the Zariski closure of the set of inverses of all matrices in X.

Remark 11.18 The optimization problem (11.15)-(11.16) has a metric interpretation as in (11.4). Namely, we can define the KL divergence between two probability distributions on $\mathbb{R}^n$ by replacing the sum in (11.2) with the corresponding integral over $\mathbb{R}^n$. For two Gaussians we obtain a certain kind of distance between the unknown Σ and the sample covariance matrix S.

The critical equations of the optimization problem (11.15)-(11.16) can be written as polynomials, since the partial derivatives of the logarithm are rational functions. These equations have finitely many complex solutions. Their number is the *ML degree* of the Gaussian statistical model X^{-1}.

In the remainder of this section we focus on Gaussian models that are described by linear constraints on either the covariance matrix or its inverse, which is the concentration matrix. Let $\mathcal{L} \subset \mathrm{Sym}_2(\mathbb{R}^n)$ be a linear space of symmetric matrices (LSSM), whose general element is assumed to be invertible. We are interested in the models $X^{-1} = \mathcal{L}$ and $X = \mathcal{L}$. It is convenient to use primal-dual coordinates (Σ, K) to write the respective critical equations.

Proposition 11.19 *Fix an LSSM $\mathcal{L}$ and its orthogonal complement $\mathcal{L}^\perp$ for the inner product $\langle X, Y\rangle = \mathrm{trace}(XY)$. The critical equations for the* linear concentration model $X^{-1} = \mathcal{L}$ *are*

$$K \in \mathcal{L} \ \text{ and } \ K\Sigma = Id_n \ \text{ and } \ \Sigma - S \in \mathcal{L}^\perp. \tag{11.17}$$

The critical equations for the linear covariance model $X = \mathcal{L}$ *are*

$$\Sigma \in \mathcal{L} \ \text{ and } \ K\Sigma = Id_n \ \text{ and } \ KSK - K \in \mathcal{L}^\perp. \tag{11.18}$$

Proof This is well-known in statistics. For proofs see [169, Propositions 3.1 and 3.3]. □

The system (11.17) is linear in the unknown matrix K, whereas the last group of equations in (11.18) is quadratic in K. The numbers of complex solutions are the *ML degree* of $\mathcal{L}$ and the *reciprocal ML degree* of $\mathcal{L}$. The former is smaller than the latter, and (11.17) is easier to solve than (11.18).

Example 11.20 Let $n = 4$ and $\mathcal{L}$ a generic LSSM of dimension k. Our degrees are as follows:

$k = \dim(\mathcal{L})$:	2	3	4	5	6	7	8	9
ML degree :	3	9	17	21	21	17	9	3
reciprocal ML degree :	5	19	45	71	81	63	29	7

These numbers and many more appear in [169, Table 1].

ML degrees and reciprocal ML degrees of linear spaces of symmetric matrices have been studied intensively in the recent literature, both for generic and special spaces $\mathcal{L}$. See [4, 20, 69] and the references therein. We now present an important result due to Manivel, Michalek, Monin, Seynnaeve, Vodička and Wiśniewski. Theorem 11.21 paraphrases highlights from their articles [127, 132].

Theorem 11.21 *The ML degree of a generic linear subspace $\mathcal{L}$ of dimension k in $Sym_2(\mathbb{R}^n)$ is the number of quadrics in $\mathbb{P}^{n-1}$ that pass through $\binom{n+1}{2} - k$ general points and are tangent to $k-1$ general hyperplanes. For fixed k, this number is a polynomial in n of degree $k-1$.*

Proof The first statement is [132, Corollary 2.6 (4)], here interpreted classically in terms of Schubert calculus. For a detailed discussion see the introduction of [127]. The second statement appears in [127, Theorem 1.3 and Corollary 4.13]. □

Example 11.22 ($n = 4$) Fix $10 - k$ points and $k - 1$ planes in $\mathbb{P}^3$. We are interested in all quadratic surfaces that contain the points and are tangent to the planes. This points and planes impose 9 constraints on $\mathbb{P}(\mathrm{Sym}_2(\mathbb{C}^4)) \simeq \mathbb{P}^9$. Passing through a point is a linear equation. Being tangent to a plane is a cubic constraint on $\mathbb{P}^9$. Bézout's Theorem suggests that there could be 3^{k-1} solutions. This is correct for $k \leq 3$ but it overcounts for $k \geq 4$. Indeed, in Example 11.20 we see $17, 21, 21, \ldots$ instead of $27, 81, 243, \ldots$.

The intersection theory approeach in [127, 132] leads to formulas for the ML degrees of linear Gaussian models. From this we obtain provably correct numerical methods for maximum likelihood estimation. Namely, after computing critical points as in [169], we can certify them as in [30]. Since the ML degree is known, one can then be sure that all solutions have been found.

Chapter 12
Tensors

Tensors are a generalization of matrices and can be viewed as tables of higher dimensions: A 2×2-matrix is a table that contains 4 numbers aligned in two directions and each direction has dimension 2; a $2 \times 2 \times 2$ tensor is a table with 8 numbers aligned in three directions where each direction has dimension 2.

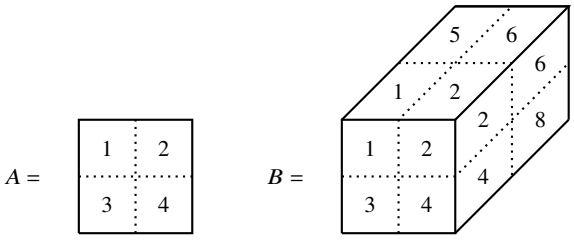

Fig. 12.1: A 2×2 matrix A and a $2 \times 2 \times 2$ tensor B.

For positive integers $n_1, \ldots, n_d$, the vector space of real $n_1 \times \cdots \times n_d$–tensors is denoted by

$$\mathbb{R}^{n_1 \times \cdots \times n_d} := \left\{ A = \left(a_{i_1,\ldots,i_d}\right)_{1 \le i_1 \le n_1, \ldots, 1 \le i_d \le n_d} \;\middle|\; a_{i_1,\ldots,i_d} \in \mathbb{R} \right\}.$$

In the literature, elements in $\mathbb{R}^{n_1 \times \cdots \times n_d}$ are also sometimes called *hypermatrices* or *Cartesian tensors*, because our definition of a tensor as a multidimensional array relies on a choice of basis. The dimension of $\mathbb{R}^{n_1 \times \cdots \times n_d}$ is $n_1 \cdots n_d$. The number d is called the *order* or *power* of the tensor. Tensors of order two are matrices. We can also consider the space of complex tensors $\mathbb{C}^{n_1 \times \cdots \times n_d}$.

A common notation for order-three tensors is by writing them as a pencil of matrices.

Example 12.1 The tensor $B = \left(b_{i,j,k}\right)_{1 \le i,j,k \le 2}$ from Figure 12.1 can be written as

$$B = \left(\begin{array}{cc|cc} 1 & 2 & 5 & 6 \\ 3 & 4 & 7 & 8 \end{array} \right) \in \mathbb{R}^{2 \times 2 \times 2}.$$

The left matrix contains the entries $b_{i,j,1}$ and the matrix on the right contains the entries $b_{i,j,2}$. ◇

As in the previous chapters, the Euclidean inner product is

$$\langle A, B \rangle := \sum_{i_1=1}^{n_1} \cdots \sum_{i_d=1}^{n_d} a_{i_1,\ldots,i_d} \cdot b_{i_1,\ldots,i_d}$$

for $A = (a_{i_1,\ldots,i_d})$ and $B = (b_{i_1,\ldots,i_d})$. The induced norm is $\|A\| = \sqrt{\langle A, A \rangle}$.

Given d vectors $\mathbf{v}_i \in \mathbb{R}^{n_i}$, $1 \le i \le d$, their *outer product* is the following tensor:

$$\mathbf{v}_1 \otimes \cdots \otimes \mathbf{v}_d := \left((\mathbf{v}_1)_{i_1} \cdots (\mathbf{v}_d)_{i_d} \right)_{1 \le i_1 \le n_1, \ldots, 1 \le i_d \le n_d}.$$

That is, the entries of $\mathbf{v}_1 \otimes \cdots \otimes \mathbf{v}_d$ are all possible products between the entries of the $\mathbf{v}_i$. In fact, we have that $(a_{i_1,\ldots,i_d}) = \sum_{i_1=1}^{n_1} \cdots \sum_{i_d=1}^{n_d} a_{i_1,\ldots,i_d}\, \mathbf{e}_{i_1} \otimes \cdots \otimes \mathbf{e}_{i_d}$.

If $n := n_1 = \cdots = n_d$ are all equal, we write the space of order-d tensors as

$$(\mathbb{R}^n)^{\otimes d} := \mathbb{R}^{n \times \cdots \times n}.$$

Each permutation $\pi \in \mathfrak{S}_d$ acts on outer products $\mathbf{v}_1 \otimes \cdots \otimes \mathbf{v}_d \in (\mathbb{R}^n)^{\otimes d}$ via $\pi(\mathbf{v}_1 \otimes \cdots \otimes \mathbf{v}_d) = \mathbf{v}_{\pi(1)} \otimes \cdots \otimes \mathbf{v}_{\pi(d)}$. This yields an action of the symmetric group $\mathfrak{S}_d$ on $(\mathbb{R}^n)^{\otimes d}$ via linear extension. That action generalizes matrix transposition.

Definition 12.2 We call a tensor $A \in (\mathbb{R}^n)^{\otimes d}$ *symmetric* if $\pi(A) = A$ for all $\pi \in \mathfrak{S}_d$. The space of symmetric tensors in $(\mathbb{R}^n)^{\otimes d}$ is denoted by

$$S^d(\mathbb{R}^n) := \{A \in (\mathbb{R}^n)^{\otimes d} \mid A \text{ is symmetric}\}.$$

Since $S^d(\mathbb{R}^n)$ is the image of the linear map $A \mapsto \sum_{\pi \in \mathfrak{S}_d} \pi(A)$, it is a linear subspace of $(\mathbb{R}^n)^{\otimes d}$. Its dimension is $\binom{n+d-1}{d}$. For $\mathbf{v} \in \mathbb{R}^n$, we write

$$\mathbf{v}^{\otimes d} := \mathbf{v} \otimes \cdots \otimes \mathbf{v} \in S^d(\mathbb{R}^n).$$

Furthermore, for $A \in S^d(\mathbb{R}^n)$,

$$F_A(\mathbf{x}) := \sum_{i_1=1}^{n} \cdots \sum_{i_d=1}^{n} a_{i_1,\ldots,i_d}\, x_{i_1} \cdots x_{i_d} \tag{12.1}$$

is a homogeneous polynomial of degree d in n variables. The map $A \mapsto F_A$ is a linear isomorphism between $S^d(\mathbb{R}^n)$ and the vector space of homogeneous polynomials of degree d in n variables. We can write the polynomial F_A from (12.1) as

$$F_A(\mathbf{x}) = \langle A, \mathbf{x}^{\otimes d} \rangle.$$

For $A \in S^d(\mathbb{R}^n)$, we have $\|A\| = \|F_A\|_{\mathrm{BW}}$, where the latter is the Bombieri-Weyl metric from Chapter 9.

Example 12.3 Consider the symmetric matrix $A = \left(\begin{smallmatrix} 1 & 2 \\ 2 & 0 \end{smallmatrix}\right) \in S^2(\mathbb{R}^2)$. The associated polynomial is

$$F_A(\mathbf{x}) = \mathbf{x}^\top A \mathbf{x} = x_1^2 + 4x_1 \cdot x_2.$$

The polynomial associated to the symmetric order-three tensor $B = \left(\begin{smallmatrix} 1 & -1 \\ -1 & 0 \end{smallmatrix} \,\middle|\, \begin{smallmatrix} -1 & 0 \\ 0 & 2 \end{smallmatrix}\right) \in S^3(\mathbb{R}^2)$ is

$$F_B(\mathbf{x}) = x_1^3 - 3x_1^2 x_2 + 2x_2^3.$$

◇

Given a d-tuple of matrices $(M_1, \ldots, M_d) \in \mathbb{R}^{k_1 \times n_1} \times \cdots \times \mathbb{R}^{k_d \times n_d}$, we define the *multilinear multiplication*

$$(M_1, \ldots, M_d).(\mathbf{v}_1 \otimes \cdots \otimes \mathbf{v}_d) := (M_1 \mathbf{v}_1) \otimes \cdots \otimes (M_d \mathbf{v}_d).$$

It extends linearly to all of $\mathbb{R}^{n_1 \times \cdots \times n_d}$, and induces a representation of $\mathrm{GL}(n_1) \times \cdots \times \mathrm{GL}(n_d)$ into the general linear group of $\mathbb{R}^{n_1 \times \cdots \times n_d}$.

Example 12.4 Let $A \in \mathbb{R}^{n_1 \times n_2}$ and $(M_1, M_2) \in \mathbb{R}^{k_1 \times n_1} \times \mathbb{R}^{k_2 \times n_2}$. Then, $(M_1, M_2).A = M_1 A M_2^\top$. Thus, multilinear multiplication is a generalization of simultaneous left–right multiplication for matrices. ◇

A central topic of this chapter are *rank-one tensors*. We say that a tensor $A \in \mathbb{R}^{n_1 \times \cdots \times n_d}$ has rank one if there exist vectors $\mathbf{v}_i \in \mathbb{R}^{n_i}$, $1 \le i \le d$, such that $A = \mathbf{v}_1 \otimes \cdots \otimes \mathbf{v}_d$.

Definition 12.5 The (real) *Segre variety* $\mathcal{S}_{n_1,\ldots,n_d}$ consists of all rank-one $n_1 \times \ldots \times n_d$-tensors:

$$\mathcal{S}_{n_1,\ldots,n_d} := \{\mathbf{v}_1 \otimes \cdots \otimes \mathbf{v}_d \mid \mathbf{v}_i \in \mathbb{R}^{n_i}, 1 \le i \le d\}.$$

We typically write simply $\mathcal{S}$ when $n_1, \ldots, n_d$ are clear from the context.

Example 12.6 The outer product of $\mathbf{v} = (v_1, v_2) \in \mathbb{R}^2$ and $\mathbf{w} = (w_1, w_2, w_3) \in \mathbb{R}^3$ is the rank-one matrix

$$\mathbf{v} \otimes \mathbf{w} = \begin{pmatrix} v_1 \cdot w_1 & v_1 \cdot w_2 & v_1 \cdot w_3 \\ v_2 \cdot w_1 & v_2 \cdot w_2 & v_2 \cdot w_3 \end{pmatrix}$$

with column space $\mathbb{R} \cdot \mathbf{v}$ and row space $\mathbb{R} \cdot \mathbf{w}$. Another common notation is $\mathbf{v}\mathbf{w}^T$. ◇

The most immediate way to see that $\mathcal{S}$ is an algebraic variety goes as follows. We can always *flatten* a tensor $A \in \mathbb{R}^{n_1 \times \cdots \times n_d}$ into d matrices $F_1, \ldots, F_d$, where $F_i \in \mathbb{R}^{n_i \times (\prod_{j \neq i} n_j)}$. Then, we have $A \in \mathcal{S}$ if and only if the column span of F_i has dimension at most one for $1 \leq i \leq d$. This is equivalent to saying that the F_i are all of rank at most 1; i.e., their 2×2–minors vanish. The dimension of the Segre variety is

$$\dim \mathcal{S} = n_1 + \cdots + n_d + 1 - d.$$

The inner product between rank-one tensors is

$$\langle \mathbf{v}_1 \otimes \cdots \otimes \mathbf{v}_d, \mathbf{w}_1 \otimes \cdots \otimes \mathbf{w}_d \rangle = \langle \mathbf{v}_1, \mathbf{w}_1 \rangle \cdots \langle \mathbf{v}_d, \mathbf{w}_d \rangle. \tag{12.2}$$

The symmetric analogue of the Segre variety is the Veronese variety.

Definition 12.7 The *Veronese variety* is the variety of symmetric rank-one tensors:

$$\mathcal{V} := \mathcal{V}_{n,d} := \{\mathbf{v}^{\otimes d} \mid \mathbf{v} \in \mathbb{R}^n\}.$$

Example 12.8 Let $\mathbf{v} = (x, y) \in \mathbb{R}^2$. Then,

$$\mathbf{v}^{\otimes 3} = \left(\begin{array}{cc|cc} x^3 & x^2y & x^2y & xy^2 \\ x^2y & xy^2 & xy^2 & y^3 \end{array}\right).$$

The four independent coordinates of this symmetric tensor give all monomials of degree three in x and y. In general, $\mathbf{v}^{\otimes d}$ is given by all monomials of degree d in the entries of $\mathbf{v}$. ◇

Since $\mathcal{V}$ is the intersection of $\mathcal{S}$ with a linear subspace, it is an algebraic variety. Its dimension is

$$\dim \mathcal{V} = n.$$

12.1 Tensor Rank

The Segre variety induces a notion of rank of a tensor $A \in \mathbb{R}^{n_1 \times \ldots \times n_d}$.

$$\operatorname{rank}(A) := \min \{r \geq 0 \mid \text{there exists } A_1, \ldots, A_r \in \mathcal{S} \text{ with } A = A_1 + \cdots + A_r\}.$$

For matrices ($d = 2$), this coincides with the usual matrix rank. We denote tensors of rank at most r by

$$\Sigma_r := \Sigma_{r,n_1,\ldots,n_d} := \left\{A \in \mathbb{R}^{n_1 \times \cdots \times n_d} \mid \operatorname{rank}(A) \leq r\right\}.$$

A tensor of order three and rank r can be visualized as follows:

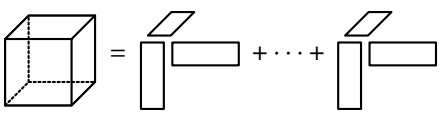

In the case of matrices, the set Σ_r is a variety for every r, defined by $(r+1)\times(r+1)$–minors. For $d \geq 3$ and $r \geq 2$, however, Σ_r is not necessarily a variety anymore. This is implied by the following result going back to the work by da Silva and Lim [52].

Proposition 12.9 *For $d \geq 3$ and $n_1 \geq 2, \ldots, n_d \geq 2$, the set Σ_2 of tensors of rank at most two is not closed in the Euclidean topology.*

Proof First consider the case $d = 3$. Let $\mathbf{x}_1, \mathbf{x}_2 \in \mathbb{R}^{n_1}$, $\mathbf{y}_1, \mathbf{y}_2 \in \mathbb{R}^{n_2}$ and $\mathbf{z}_1, \mathbf{z}_2 \in \mathbb{R}^{n_3}$ be three pairs of linearly independent vectors. Define for $\varepsilon > 0$ the tensor $A_\varepsilon \in \Sigma_2$ by

$$A_\varepsilon := \varepsilon^{-1}(\mathbf{x}_1 + \varepsilon\mathbf{x}_2) \otimes (\mathbf{y}_1 + \varepsilon\mathbf{y}_2) \otimes (\mathbf{z}_1 + \varepsilon\mathbf{z}_2) - \varepsilon^{-1}\mathbf{x}_1 \otimes \mathbf{y}_1 \otimes \mathbf{z}_1. \tag{12.3}$$

Then, $A := \lim_{\varepsilon\to 0} A_\varepsilon = \mathbf{x}_1 \otimes \mathbf{y}_1 \otimes \mathbf{z}_2 + \mathbf{x}_1 \otimes \mathbf{y}_2 \otimes \mathbf{z}_1 + \mathbf{x}_2 \otimes \mathbf{y}_1 \otimes \mathbf{z}_1$. To see that this tensor is of rank three, we first observe that $A = (P_{\mathbf{x}}, P_{\mathbf{y}}, P_{\mathbf{z}}).A$, where $P_{\mathbf{x}}$ is the projection onto the plane spanned by $\mathbf{x}_1$ and $\mathbf{x}_2$, and similar for $P_{\mathbf{y}}$ and $P_{\mathbf{z}}$. Therefore, we can assume $n_1 = n_2 = n_3 = 2$. Let us consider multilinear multiplication by $X := (I_2, I_2, \mathbf{h}^\top)$, where $\mathbf{h} \in \mathbb{R}^2$:

$$X.A = \langle \mathbf{h}, \mathbf{z}_2\rangle \cdot \mathbf{x}_1 \otimes \mathbf{y}_1 + \langle \mathbf{h}, \mathbf{z}_1\rangle \cdot \mathbf{x}_1 \otimes \mathbf{y}_2 + \langle \mathbf{h}, \mathbf{z}_1\rangle \cdot \mathbf{x}_2 \otimes \mathbf{y}_1. \tag{12.4}$$

Choosing $\mathbf{h}$ with $\langle \mathbf{h}, \mathbf{z}_1\rangle \neq 0$ yields a matrix of rank two, which shows that A has rank at least two. We suppose now for contradiction that $A = \mathbf{u}_1 \otimes \mathbf{v}_1 \otimes \mathbf{w}_1 + \mathbf{u}_2 \otimes \mathbf{v}_2 \otimes \mathbf{w}_2$ has rank two. Among the three pairs of vectors, there must be at least two that are linearly independent. We assume without restriction that the pairs $(\mathbf{u}_1, \mathbf{u}_2)$ and $(\mathbf{v}_1, \mathbf{v}_2)$ are each independent. We have

$$X.A = \langle \mathbf{h}, \mathbf{w}_1\rangle \cdot \mathbf{u}_1 \otimes \mathbf{v}_1 + \langle \mathbf{h}, \mathbf{w}_2\rangle \cdot \mathbf{u}_2 \otimes \mathbf{v}_2. \tag{12.5}$$

Let us now pick $\mathbf{h}$ such that $\langle \mathbf{h}, \mathbf{z}_1\rangle = 0$. By (12.4), $X.A$ has rank one and we must have $\langle \mathbf{h}, \mathbf{w}_1\rangle = 0$ or $\langle \mathbf{h}, \mathbf{w}_2\rangle = 0$ by (12.5). Without restriction we assume $\langle \mathbf{h}, \mathbf{w}_1\rangle = 0$. This implies that $\mathbf{w}_1$ is a multiple of $\mathbf{z}_1$, since they both satisfy the linear equation imposed by $\mathbf{h}$. Now we distinguish two cases.

First, if the pair $(\mathbf{w}_1, \mathbf{w}_2)$ is linearly independent, there is another $\mathbf{h}'$ with $\langle \mathbf{h}', \mathbf{w}_1\rangle \neq 0$ but $\langle \mathbf{h}', \mathbf{w}_2\rangle = 0$. Then, $\langle \mathbf{h}', \mathbf{z}_1\rangle \neq 0$ and so $X.A$ has rank two by (12.4) and it has rank one by (12.5); a contradiction. Second, if $\mathbf{w}_1$, $\mathbf{w}_2$ and $\mathbf{z}_1$ are multiples of one another, then A is of the form $A = (\lambda_1\mathbf{u}_1 \otimes \mathbf{v}_1 + \lambda_2\mathbf{u}_2 \otimes \mathbf{v}_2) \otimes \mathbf{z}_1$ (i.e., its "third row space" is spanned by $\mathbf{z}_1$). This is a contradiction to the definition of A under (12.3).

In both cases, we have derived a contradiction, so A cannot have rank two. Finally, for $d \geq 3$, we tensor A with as many factors as needed. □

A decomposition of the form $A = A_1 + \cdots + A_r$ with $A_i \in \mathcal{S}$ is called a *rank-r decomposition*. In the signal processing literature it is also called *canonical polyadic decomposition*. One appealing property of higher order tensors is *identifiability*. That is, many tensor decompositions are actually unique (rank decompositions of matrices are never unique). The following is [46, Theorem 1.1] and [149, Lemma 28].

Theorem 12.10 *Let $n_1 \geq \cdots \geq n_d$ with $\prod_{i=1}^d n_i \leq 15000$ and*

$$r_0 = \left\lceil \frac{\dim \mathbb{R}^{n_1\times\cdots\times n_d}}{\dim \mathcal{S}} \right\rceil = \left\lceil \frac{n_1 \cdots n_d}{1 + \sum_{i=1}^d (n_i - 1)} \right\rceil.$$

Suppose that $r < r_0$ and $(n_1, \ldots, n_d, r)$ is not one of the following cases

$(n_1, \ldots, n_d)$	r
$(4,4,3)$	5
$(4,4,4)$	6
$(6,6,3)$	8
$(n,n,2,2)$	$2n-1$
$(2,2,2,2,2)$	5
$n_1 > \prod_{i=2}^d n_i - \sum_{i=2}^d (n_i - 1)$	$r \geq \prod_{i=2}^d n_i - \sum_{i=2}^d (n_i - 1)$

Then, a general tensor in Σ_r has a unique rank-r decomposition.

Remark 12.11 Another important decomposition is the so-called *block term decomposition*. This is a decomposition of the form $A = A_1 + \cdots + A_r$, where the A_i are tensors of *low multilinear-rank*. A block term decomposition models a mixture of distributions which allow correlations between the variables, other than the rank decomposition, which models a mixture of independence models. An example, where this is relevant, is detecting epileptic seizures [105]. The interaction between the variables in this case is extremely complex, so that a mixture of independence models is not the appropriate model.

The definition of the block term decomposition is as follows: Let $\boldsymbol{k} = (k_1, \ldots, k_d)$ be a vector of integers with $1 \leq k_i \leq n_i$. Let $A \in \mathbb{R}^{n_1 \times \cdots \times n_d}$ and $F_1, \ldots, F_d$ be the flattenings of A. Then, we say that A has *multilinear-rank* (at most) $\boldsymbol{k}$ if $\operatorname{rank}(F_j) \leq k_j$ for all $1 \leq j \leq d$. Note that the rank decomposition above is the special case $k = (1, \ldots, 1)$. For order-three tensors, a block term decomposition can be visualized as follows:

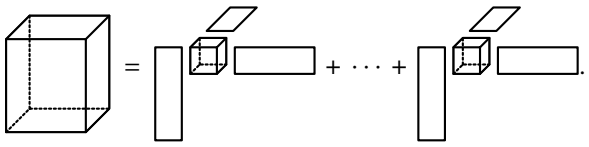

Identifiability of block term decompositions is less well-studied than for rank-r decompositions. Results exist for the decomposition of tensors into tensors of multilinear-rank $(1, k_1, k_2)$ [181], $(1, k, k)$ [51, 58], $(k_1, k_2, 1)$ [163], and (k_1, k_2, k_3) [119]. ◇

12.2 Singular Vectors and Eigenvectors

We study the Euclidean distance degree of the Segre- and of the Veronese variety. A key property of both the Segre and Veronese variety is that they are *unirational*. One can see that each of them is the image of a polynomial map:

$$\psi : \mathbb{R}^{n_1} \times \cdots \times \mathbb{R}^{n_d} \to \mathcal{S},\ (\mathbf{v}_1, \ldots, \mathbf{v}_d) \mapsto \mathbf{v}_1 \otimes \cdots \otimes \mathbf{v}_d, \tag{12.6}$$

and

$$\nu : \mathbb{R}^n \to \mathcal{V},\ \mathbf{v} \mapsto \mathbf{v}^{\otimes d}. \tag{12.7}$$

These maps are called the Segre– and Veronese–map, respectively.

Remark 12.12 Proposition 12.9 implies that for tensors of order $d \geq 3$ the problem of computing $\min_{B \in \Sigma_r} \|A - B\|$ for a tensor A can be ill-posed (the minimizer does not need to exist). In fact, da Silva and Lim [52] prove that there is full-dimensional open subset of tensors such that this problem is ill-posed. This is different for matrices, where the Eckhart-Young Theorem (Theorem 2.6) provides an explicit algorithm for computing the minimizer. By contrast, the Segre- and the Veronese-variety are closed (both in the Euclidean and Zariski topology).

We first study the Euclidean distance degree of the Segre variety $\mathcal{S}$. For this, we consider a tensor $A \in \mathbb{R}^{n_1 \times \cdots \times n_d}$ and the optimization problem

$$\min_{B \in \mathcal{S}} \|A - B\| = \min_{\mathbf{v}_i \in \mathbb{R}^{n_i}} \|A - \psi(\mathbf{v}_1, \ldots, \mathbf{v}_d)\|.$$

The polynomial map ψ is a smooth map of constant rank away from the fiber of zero, which implies that the critical values of the distance function $\mathcal{S} \to \mathbb{R}, B \mapsto \|A - B\|$ are in one-to-one correspondence to the critical values of $\|A - \psi(\mathbf{v}_1, \ldots, \mathbf{v}_d)\|$ up to scaling $(\mathbf{v}_1, \ldots, \mathbf{v}_d) \mapsto (t_1\mathbf{v}_1, \ldots, t_d\mathbf{v}_d)$ with $t_1 \cdots t_d = 1$. Let us write

$$\|A - \psi(\mathbf{v}_1, \ldots, \mathbf{v}_d)\|^2 = \|A\|^2 - 2\langle A, \psi(\mathbf{v}_1, \ldots, \mathbf{v}_d)\rangle + \|\psi(\mathbf{v}_1, \ldots, \mathbf{v}_d)\|^2.$$

By (12.2), we have $\|\psi(\mathbf{v}_1, \ldots, \mathbf{v}_d)\|^2 = \|\mathbf{v}_1\|^2 \cdots \|\mathbf{v}_d\|^2$. We use this to get the critical equation

$$\begin{aligned} 0 &= \tfrac{\mathrm{d}}{\mathrm{d}\mathbf{v}_i}\|A - \psi(\mathbf{v}_1, \ldots, \mathbf{v}_d)\|^2 \\ &= -2\tfrac{\mathrm{d}}{\mathrm{d}\mathbf{v}_i}\langle A, \psi(\mathbf{v}_1, \ldots, \mathbf{v}_d)\rangle + \tfrac{\mathrm{d}}{\mathrm{d}\mathbf{v}_i}(\|\mathbf{v}_1\|^2 \cdots \|\mathbf{v}_d\|^2) \\ &= -2\begin{pmatrix} \langle A, \mathbf{v}_1 \otimes \cdots \otimes \mathbf{v}_{i-1} \otimes \mathbf{e}_1 \otimes \mathbf{v}_{i+1} \otimes \cdots \otimes \mathbf{v}_d\rangle \\ \vdots \\ \langle A, \mathbf{v}_1 \otimes \cdots \otimes \mathbf{v}_{i-1} \otimes \mathbf{e}_{n_i} \otimes \mathbf{v}_{i+1} \otimes \cdots \otimes \mathbf{v}_d\rangle \end{pmatrix} + \Big(2\prod_{j \neq i} \|\mathbf{v}_j\|^2\Big)\mathbf{v}_i, \end{aligned} \tag{12.8}$$

where $\mathbf{e}_1, \ldots, \mathbf{e}_{n_i}$ denotes the standard basis of $\mathbb{R}^{n_i}$. We denote $\sigma_i := \prod_{j \neq i} \|\mathbf{v}_j\|^2$. It is then convenient to write the critical equation (12.8) using the short-hand notation $A \bullet \otimes_{j \neq i} \mathbf{v}_j = \sigma_i \cdot \mathbf{v}_i$. For $d = 3$, we can visualize this as follows

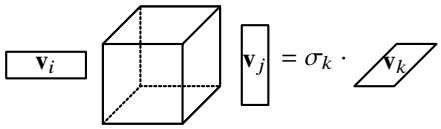

(12.9)

The critical points of the critical equations over the complex numbers are called singular vectors.

Definition 12.13 Let $A \in \mathbb{R}^{n_1 \times \cdots \times n_d}$. We say that $(\mathbf{v}_1, \ldots, \mathbf{v}_d) \in \mathbb{C}^{n_1} \times \cdots \times \mathbb{C}^{n_d}$, $\mathbf{v}_i \neq 0$, is a *singular vector tuple* for A if there exists $(\sigma_1, \ldots, \sigma_d) \in \mathbb{C}$ with

$$A \bullet \otimes_{j \neq i} \mathbf{v}_j = \sigma_i \cdot \mathbf{v}_i \qquad \text{for } i = 1, \ldots, d.$$

If $A \bullet \otimes_{j \neq i} \mathbf{v}_j = \sigma_i \cdot \mathbf{v}_i$, then also $A \bullet \otimes_{j \neq i}(t_j\mathbf{v}_j) = \sigma_i' \cdot (t_i\mathbf{v}_i)$, where $\sigma_i' = t_i^{-1} \cdot (\prod_{j \neq i} t_j) \cdot \sigma_i$, by multilinearity. Therefore, one considers singular value tuples only up to scaling.

For $d = 2$, this coincides with the classic definition of singular vector pairs for matrices. The singular value decomposition implies that for a general matrix $A \in \mathbb{R}^{n_1 \times n_2}$ there are precisely $\min\{n_1, n_2\}$ singular vector pairs that are all real. For higher order tensors not all singular vectors need to be real. The number of singular vectors – and hence the Euclidean distance degree of $\mathcal{S}$ – is given by the following theorem due to Friedland and Ottaviani [70].

Theorem 12.14 *Let $A \in \mathbb{R}^{n_1 \times \cdots \times n_d}$ be a general tensor. The number of singular vector tuples of A, up to scaling $(\mathbf{v}_1, \ldots, \mathbf{v}_d) \mapsto (t_1\mathbf{v}_1, \ldots, t_d\mathbf{v}_d)$ is the coefficient of the monomial $x_1^{n_1-1} \cdots x_d^{n_d-1}$ in the polynomial*

$$\prod_{i=1}^{d} \frac{f_i^{n_i} - x_i^{n_i}}{f_i - x_i}, \qquad \text{where } f_i := \sum_{j \neq i} x_j.$$

Example 12.15 We consider the formula in Theorem 12.14 for binary tensors $A \in \mathbb{R}^{2\times\cdots\times 2}$. In this case,

$$\prod_{i=1}^{d} \frac{f_i^2 - x_i^2}{f_i - x_i} = \prod_{i=1}^{d} (f_i + x_i) = (x_1 + \cdots + x_d)^d.$$

The coefficient of $x_1 \cdots x_d$ in this polynomial is $d!$. Consequently, the Euclidean distance degree of the Segre variety in $\mathbb{R}^{2\times 2\times 2}$ is $3! = 6$. ◇

If we follow the approach above for symmetric tensors and the Veronese variety, we arrive at the notion of *eigenpairs of tensors*. In this case, the critical equations are $\left(\langle A, \mathbf{e}_1 \otimes \mathbf{v}^{\otimes(d-1)}\rangle, \ldots, \langle A, \mathbf{e}_n \otimes \mathbf{v}^{\otimes(d-1)}\rangle\right) = \lambda \mathbf{v}$. We abbreviate this as $A \bullet \mathbf{v}^{\otimes(d-1)} = \lambda \mathbf{v}$. Similarly to (12.9), we can visualize this in the case $d = 3$:

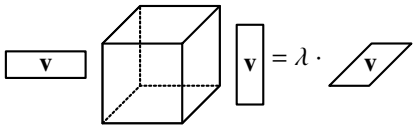

Definition 12.16 Let $A \in S^d(\mathbb{R}^n)$. We call $\mathbf{v} \in \mathbb{C}^n \setminus \{0\}$ an *eigenvector* of A if there exists $\lambda \in \mathbb{C}$ with

$$A \bullet \mathbf{v}^{\otimes(d-1)} = \lambda \mathbf{v}.$$

The pair $(\mathbf{v}, \lambda)$ is called an *eigenpair* of A.

Eigenpairs have another interesting interpretation, next to being critical points for the Euclidean distance function on the real Veronese variety. Recall that, if $A \in S^d(\mathbb{R}^n)$ is symmetric, then $F_A(\mathbf{x}) = \langle A, \mathbf{x}^{\otimes d}\rangle$ is a homogeneous polynomial of degree d in n variables. Eigenpairs correspond to fixed points of the rational map $\mathbb{P}^{n-1} \dashrightarrow \mathbb{P}^{n-1}, \mathbf{x} \mapsto (\partial F_A/\partial x_1, \ldots, \partial F_A/\partial x_n)$ given by the gradient of F_A.

Example 12.17 Consider the symmetric matrix $A = \left(\begin{smallmatrix} 1 & 2 \\ 2 & 0 \end{smallmatrix}\right) \in S^2(\mathbb{R}^2)$ from Example 12.3. The eigenvectors equations of A are

$$\begin{pmatrix} \partial F_A/\partial x_1 \\ \partial F_A/\partial x_2 \end{pmatrix} = \begin{pmatrix} 2x_1 + 4x_2 \\ 4x_1 \end{pmatrix} = 2A\mathbf{x} = 2\lambda\mathbf{x}.$$

For the tensor $B = \left(\begin{smallmatrix} 1 & -1 \\ -1 & 0 \end{smallmatrix} \middle| \begin{smallmatrix} -1 & 0 \\ 0 & 2 \end{smallmatrix}\right) \in S^3(\mathbb{R}^2)$ from Example 12.3, the eigenvector equations for B are

$$\begin{pmatrix} \partial F_B/\partial x_1 \\ \partial F_B/\partial x_2 \end{pmatrix} = \begin{pmatrix} 3x_1^2 - 6x_1x_2 \\ -3x_1^2 + 6x_2^2 \end{pmatrix} = 3\lambda\mathbf{x}.$$

These are systems of polynomial equations for the unknowns x_1, x_2, λ. ◇

In fact, we can remove the assumption that A is symmetric from Definition 12.16 and define eigenpairs for general tensors as well. That way, we lose the interpretations above, but we have a more general definition. Let us count the number of eigenpairs of a general tensor. The following theorem was first proved by Cartwright and Sturmfels in [38] using intersection theory. Here, we give an alternative proof.

Theorem 12.18 *Let $A \in (\mathbb{R}^n)^{\otimes d}$ be general. The number of eigenvectors of A, up to scaling $\mathbf{v} \mapsto t\mathbf{v}$, is*

$$\sum_{i=0}^{n-1} (d-1)^i.$$

Proof For $d = 2$, the formula of Theorem 12.18 gives n, which is the number of eigenpairs of a general matrix $A \in \mathbb{R}^{n\times n}$. Hence, we assume $d > 2$ from now on. We use the same proof strategy as for Corollary 3.15.

Let us first prove the statement for a general $A \in S^d(\mathbb{R}^n)$. Consider the symmetric tensor A with $F_A(\mathbf{x}) = x_1^d + \cdots + x_n^d$ (for $d = 3$ and $n = 2$, this gives the tensor from Example 12.19). The equations for eigenpairs are then

$$x_1^{d-1} - \xi^{d-2}x_1 = \cdots = x_n^{d-1} - \xi^{d-2}x_n = 0,$$

where $\lambda = \xi^{d-2}$ is the eigenvalue. We count that this system of homogeneous polynomial equations has precisely $(d-1)^n$ regular solutions in $\mathbb{P}^n$. By Bézout's theorem, a general system of n polynomials with degrees $(d-1,\ldots,d-1)$ also has $(d-1)^n$ regular zeros. The Parameter Continuation Theorem 3.18 then implies that the family of systems

$$\mathcal{F} := \left\{ \tfrac{1}{d}\nabla F_A(\mathbf{v}) - \xi^{d-2}\mathbf{v} \mid A \in S^d(\mathbb{R}^n) \right\}$$

has $(d-1)^n$ regular zeros for a general $A \in S^d(\mathbb{R}^n)$ (Theorem 3.18 works for non-homogeneous systems; we can dehomogenize the systems in $\mathcal{F}$ by considering a random affine patch in $\mathbb{C}^{n+1}$. Moreover, for general A and a zero $\frac{1}{d}\nabla F_A(\mathbf{v}) - \xi^{d-2}\mathbf{v} = 0$, we must have $\xi \neq 0$, because $\nabla F_A(\mathbf{v}) \neq 0$, since it is a general system of n homogeneous equations in n variables). The number of eigenpairs for a general A therefore is

$$\frac{(d-1)^n - 1}{d-2} = \sum_{i=0}^{n-1}(d-1)^i,$$

because we have to remove $\mathbf{v} = 0$ from the count and divide the count by $(d-2)$ to account for scaling of ξ with $(d-2)$–th roots of unity.

Finally, since $S^d(\mathbb{R}^n) \subset (\mathbb{R}^n)^{\otimes d}$ the above argument shows that the number of eigenvalues of a general tensor in $(\mathbb{R}^n)^{\otimes d}$ is lower bounded by $\sum_{i=0}^{n-1}(d-1)^i$. This is also an upper bound by Bézout's theorem.

Example 12.19 The polynomial $F_A(\mathbf{x}) = x_1^3 + x_2^3$ corresponds to a $2\times 2\times 2$–tensor A. The eigenpairs of A are solutions to the system of equations

$$v_1^2 - \lambda v_1 = v_2^2 - \lambda v_2 = 0.$$

If $\lambda = 0$, then $\mathbf{v} = 0$, which by definition is not an eigenvector. So, we can set $\lambda = 1$. The other solutions are $\mathbf{v} \in \{(1,1),\ (0,1),\ (1,0)\}$. So, we have three eigenvectors up to scaling, which is consistent with the formula in Theorem 12.18. ◇

For matrices, every n-tuple of linearly independent vectors can be eigenvectors of a matrix. For tensors this is not so. Abo, Sturmfels and Seigal proved in [1] that a set of d points $\mathbf{v}_1,\ldots,\mathbf{v}_d$ in $\mathbb{C}^2$ is the eigenconfiguration of a symmetric tensor in $S^d(\mathbb{C}^2)$ if and only if d is odd, or $d = 2k$ is even and the differential operator $(\frac{\partial^2}{\partial x^2} + \frac{\partial^2}{\partial y^2})^k$ annihilates the binary form $f_{\mathbf{v}_i}(x,y) := \prod_{i=1}^d (b_i x - a_i y)$, where $\mathbf{v}_i = (a_i, b_i)$, for all $i = 1,\ldots,d$.

12.3 Volumes of Rank-One Varieties

We now address the problem of computing the volumes of the complex Segre variety $\mathcal{S}_{\mathbb{C}} := \overline{\mathcal{S}}$ and of the complex Veronese variety $\mathcal{V}_{\mathbb{C}} := \overline{\mathcal{V}}$, where $\overline{\ }$ denotes complex Zariski closure. This is an important problem in metric algebraic geometry by itself. We discuss volumes of real semialgebraic sets in Section 6.3

and Chapter **??**. In this section, we measure volumes in $\mathbb{C}^{n_1 \times \cdots \times n_d}$ relative to the Euclidean inner product $\mathrm{Re}(\langle A, B\rangle_{\mathbb{C}})$, where the Hermitian inner product is

$$\langle A, B\rangle_{\mathbb{C}} := \sum_{i_1=1}^{n_1} \cdots \sum_{i_d=1}^{n_d} \overline{a_{i_1,\ldots,i_d}} \cdot b_{i_1,\ldots,i_d}$$

The complex Segre variety $\mathcal{S}_{\mathbb{C}}$ consists of rank-one tensors $\mathbf{v}_1 \otimes \cdots \otimes \mathbf{v}_d$, where the $\mathbf{v}_i \in \mathbb{C}^{n_i}$ are complex vectors. Similarly, $\mathcal{V}_{\mathbb{C}}$ consists of vectors $\mathbf{v}^{\otimes d}$ for $\mathbf{v} \in \mathbb{C}^n$. We observe that both $\mathcal{S}_{\mathbb{C}}$ and $\mathcal{V}_{\mathbb{C}}$ are cones; i.e., closed under scaling. In particular, they are not compact and do not have finite volume. To make a meaningful computation, we pass to complex projective space $\mathbb{P}^N$, where $N = n_1 \cdots n_d - 1$ (or $N = n^d - 1$ if the n_i are all equal) and measure the volume of the projective Segre variety and projective Veronese variety. Let us denote them by

$$\mathcal{S}_{\mathbb{P}} := \left\{\mathbf{v}_1 \otimes \cdots \otimes \mathbf{v}_d \in \mathbb{P}^N \mid \mathbf{v}_i \in \mathbb{P}^{n_i - 1}, 1 \le i \le d\right\} \quad \text{and} \quad \mathcal{V}_{\mathbb{P}} := \left\{\mathbf{v}^{\otimes d} \in \mathbb{P}^N \mid \mathbf{v}_i \in \mathbb{P}^{n-1}\right\}. \tag{12.10}$$

Furthermore, let us denote the sphere in $\mathbb{C}^n$ by

$$\mathbb{S}^{2n-1} := \{\mathbf{a} \in \mathbb{C}^n \mid \langle \mathbf{a}, \mathbf{a}\rangle_{\mathbb{C}} = 1\},$$

where, as above in the space of tensors, $\langle \mathbf{a}, \mathbf{b}\rangle_{\mathbb{C}} = \mathbf{a}^*\mathbf{b}$ is the standard Hermitian inner product. The sphere is a real manifold of real dimension $\dim_{\mathbb{R}} \mathbb{S}^{2n-1} = 2n - 1$. We have the projection $\pi : \mathbb{S}^{2n-1} \to \mathbb{P}^{n-1}$ that sends a point $\mathbf{a} \in \mathbb{S}^{2n-1}$ to its projective class. The tangent space of $\mathbb{S}^{2n-1}$ at a point $\mathbf{a}$ is

$$T_{\mathbf{a}}\mathbb{S}^{2n-1} = \{\mathbf{t} \in \mathbb{C}^n \mid \mathrm{Re}(\langle \mathbf{a}, \mathbf{t}\rangle_{\mathbb{C}}) = 0\}.$$

We have $\mathrm{Re}(\langle \mathbf{a}, \mathbf{b}\rangle_{\mathbb{C}}) = 0$ if and only if $\langle \mathbf{a}, \mathbf{b}\rangle_{\mathbb{C}} = 0$ or $\mathbf{a} = \sqrt{-1} \cdot \mathbf{b}$. Thus, we can interpret the tangent space of projective space as

$$T_{\mathbf{x}}\mathbb{P}^{n-1} = \{\mathbf{t} \in \mathbb{C}^n \mid \langle \mathbf{a}, \mathbf{t}\rangle_{\mathbb{C}} = 0\}, \qquad \text{where } \mathbf{x} = \pi(\mathbf{a}) \text{ for } \mathbf{a} \in \mathbb{S}^{2n-1}.$$

Complex projective space $\mathbb{P}^{n-1}$ is a Riemannian manifold relative to the Euclidean structure $\mathrm{Re}(\langle \mathbf{a}, \mathbf{b}\rangle)_{\mathbb{C}}$. This induces a notion of volume for subsets of $\mathbb{P}^{n-1}$. We have defined the metric structures of $\mathbb{S}^{2n-1}$ and $\mathbb{P}^{n-1}$ so that the projection π is a Riemannian submersion. This implies that the m-dimensional real volume of a measurable subset $U \subset \mathbb{P}^{n-1}$ is

$$\mathrm{vol}_m(U) = \tfrac{1}{2\pi}\,\mathrm{vol}_{m+1}(\pi^{-1}(U)),$$

since the preimage $\pi^{-1}(\mathbf{x})$ for $\mathbf{x} \in \mathbb{P}^{n-1}$ is a circle. For instance, the volume of projective space is

$$\mathrm{vol}_{2(n-1)}(\mathbb{P}^{n-1}) := \frac{1}{2\pi}\mathrm{vol}_{2n-1}(\mathbb{S}^{2n-1}) = \frac{\pi^{n-1}}{(n-1)!}. \tag{12.11}$$

In the following, we sometimes omit the subscript from vol when the dimension is clear from the context.

Proposition 12.20 *Let $m := \dim_{\mathbb{R}} \mathcal{S}_{\mathbb{P}}$. The m-dimensional volume of $\mathcal{S}_{\mathbb{P}}$ in* (12.10) *is*

$$\mathrm{vol}(\mathcal{S}_{\mathbb{P}}) = \mathrm{vol}(\mathbb{P}^{n_1-1}) \cdots \mathrm{vol}(\mathbb{P}^{n_d-1}).$$

Proof We define the Segre map (12.6) for projective space: $\psi_{\mathbb{P}} : \mathbb{P}^{n_1-1} \times \cdots \times \mathbb{P}^{n_d-1} \to \mathcal{S}_{\mathbb{P}}$. Then, $\psi_{\mathbb{P}}$ is a smooth embedding. Let $(\mathbf{x}_1, \ldots, \mathbf{x}_d) \in \mathbb{P}^{n_1-1} \times \cdots \times \mathbb{P}^{n_d-1}$ and $\mathbf{a}_i \in \mathbb{S}^{2n_i-1}$ with $\pi(\mathbf{a}_i) = \mathbf{x}_i$ be a fixed representative for $\mathbf{x}_i$. Let also $\mathbf{t}_i \in \mathbb{C}^{n_i}$ with $\langle \mathbf{a}_i, \mathbf{t}_i\rangle = 0$.

The derivative of $\psi_{\mathbb{P}}$ maps $(\mathbf{t}_1, \ldots, \mathbf{t}_d) \in T_{(\mathbf{x}_1,\ldots,\mathbf{x}_d)}(\mathbb{P}^{n_1-1} \times \cdots \times \mathbb{P}^{n_d-1})$ to

$$\theta := \mathbf{t}_1 \otimes \mathbf{a}_2 \otimes \cdots \otimes \mathbf{a}_d + \mathbf{a}_1 \otimes \mathbf{t}_2 \otimes \cdots \otimes \mathbf{a}_d + \cdots + \mathbf{a}_1 \otimes \mathbf{a}_2 \otimes \cdots \otimes \mathbf{t}_d.$$

It follows from (12.2) that the terms in this sum are pairwise orthogonal. Therefore

$$\|\theta\|^2 = \|\mathbf{t}_1\|^2 + \|\mathbf{t}_2\|^2 + \cdots + \|\mathbf{t}_d\|^2.$$

This shows that the derivative of $\psi_{\mathbb{P}}$ preserves norms. This implies that $\psi_{\mathbb{P}}$ is volume preserving. □

Proposition 12.21 *The $2(n-1)$-dimensional volume of the projective Veronese variety in* (12.10) *is*

$$\operatorname{vol}(\mathcal{V}_{\mathbb{P}}) = d^{n-1} \cdot \operatorname{vol}(\mathbb{P}^{n-1}).$$

Proof The proof is similar to that of Proposition 12.20. We denote the projective Veronese map by $\nu_{\mathbb{P}} : \mathbb{P}^{n-1} \to \mathcal{V}_{\mathbb{P}}$. Then, also $\nu_{\mathbb{P}}$ is a smooth embedding. Let $\mathbf{x} \in \mathbb{P}^{n-1}$ and $\mathbf{a} \in \mathbb{S}^{2n-1}$ be a representative for $\mathbf{x}$; i.e., $\pi(\mathbf{a}) = \mathbf{x}$. Let $\mathbf{t} \in \mathbb{C}^n$ with $\langle \mathbf{a}, \mathbf{t} \rangle = 0$. The derivative of $\nu_{\mathbb{P}}$ maps $\mathbf{t} \in T_{\mathbf{x}}\mathbb{P}^{n-1}$ to

$$\theta := \mathbf{t} \otimes \mathbf{a} \otimes \cdots \otimes \mathbf{a} + \mathbf{a} \otimes \mathbf{t} \otimes \cdots \otimes \mathbf{a} + \cdots + \mathbf{a} \otimes \mathbf{a} \otimes \cdots \otimes \mathbf{t}.$$

It follows from (12.2) that the terms in this sum are pairwise orthogonal, so $\|\theta\|^2 = d\|\mathbf{t}\|^2$. This shows that the derivative of $\nu_{\mathbb{P}}$ scales norms by $\sqrt{d}$. This implies that

$$\operatorname{vol}(\mathcal{V}_{\mathbb{P}}) = \left(\sqrt{d}\,\right)^{\dim_{\mathbb{R}} \mathbb{P}^{n-1}} \cdot \operatorname{vol}(\mathbb{P}^{n-1}) = d^{n-1} \cdot \operatorname{vol}(\mathbb{P}^{n-1}).$$

Propositions 12.20 and 12.21 can be applied to intersection theory using Howard's *Kinematic Formula* [97]. This is a general formula for the average volume of intersections of submanifolds in homogeneous spaces. For complex projective space, we have the following; see [97, Theorem 3.8 & Corollary 3.9]. Let $M \subset \mathbb{P}^N$ be a smooth manifold of complex dimension m. Then, the Kinematic formula for complex projective space is

$$\mathbb{E}_U \#(M \cap U \cdot (\mathbb{P}^{N-m} \times \{0\}^m)) = \frac{\operatorname{vol}_{2m}(M)}{\operatorname{vol}_{2m}(\mathbb{P}^m)},$$

where the expectation is taken relative to the probability measure on the unitary group $U(N+1)$ induced by the Haar measure. If $X \subset \mathbb{P}^N$ is a smooth algebraic variety of complex dimension m, then the number of intersection points $\#(X \cap U \cdot (\mathbb{P}^{N-m} \times \{0\}^m))$ equals the degree of X for almost all U. Thus, we are taking the expected value of a constant function. This shows

$$\deg(X) = \frac{\operatorname{vol}_{2m}(X)}{\operatorname{vol}_{2m}(\mathbb{P}^m)}, \qquad \text{where } m = \dim_{\mathbb{C}}(X). \tag{12.12}$$

Combined with the theorems above we obtain the following result.

Corollary 12.22

1. $\deg(\mathcal{S}_{\mathbb{P}}) = \dfrac{(n_1 + \cdots + n_d - d)!}{(n_1 - 1)! \cdots (n_d - 1)!}$.
2. $\deg(\mathcal{V}_{\mathbb{P}}) = d^{n-1}$.

Proof The second formula follows directly from Proposition 12.21 and (12.12). For the first formula, we recall from (12.11) the volume of projective space: $\operatorname{vol}_{2(n-1)}(\mathbb{P}^{n-1}) = \frac{\pi^{n-1}}{(n-1)!}$. We set

$$m := n_1 + \cdots + n_d - d = \dim_{\mathbb{C}} \mathcal{S}_{\mathbb{P}}.$$

Using Proposition 12.20 and (12.12) we then have

$$\deg(\mathcal{S}_{\mathbb{P}}) = \frac{\operatorname{vol}(\mathbb{P}^{n_1-1})\cdots\operatorname{vol}(\mathbb{P}^{n_d-1})}{\operatorname{vol}(\mathbb{P}^m)} = \frac{\pi^{\sum_{i=1}^d (n_i-1)}}{\pi^m} \cdot \frac{m!}{(n_1-1)!\cdots(n_d-1)!}$$
$$= \frac{(n_1+\cdots+n_d-d)!}{(n_1-1)!\cdots(n_d-1)!}.$$

Remark 12.23 By (12.1), a linear equation of $\deg(\mathcal{V}_{\mathbb{P}})$ corresponds to the evaluation of a homogeneous polynomial of degree d in n variables. Thus, $\deg(\mathcal{V}_{\mathbb{P}}) = d^{n-1}$ means that a general system of $n-1$ homogeneous polynomials of degree d has d^{n-1} zeros.

Remark 12.24 Howard's Kinematic Formula from [97] also provides the following result for real projective space. Let $\mathbb{P}^N_{\mathbb{R}}$ denote real projective space and let $M \subset \mathbb{P}^N_{\mathbb{R}}$ be a real submanifold of real dimension m. Then, $\mathbb{E}_U \#(M \cap U \cdot (\mathbb{P}^{N-m}_{\mathbb{R}} \times \{0\}^m)) = \frac{\operatorname{vol}_m(M)}{\operatorname{vol}_m(\mathbb{P}^m_{\mathbb{R}})}$, where here the expectation is taken relative to the probability measure on the orthogonal group $O(n+1)$. Thus, the volume of real projective varieties can be interpreted as an "average degree". We can use the same proof strategies as above to show that the projective volume of the real Segre variety $\mathcal{S}$ is equal to $\operatorname{vol}(\mathbb{P}^{n_1-1}_{\mathbb{R}})\cdots\operatorname{vol}(\mathbb{P}^{n_d-1}_{\mathbb{R}})$ and the projective volume of the real Veronese $\mathcal{V}$ is $\sqrt{d^{n-1}} \cdot \operatorname{vol}(\mathbb{P}^{n-1}_{\mathbb{R}})$. The latter result was first observed by Edelman and Kostlan in their seminal paper [67] to show that a homogeneous polynomial of degree d in n variables has on the average $\sqrt{d}$ many real zeros.

Chapter 13
Computer Vision

The research field of computer vision studies how computers can gain understanding from images and videos, similarly to human cognitive abilities. One of the classical challenges is to reconstruct a 3D object from many images taken by unknown cameras. The simplest mathematical model of a camera is a surjective linear projection $C : \mathbb{P}^3 \dashrightarrow \mathbb{P}^2$. Such a *projective* or *uncalibrated camera* is given by an arbitrary full-rank 3×4 matrix A, i.e., $C(\mathbf{x}) = A\mathbf{x}$.

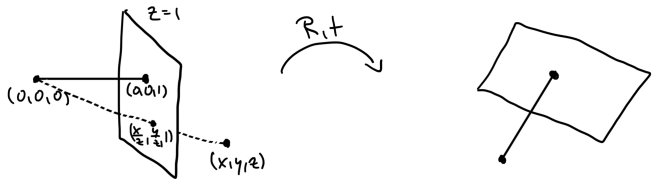

Fig. 13.1: Calibrated cameras: in standard position (on the left) and arbitrary (on the right).

In most real-life applications, one does not allow arbitrary matrices A, as one assumes several internal camera parameters, such as focal length, to be known. *Calibrated cameras* are those that can be obtained from rotation and translation from a camera in standard position; see Figure13.1. Projectively, the standard camera is $\mathbb{P}^3 \dashrightarrow \mathbb{P}^2$, $[x_1 : x_2 : x_3 : x_4] \mapsto [x_1 : x_2 : x_3]$, given by the 3×4 matrix $A = [I_3|0]$. Thus, all calibrated cameras are given by $A = [R|t]$, where $R \in \mathrm{SO}(3)$ and $t \in \mathbb{R}^3$. Between uncalibrated and calibrated cameras, there are also partially calibrated camera models; see [83, Chapter 6].

To be able to do 3D reconstruction from given images, one needs at least two cameras. The *joint camera map* is

$$\Phi : C_m \times X \dashrightarrow Y \tag{13.1}$$

that maps an m-tuple of cameras $(C_1, \ldots, C_m) \in C_m$ and an algebraic 3D object $\mathbf{x} \in X$ to the m images $(C_1(\mathbf{x}), \ldots, C_m(\mathbf{x})) \in Y$. For instance, the 3D object $\mathbf{x}$ could be a single point (i.e., $X = \mathbb{P}^3$), a line (i.e., $X = \mathrm{Gr}(1, \mathbb{P}^3)$), an arrangement of points and lines with prescribed incidences, a curve, or a surface. Formally, the task of 3D reconstruction means to compute fibers under the joint camera map Φ.

Example 13.1 For $m = 2$ projective cameras observing k points, the joint camera map is

$$\begin{aligned} \Phi : (\mathbb{P}\mathbb{R}^{3\times 4})^2 \times (\mathbb{P}^3_{\mathbb{R}})^k &\dashrightarrow (\mathbb{P}^2_{\mathbb{R}})^k \times (\mathbb{P}^2_{\mathbb{R}})^k, \\ (A_1, A_2, \mathbf{x}_1, \ldots, \mathbf{x}_k) &\mapsto (A_1\mathbf{x}_1, \ldots, A_1\mathbf{x}_k, A_2\mathbf{x}_1, \ldots, A_2\mathbf{x}_k). \end{aligned} \tag{13.2}$$

It is defined whenever none of the space points $\mathbf{x}_i$ is the kernel of A_1 nor A_2. The kernel of the matrix A_i is called the *camera center* of C_i. For calibrated cameras given by matrices of the form $A_i = [R_i|t_i]$, the joint camera map becomes

$$\Phi : (\mathrm{SO}(3) \times \mathbb{R}^3)^2 \times (\mathbb{P}^3_{\mathbb{R}})^k \dashrightarrow (\mathbb{P}^2_{\mathbb{R}})^k \times (\mathbb{P}^2_{\mathbb{R}})^k. \tag{13.3}$$

13.1 Multiview Varieties

For fixed cameras $C = (C_1, \ldots, C_m) \in C_m$, the joint camera map specializes to $\Phi_C : X \dashrightarrow Y$. The Zariski closure of the image of that map is the *multiview variety* $\mathcal{M}_C$ of the cameras C. We focus in this section on the multiview variety of a point, i.e., when $X = \mathbb{P}^3$. In that case, the multiview variety is parametrized

by

$$\Phi_C : \mathbb{P}^3 \dashrightarrow (\mathbb{P}^2)^m. \tag{13.4}$$

For $m \geq 2$ cameras whose camera centers do not all agree, the multiview variety $\mathcal{M}_C$ is a threefold. An implicit description of $\mathcal{M}_C$ is given by the maximal minors of the $3m \times (m+4)$ matrix

$$M_A := \begin{bmatrix} A_1 & \mathbf{y}_1 & 0 & \cdots & 0 \\ A_2 & 0 & \mathbf{y}_2 & \cdots & 0 \\ \vdots & & & \ddots & \\ A_m & 0 & 0 & \cdots & \mathbf{y}_m \end{bmatrix}, \tag{13.5}$$

where the A_i are the 3×4 matrices that define the cameras C_i and $(\mathbf{y}_1, \ldots, \mathbf{y}_m)$ are the coordinates on $(\mathbb{P}^2)^m$.

Proposition 13.2 *The multiview variety of a single point under m cameras $C = (C_1, \ldots, C_m)$ with at least two distinct camera centers is*

$$\mathcal{M}_C = \{(\mathbf{y}_1, \ldots, \mathbf{y}_m) \in (\mathbb{P}^2)^m \mid \operatorname{rk} M_A(\mathbf{y}_1, \ldots, \mathbf{y}_m) < m+4\}.$$

Proof (Idea) Computer vision researchers first discussed the defining polynomials of the multiview variety of a point in [90]. A tuple $(\mathbf{y}_1, \ldots, \mathbf{y}_m) \in (\mathbb{P}^2)^m$ is in the image of Φ_C in (13.4) if and only if there is a space point $\mathbf{x} \in \mathbb{P}^3$ and nonzero scalars λ_i such that $A_i\mathbf{x} = \lambda_i \mathbf{y}_i$ (for all $i = 1, \ldots, m$). The latter condition is equivalent to the vector $(\mathbf{x}^\top, -\lambda_1, \ldots, -\lambda_m)^\top$ being in the kernel of the matrix M_A in (13.5). Taking the closure, we obtain that the multiview variety $\mathcal{M}_C$ consists of those tuples $(\mathbf{y}_1, \ldots, \mathbf{y}_m)$ such that M_A has a non-trivial kernel vector. □

Example 13.3 For $m = 2$ cameras, the matrix M_A in (13.5) is a 6×6 matrix. Hence, $\mathcal{M}_C$ is the vanishing locus of its determinant, which is a bilinear form in $(\mathbf{y}_1, \mathbf{y}_2)$. This means that there is a 3×3 matrix F such that $\det(M_A) = \mathbf{y}_2^\top F \mathbf{y}_1$. The matrix F is called the *fundamental matrix* in the case of two projective cameras (C_1, C_2) and the *essential matrix* in the case of calibrated cameras. The matrix F has rank two. In fact, its kernel is the image of the camera center of C_2 under the camera C_1. Similarly, the cokernel of F is the image of the camera center of C_1 under the camera C_2; see Figure 13.2.

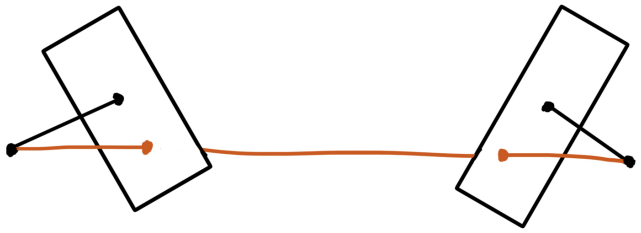

Fig. 13.2: The image of the center of one camera under the other camera (orange points) is the (co)kernel of the fundamental matrix.

In computer vision, the term *triangulation* refers to the task of 3D reconstruction once the cameras C are known. This task essentially means to compute fibers under the specialized joint camera map Φ_C. However, for $m \geq 2$ cameras, the generic fiber under Φ_C in (13.4) is empty. Since measurements

$\mathbf{y} := (\mathbf{y}_1, \ldots, \mathbf{y}_m)$ on the images are typically noisy, they do not lie on the multiview variety $\mathcal{M}_C$, and to triangulate a corresponding space point $\mathbf{x} \in \mathbb{P}^3$ we first need to find a point $\tilde{\mathbf{y}}$ on $\mathcal{M}_C$ closest to $\mathbf{y}$ and then compute its fiber $\Phi_C^{-1}(\tilde{\mathbf{y}})$. Hence, the algebraic complexity of triangulating a single point from m images is determined by the ED degree of the multiview variety $\mathcal{M}_C$.

In real-life applications, the image measurements $(\mathbf{y}_1, \ldots, \mathbf{y}_m)$ come from an affine chart $(\mathbb{R}^2)^m$ inside $(\mathbb{P}^2)^m$. Thus, triangulation requires to find a closest point to the measurements on the *affine multiview variety* $\mathcal{M}_C^\circ := \mathcal{M}_C \cap (\mathbb{R}^2)^m$ in that affine chart. The algebraic complexity of that problem is the ED degree of the affine variety $\mathcal{M}_C^\circ$. The interest in that ED degree was originally posed in the computer vision community. Indeed, computer vision experts computed the ED degree of $\mathcal{M}_C^\circ$ for $m \geq 7$ cameras [82,164]. The latter article titled *How hard is 3-view triangulation really?* was in fact one of the main motivations for the development of the general notion of ED degrees of algebraic varieties in [60, Example 3.3]. There, the authors conjectured a formula for the ED degree of the affine multiview variety $\mathcal{M}_C^\circ$ for arbitrarily many cameras. That conjecture was proven in [128]:

Theorem 13.4 *The ED degree of the affine multiview variety $\mathcal{M}_C^\circ$ for $m \geq 2$ cameras in general position is*

$$\frac{9}{2}m^3 - \frac{21}{2}m^2 + 8m - 4.$$

13.2 Grassmann Tensors

The fundamental / essential matrix from Example 13.3 can be generalized to more than two cameras, even to higher-dimensional surjective projections

$$C_i : \mathbb{P}^N \dashrightarrow \mathbb{P}^{n_i}. \tag{13.6}$$

Such projections can be for instance used to model basic dynamics [99,180]. The *camera center* of such a camera is its base locus. To generalize fundamental matrices to that setting, the computer vision article [81] studies proper projective subspaces L_i of the image spaces $\mathbb{P}^{n_i}$ that meet the multiview variety of a single point. More concretely, for fixed cameras C_i as in (13.6) and fixed integers $c_1, \ldots, c_m$ with $1 \leq c_i \leq n_i$ denoting the codimension of the L_i, we write $\Gamma_{C,c}$ for the Zariski closure of

$$\begin{aligned}\{(L_1, \ldots, L_m) \in \mathrm{Gr}(n_1 - c_1, \mathbb{P}^{n_1}) \times \ldots \times \mathrm{Gr}(n_m - c_m, \mathbb{P}^{n_m}) \mid \\ \exists \mathbf{x} \in \mathbb{P}^N : C_1(\mathbf{x}) \in L_1, \ldots, C_m(\mathbf{x}) \in L_m\}.\end{aligned} \tag{13.7}$$

Theorem 13.5 *Assume that the intersection of all m camera centers of the cameras $C = (C_1, \ldots, C_m)$ is empty. The variety $\Gamma_{C,c}$ is a hypersurface if and only if $c_1 + \ldots + c_m = N + 1$. In that case, its defining equation in the Plücker coordinates of the $\mathrm{Gr}(n_i - c_i, \mathbb{P}^{n_i})$ is multilinear.*

In the case that $\Gamma_{C,c}$ is a hypersurface, its multilinear defining equation is given by an m-dimensional tensor, called the *Grassmann tensor*.

Example 13.6 Let us consider the standard setting in computer vision: $N = 3$ and $n_i = 2$ for all $i = 1, \ldots, m$. For $m = 2$ cameras, the only two integers $1 \leq c_i \leq 2$ summing to $N + 1 = 4$ are $c_1 = c_2 = 2$. The hypersurface $\Gamma_{(C_1,C_2),(2,2)}$ is the multiview variety $\mathcal{M}_{C_1,C_2}$ in Example 13.3. The corresponding Grassmann tensor is the fundamental / essential matrix.

For $m = 3$ cameras, there are three choices of integers c_i such that $\Gamma_{C,c}$ is a hypersurface: $(c_1, c_2, c_3) \in \{(2,1,1), (1,2,1), (1,1,2)\}$. For $m = 4$ cameras, there is a single choice, namely $c_1 = c_2 = c_3 = c_4 = 1$. The corresponding Grassmann tensors are known as the *trifocal* and *quadrifocal tensors*, respectively. There are no Grassmann tensors for $m \geq 5$.

Proof (of Theorem 13.5) This was essentially argued in [81]. We provide an independent proof.

For a general $L_i \in \mathrm{Gr}(n_i - c_i, \mathbb{P}^{n_i})$, the *back-projected linear space* $\tilde{L}_i := \overline{C_i^{-1}(L_i)}$ has the same codimension c_i, i.e., $\tilde{L}_i \in \mathrm{Gr}(N - c_i, \mathbb{P}^N)$. If $\sum c_i \leq N$, the back-projected subspaces $\tilde{L}_1, \ldots, \tilde{L}_m$ always intersect, meaning that $\Gamma_{C,c}$ is equal to its ambient space.

Now let us consider the case that $\sum c_i = N + 1$. Since camera centers do not have a common point of intersection, the multiview variety $\mathcal{M}_C$ of a single point (that is, the Zariski closure of the image of $\Phi_C : \mathbb{P}^N \dashrightarrow \mathbb{P}^{n_1} \times \ldots \times \mathbb{P}^{n_m}$) has dimension N. Hence, the product $L_1 \times \ldots \times L_m$ of general subspaces $L_i \subseteq \mathbb{P}^{n_i}$ of codimension c_i does not intersect the multiview variety $\mathcal{M}_C$. This shows that $\Gamma_{C,c}$ is at most a hypersurface. We show that it is a hypersurface and simultaneously compute its multidegree by intersecting it with generic pencils in $\mathrm{Gr}(n_1 - c_1, \mathbb{P}^{n_1}) \times \ldots \times \mathrm{Gr}(n_m - c_m, \mathbb{P}^{n_m})$. Indeed, it is sufficient to show that every general pencil meets $\Gamma_{C,c}$ in exactly one point. Such a pencil is of the form $L_1 \times \ldots \times \mathcal{L}_k \times \ldots \times L_m$, where L_i (for $i \neq k$) is a general point in the Grassmannian $\mathrm{Gr}(n_i - c_i, \mathbb{P}^{n_i})$ and

$$\mathcal{L}_k = \{L \in \mathrm{Gr}(n_k - c_k, \mathbb{P}^{n_k}) \mid V_k \subset L \subset W_k\},$$

where $V_k, W_k \subseteq \mathbb{P}^{n_k}$ are general projective subspaces of codimension $c_k + 1$ and $c_k - 1$, respectively. The back-projected subspaces $\tilde{L}_1, \ldots, \tilde{W}_k, \ldots, \tilde{L}_m$ intersect in a single point $\mathbf{x} \in \mathbb{P}^N$. That point $\mathbf{x}$ does not lie in the back-projected subspace $\tilde{V}_k$, because otherwise, for a general $L \in \mathcal{L}_k$, the general point $L_1 \times \ldots \times L \times \ldots \times L_m$ would be contained in $\Gamma_{C,c}$; the latter is a contradiction since the codimension of $\Gamma_{C,c}$ is at least one. Thus, there is exactly one $L \in \mathcal{L}_k$ (namely, the span of V_k with $C_k(\mathbf{x})$) with the property that $L_1 \times \ldots \times L \times \ldots \times L_m \in \Gamma_{C,c}$. This shows that $\Gamma_{C,c}$ is a hypersurface of multidegree $(1, \ldots, 1)$. The multidegree of a hypersurface in a product of Grassmannians coincides with the multidegree of its defining equation in Plücker coordinates.

Similar arguments show that the codimension of $\Gamma_{C,c}$ is larger than one if $\sum c_i > N + 1$. □

13.3 3D Reconstruction

In this section, we consider the joint camera map Φ introduced in (13.1). Recall that 3D reconstruction from images taken by unknown cameras is equivalent to computing fibers under Φ. Typically, a nontrivial group G acts on the fibers since global 3D transformations that act simultaneously on the cameras and the 3D scene do not change the resulting images.

Example 13.7 For a projective camera given by a 3×4 matrix A that observes a point $\mathbf{x} \in \mathbb{P}^3$, the projective linear group acts via $\mathrm{PGL}(4) \ni g \mapsto (Ag^{-1}, g\mathbf{x})$ on the space of cameras and points without changing the resulting image $Ag^{-1} \cdot g\mathbf{x} = A\mathbf{x}$. Hence, $\mathrm{PGL}(4)$ acts on the fibers of the joint camera map in (13.2), where two projective cameras observe k points. This means that 3D reconstruction is only possible up to a projective transformation.

The action of the projective linear group $\mathrm{PGL}(4)$ does not map calibrated cameras to calibrated cameras. The largest subgroup of $\mathrm{GL}(4)$ that preserves the structure of calibrated camera matrices $[R|t] \in \mathrm{SO}(3) \times \mathbb{R}^3$ is the scaled special Euclidean group of $\mathbb{R}^3$:

$$G = \{g \in \mathrm{GL}(4) \mid g = \left[\begin{smallmatrix} R & t \\ 0 & \lambda \end{smallmatrix}\right] \text{ for some } R \in \mathrm{SO}(3), t \in \mathbb{R}^3, \lambda \in \mathbb{R} \setminus \{0\}\}. \tag{13.8}$$

In other words, 3D reconstruction with calibrated cameras is only possible up to a proper rigid motion and a nonzero scale.

The state-of-the-art 3D reconstruction algorithms compute fibers under joint camera maps Φ that are dominant and have generically finite fibers, after modding out the group G. These properties mean that

computing the fibers can be modeled as solving a *square* parametrized system of polynomial equations. 3D reconstruction problems that satisfy these properties are called *minimal problems* since they use the minimal amount of data on the images while having finitely many solutions. The generic number of solutions (over the complex numbers) of a minimal problem is its *algebraic degree*.

Example 13.8 We consider the setting of $m \geq 2$ projective cameras observing k points. The joint camera map for the case $m = 2$ was given in (13.2). This 3D reconstruction problem is minimal only if domain and codomain of the joint camera map, after modding out the group G acting on the fibers, have the same dimension. This domain is the quotient $\left((\mathbb{P}\mathbb{R}^{3\times 4})^m \times (\mathbb{P}^3_{\mathbb{R}})^k\right)/\mathrm{PGL}(4)$, while the codomain is $\left((\mathbb{P}^2)^k\right)^m$. Both have the same dimension if and only if $11m + 3k - 15 = 2km$. This equation has exactly two integer solutions with $m \geq 2$ and $k \geq 1$, namely $(m, k) \in \{(2, 7), (3, 6)\}$. Both solutions yield minimal problems of algebraic degree three [80]. That degree was already known by Hesse [89] and Sturm [166] in the 19th century.

For $m \geq 2$ calibrated cameras observing k points, the domain of the joint camera map, after modding out the special Euclidean group G in (13.8), is $\left((\mathrm{SO}(3) \times \mathbb{R}^3)^m \times (\mathbb{P}^3)^k\right)/G$. Thus, domain and codomain have the same dimension if and only if $6m + 3k - 7 = 2km$. The only integer solution with $m \geq 2$ and $k \geq 1$ is $(m, k) = (2, 5)$. This yields a minimal problem of algebraic degree 20 [64]. It is in fact the most common minimal problem in practical 3D reconstruction algorithms.

We explain the practical usage of minimal problems in 3D reconstruction algorithms at the previous example. Imagine two calibrated cameras observe 100 points. Then the joint camera map Φ in (13.3) for $k = 100$ is not dominant. Hence, the fiber under Φ of two noisy images is empty. Therefore, given two noisy images, we first need to find a closest point on the image of Φ, before we can compute the fiber of that closest point (similarly to the triangulation problem described at the end of Section 13.1). To avoid solving that optimization problem, one chooses five of the given 100 point pairs and solves the resulting minimal problem described in Example 13.8. This process gets repeated many times and the solutions of the many minimal problems get patched together via random sample consensus (RANSAC), until all 100 points (and both cameras) are reconstructed. This approach can also detect if some of the given 100 point pairs are incorrect. For more details on 3D reconstruction algorithms, see [107].

Since minimal problems have to be solved many times in practical algorithms, it is crucial that their formulation as a square polynomial system is efficient. A common strategy to make the polynomial systems simpler is to first only reconstruct the cameras and afterward recover the 3D scene via triangulation. Hence, instead of solving the full minimal problem at once, one starts by solving a polynomial system whose only unknowns are the camera parameters. The number of camera parameters can be further reduced by modding out the group G that acts on the fibers of the joint camera map. Indeed, the Grassmann tensors introduced in Section 13.2 encode projective cameras modulo $\mathrm{PGL}(N + 1)$. Formally, let $C_i : \mathbb{P}^N \dashrightarrow \mathbb{P}^{n_i}$ (for $i = 1, \ldots, m$) be surjective projections that do not have a common point in their base loci and let $c_1, \ldots, c_m$ be integers satisfying $1 \leq c_i \leq n_i$ and $c_1 + \ldots + c_m = N + 1$. Then the Grassmann tensor $T_{C,c}$ exists by Theorem 13.5. Thus, we have a rational map

$$\gamma_c : \mathbb{P}\mathbb{R}^{(n_1+1)\times(N+1)} \times \ldots \times \mathbb{P}\mathbb{R}^{(n_m+1)\times(N+1)} \dashrightarrow \mathbb{P}\mathbb{R}^{\binom{n_1+1}{c_1}\times\cdots\times\binom{n_m+1}{c_m}},$$

that sends the $(n_i + 1) \times (N + 1)$ matrices defining the projections C_i to their m-dimensional Grassmann tensor in the Plücker coordinates of the Grassmannians appearing in (13.7).

Proposition 13.9 ([81]) *The projective linear group* $\mathrm{PGL}(N+1)$ *acts on the fibers of* γ_c *by componentwise right-multiplication. Moreover, after modding out* $\mathrm{PGL}(N + 1)$ *from the domain of* γ_c*, that map becomes birational.*

Example 13.10 For $m = 2$ standard projective cameras (i.e., $N = 3, n_1 = n_2 = 2$), we have $c_1 = c_2 = 2$ (see Example 13.6) and γ_c is the map that sends two 3×4 matrices (A_1, A_2) to their fundamental matrix

F as in Example 13.3. The Zariski closure of the image of γ_c is the set $\mathcal{F} \subseteq \mathbb{R}^{3\times 3}$ of matrices with rank at most two. Hence, that variety $\mathcal{F}$ is birational to pairs of projective cameras modulo PGL(4). Working with this moduli space $\mathcal{F}$ reduces the number of camera parameters that have to be reconstructed: The rank-two 3×3 matrices (up to global scaling) have seven degrees of freedom, while pairs of projective cameras have 22 degrees of freedom. Any pair of image points $(\mathbf{y}_1, \mathbf{y}_2) \in \mathbb{P}^2 \times \mathbb{P}^2$ imposes a linear condition on the sought-after fundamental matrix: $\mathbf{y}_2^\top F \mathbf{y}_1 = 0$; see Example 13.3. Therefore, reconstructing a fundamental matrix means to intersect the seven-dimensional variety $\mathcal{F}$ with seven hyperplanes. This shows that two projective cameras observing seven points is a minimal problem of algebraic degree $\deg(\mathcal{F}) = 3$, as claimed in the first paragraph of Example 13.8.

When restricting the map γ_c to pairs of calibrated cameras and then modding out the scaled special Euclidean group G in (13.8) from the domain, the resulting map is no longer birational: Its generic fiber consists of two points. Its image is the set of all essential matrices E, which is the set of all 3×3 matrices of rank two whose two non-zero singular values are equal. The Zariski closure $\mathcal{E}$ of that image has dimension five, degree ten, and is defined by the equations

$$\det E = 0 \text{ and } EE^\top E - \frac{1}{2}\operatorname{tr}(EE^\top)E = 0;$$

see [53]. As for fundamental matrices, reconstructing an essential matrix means to intersect the variety $\mathcal{E}$ with hyperplanes $\mathbf{y}_2^\top E \mathbf{y}_1 = 0$ defined by pairs of image points $(\mathbf{y}_1, \mathbf{y}_2)$. For five $(= \dim \mathcal{E})$ such points pairs, there are ten $(= \deg \mathcal{E})$ complex solutions. Each solution E comes from two possible pairs of calibrated cameras (modulo PGL(4)), which shows that the minimal problem of two calibrated cameras observing five points has algebraic degree $20 = 2 \cdot 10$, as claimed in Example 13.8.

The procedure described above (i.e., first reconstructing an essential matrix by intersecting the variety $\mathcal{E}$ with five hyperplanes, then recovering the calibrated cameras, and finally reconstructing the 3D scene using triangulation) is in fact the standard implementation in state-of-the-art reconstruction algorithms. It would be interesting to study the condition number of intersecting the variety $\mathcal{E}$ with five hyperplanes $\mathbf{y}_2^\top E \mathbf{y}_1 = 0$ given by five image point pairs $(\mathbf{y}_1, \mathbf{y}_2)$ and to make use of those condition numbers in homotopy continuation solvers. More generally, the condition number of intersecting the variety $\mathcal{G}_c := \overline{\operatorname{im}(\gamma_c)}$ of Grassmann tensors with $\dim \mathcal{G}_c$ many hyperplanes given by $(L_1, \ldots, L_m)$ in (13.7) has not been studied. The condition number of intersecting a fixed projective variety with varying linear subspaces of complementary dimension has already been investigated in [35]. However, that theory does not immediately apply to the problem of reconstructing essential matrices, since there only *special* linear spaces are allowed (namely, those that are intersections of five hyperplanes of the form $\mathbf{y}_2^\top E \mathbf{y}_1 = 0$).

Chapter 14
Volumes

In this chapter we discuss the problem of computing the volume of a subset X of $\mathbb{R}^n$ that is full-dimensional and semialgebraic. Being *semialgebraic* means that X is described by a finite Boolean combination of polynomial inequalities. We say that X is *basic semialgebraic* if that description is a conjunction of polynomial inequalities. This means that our set admits a representation of the form

$$X \;=\; \bigl\{ \mathbf{x} \in \mathbb{R}^n \,:\, f_1(\mathbf{x}) \,\geq\, 0 \;\text{ and }\; f_2(\mathbf{x}) \,\geq\, 0 \;\text{ and }\; \cdots \;\text{ and }\; f_k(\mathbf{x}) \,\geq\, 0 \bigr\},$$

where $f_1, f_2, \ldots, f_k$ are polynomials in n unknowns with real coefficients. Our task is to compute the volume of X, as reliably and accurately as possible, when the input consists of the polynomials $f_1, f_2, \ldots, f_k$.

14.1 Calculus and Beyond

The simplest scenario arises when $k = 1$, so our semialgebraic set X is the domain of nonnegativity of one polynomial $f(\mathbf{x}) = f(x_1, \ldots, x_n)$ with real coefficients. We wish to evaluate the integral

$$\mathrm{Vol}(X) \;=\; \int_X 1 \cdot d\mathbf{x}, \tag{14.1}$$

where $d\mathbf{x}$ denotes Lebesgue measure on $\mathbb{R}^n$. Of course, it makes perfect sense to also consider integrals $\int_X g(\mathbf{x}) d\mathbf{x}$, where $g(\mathbf{x})$ is some polynomial function. The value of such an integral is a real number which is called a *period* [116]. Our integrals are special cases of *period integrals*.

We begin with an instance where the volume can be computed explicitly using calculus.

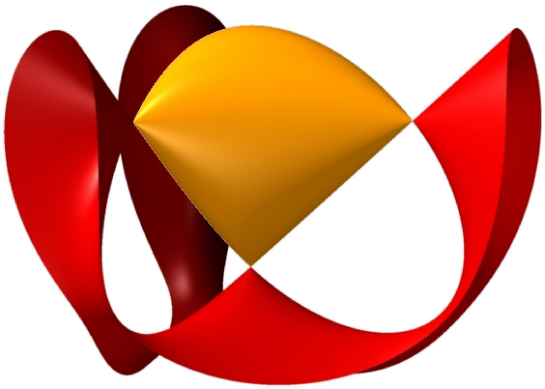

Fig. 14.1: The yellow convex body is the elliptope. It is bounded by Cayley's cubic surface.

Example 14.1 (Elliptope) Consider the set X of all points (x, y, z) in $\mathbb{R}^3$ such that the matrix

$$M \;=\; \begin{pmatrix} 1 & x & y \\ x & 1 & z \\ y & z & 1 \end{pmatrix}$$

is positive semidefinite. The set X is convex and semialgebraic: it consists of all points (x, y, z) in the cube $[-1, 1]^3$ such that $\det(M) \;=\; 2xyz - x^2 - y^2 - z^2 + 1$ is nonnegative. Figure 14.1 appears in [133, Figure 1.1] and it serves as the logo of the Nonlinear Algebra group at the Max-Planck Institute for Mathematics

in the Sciences in Leipzig. It illustrates several applications of algebraic geometry. In statistics, the convex set X is the set of all correlation matrices. In optimization, it is the feasible region of a semidefinite programming problem [133, Chapter 12], and it is known as the *elliptope*.

We now compute the volume of the elliptope. We begin by rewriting of its boundary surface. Solving the equation $\det(M) = 0$ for z with the quadratic formula, we obtain

$$z \;=\; xy \pm \sqrt{x^2y^2 - x^2 - y^2 + 1} \;=\; xy \pm \sqrt{(1-x^2)(1-y^2)} \qquad \text{for } (x,y) \in [-1,1]^2,$$

The plus sign gives the upper yellow surface and the minus sign gives the lower yellow surface. The volume of the elliptope X is obtained by integrating the difference between the upper function and the lower function over the square. Hence the desired volume equals

$$\mathrm{vol}(X) \;=\; \int_{-1}^{1}\int_{-1}^{1} 2\sqrt{(1-x^2)(1-y^2)}\,dxdy \;=\; 2\left[\int_{-1}^{1}\sqrt{1-t^2}\,dt\right]^2.$$

The univariate integral on the right gives the area of a semicircle with radius 1. We know from trigonometry that this area equals $\pi/2$, where $\pi = 3.14159265\ldots$. We conclude that

$$\mathrm{vol}(X) \;=\; \pi^2/2 \;=\; 4.934802202\ldots$$

Thus our elliptope covers about 61.7 % of the volume of the cube $[-1,1]^3$ that surrounds it.

The number $\pi^2/2$ we found is an example of a period. It is generally much more difficult to accurately evaluate such integrals. In fact, this challenge has played an important role in the history of mathematics. Consider the problem of computing the arc length of an ellipse. This requires us to integrate the reciprocal square root of cubic polynomial $f(t)$. Such integrals are called *elliptic integrals*, and they represent periods of elliptic curves. Furthermore, in an 1841 paper, Abel introduced *abelian integrals*, where $g(t)$ is an algebraic function in one variable t. How to evaluate such an integral? This question leads us to Riemann surface and then to their Jacobians. And, voilà, we arrived at the theory of *abelian varieties*.

This chapter presents two current paradigms for accurately computing integrals like (14.1). The first method rests on the theory of D-modules, that is, on the algebraic study of linear differential equations with polynomial coefficients. Our volume is found as a special value of a parametric volume function that is encoded by means of its *Picard-Fuchs differential equation*. This method, which tends to appeal to algebraic geometers, was introduced by Lairez, Mezzarobba and Safey El Din in [117].

The second approach is due to Lasserre and his collaborators [88, 172, 173]. On first glance it might appeal more to analysts and optimizers, but there is also plenty of deep algebraic structure under the hood. The idea is to consider all moments $m_{\mathbf{a}} = \int_X \mathbf{x}^{\mathbf{a}} d\mathbf{x}$ of our semialgebraic set X, where again $d\mathbf{x}$ is Lebesgue measure, and to use relations among these moments to infer an accurate approximation of $m_0 = \mathrm{vol}(X)$. That numerical inference rests on semidefinite programming [133, Chapter 12].

14.2 D-Modules

In calculus, we learn about definite integrals in order to determine the area under a graph. Likewise, in multivariable calculus, we examine the volume enclosed by a surface. We are here interested in areas and volumes of semi-algebraic sets. When these sets depend on one or more parameters, their volumes are holonomic functions of the parameters. We explain what this means and how it can be used for accurate evaluation of volume functions. We present the method of [117], following the exposition given in [160].

Suppose that M is a D-module. The letter D denotes the *Weyl algebra* (cf. [156, 160]), written here as

$$D \;=\; \mathbb{C}\langle x_1, \ldots, x_n, \partial_1, \ldots, \partial_n \rangle.$$

In applications, M is usually a space of infinitely differentiable functions on a subset of $\mathbb{R}^n$ or $\mathbb{C}^n$. Such D-modules are torsion-free. For a function $f \in M$, its *annihilator* is the D-ideal

$$\mathrm{Ann}_D(f) \;:=\; \{\, P \in D \mid P \bullet f = 0 \,\}.$$

In general, it is a non-trivial task to compute this annihilating ideal. But, in some cases, computer algebra systems can help us to compute holonomic annihilating ideals. For rational functions $r \in \mathbb{Q}(x_1, \ldots, x_n)$ this can be done in `Macaulay2` with a built-in command as follows:

```
needsPackage "Dmodules"; D = QQ[x1,x2,d1,d2, WeylAlgebra => {x1=>d1,x2=>d2}];
rnum = x1;  rden = x2;   I = RatAnn(rnum,rden)
```

This code fragment shows that $r = x_1/x_2$ has $\mathrm{Ann}_D(r) = D\{\partial_1^2,\, x_1\partial_1 - 1,\, x_2\partial_1\partial_2 + \partial_1\}$.

Suppose now that $f(x_1, \ldots, x_n)$ is an algebraic function. This means that f satisfies some polynomial equation $F(f, x_1, \ldots, x_n) = 0$. Using the polynomial F as its input, the `Mathematica` package `HolonomicFunctions` can compute a holonomic representation of f. The output is a linear differential operator of lowest degree annihilating f. See Example 14.3.

Let M be a D-module and $f \in M$. We say that f is *holonomic* if, for each $i \in \{1, \ldots, n\}$, there is an operator $P_i \in \mathbb{C}[x_1, \ldots, x_n]\langle \partial_i \rangle \backslash \{0\}$ that annihilates f. If this holds then we say that $\mathrm{Ann}_D(f)$ is a *holonomic D-ideal*. Suppose this is the case, and fix a general point $x_0 \in \mathbb{C}^n$. Let $m_1, \ldots, m_n$ denote the orders of the differential operators $P_1, \ldots, P_n$ in the definition of holonomic. Thus, P_k is an operator in ∂_k of order m_k whose coefficients are polynomials in $x_1, \ldots, x_n$.

We fix initial conditions for f by specifying the following $m_1 m_2 \cdots m_n$ numerical values:

$$(\partial_1^{i_1} \cdots \partial_n^{i_n} \bullet f)|_{x=x_0} \quad \text{where } 0 \le i_k < m_k \text{ for } k = 1, \ldots, n. \tag{14.2}$$

Then the operators $P_1, \ldots, P_n$ together with the initial conditions (14.2) specify the function f.

Many interesting functions are holonomic. To begin with, every rational function r in $\mathbf{x} = (x_1, \ldots, x_n)$ is holonomic, because r is annihilated by $r(\mathbf{x})\partial_i - \partial r/\partial x_i$ for $i = 1, 2, \ldots, n$. By clearing denominators in this operator, we obtain a non-zero $P_i \in \mathbb{C}[\mathbf{x}]\langle \partial_i \rangle$ with $m_i = 1$ that annihilates r. See the `Macaulay2` example above. These operators, together with fixing the value $r(\mathbf{x}_0)$ at a general point $\mathbf{x}_0 \in \mathbb{C}^n$, constitute a canonical holonomic representation of the rational function r.

Holonomic functions in one variable are solutions to ordinary linear differential equations with rational function coefficients. Examples include algebraic functions, some elementary trigonometric functions, hypergeometric functions, Bessel functions, period integrals, and many more. But, not every nice function is holonomic. A necessary condition for a meromorphic function $f(x)$ to be holonomic is that it has only finitely many poles in $\mathbb{C}$. For a concrete example, we start with the holonomic function $\sin(x)$. This is annihilated by the operator $\partial^2 + 1$. Its reciprocal $f(x) = \frac{1}{\sin(x)}$ has infinitely many poles, so is not holonomic. Hence the class of holonomic functions is not closed under division. It is also not closed under composition of functions, since both $\frac{1}{x}$ and $\sin(x)$ are holonomic. We record the following fact:

Proposition 14.2 *Let $f(\mathbf{x})$ be holonomic and $g(\mathbf{x})$ algebraic. Then $f(g(\mathbf{x}))$ is holonomic.*

For the proof see [160, Proposition 2.3]. The term "holonomic function" is due to Zeilberger [182]. Koutschan [115] developed practical algorithms for manipulating holonomic functions. These are implemented in his `Mathematica` package `HolonomicFunctions`, as seen below.

Example 14.3 Every algebraic function $f(\mathbf{x})$ in n variables is holonomic. Let $n = 2$ and consider the function $y = f(x)$ that is defined by $y^4 + x^4 + \frac{xy}{100} - 1 = 0$. Its annihilator in D can be computed as follows:

```
<< RISC‘HolonomicFunctions‘
q = y^4 + x^4 + x*y/100 - 1
ann = Annihilator[Root[q, y, 1], Der[x]]
```

This `Mathematica` code determines an operator P of lowest order in $\mathrm{ann}_D(f)$. We find

$$\begin{aligned} P \;=\; & (2x^4+1)^2(25600000000x^{12}-76800000000x^8+76799999973x^4-25600000000)\,\partial^3 \\ & +6x^3(2x^4+1)(51200000000x^{12}+76800000000x^8-307199999946x^4+179199999973)\,\partial^2 \\ & +3x^2(102400000000x^{16}+204800000000x^{12}+2892799999572x^8-3507199999444x^4+307199999953)\,\partial \\ & -3x(102400000000x^{16}+204800000000x^{12}+1459199999796x^8-1049599999828x^4+51199999993). \end{aligned}$$

This operator is an encoding of the algebraic function $y = f(x)$ as a holonomic function.

In computer algebra, one represents a real algebraic number as a root of a polynomial with coefficients in $\mathbb{Q}$. However, this *minimal polynomial* does not specify the number uniquely. For that, one also needs an isolating interval or sign conditions on derivatives. The situation is analogous for encoding a holonomic function f in n variables. We specify f by a holonomic system of linear PDEs together with a list of initial conditions. The canonical holonomic representation is one possibility. Initial conditions such as (14.2) are designed to determine the function uniquely inside the linear space $\mathrm{Sol}(I)$, where $I \subseteq \mathrm{Ann}_D(f)$.

For instance, in Example 14.3, we would need three initial conditions to specify the function $f(\mathbf{x})$ uniquely inside the 3-dimensional solution space to our operator P. We could fix the values at three distinct points, or we could fix the value and the first two derivatives at one special point.

To be more precise, we generalize the canonical representation (14.2) as follows. A *holonomic representation* of a function f is a holonomic D-ideal $I \subseteq \mathrm{ann}_D(f)$ together with a list of linear conditions that specify p uniquely inside the finite-dimensional solution space of holomorphic solutions. The existence of this representation makes f a *holonomic function*. The next example is meant to show the relevance of holonomic functions for metric algebraic geometry.

Example 14.4 (The area of a TV screen) Fix the quartic polynomial

$$q(x,y) \;=\; x^4+y^4+\frac{1}{100}xy-1. \tag{14.3}$$

We are interested in the semi-algebraic set $S = \{(x,y) \in \mathbb{R}^2 \mid q(x,y) \le 0\}$. This convex set is a slight modification of a set known in the optimization literature as "the TV screen". Our aim is to compute the area of the semi-algebraic convex set S as accurately as is possible.

One can get a rough idea of the area of S by sampling. This is illustrated in Figure 14.2. From the polynomial $q(x,y)$ we read off that S is contained in the square defined by $-1.2 \le x, y \le 1.2$. We sampled 10000 points uniformly from that square, and for each sample we checked the sign of q. Points inside S are drawn in blue and points outside S are drawn in pink. By multiplying the area $(2.4)^2 = 5.76$ of the square with the fraction of the number of blue points among the samples, we learn that the area of the TV screen is approximately 3.7077.

We now compute the area more accurately using D-modules. Let $\mathrm{pr}\colon S \to \mathbb{R}$ be the projection on the x-coordinate, and write $v(x) = \ell\left(\mathrm{pr}^{-1}(x) \cap S\right)$ for the length of a fiber. This function is holonomic and it satisfies the third-order differential operator in Example 14.3.

The map pr has two branch points $x_0 < x_1$. They are the real roots of the resultant

$$\mathrm{Res}_y(q, \partial q/\partial y) \;=\; 256000000000x^{12}-76800000000x^8+76799999973x^4-25600000000. \tag{14.4}$$

These values can be written in radicals, but we take an accurate floating point representation:

$$x_1 \;=\; -x_0 \;=\; 1.000254465850258845478545766643566750080196276158976351763236\ldots$$

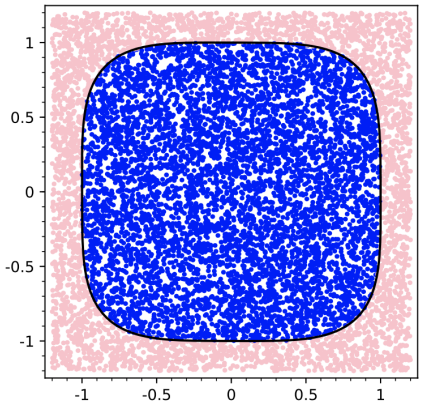

Fig. 14.2: The TV screen is the convex region consisting of the blue points.

The desired area equals $\mathrm{vol}(S) = w(x_1)$, where w is the holonomic function

$$w(x) \;=\; \int_{x_0}^{x} v(t)dt.$$

One operator that annihilates w is $P\partial$, where $P \in \mathrm{ann}_D(v)$ is the third-order operator above. To get a holonomic representation of w, we also need some initial conditions. Clearly, $w(x_0) = 0$. Further initial conditions on w' are derived by evaluating v at other points. By plugging values for x into (14.3) and solving for y, we find $w'(0) = 2$ and $w'(\pm 1) = 1/\sqrt[3]{100}$. Thus, we now have four linear constraints on our function w, albeit at different points.

Our goal is to determine a unique function $w \in \mathrm{Sol}(P\partial)$ by incorporating these four initial conditions, and then to evaluate w at x_1. To this end, we proceed as follows. Let $x_{\mathrm{ord}} \in \mathbb{R}$ be any point at which $P\partial$ is not singular. Using the command `local_basis_expansion` that is built into the `SAGE` package `ore_algebra`, we compute a basis of local series solutions to $P\partial$ at the point x_{ord}. Since that point is non-singular, that basis has the following form:

$$\begin{aligned}
s_{x_{\mathrm{ord}},0}(x) &= \quad 1 \quad + O((x-x_{\mathrm{ord}})^4),\\
s_{x_{\mathrm{ord}},1}(x) &= (x-x_{\mathrm{ord}}) + O((x-x_{\mathrm{ord}})^4),\\
s_{x_{\mathrm{ord}},2}(x) &= (x-x_{\mathrm{ord}})^2 + O((x-x_{\mathrm{ord}})^4),\\
s_{x_{\mathrm{ord}},3}(x) &= (x-x_{\mathrm{ord}})^3 + O((x-x_{\mathrm{ord}})^4).
\end{aligned} \tag{14.5}$$

Locally at x_{ord}, our solution is given by a unique choice of four coefficients $c_{x_{\mathrm{ord}},i}$, namely

$$w(x) \;=\; c_{x_{\mathrm{ord}},0} \cdot s_{x_{\mathrm{ord}},0}(x) \,+\, c_{x_{\mathrm{ord}},1} \cdot s_{x_{\mathrm{ord}},1}(x) \,+\, c_{x_{\mathrm{ord}},2} \cdot s_{x_{\mathrm{ord}},2}(x) \,+\, c_{x_{\mathrm{ord}},3} \cdot s_{x_{\mathrm{ord}},3}(x).$$

At a regular singular point x_{rs}, complex powers of x and $\log(x)$ can appear in the local basis at x_{rs}. Any initial condition at that point determines a linear constraint on these coefficients. For instance, $w'(0) = 2$ implies $c_{0,1} = 2$, and similarly for our initial conditions at $-1, 1$ and x_0. One challenge is that the initial conditions pertain to different points. To address this, we calculate transition matrices that relate the basis (14.5) of series solutions at one point to the basis at another point. These are invertible 4×4 matrices.

With the method described above, we find the basis of series solutions at x_1, along with a system of four linear constraints on the four coefficients $c_{x_1,i}$. These constraints are derived from the initial conditions at 0, ± 1 and x_0, using the 4×4 transition matrices. By solving these linear equations, we compute the

desired function value up to any desired precision:

$$w(x_1) \;=\; 3.708159944742162288348225561145865371243065819913934709438572....$$

In conclusion, this number is the area of the TV screen S defined by the polynomial $q(x, y)$.

Before computing an example in 3-space, let us first come back to properties of holonomic functions. Holonomic functions are very well-behaved with respect to many operations. They turn out to have remarkable closure properties. In the following, let f and g be functions in n variables $\mathbf{x} = (x_1, \ldots, x_n)$.

Proposition 14.5 *If f, g are holonomic functions, then both $f + g$ and $f \cdot g$ are holonomic.*

Proof For each index $i \in \{1, 2, \ldots, n\}$, there exist non-zero operators P_i and Q_i in $\mathbb{C}[\mathbf{x}]\langle\partial_i\rangle$ which satisfy $P_i \bullet f = Q_i \bullet g = 0$. Set $n_i = \text{order}(P_i)$ and $m_i = \text{order}(Q_i)$. The $\mathbb{C}(\mathbf{x})$-linear span of the set $\{\partial_i^k \bullet f\}_{k=0,\ldots,n_i}$ has dimension $\leq n_i$. Similarly, the span of the set $\{\partial_i^k \bullet g\}_{k=0,\ldots,m_i}$ has dimension $\leq m_i$.

Now consider $\partial_i^k \bullet (f + g) = \partial_i^k \bullet f + \partial_i^k \bullet g$. The $\mathbb{C}(\mathbf{x})$-linear span of $\{\partial_i^k \bullet (f + g)\}_{k=0,\ldots,n_i+m_i}$ has dimension $\leq n_i + m_i$. Hence, there exists a non-zero operator $S_i \in \mathbb{C}[\mathbf{x}]\langle\partial_i\rangle$, such that $S_i \bullet (f + g) = 0$. Since this holds for all indices i, we conclude that the sum $f + g$ is holonomic.

A similar proof works for the product $f \cdot g$. For each $i \in \{1, 2, \ldots, n\}$, we now consider the set $\{\partial_i^k \bullet (f \cdot g)\}_{k=0,1,\ldots,n_i m_i}$. By applying Leibniz' rule for taking derivatives of a product, we find that the $m_i n_i + 1$ generators are linear dependent over the rational function field $\mathbb{C}(\mathbf{x})$. Hence, there is a non-zero operator $T_i \in \mathbb{C}[\mathbf{x}]\langle\partial_i\rangle$ such that $T_i \bullet (f \cdot g) = 0$. We conclude that the product $f \cdot g$ is holonomic. □

The proof above gives a linear algebra method for computing an annihilating D-ideal I of finite holonomic rank for $f + g$ (resp. of $f \cdot g$), starting from such D-ideals for f and g. The following example, similar to one in [182, Section 4.1], illustrates Proposition 14.5.

Example 14.6 ($n = 1$) Consider the functions $f(x) = \exp(x)$ and $g(x) = \exp(-x^2)$. Their canonical holonomic representations are $I_f = \langle\partial - 1\rangle$ with $f(0) = 1$ and $I_g = \langle\partial + 2x\rangle$ with $g(0) = 1$. We are interested in the function $h = f + g$. Its first partial derivatives are

$$\begin{pmatrix} h \\ \partial \bullet h \\ \partial^2 \bullet h \end{pmatrix} \;=\; \begin{pmatrix} 1 & 1 \\ 1 & -2x \\ 1 & 4x^2 - 2 \end{pmatrix} \cdot \begin{pmatrix} f \\ g \end{pmatrix}.$$

By computing the left kernel of this 3×2-matrix, we find that $h = f + g$ is annihilated by

$$I_h \;=\; \langle (2x + 1)\partial^2 + (4x^2 - 3)\partial - 4x^2 - 2x + 2\rangle, \quad \text{with } h(0) = 2,\ h'(0) = 1.$$

For the product $j = f \cdot g$ we have $j' = f'g + fg' = f \cdot g + f \cdot (-2xg) = (1 - 2x)j$, so the canonical holonomic representation of j is the D-ideal $I_j = \langle\partial + 2x - 1\rangle$ with $j(0) = 1$.

Proposition 14.7 *Let f be holonomic in n variables and $m < n$. Then the restriction of f to the coordinate subspace $\{x_{m+1} = \ldots = x_n = 0\}$ is a holonomic function in the first m variables $x_1, \ldots, x_m$.*

Proof For $i \in \{m + 1, \ldots, n\}$, we consider the right ideal $x_i D$ in the Weyl algebra D. This ideal is a left module over $D_m = \mathbb{C}\langle x_1, \ldots, x_m, \partial_1, \ldots, \partial_m\rangle$. The sum of these ideals with $\text{Ann}_D(f)$ is hence a left D_m-module. Its intersection with D_m is called the *restriction ideal*:

$$(\text{Ann}_D(f) + x_{m+1}D + \cdots + x_n D) \;\cap\; D_m. \tag{14.6}$$

By [156, Prop. 5.2.4], this D_m-ideal is holonomic and it annihilates $f(x_1, \ldots, x_m, 0, \ldots, 0)$. □

Proposition 14.8 *The partial derivatives of a holonomic function are holonomic functions.*

Proof Let f be holonomic and $P_i \in \mathbb{C}[x]\langle\partial_i\rangle\backslash\{0\}$ with $P_i \bullet f = 0$ for all i. We can write P_i as $P_i = \widetilde{P}_i\partial_i + a_i(x)$, where $a_i \in \mathbb{C}[x]$. If $a_i = 0$, then $\widetilde{P}_i \bullet \frac{\partial f}{\partial x_i} = 0$ and we are done. Assume $a_i \neq 0$. Since both a_i and f are holonomic, by Proposition 14.5, there is a non-zero linear operator $Q_i \in \mathbb{C}[x]\langle\partial_i\rangle$ such that $Q_i \bullet (a_i \cdot f) = 0$. Then $Q_i\widetilde{P}_i$ annihilates $\partial f/\partial x_i$. □

A key insight from the theory of D-modules (see [156, Section 5.5]) is that integration is dual, in the sense of the Fourier transform, to restriction. Here is the dual to Proposition 14.7.

Proposition 14.9 *Let $f\colon \mathbb{R}^n \to \mathbb{C}$ be a holonomic function. Then the definite integral*

$$F(x_1,\ldots,x_{n-1}) \;=\; \int_a^b f(x_1,\ldots,x_{n-1},x_n)dx_n$$

is a holonomic function in $n-1$ variables, assuming the integral converges.

By dualizing (14.6), we obtain the following D_m-ideal, known as the *integration ideal*:

$$\big(\mathrm{Ann}_D(f) \;+\; \partial_{m+1}D + \cdots + \partial_n D\big) \cap D_m \qquad \text{for } m < n.$$

The expression is dual to the restriction ideal (14.6) under the Fourier transform. This exchanges x_i and ∂_i. If $m = n-1$ then the integration ideal annihilates the holonomic function F above.

Equipped with our tools for holonomic functions, we now return to computing volumes of compact semi-algebraic sets. We follow the work of Lairez, Mezzarobba and Safey El Din in [117]. They compute this volume by deriving a differential operator that encodes the period of a certain integral [116]. Here is the definition. Let $R(t,x_1,\ldots,x_n)$ be a rational function and consider the formal period integral

$$\oint R(t,x_1,\ldots,x_n)dx_1\cdots dx_n. \tag{14.7}$$

Fix an open subset Ω of either $\mathbb{R}$ or $\mathbb{C}$. An analytic function $\phi\colon \Omega \to \mathbb{C}$ is a *period* of the integral (14.7) if, for any $s \in \Omega$, there exists a neighborhood $\Omega' \subseteq \Omega$ of s and an n-cycle $\gamma \subset \mathbb{C}^n$ with the following property. For all $t \in \Omega'$, γ is disjoint from the poles of $R_t := R(t,\bullet)$ and

$$\phi(t) \;=\; \int_\gamma R(t,x_1,\ldots,x_n)dx_1\cdots dx_n. \tag{14.8}$$

If this holds, then there exists an operator $P \in D\backslash\{0\}$ of the Fuchsian class annihilating $\phi(t)$.

Let $S = \{f \leq 0\} \subset \mathbb{R}^n$ be a compact basic semi-algebraic set, defined by a polynomial $f \in \mathbb{Q}[x_1,\ldots,x_n]$. Let $\mathrm{pr}\colon \mathbb{R}^n \to \mathbb{R}$ denote the projection on the first coordinate. The set of *branch points* of pr is the following subset of the real line, which is assumed to be finite:

$$\Sigma_f \;=\; \Big\{p \in \mathbb{R} \mid \exists\, x = (x_2,\ldots,x_n) \in \mathbb{R}^{n-1} : f(p,x) = 0 \text{ and } \tfrac{\partial f}{\partial x_i}(p,x) = 0 \text{ for } i = 2,\ldots,n\Big\}.$$

The polynomial in the unknown p that defines Σ_f is obtained by eliminating $x_2,\ldots,x_n$. It can be represented as a multivariate resultant, generalizing the Sylvester resultant in (14.4).

Fix an open interval I in $\mathbb{R}$ with $I \cap \Sigma_f = \emptyset$. For any $x_1 \in I$, the set $S_{x_1} := \mathrm{pr}^{-1}(x_1) \cap S$ is compact and semi-algebraic in $(n-1)$-space. We are interested in its volume. By [117, Theorem 9], the function $v\colon I \to \mathbb{R}$, $x_1 \mapsto \mathrm{vol}_{n-1}\left(S_{x_1}\right)$ is a period of the rational integral

$$\frac{1}{2\pi i}\oint \frac{x_2}{f(x_1,x_2,\ldots,x_n)}\frac{\partial f(x_1,x_2,\ldots,x_n)}{\partial x_2}dx_2\cdots dx_n. \tag{14.9}$$

Let $e_1 < e_2 < \cdots < e_K$ be the branch points in Σ_f and set $e_0 = -\infty$ and $e_{K+1} = \infty$. This specifies the pairwise disjoint open intervals $I_k = (e_k, e_{k+1})$. They satisfy $\mathbb{R}\backslash\Sigma_f = \bigcup_{k=0}^{K} I_k$. Fix the holonomic functions $w_k(t) = \int_{e_k}^{t} v(x_1)dx_1$. The volume of S then is obtained as

$$\mathrm{vol}_n\,(S) \;=\; \int_{e_1}^{e_K} v(x_1)dx_1 \;=\; \sum_{k=1}^{K-1} w_k\,(e_{k+1})\,.$$

How does one compute such an expression? As a period of the rational integral (14.9), the volume v is a holonomic function on each interval I_k. A key step is to find an operator $P \in D_1$ that annihilates $v|_{I_k}$ for all k. Then the product $P\partial$ annihilates the functions $w_k(x_1)$ for all k. By imposing sufficiently many initial conditions, we can reconstruct the functions w_k from the operator $P\partial$. One initial condition that comes for free for each k is $w_k(e_k) = 0$.

The differential operator P is known as the *Picard–Fuchs equation* of the period in question. The following software packages can be used to compute such Picard–Fuchs equations:

- `HolonomicFunctions` by C. Koutschan in `Mathematica`,
- `ore_algebra` by M. Kauers in `SAGE`,
- `periods` by P. Lairez in `MAGMA`,
- `Ore_Algebra` by F. Chyzak in `Maple`.

We now apply this to compute volumes. Starting from the polynomial f, we compute the Picard–Fuchs operator $P \in D_1$ along with sufficiently many compatible initial conditions. For each interval I_k, where $k = 1, \ldots, K-1$, we perform the following steps, here described for the `ore_algebra` package in `SAGE`:

1. Using the command `local_basis_expansion`, compute a local basis of series solutions for the linear differential operator $P\partial$ at various points in $[e_k, e_{k+1})$.
2. Using the command `op.numerical_transition_matrix`, numerically compute a transition matrix for the series solution basis from one point to another one.
3. From the initial conditions construct linear relations between the coefficients in the local basis extensions. Using step (ii), transfer them to the branch point e_{k+1}.
4. Plug in to the local basis extension at e_{k+1} and thus evaluate the volume of $S \cap \mathrm{pr}^{-1}\,(I_k)$.

We illustrate this recipe by computing the volume of a convex body in 3-space, shown in Figure 14.3.

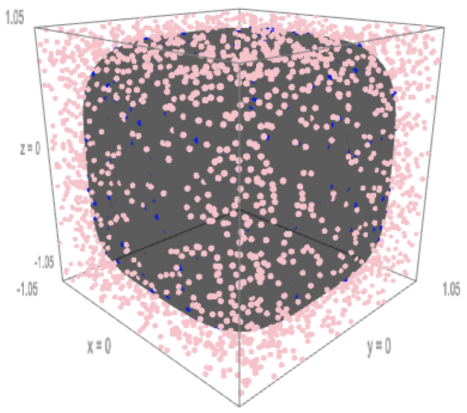

Fig. 14.3: The quartic bounds the convex region consisting of the gray points.

Example 14.10 (Quartic surface) Fix the quartic polynomial

$$f(x,y,z) \;=\; x^4+y^4+z^4+\frac{x^3y}{20}-\frac{xyz}{20}-\frac{yz}{100}+\frac{z^2}{50}-1, \tag{14.10}$$

and consider the set $S=\{(x,y,z)\in\mathbb{R}^3 \mid f(x,y,z)\le 0\}$. Our aim is to compute $\mathrm{vol}_3(S)$.

As in Example 14.4 with the TV screen, we can get a rough idea of the volume of S by sampling. This is illustrated in Figure 14.3. Our set S is compact, convex, and contained in the cube defined by $-1.05\le x,y,z\le 1.05$. We sampled 10000 points uniformly from that cube. For each sample we checked the sign of $f(x,y,z)$. By multiplying the volume $(2.1)^3=9.261$ of the cube by the fraction of the number of gray points and the number of sampled points, `SAGE` found within few seconds that $\mathrm{vol}(S)\approx 6.4771$. In order to obtain a higher precision, we now compute the volume of our set S with help of D-modules.

Let $\mathrm{pr}\colon\mathbb{R}^3\to\mathbb{R}$ be the projection onto the x-coordinate. Let $v(x)=\mathrm{vol}_2\left(\mathrm{pr}^{-1}(x)\cap S\right)$ denote the area of the fiber over any point x in $\mathbb{R}$. We write $e_1<e_2$ for the two branch points of the map pr restricted to the quartic surface $\{f=0\}$. They can be computed with resultants. The projection has 36 complex branch points. The first two of them are real and therefore are the branch points of pr. We obtain $e_1\approx -1.0023512$ and $e_2\approx 1.0024985$. By [117, Theorem 9], the area function $v(x)$ is a period of the rational integral

$$\frac{1}{2\pi i}\oint \frac{y}{f(x,y,z)}\frac{\partial f(x,y,z)}{\partial y}dydz.$$

We set $w(t)=\int_{e_1}^{t} v(x)dx$. The desired 3-dimensional volume equals $\mathrm{vol}_3(S)=w(e_2)$.

Using Lairez' implementation `periods` in `MAGMA`, we compute a differential operator P of order eight that annihilates $v(x)$. Again, $P\partial$ then annihilates $w(x)$. One initial condition is $w(e_1)=0$. We obtain eight further initial conditions $w'(x)=\mathrm{vol}_2(S_x)$ for points $x\in(e_1,e_2)$ by running the same algorithm for the 2-dimensional semi-algebraic slices $S_x=\mathrm{pr}^{-1}(x)\cap S$. In other words, we make eight subroutine calls to an area measurement as in Example 14.4. From these nine initial conditions we derive linear relations of the coefficients in the local basis expansion at e_2. These computations are run in `SAGE` as described in steps (i), (ii), (iii) and (iv) above. We find the approximate volume of our convex body S to be

$$\begin{aligned}\approx\ & 6.43883248057289354474073389596995618895842088923511697626632892312882691552738876421620914955839890382943113760889345269035255600976010241711908047694055348265581142127661353806139597579353052710220894191557015215864701708740021943845291406868562277595417150971133991347340596176328922060720855163323979691633837600707387601073182477520615047143672504609009234090663777322733903968222962352149636232866131175579306875441483607212256810534811787600582647388671058103268189115784483237585367671687074425321460297537625942615789204778597.\end{aligned}$$

This numerical value is guaranteed to be accurate up to 550 digits.

14.3 Lasserre's Method

In this section we present the second method for computing volumes, based on semidefinite programming. This was developed by Lasserre and his collaborators. See [88, 172, 173] and references therein. We consider an inclusion of semialgebraic sets $K\subset B\subset\mathbb{R}^n$, where K and B are compact. Here B is a set that serves as a bounding box, like $B=[-1,1]^n$. We assume that the moments of Lebesgue measure on B are known or easy-to-compute. In other words, we assume that we have access to the values of the integrals

$$\beta_{\mathbf{u}} \;=\; \int_B \mathbf{x}^{\mathbf{u}} d\mathbf{x} \;=\; \int_B x_1^{u_1} x_2^{u_2} \cdots x_n^{u_n}\, dx_1 dx_2 \cdots dx_n \qquad \text{for } \mathbf{u} \in \mathbb{N}^n.$$

The moments $m_{\mathbf{u}}$ of Lebesgue measure on K are unknown. These will be our decision variables:

$$m_u \;=\; \int_K \mathbf{x}^u dx \;=\; \int_K x_1^{u_1} x_2^{u_2} \cdots x_n^{u_n}\, dx_1 dx_2 \cdots dx_n \qquad \text{for } u \in \mathbb{N}^n. \tag{14.11}$$

Our aim is to compute $m_0 = \mathrm{vol}(K)$. The idea is to use the following infinite-dimensional linear program: *Maximize the integral $\int d\mu$, where μ and $\hat{\mu}$ range over measures on $\mathbb{R}^n$, where μ is supported on K, $\hat{\mu}$ is supported on B, and the sum $\mu + \hat{\mu}$ is Lebesgue measure on B.*

The unique optimal solution $(\mu, \hat{\mu})$ to this linear program can be characterized as follows: μ^* is Lebesgue measure on K, $\hat{\mu}^*$ is Lebesgue measure on $B \backslash K$, and the optimal value is $\mathrm{vol}(K) = \int d\mu^*$. This is described in [173, equation (1)]. The linear programming (LP) dual is given in [173, equation (2)].

We can express our linear program in terms of the moment sequences $\mathbf{m} = (m_{\mathbf{u}})$ and $\hat{\mathbf{m}} = (\hat{m}_{\mathbf{u}})$ of the two unknown measures μ and $\hat{\mu}$. Namely, we paraphrase: *Maximize m_0 subject to $m_{\mathbf{u}} + \hat{m}_{\mathbf{u}} = \beta_u$ for all $\mathbf{u} \in \mathbb{N}^d$, where $\mathbf{m}$ and $\hat{\mathbf{m}}$ are valid moment sequences of measures on $\mathbb{R}^n$, with m supported on K.* This brings us to the moment problem, which is the question how to characterize valid moment sequences. This is problem with a long history in mathematics, and an exact characterization is very difficult. However, in recent years, it has been realized that there are effective necessary conditions. These involve semidefinite programming formulations in finite dimensions, which are built via the *localizing matrices* we now define.

Let $K = \{\mathbf{x} \in \mathbb{R}^n \,:\, f(\mathbf{x}) \geq 0\}$ be defined by a single polynomial $f = \sum_{\mathbf{w}} c_{\mathbf{w}} \mathbf{x}^{\mathbf{w}}$ in n variables. Fix an integer d that exceeds the degree of f. We shall construct three symmetric matrices of format $\binom{n+d}{d} \times \binom{n+d}{d}$ whose entries are linear in the decision variables. The rows and columns of our matrices are indexed by elements $\mathbf{u} \in \mathbb{N}^n$ with $|\mathbf{u}| = u_1 + \cdots + u_n$ at most d. These correspond to monomials $\mathbf{x}^{\mathbf{u}}$ of degree $\leq d$.

Our first matrix $M_d(\mathbf{m})$ has the entry $m_{\mathbf{u}+\mathbf{v}}$ in row $\mathbf{u}$ and column $\mathbf{v}$. Our second matrix $M_d(\hat{\mathbf{m}})$ has the entry $\hat{m}_{\mathbf{u}+v}$ in row $\mathbf{u}$ and column $\mathbf{v}$. And, finally, our third matrix $M_d(f\mathbf{m})$ has the entry $\sum_{\mathbf{w}} c_{\mathbf{w}} m_{\mathbf{u}+\mathbf{v}+\mathbf{w}}$ in row $\mathbf{u}$ and column $\mathbf{v}$. We consider the following semidefinite program:

$$\begin{array}{c} \text{Maximize } \; m_0 \; \text{ subject to } \; m_u + \hat{m}_u = \beta_u \;\; \text{ for all } u \in \mathbb{N}^d \text{ with } |u| \leq d, \text{ where} \\ \text{the symmetric matrices } M_d(m), M_d(\hat{m}) \;\text{ and }\; M_d(f\mathbf{m}) \text{ are positive semidefinite.} \end{array} \tag{14.12}$$

Here, the third matrix is usually replaced by $M_{d'}(f\mathbf{m})$ where $d' = d - \lceil \deg(f)/2 \rceil$. The objective function value depends on d, and it decreases as d increases. The limit for $d \longrightarrow \infty$ is equal to the volume of X. Indeed, this sequence of SDP problems is an approximation to the infinite-dimensional linear programming problem above. The convergence property was proved in [88].

The remainder of this section will demonstrate how one can solve (14.12) in practice. It is based on [88, 172, 173], and we discuss an implementation in `Mathematica`. This material was developed by Chiara Meroni, and we are very grateful to her for allowing us to include it in these lecture notes.

Our point of departure is the following question: given a sequence of real numbers $\mathbf{m} = (m_\alpha)_\alpha$, does there exist a set S and a measure μ_S supported on S such that (14.11) holds? Given $d \in \mathbb{N}$, denote by $\mathbb{N}^n_d$ the set of multiindices $\alpha \in \mathbb{N}^n$ such that $|\alpha| = \alpha_1 + \ldots + \alpha_n \leq d$. Fix a semialgebraic set K as above, let $r = \lceil \frac{\deg f}{2} \rceil$, and consider an arbitrary sequence of real numbers $\mathbf{m} = (m_\alpha)_\alpha$ that is indexed by $\mathbb{N}^n$.

The *moment matrix* and the *localizing matrix* associated with this sequence are respectively

$$M_d(\mathbf{m}) = \Big(m_{\alpha+\beta}\Big)_{\alpha,\beta \in \mathbb{N}^n_d}, \qquad M_{d-r}(f\mathbf{m}) = \Big(\sum_{w \in W} c_w m_{w+\alpha+\beta}\Big)_{\alpha,\beta \in \mathbb{N}^n_{d-r}}. \tag{14.13}$$

The moment matrix has size $\binom{n+d}{d} \times \binom{n+d}{d}$ whereas the localizing matrix has size $\binom{n+d-r}{d-r} \times \binom{n+d-r}{d-r}$. A necessary condition for a sequence $\mathbf{m} = (m_\alpha)_\alpha$ to have a representing measure supported on K is that for

every $d \in \mathbb{N}$ the matrix inequalities $M_d(\mathbf{m}) \succcurlyeq 0$ and $M_{d-r}(f\mathbf{m}) \succcurlyeq 0$ hold. This result is a formulation of Putinar's Positivstellensatz [88, Theorem 2.2]. In particular, the positive definiteness of the moment matrix is a necessary condition for $\mathbf{m}$ to have a representing measure; the inequality with the localizing matrix forces the support of the representing measure to be contained in the superlevel set $\{f(\mathbf{x}) \geq 0\}$, namely K.

Example 14.11 As a sanity check, consider the disc $K = \{(x, y) \in \mathbb{R}^2 \mid f = 1 - x^2 - y^2 \geq 0\}$. Its moments are

$$m_{(\alpha_1,\alpha_2)} = \left((-1)^{\alpha_1} + 1\right)\left((-1)^{\alpha_2} + 1\right) \frac{\Gamma\left(\frac{\alpha_1+1}{2}\right)\Gamma\left(\frac{\alpha_2+1}{2}\right)}{4\Gamma\left(\frac{1}{2}(\alpha_1+\alpha_2+4)\right)},$$

where Γ denotes the usual Gamma function. For $d = 3$, the moment and localizing matrices in (14.13) are

$$M_3(\mathbf{m}) = \begin{pmatrix}
\pi & 0 & \frac{\pi}{4} & 0 & 0 & 0 & 0 & \frac{\pi}{4} & 0 & 0 \\
0 & \frac{\pi}{4} & 0 & \frac{\pi}{8} & 0 & 0 & 0 & 0 & \frac{\pi}{24} & 0 \\
\frac{\pi}{4} & 0 & \frac{\pi}{8} & 0 & 0 & 0 & 0 & \frac{\pi}{24} & 0 & 0 \\
0 & \frac{\pi}{8} & 0 & \frac{5\pi}{64} & 0 & 0 & 0 & 0 & \frac{\pi}{64} & 0 \\
0 & 0 & 0 & 0 & \frac{\pi}{4} & 0 & \frac{\pi}{24} & 0 & 0 & \frac{\pi}{8} \\
0 & 0 & 0 & 0 & 0 & \frac{\pi}{24} & 0 & 0 & 0 & 0 \\
0 & 0 & 0 & 0 & \frac{\pi}{24} & 0 & \frac{\pi}{64} & 0 & 0 & \frac{\pi}{64} \\
\frac{\pi}{4} & 0 & \frac{\pi}{24} & 0 & 0 & 0 & 0 & \frac{\pi}{8} & 0 & 0 \\
0 & \frac{\pi}{24} & 0 & \frac{\pi}{64} & 0 & 0 & 0 & 0 & \frac{\pi}{64} & 0 \\
0 & 0 & 0 & 0 & \frac{\pi}{8} & 0 & \frac{\pi}{64} & 0 & 0 & \frac{5\pi}{64}
\end{pmatrix}, \quad M_2(f\mathbf{m}) = \begin{pmatrix}
\frac{\pi}{2} & 0 & \frac{\pi}{12} & 0 & 0 & \frac{\pi}{12} \\
0 & \frac{\pi}{12} & 0 & 0 & 0 & 0 \\
\frac{\pi}{12} & 0 & \frac{\pi}{32} & 0 & 0 & \frac{\pi}{96} \\
0 & 0 & 0 & \frac{\pi}{12} & 0 & 0 \\
0 & 0 & 0 & 0 & \frac{\pi}{96} & 0 \\
\frac{\pi}{12} & 0 & \frac{\pi}{96} & 0 & 0 & \frac{\pi}{32}
\end{pmatrix},$$

These two matrices are symmetric and positive definite.

We consider the infinite-dimensional *linear program* on measures whose optimal value is the volume of $K \subset B$. The program was stated above. We use the formulation in [88, Equation 3.1] and [173, Equation 1]:

$$\begin{aligned} P: \qquad & \max_{\mu_K, \mu_{B\setminus K}} \int d\mu_K \\ & \text{s.t. } \mu_K + \mu_{B\setminus K} = \mu_B^*. \end{aligned} \tag{14.14}$$

Here μ_S is a positive finite Borel measure supported on S, and μ_B^* is the Lebesgue measure on B. The adjective "infinite-dimensional" refers to the fact that we are optimizing over a set of measures, which is uncountable. Based on the theory of dual Banach spaces, one can talk about dual convex bodies, and construct a duality theory for LP. In our case, the dual to the space of positive finite Borel measures is the set of positive continuous functions. This observation leads to the definition of an LP dual to P:

$$\begin{aligned} P^*: \qquad & \inf_{\gamma} \int \gamma \, d\mu_B^* \\ & \text{s.t. } \gamma \geq \mathbf{1}_K, \end{aligned} \tag{14.15}$$

where γ is a positive continuous function on B and $\mathbf{1}_K$ is the indicator function of K. There is no duality gap between P and P^*, i.e. the optimal values of (14.14) and (14.15) coincide. Note that the optimal value of P^* is an infimum and not a minimum, since we are approximating the *discontinuous* indicator function $\mathbf{1}_K$ using continuous functions. This detail explains the slow rate of approximation of the basic method.

The infinite-dimensional LP can be approximated by a hierarchy of finite-dimensional *semidefinite programs* [118]. The optimal values of the hierarchy converge monotonically to the optimal value of the LP [88, Theorem 3.2]. There is again a primal and dual version of the SDP. In our setting, the primal is

$$P_d: \quad \max_{\mathbf{m},\widehat{\mathbf{m}}} \ m_{\mathbf{0}} \quad \text{s.t. } \mathbf{m}+\widehat{\mathbf{m}}=\mathbf{b},\ M_d(\mathbf{m}) \succcurlyeq 0,\ M_d(\widehat{\mathbf{m}}) \succcurlyeq 0,\ M_{d-r}(f\mathbf{m}) \succcurlyeq 0. \tag{14.16}$$

Here $\mathbf{m} = (m_\alpha)_{\alpha\in\mathbb{N}^n_{2d}}$, $\widehat{\mathbf{m}} = (\widehat{m}_\alpha)_{\alpha\in\mathbb{N}^n_{2d}}$, and $\mathbf{b}$ contains the moments of B indexed by $\mathbb{N}^n_{2d}$. This formulation is [173, Equation 3]. The optimal value of P_d is an upper bound for $\mathrm{vol}(K)$, since we are optimizing over a larger set. The dual SDP is [88, Equation 3.6], which is formulated using sums of squares of polynomials. The authors of [88, 172, 173] implemented the SDPs using `GloptiPoly MATLAB`. Our computations in the next examples are performed in `Mathematica`. We are going to include the linear condition $\mathbf{m}+\widehat{\mathbf{m}}=\mathbf{b}$ inside the condition on the moment matrix of $\widehat{\mathbf{m}}$, by imposing directly that $M_d(\mathbf{b}-\mathbf{m}) \succcurlyeq 0$.

Example 14.12 (TV screen) Fix $K_1 = \{(x,y) \in [-1.2, 1.2]^2 \mid f_1(x,y) \geq 0\} \subset \mathbb{R}^2$ where $f_1 = -q$ is the quartic in (14.3). This convex set shown in Figures 14.2 and 14.4. Recall that $\mathrm{vol}(K_1) = 3.7081599447\ldots$.

Let us now try the SDP formulation above, with $d = 10$. The moment matrices $M_{10}(\mathbf{m})$ and $M_{10}(\mathbf{b}-\mathbf{m})$ have format 66×66. For instance, the second matrix looks like

$$M_{10}(\mathbf{b}-\mathbf{m}) \ = \ \begin{pmatrix} 4-m_{(0,0)} & -m_{(0,1)} & \frac{4}{3}-m_{(0,2)} & -m_{(0,3)} & \cdots \\ -m_{(0,1)} & \frac{4}{3}-m_{(0,2)} & -m_{(0,3)} & \frac{4}{5}-m_{(0,4)} & \cdots \\ \frac{4}{3}-m_{(0,2)} & -m_{(0,3)} & \frac{4}{5}-m_{(0,4)} & -m_{(0,5)} & \cdots \\ -m_{(0,3)} & \frac{4}{5}-m_{(0,4)} & -m_{(0,5)} & \frac{4}{7}-m_{(0,6)} & \cdots \\ \vdots & \vdots & \vdots & \vdots & \ddots \end{pmatrix}.$$

The localizing matrix $M_8(f_1\mathbf{m})$ has format 45×45. Its (α,β) entry equals

$$m_{\alpha+\beta} - m_{(4,0)+\alpha+\beta} - m_{(0,4)+\alpha+\beta} - \frac{1}{100} m_{(1,1)+\alpha+\beta}.$$

The optimal value of the semidefinite program P_{10} is 4.4644647361..., the optimal value of P_{14} is 4.3679560947..., and for P_{18} we get 4.3241824171.... These numbers are upper bounds for the actual volume, as predicted. However, these bounds are still far from the truth.

Example 14.13 (Elliptope) Set $f_2(x,y) = 1-x^2-y^2-z^2+2xyz$. This defines the elliptope $K_2 = \{x,y \in [-1,1]^3 \mid f_2(x,y) \geq 0\} \subset \mathbb{R}^3$, which in shown in Figures 14.1 and 14.4. We already know $\mathrm{vol}\, K_2 = \frac{\pi^2}{2} = 4.934802202\ldots$. The upper bounds computing from the semidefinite program for $d = 4, 8, 12$ are respectively 7.3254012963..., 6.6182632506..., and 6.303035372.... This is still pretty bad.

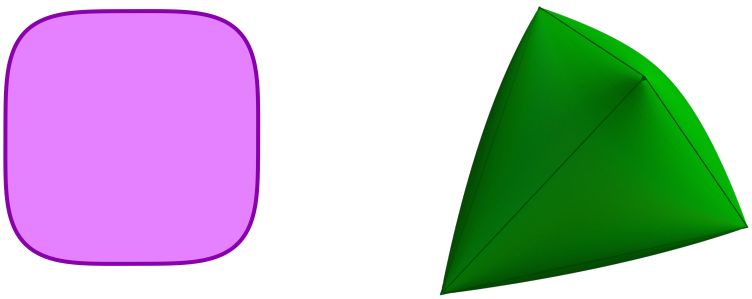

Fig. 14.4: Left: the TV screen from Example 14.12. Right: the elliptope from Example 14.13.

Examples 14.12 and 14.13 suggest that the convergence of the SDP approximation is quite slow. To improve the convergence, one uses the method of *Stokes constraints*. This was introduced and analyzed

in [172, 173] and we shall now explain it. In the infinite-dimensional linear program P^* (and in the SDP hierarchy) we aim to approximate a piecewise-differentiable function, $\mathbf{1}_K$ with continuous functions (respectively, polynomials). This produces the well-known *Gibbs effect*, creating many oscillations near the boundary of K in the polynomial solutions of the SDP. To remedy this, we add linear constraint that do not modify the infinite-dimensional LP problem but add more information to the finite-dimensional SDP. One concrete way to do this uses Stokes' theorem and the fact that f vanishes on the boundary ∂K of K.

Let U be an open region in $\mathbb{R}^n$ such that the Euclidean closure of U is our semialgebraic set K. Since ∂K is smooth almost everywhere, the classical Stokes Theorem applies. This theorem states that

$$\int_{\partial K} \omega \;=\; \int_K d\omega$$

for any $(n-1)$-differential form ω on $\mathbb{R}^n$. One consequences of Stokes' Theorem is *Gauss' formula*

$$\int_{\partial K} V(\mathbf{x}) \cdot \widehat{n}(\mathbf{x})\; d\mathcal{H}^{n-1}(\mathbf{x}) \;=\; \int_K \operatorname{div} V(\mathbf{x})\; d\mathbf{x}.$$

Here $V(\mathbf{x})$ is a vector field, div denotes divergence, $\widehat{n}(\mathbf{x})$ is the exterior normal vector at $\mathbf{x} \in \partial K$, and $\mathcal{H}^{n-1}$ is $(n-1)$-dimensional Hausdorff measure. If the vector field is a scalar field times a constant vector $\mathbf{c} \in \mathbb{R}^n$, say $V(\mathbf{x}) = v(\mathbf{x})\mathbf{c}$, then we obtain the following equations:

$$\mathbf{c} \cdot \left(\int_{\partial K} v(\mathbf{x}) \widehat{n}(\mathbf{x})\; d\mathcal{H}^{n-1}(\mathbf{x}) \right) \;=\; \int_K \operatorname{div}\big(v(\mathbf{x})\mathbf{c}\big)\; d\mathbf{x} \;=\; \mathbf{c} \cdot \left(\int_K \nabla v(\mathbf{x})\; d\mathbf{x} \right).$$

This holds because $\operatorname{div}\big(v(\mathbf{x})\mathbf{c}\big) = \nabla v(\mathbf{x}) \cdot \mathbf{c} + v(\mathbf{x}) \operatorname{div} \mathbf{c}$ and the divergence of a constant vector is zero. Since this identity holds for every $\mathbf{c} \in \mathbb{R}^n$, we have

$$\int_{\partial K} v(\mathbf{x}) \widehat{n}(\mathbf{x})\; d\mathcal{H}^{n-1}(\mathbf{x}) = \int_K \nabla v(\mathbf{x})\; d\mathbf{x}. \tag{14.17}$$

If $v = 0$ on ∂K, then the left hand side of (14.17) is zero. This condition can be expressed in terms of measures and distributions, and added to (14.14) and (14.15) as in [173, Equation 17 and Remark 3].

In the setting of our SDP hierarchy, the Stokes constraints are written as follows. Let $v(\mathbf{x}) = f(\mathbf{x})\mathbf{x}^\alpha$ for any multiindex $\alpha \in \mathbb{N}^n$ with $|\alpha| \le d + 1 - \deg f$. Then we require

$$\nabla\big(f(\mathbf{x})\mathbf{x}^\alpha\big)\big|_{\mathbf{x}^\beta \to m_\beta} \;=\; 0.$$

We now replace each monomial by its moment. This yields n new linear conditions for each α as above.

Example 14.14 For the SDP in Examples 14.12 and 14.13, the Stokes constraints for a given α are:

$$\begin{aligned}
&K_1: \\
&\alpha_1 m_{\alpha+(-1,0)} - (\alpha_1+4) m_{\alpha+(3,0)} - \alpha_1 m_{\alpha+(-1,4)} - \tfrac{\alpha_1+1}{100} m_{\alpha+(0,1)} = 0, \\
&\alpha_2 m_{\alpha+(0,-1)} - \alpha_2 m_{\alpha+(4,-1)} - (\alpha_2+4) m_{\alpha+(0,3)} - \tfrac{\alpha_2+1}{100} m_{\alpha+(1,0)} = 0, \\
&K_2: \\
&\alpha_1 m_{\alpha+(-1,0,0)} - (\alpha_1+2) m_{\alpha+(1,0,0)} - \alpha_1 m_{\alpha+(-1,2,0)} - \alpha_1 m_{\alpha+(-1,0,2)} + 2(\alpha_1+1) m_{\alpha+(0,1,1)} = 0, \\
&\alpha_2 m_{\alpha+(0,-1,0)} - \alpha_2 m_{\alpha+(2,-1,0)} - (\alpha_2+2) m_{\alpha+(0,1,0)} - \alpha_2 m_{\alpha+(0,-1,2)} + 2(\alpha_2+1) m_{\alpha+(1,0,1)} = 0, \\
&\alpha_3 m_{\alpha+(0,0,-1)} - \alpha_3 m_{\alpha+(2,0,-1)} - \alpha_3 m_{\alpha+(0,2,-1)} - (\alpha_3+2) m_{\alpha+(0,0,1)} + 2(\alpha_3+1) m_{\alpha+(1,1,0)} = 0.
\end{aligned}$$

Table 14.1 compares the optimal values of the SDP (14.13) with and without Stokes constraints.

K	Volume	d	without Stokes		with Stokes	
			max P_d	time	max P_d	time
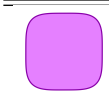	3.708159…	10	4.464464…	0.621093	3.709994…	0.482376
		15	4.367956…	3.545369	3.708191…	3.738137
		20	4.324182…	14.906281	3.708163…	20.592531
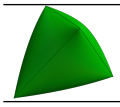	4.934802…	4	7.325401…	0.124392	5.612716…	0.077315
		8	6.618263…	7.222441	4.976796…	7.178571
		12	6.303035…	696.886298	4.937648…	1105.619231

Table 14.1: The optimal values of (14.13) with and without Stokes constraints for Examples 14.12 and 14.13. The column "max P_d" displays the optimal value, whereas the column "time" gives the time, in seconds, for running the command `SemidefiniteOptimization` in `Mathematica`.

As Table 14.1 shows, the convergence with Stokes constraints is much faster than without them. The intuition is that now, with the (dual) Stokes constraints added to P^*, the function we approximate is not just the indicator function of K. A detailed explanation, for a variant of the Stokes constraints, is given in [172]. The authors prove that, when adding this new type of constraints, the optimal solution of the new P^* becomes a minimum. This eliminates any kind of Gibbs effect, and guarantees faster convergence. In [172], the authors mention that, from numerical experiments, it is reasonable to expect that the original Stokes constraints and the new Stokes constraints are equivalent, but there is no formal proof of this statement yet. We close with the remark that general semialgebraic sets fit into this framework; see [88, 172, 173].

Chapter 15
Sampling

This chapter is about methods for sampling from a real algebraic variety $X \subset \mathbb{R}^n$. In other words, we want to compute a finite subset $S \subset X$, which we call a *sample*. An example of a sample on a curve is shown in Figure 15.1. The sample S yields a discrete approximation of X that can be used to explore properties of the variety. For instance, if $g : X \to \mathbb{R}$ is a function, we can find a lower bound for the optimization problem $\max_{\mathbf{x}\in X} g(\mathbf{x})$ by computing $\max_{\mathbf{s}\in S} g(\mathbf{s})$, or we can estimate the integral $\int_{\mathbf{x}\in X} g(\mathbf{x})d\mathbf{x} \,/\, \mathrm{vol}(X)$ (provided X has finite volume) by $\frac{1}{|S|}\sum_{\mathbf{s}\in S} g(\mathbf{x})$. Asmussen and Glynn [7] underline the importance of sampling methods as follows:

> "Sampling-based computational methods are a fundamental part of the numerical toolset across an enormous number of different applied domains".

In Section 15.1, we discuss in detail how samples can be used to compute topological information of X.

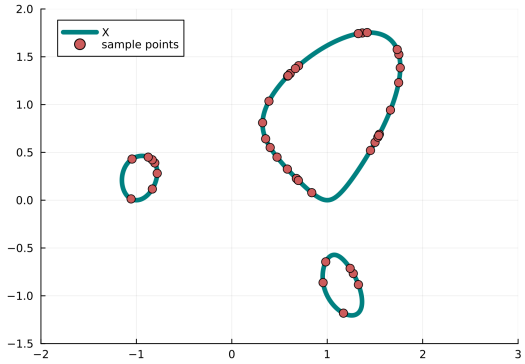

Fig. 15.1: A sample of points on the curve $X = \{x^4 + y^4 - 2x^2 - 2xy^2 - y + 1 = 0\}$.

In Sections 15.2 and 15.3, we discuss two approaches to sampling. The first approach concerns sampling methods with density guarantees. These methods have in common that they generate a (possibly random) sample $S \subset X$ that is ε-*dense* in X.

Definition 15.1 A finite subset $S \subset X$ is called ε-*dense* in X or an ε-*dense sample* for X if, for all $\mathbf{x} \in X$, there exists $\mathbf{s} \in S$ with $\|\mathbf{x} - \mathbf{s}\| < \varepsilon$.

The second approach to sampling is to generate points from a prescribed probability distribution on X. For instance, if X is compact, we could be interested in sampling from the uniform distribution.

Since we are computing random samples, it is enough to replace the variety X by its smooth locus X^{sm} and sample from X^{sm}. To keep the notation simple, though, we assume throughout the remainder of this chapter that X is a smooth manifold embedded in $\mathbb{R}^n$.

15.1 Computing the Homology from Finite Samples

We first recall a theorem due to Niyogi, Smale and Weinberger [142]. Their result gives conditions for when the homology of a smooth manifold X embedded in $\mathbb{R}^n$ can be computed from a finite sample S. The idea is to compute the homology of the union of ε-balls $U = \bigcup_{\mathbf{s}\in S} B_\varepsilon(\mathbf{s})$ of an ε-sample S. The homology groups of a union of balls U can be computed from the associated Čech-complex. The theorem explains how small ε must be for this to work.

Theorem 15.2 *Let $\varepsilon > 0$, $S \subset X$ be an ε-sample for X, and $U = \bigcup_{\mathbf{s}\in S} B_\varepsilon(\mathbf{s})$ be the union of ε-balls around points in S. Let $\tau(X)$ be the reach of X. If $\varepsilon < \sqrt{\frac{3}{20}}\,\tau$, then X is a deformation retract of U. In particular, the homology of X equals the homology of U.*

Proof See [142, Proposition 3.1]. □

It was shown in [154] that we can replace the reach $\tau(X)$ in Theorem 15.2 by what is called the *local reach* $\tau(\mathbf{x})$. For $\mathbf{x} \in X$, the local reach is defined as

$$\tau(\mathbf{x}) := \sup\{r \geq 0 \mid \text{ for all } \mathbf{u} \in B_r(\mathbf{x}) \text{ there is a unique minimizer of } X \to \mathbb{R}, \mathbf{x}' \mapsto \|\mathbf{x}' - \mathbf{u}\|\}\,.$$

In other words, the local reach $\tau(\mathbf{x})$ is the distance from the point $\mathbf{x} \in X$ to the medial axis $\mathrm{Med}(X)$ of X (cf. Chapter 7). Hence, the global reach $\tau(X)$ is upper bounded by the local reach at each point; in fact, $\tau(X) = \inf_{\mathbf{x}\in X} \tau(\mathbf{x})$. Thus, using the local reach instead of the global reach for upper bounding ε can make a significant difference. The result from [154] is: If $\varepsilon < \frac{4}{5}\,\tau(\mathbf{s})$ for all points $\mathbf{s}$ in a ε-dense sample $S \subset X$, then X is a deformation retract of $U = \bigcup_{\mathbf{s}\in S} B_\varepsilon(\mathbf{s})$.

Interestingly, if we only want to compute homology for small dimensions, we can relax the conditions on ε even more. For that, we recall the definition of *weak feature size* from [44]. We first need to introduce the notion of *k-bottlenecks*.

Definition 15.3 Let $k \geq 2$. For $B = \{\mathbf{x}_1, \ldots, \mathbf{x}_k\} \subset X$ (with $|B| = k$), let $\Gamma(B)$ be the union of the centers of all $(n-1)$-spheres passing through $\mathbf{x}_1, \ldots, \mathbf{x}_k$. If $N_{\mathbf{x}_1} X \cap \cdots \cap N_{\mathbf{x}_k} X \cap \Gamma(B) \cap \mathrm{conv}(B) \neq \emptyset$, we call B a *k-bottleneck* of X. Its *width* is $\ell(B) := \inf_{\mathbf{u}\in\Gamma(B)} \|\mathbf{x}_1 - \mathbf{u}\|$.

For instance, the 2-bottlenecks of X are precisely the bottlenecks studied in Section 7.1. The *weak feature size* is the smallest width of a k-bottleneck:

$$\mathrm{wfs}(X) := \min_{2\leq k\leq \mathrm{EDdegree}(X)} \inf\{\ell(B) \mid B \text{ is a } k\text{-bottleneck of } X\}.$$

The weak feature size is always greater or equal than the reach, because the exponential map φ_ε in (6.10) cannot be injective when $\varepsilon > \ell(B)$ for a k-bottleneck $B = \{\mathbf{x}_1, \ldots, \mathbf{x}_k\}$. In fact, in that case, the point $\mathbf{u} \in \Gamma(B)$ with $\ell(B) = \|\mathbf{x}_1 - \mathbf{u}\|$ has k points $(\mathbf{x}_1, \mathbf{v}_1), \ldots, (\mathbf{x}_k, \mathbf{v}_k)$ in its fiber under φ_ε. The following was proved in [154].

Theorem 15.4 *Let $\varepsilon < \mathrm{wfs}(X)$ and $S \subset X$ be an ε-dense sample. Construct the two-dimensional Vietoris-Rips complex C with vertices S as follows: Add the edge spanned by $\mathbf{x}, \mathbf{y} \in S$ to C if and only if one of the following two conditions is satisfied:*

1. *$\|\mathbf{x} - \mathbf{y}\| \leq 2\varepsilon$, or*
2. *$\|\mathbf{x} - \mathbf{y}\| \leq \sqrt{8}\varepsilon$ and there is $\mathbf{z} \in S$ with $\|\mathbf{x} - \mathbf{z}\| \leq 2\varepsilon$ and $\|\mathbf{y} - \mathbf{z}\| \leq 2\varepsilon$.*

Moreover, add the 2-simplex spanned by $\mathbf{x}, \mathbf{y}, \mathbf{z} \in S$ to C if and only if there is an edge between $\mathbf{x}$ and $\mathbf{y}$, between $\mathbf{x}$ and $\mathbf{z}$, and between $\mathbf{y}$ and $\mathbf{z}$. Then, $H_0(X) \cong H_0(C)$ and $H_1(X) \cong H_1(C)$.

Remark 15.5 Theorem 15.4 is based on [44, Theorem 1], where it is shown that for $\varepsilon < \mathrm{wfs}(X)$ the tubular neighborhood $\bigcup_{\mathbf{x}\in X} B_\varepsilon(\mathbf{x})$ is homotopy equivalent to X.

15.2 Sampling with Density Guarantees

This section presents two sampling algorithms that guarantee to compute an ε-sample. Both algorithms compute a sample of $X \cap R$, where

$$R = [a_1, b_1] \times \cdots \times [a_n, b_n] \subset \mathbb{R}^n$$

is a box. If X is compact, we can compute a box R such that $X \subset R$ as follows. We first sample a point $\mathbf{u} \in \mathbb{R}^n$ at random. Then, we compute the ED critical points on X with respect to $\mathbf{u}$; i.e., the critical points of the Euclidean distance function $X \to \mathbb{R}, \mathbf{x} \mapsto \|\mathbf{x} - \mathbf{u}\|$. From this, we infer $r := \max_{\mathbf{x} \in X} \|\mathbf{x} - \mathbf{u}\|$ and set R to be the box with center $\mathbf{u}$ and side length $2r$.

The first sampling algorithm we present is from [65]. Let $R = [a_1, b_1] \times \cdots \times [a_n, b_n]$ be a box. The basic idea for sampling from $X \cap R$ is to sample points $\mathbf{u} \in \mathbb{R}^n$ and then to collect the ED critical points with respect to $\mathbf{u}$. The complexity of this approach therefore depends on the Euclidean Distance Degree of X.

The algorithm in [65] works recursively by dividing the sides of the box R in half, thus splitting R into 2^n subboxes. In addition, one implements a database $\mathcal{D}$ that contains information about all the regions in R that already have been covered by at least one sample point. Algorithm 4 provides a complete description. The correctness of that algorithm is proved in [65].

Theorem 15.6 (Theorem 4.4 in [65]) *Algorithm 4 terminates and outputs an ε-dense sample of $X \cap R$.*

Algorithm 4: The algorithm from [65].

Input: A real algebraic variety $X \subset \mathbb{R}^n$, a real number $\varepsilon > 0$, and a box $R = [a_1, b_1] \times \cdots \times [a_n, b_n]$
Output: An ε-dense sample $S \subset X \cap R$.
Initialize $S = \emptyset$ and $\mathcal{D} = \emptyset$. The set S will contain the sample points. The set $\mathcal{D}$ serves as a database containing balls in $\mathbb{R}^n$ that have already been covered in the process of the algorithm.
for *each subbox R' of R that is not yet covered* **do**
    Compute the midpoint $\mathbf{u}$ of R'.
    Compute the real ED critical points $E \subset X$ with respect to $\mathbf{u}$ and compute $r := \min_{\mathbf{x} \in X} \|x - \mathbf{u}\|$.
    Add the points in E to S.
    Add $B_r(\mathbf{u})$ to $\mathcal{D}$ (this open ball does not contain any point in X, so we do not need to consider this region any further and can label it as being covered).
    Add $B_\varepsilon(\mathbf{y})$ for $\mathbf{y} \in E$ to $\mathcal{D}$.
    if *the union of balls in $\mathcal{D}$ cover R'* **then**
        Label R' and all of its subboxes as covered.
    else
        Split R' into 2^n smaller subboxes.
    end
end
if *all subboxes of R are labeled as covered* **then**
    return S.

The second algorithm we present is from [154]. That algorithm is also based on computing ED critical points on X, but in addition adds linear slices to the sampling. We need a few definitions. We set $d := \dim X$. For every $1 \le k \le d$, denote by $\mathcal{T}_k$ the set of subsets of $\{1, \ldots, n\}$ with k elements. Given a set $T = \{t_1, \ldots, t_k\} \in \mathcal{T}_K$, we let $V_T \subseteq \mathbb{R}^n$ be the k-dimensional coordinate plane spanned by $\mathbf{e}_{t_1}, \ldots, \mathbf{e}_{t_k}$. For $\delta > 0$, consider the grid

$$G_T(\delta) := \left\{ \delta \cdot (a_1 \cdot \mathbf{e}_{t_1} + \cdots + a_d \cdot \mathbf{e}_{t_k}) \mid a_1, \ldots, a_k \in \mathbb{Z} \right\} \cong \delta \cdot \mathbb{Z}^k.$$

Let $\pi_T : \mathbb{R}^n \to V_T$ be the projection. Then, the linear spaces $\pi_T^{-1}(g)$ for $g \in G_T(\delta)$ are given by the faces of a cubical tessellation with side length δ.

Let $B(X)$ be the width of the smallest bottleneck of X. The algorithm from [154] takes as input a number $0 < \delta < \frac{1}{\sqrt{n}} \min\{\varepsilon, 2B(X)\}$. Then, the sample is given by

$$S_\delta := \bigcup_{T \in \mathcal{T}_d} \bigcup_{g \in G_T(\delta)} X \cap \pi_T^{-1}(g); \tag{15.1}$$

i.e., S_δ consists of the points that are obtained by intersecting X with the collection of linear spaces $\pi_T^{-1}(g)$ ranging over $T \in \mathcal{T}_d$ and $g \in G_T(\delta)$. The dimension of $\pi_T^{-1}(g)$ equals the codimension of X. To ensure transversal intersections, we can always modify $G_T(\delta)$ by a random translation.

If $d = \dim X > 1$, the algorithm computes an additional sample. First, we sample a random point $\mathbf{u} \in \mathbb{R}^n$. Denote by $E(T, g, \mathbf{u})$ the ED critical points on $X \cap \pi_T^{-1}(g)$ with respect to $\mathbf{u}$. The additional sample is

$$S'_\delta = \bigcup_{k=1}^{d-1} \bigcup_{T \in \mathcal{T}_k} \bigcup_{g \in G_T(\delta)} E(T, g, \mathbf{u}). \tag{15.2}$$

The motivation for this extra sample is that $E(T, g, \mathbf{u})$ contains a point on every connected component of $X \cap \pi_T^{-1}(g)$. The algorithm is summarized in Algorithm 5.

Theorem 15.7 (Theorem 4.6 in [154]) *Algorithm 5 outputs an ε-dense sample of $X \cap R$.*

Algorithm 5: The algorithm from [154].

Input: A real algebraic variety $X \subset \mathbb{R}^n$, a real number $\delta > 0$ with $\delta < \frac{1}{\sqrt{n}} \min\{\varepsilon, 2B(X)\}$, and a box $R = [a_1, b_1] \times \cdots \times [a_n, b_n]$.
Output: An ε-dense sample $S \subset X \cap R$.
Initialize $S_\delta = \emptyset$ and $S'_\delta = \emptyset$.
Set $d := \dim X$.
for $T \in \mathcal{T}_d$ *and* $g \in G_T(\delta)$ **do**
    Compute $X \cap \pi_T^{-1}(g)$.
    Add the points in $X \cap \pi_T^{-1}(g)$ to S_δ.
end
if $d > 1$ **then**
    for $1 \le k < d$ **do**
        for $T \in \mathcal{T}_k$ *and* $g \in G_T(\delta)$ **do**
            Sample a random point $\mathbf{u} \in \mathbb{R}^n$.
            Compute $E(T, g, \mathbf{u})$, which are the ED critical points on $X \cap \pi_T^{-1}(g)$ with respect to $\mathbf{u}$.
            Add the points in $E(T, g, \mathbf{u})$ to S'_δ.
        end
    end
Set $S := S_\delta \cup S'_\delta$.
return S.

15.3 Sampling from Probability Distributions

Let π be a probability measure on X. In this section, we discuss algorithms for sampling from π. In this context, π is also called the *target distribution*. We will review one popular class of methods for sampling from probability distributions on X, namely *Markov-Chain Monte Carlo* (MCMC) methods. In the following, $\mathcal{A}$ denotes the σ-algebra of X.

Example 15.8 Let X be compact and $\mathrm{d}\mathbf{x}$ be the Lebesgue measure on X. For a measurable set $A \in \mathcal{A}$, let $\mathrm{vol}(A) = \int_A \mathrm{d}\mathbf{x} < \infty$ be the volume of A. The probability distribution with probability measure given

by $\pi(A) := \mathrm{vol}(A) \,/\, \mathrm{vol}(X)$ is called the *uniform distribution* on X. For instance, the sample in Figure 15.1 consists of i.i.d. (independent and uniformly distributed) points from the uniform distribution on a plane curve $X = \{x^4 + y^4 - 2x^2 - 2xy^2 - y + 1 = 0\}$.

Before we discuss sampling algorithms, let us briefly recall the following result by Niyogi, Smale and Weinberger [142], which implies that sampling from the uniform distribution on X can be used to generate ε-samples with high probability.

Proposition 15.9 *Let $\varepsilon > 0$ and $0 < \delta < 1$. Suppose X is compact of dimension $d := \dim X$ and with positive reach $\tau(X) > 0$. Set*

$$\theta := \arcsin\left(\tfrac{\varepsilon}{\tau}\right), \qquad \omega := \frac{\mathrm{vol}(X)}{\cos^d \theta}, \qquad \beta_1 := \frac{\omega}{\mathrm{vol}(B_\varepsilon(\mathbf{0}))}, \qquad \beta_2 := \frac{\omega}{\mathrm{vol}(B_{\varepsilon/8}(\mathbf{0}))}$$

(here, $B_\varepsilon(\mathbf{0})$ is the unit ball of radius ε). Let $n > \beta_1(\log\beta_2 - \log\delta)$. For a sample of i.i.d. points $S = \{\mathbf{x}_1, \ldots, \mathbf{x}_n\}$ from the uniform distribution on X, we have $\mathrm{Prob}(S \text{ is an } \varepsilon\text{-sample for } X) > 1 - \delta$.

Let us now put the focus on sampling by using MCMC methods. These methods set up a *Markov process* on X. Let us recall some basic definitions from the theory of Markov chains; see, e.g., [131, Chapter 3]. In this context, X is also called a *state space*. A *Markov kernel* is a map $p : X \times \mathcal{A} \to [0, 1]$, such that

1. $p(\mathbf{x}, \cdot\,)$ is a probability measure for all $\mathbf{x} \in X$;
2. $p(\,\cdot\,, A)$ is a measurable function for all $A \in \mathcal{A}$.

A stochastic process $\mathbf{x}_0, \mathbf{x}_1, \mathbf{x}_2, \mathbf{x}_3, \ldots$ on X is a sequence of random points on X. Markov processes encompass a special type of stochastic processes. Let $\mathbf{x} \in X$ be a fixed point. A (time-homogeneous) Markov process with starting point $\mathbf{x}$ is the stochastic process defined by $\mathbf{x}_0 = \mathbf{x}$ and for $k \geq 1$:

$$\mathrm{Prob}(\mathbf{x}_1 \in A_1, \ \ldots\ , \mathbf{x}_k \in A_k \mid \mathbf{x}_0 = \mathbf{x}) := \int_{\mathbf{y}_1 \in A_1} \cdots \int_{\mathbf{y}_{k-1} \in A_{k-1}} p(\mathbf{x}, \mathrm{d}\mathbf{y}_1) p(\mathbf{y}_1, \mathrm{d}\mathbf{y}_2) \cdots p(\mathbf{y}_{k-1}, A_k).$$

For fixed $\mathbf{z} \in X$, we have

$$\mathrm{Prob}(\mathbf{x}_k \in A \mid \mathbf{x}_{k-1} = \mathbf{z},\ \mathbf{x}_{k-2},\ \ldots,\ \mathbf{x}_0) = \mathrm{Prob}(\mathbf{x}_k \in A \mid \mathbf{x}_{k-1} = \mathbf{z}) = p(\mathbf{z}, A); \tag{15.3}$$

see, e.g., [131, Proposition 3.4.3]. Equation (15.3) is called the *Markov property*. It means that the probability law of the next point in the process only depends on the current state, but not on earlier states. Due to its role in (15.3), the kernel p is also called *transition probability*.

Example 15.10 (Markov Chains in $\mathbb{R}^2$) Let us consider two examples of Markov Chains in $\mathbb{R}^2$ starting at the origin. For the first, we take the kernel $p_1(\mathbf{x}, \mathrm{d}\mathbf{y}) = (2\pi)^{-1} \cdot \exp(-\frac{1}{2}\|\mathbf{y}\|^2)\,\mathrm{d}\mathbf{y}$. The stochastic process arising from this passes from the state $\mathbf{x} \in \mathbb{R}^2$ to the next state by sampling a normal vector in $\mathbb{R}^2$ with covariance matrix the identity and mean value $\mathbf{0}$. In particular, the transition probability is independent of the current state.

The second example has the kernel $p_2(\mathbf{x}, \mathrm{d}\mathbf{y}) = (2\pi)^{-1} \exp(-\frac{1}{2}\|\mathbf{x} - \mathbf{y}\|^2)\,\mathrm{d}\mathbf{y}$. In this case, passing from a state $\mathbf{x} \in \mathbb{R}^2$ to the next state works by sampling a normal vector in $\mathbb{R}^2$ with covariance matrix the identity and mean value $\mathbf{x}$. We can simulate the first $n = 10$ steps in this chain in `Julia` as follows.

```
x0 = [0; 0]
states = []
push!(states, x0)

n = 10
for k in 1:n
```

```
    x = states[k]
    y = x + randn(2)
    push!(states, y)
end
```

Figure 15.2 shows one realization of this chain.

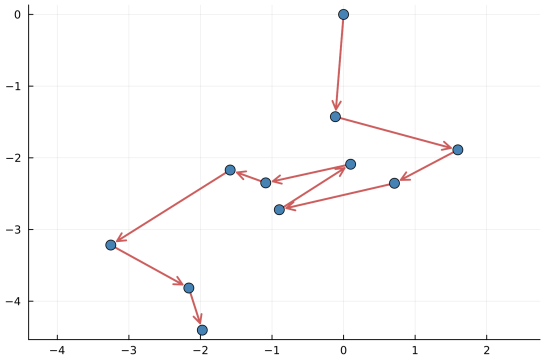

Fig. 15.2: The picture shows one sample of the first 10 steps of the Markov Chain with transition probability at state $\mathbf{x}$ given by sampling a normal vector in $\mathbb{R}^2$ with covariance matrix the identity and mean value $\mathbf{x}$. See Example 15.10.

Example 15.11 (A Markov Chain on a Real Variety) Let $X \subset \mathbb{R}^n$ be a real variety of dimension d and degree at least two. We can create a Markov chain on X as follows. Suppose that chain is in state $\mathbf{x} \in X$. We sample a random linear space L of complimentary dimension passing through $\mathbf{x}$. Then, we sample a point uniformly at random from $X \cap L$. This is the next state. As an example, we take the surface defined by $z - xy = 0$. Given a point $\mathbf{x}$ on this surface, we sample the line $L = \{A\mathbf{x} = \mathbf{b}\}$ by sampling A with Gaussian entries and setting $\mathbf{b} = A\mathbf{x}$. In addition, we only accept states in the box $R = [-8, 8] \times [-8, 8] \times [-64, 64]$. The first few steps in this chain starting at $\mathbf{x}_0 = (0, 0, 0)$ are implemented in `Julia` [18] as follows.

```
using HomotopyContinuation
@var x y z
f = System([z - x * y], variables = [x; y; z])
is_in_R(p) = abs(p[1])<8 && abs(p[2])<8 && abs(p[3])<64

n = 10
x0 = [0.0; 0.0; 0.0]
states = [x0]
for k in 1:n
    p = last(states)
    A = randn(2,3); b = A*p
    L = LinearSubspace(A, b)

    S = solve(f, target_subspace = L)
    points = real_solutions(S)
    filter!(is_in_R, points)
    push!(states, rand(points))
end
```

One realization of this example is shown in Figure 15.3.

Let us now work towards sampling. We will recall results from the survey [153] by Roberts and Rosenthal. A probability measure π on X is called a *stationary distribution* if

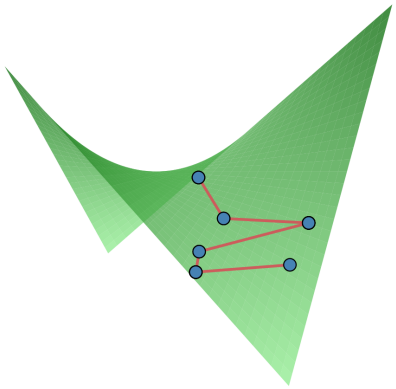

Fig. 15.3: The picture shows first few steps of the Markov Chain from Example 15.11 on the surface $z - xy = 0$.

$$\int_{\mathbf{x}\in X} \pi(\mathrm{d}\mathbf{x}) \cdot p(\mathbf{x}, \mathrm{d}\mathbf{y}) = \pi(\mathrm{d}\mathbf{y}) \quad \text{for all } \mathbf{y} \in X. \tag{15.4}$$

The idea of MCMC methods for sampling from a probability distribution π is to set up a Markov process on X starting at $\mathbf{x}$ such that π is stationary and such that the probability measure

$$\mu^k(\mathbf{x}, \cdot) : A \mapsto \mathrm{Prob}(\mathbf{x}_k \in A \mid \mathbf{x}_0 = \mathbf{x})$$

converges to π as $k \to \infty$. Convergence is measured by the *total variation distance*. The total variation distance between two measures μ and ν is $d_{\mathrm{TV}}(\mu, \nu) := \sup_{A\in\mathcal{A}} |\mu(A) - \nu(A)|$. Thus, we want to define a Markov process starting at a point $\mathbf{x} \in X$ such that $\lim_{k\to\infty} d_{\mathrm{TV}}(\pi, \mu^k(\mathbf{x}, \cdot)) = 0$. The key properties for achieving this are *irreducibility* and *aperiodicity*.

Definition 15.12 A Markov chain with kernel p is called *irreducible* if, for all states $\mathbf{x} \in X$ and all measurable sets $A \in \mathcal{A}$ with $\mathrm{vol}(A) > 0$, there exists $k \in \mathbb{N}$ such that $\mu^k(\mathbf{x}, A) > 0$.

The interpretation of irreducibility is that all sets with positive volume can eventually be reached by the Markov chain starting at any point $\mathbf{x} \in X$.

Remark 15.13 One can replace the Lebesgue measure in the definition by any other measure ϕ. In that case, one speaks of ϕ-irreducible Markov chains.

Definition 15.14 Consider a Markov chain with kernel p and suppose that it has a stationary distribution π. Let $d \geq 2$. We call the chain *periodic* with period d if there exist disjoint subsets $A_1, \ldots, A_d \in \mathcal{A}$ that satisfy

1. $\pi(A_i) > 0$ and
2. $p(\mathbf{x}, A_{i+1 \bmod d}) = 1$ for all $\mathbf{x} \in A_i$

for all i. Otherwise, the chain is called *aperiodic*.

The geometric interpretation of aperiodicity is that the Markov process does not move periodically between disjoint subset $A_1, \ldots, A_d$. Given an irreducible and aperiodic Markov chain with stationary distribution π, we have the following convergence result.

Theorem 15.15 *Let $\mathbf{x}_0, \mathbf{x}_1, \mathbf{x}_2, \ldots$ be a Markov chain with kernel p and stationary distribution π. Suppose that the chain is irreducible and aperiodic. Then,*

$$\lim_{k\to\infty} d_{\mathrm{TV}}(\pi,\ \mu^k(\mathbf{x},\ \cdot\ )) = 0$$

for almost all $\mathbf{x} \in X$.

Proof See [153, Theorem 4]. □

Remark 15.16 For this theorem, it is enough that X is a state space with countably generated σ-algebra. Smooth submanifolds of $\mathbb{R}^n$ always satisfy this hypothesis.

The next result gives, under some assumptions, the speed of convergence in Theorem 15.15. Roberts and Rosenthal [153] attribute this theorem to Doeblin, Doob and also to Markov.

Theorem 15.17 *Consider a Markov Chain with stationary distribution π. Suppose that there exist $n \in \mathbb{N}$, $\varepsilon > 0$ and a probability measure ν on X such that*

$$\mu^n(\mathbf{x}, A) \geq \varepsilon \cdot \nu(A) \quad \text{for all } \mathbf{x} \in X \text{ and } A \in \mathcal{A}.$$

Then, we have

$$d_{\mathrm{TV}}(\pi,\ \mu^k(\mathbf{x},\ \cdot\ )) < (1-\varepsilon)^{\lfloor \frac{k}{n} \rfloor}.$$

Proof See [153, Theorem 8]. □

The condition in Theorem 15.17 intuitively means that all n step transitions have a component of probability at least ε in common.

Theorems 15.15 and 15.17 have the following algorithmic consequence. For sampling from a distribution π, we set up an irreducible and aperiodic Markov chain with stationary distribution π. Then, if we let the Markov chain run long enough, the points in the process will have a probability distribution close to π. This is the idea underlying MCMC methods. The key task is thus to find and implement such a chain. The first subtask is to find a chain whose stationary distribution is π. It is often easier to show that a Markov chain is *reversible* with respect to π.

Definition 15.18 A Markov chain with kernel p is reversible with respect to a probability distribution π if $\pi(\mathrm{d}\mathbf{x}) \cdot p(\mathbf{x}, \mathrm{d}\mathbf{y}) = \pi(\mathrm{d}\mathbf{y}) \cdot p(\mathbf{y}, \mathrm{d}\mathbf{x})$ for all $\mathbf{x}, \mathbf{y} \in X$.

Lemma 15.19 *If a Markov chain with kernel p is reversible with respect to a probability distribution π, then π is a stationary distribution.*

Proof We have to check the equation in (15.4). Fix $\mathbf{y} \in X$. Then

$$\int_{\mathbf{x}\in X} \pi(\mathrm{d}\mathbf{x}) \cdot p(\mathbf{x}, \mathrm{d}\mathbf{y}) = \int_{\mathbf{x}\in X} \pi(\mathrm{d}\mathbf{y}) \cdot p(\mathbf{y}, \mathrm{d}\mathbf{x}) = \pi(\mathrm{d}\mathbf{y}) \cdot \int_{\mathbf{x}\in X} p(\mathbf{y}, \mathrm{d}\mathbf{x}) = \pi(\mathrm{d}\mathbf{y}),$$

since $p(\mathbf{y},\ \cdot\ )$ is a probability measure. □

Using Lemma 15.19, it is straighforward to show that the *Metropolis Hastings algorithm* (Algorithm 6) creates a Markov chain with stationary distribution π; see, e.g., [153, Proposition 2].

The Metropolis Hastings algorithm works for a target distribution π that has a density ϕ. The basic idea is to take another Markov chain whose kernel $p(\mathbf{x}, A)$ has a density $q(\mathbf{x}, \mathbf{y})$; i.e., $p(\mathbf{x}, \mathrm{d}\mathbf{y}) = q(\mathbf{x}, \mathbf{y})\,\mathrm{d}\mathbf{y}$.

The density q is called a *proposal density*. Sampling from the proposal density creates a random proposal point $\mathbf{y}$, which is either accepted or rejected depending on how likely it is that the proposal point $\mathbf{y}$ was sampled from π. Notice that in the algorithm we only need to evaluate $\phi(\mathbf{y})$ and $q(\mathbf{x}, \mathbf{y})$ up to scaling.

Algorithm 6: The Metropolis Hastings algorithm.

1 **Input:** A probability measure π on X with a density $\phi(\mathbf{y})$. A Markov kernel $p(\mathbf{x}, A)$ on X with density $q(\mathbf{x}, \mathbf{y})$. A fixed starting point $\mathbf{x} \in X$.
2 **Output:** A Markov chain on X with stationary distribution π.
3 Set $\mathbf{x}_0 = \mathbf{x}$.
4 **for** $k = 0, 1, 2, \ldots$ **do**
5 Sample $\mathbf{y} \sim p(\mathbf{x}_k, \cdot)$.
6 **if** $\phi(\mathbf{x}_k) = 0$ *or* $q(\mathbf{x}_k, \mathbf{y}) = 0$ **then**
7 Set $w(\mathbf{x}_k, \mathbf{y}) = 0$
8 **else**
9 Compute $w(\mathbf{x}_k, \mathbf{y}) = \min\left\{1, \dfrac{\phi(\mathbf{y}) \cdot q(\mathbf{y}, \mathbf{x}_k)}{\phi(\mathbf{x}_k) \cdot q(\mathbf{x}_k, \mathbf{y})}\right\}$.
10 **end**
11 Sample a Bernoulli random variable $\beta \in \{0, 1\}$ with $\text{Prob}\{\beta = 1\} = w(\mathbf{x}_k, \mathbf{y})$.
12 **if** $\beta = 1$ **then**
13 Set $\mathbf{x}_{k+1} := \mathbf{y}$.
14 **else**
15 Return to line 5.
16 **end**
17 **end**

Example 15.20 (The Symmetric Metropolis Algorithm) For a symmetric density $q(\mathbf{x}, \mathbf{y}) = q(\mathbf{y}, \mathbf{x})$, the Metropolis Hastings algorithm (Algorithm 6) is called *Symmetric Metropolis Algorithm*. For instance, the Markov kernel with density $q(\mathbf{x}, \mathbf{y}) \propto \exp(-\frac{1}{2}\|\mathbf{x} - \mathbf{y}\|^2)$ from Example 15.10 is symmetric.

Example 15.21 (Random Walks) We speak of a *Random Walk Metropolis Hastings Algorithm* if the proposal density $q(\mathbf{x}, \mathbf{y})$ has the form $q(\mathbf{x}-\mathbf{y})$. An example for this is the density $q(\mathbf{x}, \mathbf{y}) \propto \exp(-\frac{1}{2}\|\mathbf{x}-\mathbf{y}\|^2)$ from Example 15.10.

Example 15.22 (Independence Sampler) We call Algorithm 6 an *independence sampler* if $q(\mathbf{x}, \mathbf{y})$ does not depend on $\mathbf{x}$. In this case, the samples obtained from Algorithm 6 are independent.

Example 15.23 (The Langevin Algorithm) The Langevin Algorithm works for sampling in $X = \mathbb{R}^n$. Suppose that the density $\phi(\mathbf{y})$ of the target distribution π in Algorithm 6 is differentiable. Denote by $\nabla\phi(\mathbf{y})$ the gradient. The Langevin Algorithm generates a proposal $\mathbf{y}$ by sampling $\mathbf{y} \sim N(\mathbf{x}_k + \delta \cdot \nabla\phi(\mathbf{x}_k), 2\delta)$, where $\mathbf{x}_k$ is the current state. This choice is motivated by a discrete approximation to a Langevin diffusion processes.

Example 15.24 (Sampling points that are close to a variety) This example is inspired by an idea first suggested by Jon Hauenstein and David Kahle [84]. We can use Algorithm 6 for sampling points near a variety as follows. Choose a box $R \subset \mathbb{R}^n$ and consider the probability measure π on R given by the density

$$\phi(\mathbf{u}) \propto \exp\Big(-\tfrac{1}{2\sigma^2}\, d(\mathbf{u}, X)^2\Big),$$

where $\sigma^2 > 0$ and $d(\mathbf{u}, X) = \min_{\mathbf{x}\in X} \|\mathbf{x} - \mathbf{u}\|$ is the Euclidean distance from $\mathbf{u}$ to X. Sampling from π produces points that have a high probability of being close to X. Let us sample from this distribution for

the Trott curve $X = \{144(x^4+y^4) - 225(x^2+y^2) + 350x^2 * y^2 + 81 = 0\}$ and the box $R = [-2,2] \times [-2,2]$. We implement the Metropolis-Hasting algorithm in `Julia` [18] using the proposal density

$$q(\mathbf{x}, \mathbf{y}) \propto \exp(-\tfrac{1}{2} \|\mathbf{y}\|^2);$$

i.e., the proposals are sampled from the two-dimensional standard normal distribution (so we use an independence sampler as described in Example 15.22). First, we implement the system that we need to solve in order to compute $d(\mathbf{u}, X)$, and we solve it for a general complex point $\mathbf{u}$ that we will use later for doing parameter homotopies.

```
using HomotopyContinuation
@var x[1:2] u[1:2] l
f = 144(x[1]^4 + x[2]^4) - 225(x[1]^2 + x[2]^2) + 350x[1]^2*x[2]^2 + 81
df = differentiate(f, x)
F = System([f; df - l .* (x-u)], variables = [x; l], parameters = u)

uC = randn(ComplexF64, 2)
SC = solve(F, target_parameters = uC)
```

Next, we implement the densities q and ϕ (for $\sigma^2 = 1/100$) and a function that detects whether or not a point is in R.

```
is_in_R(p) = abs(p[1])<2 && abs(p[2])<2
q(u, v) = exp(-1/2 * norm(v)^2)
sigma_sq = 1/100
function phi(u)
    S = solve(F, solutions(SC), start_parameters = uC,
                                target_parameters = u,
                                show_progress = false)
    R = map(s -> s[1:2], real_solutions(S))
    d = minimum([norm(r - u) for r in R])
    exp(-d^2 / (2*sigma_sq))
end
```

Finally, we run the Metropolis-Hastings algorithm for 10.000 steps. The result can be seen in Figure 15.4.

```
n = 10000
u0 = randn(2)
states = [u0]
for k in 1:n
    uk = last(states)
    v = randn(2)
    if is_in_R(v)
        a = min(1, phi(v) * q(v, uk) / (phi(uk) * q(uk, v)))
        b = rand()
        if a > b
            push!(states, v)
        end
    end
end
```

One issue with Algorithm 6 when sampling from a nonlinear manifold X is to find a suitable proposal distribution with a density. Take, for instance, the Markov chain from Example 15.11, where the next step $\mathbf{x}_{k+1} \in X$ was computed from the current step $\mathbf{x}_k$ by taking a random linear space L trough $\mathbf{x}_k$ and sampling uniformly from the intersections points in $X \cap L$. It is straightforward to describe the generation of this random variable. But it is not clear how to compute its density (or if such a density even exists). In such a scenario, we must prove that the chain is reversible with respect to π. A further complication

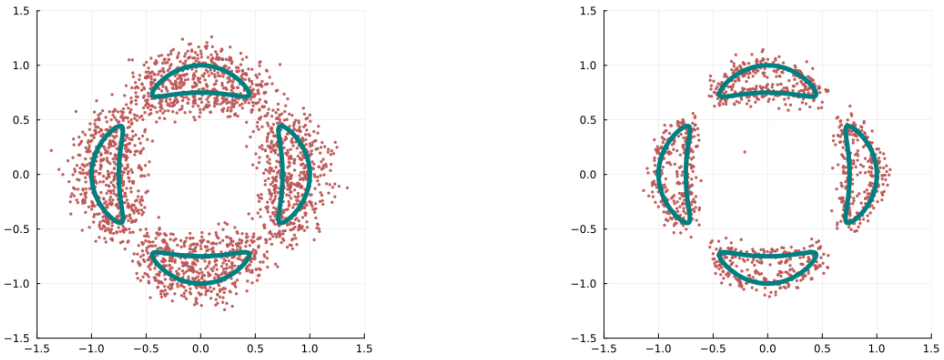

Fig. 15.4: Two samples of points near the Trott curve. They were generated using the approach from Example 15.24 with $\sigma^2 = 1/100$ (left) and $\sigma^2 = 1/400$ (right).

arises when X is not connected. In that case, the proposals must be chosen in a way that no connected component of X is missed.

In the remainder of this section, we present two alternative approaches to Metropolis Hastings that do not require the knowledge of a proposal density. The first is the algorithm in [23] using an independence sampler. Second, we consider the algorithm in [124] based on a random walk.

The algorithm in [23] is based on the idea of linear slicing. However, instead of considering a Markov chain in X, the paper considers a Markov chain in the Grassmannian $\mathrm{Gr}(c, \mathbb{R}^n)$, where $c = \operatorname{codim} X$. The algorithm is an independence sampler. The following theorem describes the density with which we have to sample $L \in \mathrm{Gr}(c, \mathbb{R}^n)$. As before, we assume that the target distribution π has a density $\phi(\mathbf{y})$. For $(A, \mathbf{b}) \in \mathbb{R}^{d \times n} \times \mathbb{R}^d$, we introduce the new function

$$\overline{\phi}(A, \mathbf{b}) := \sum_{\mathbf{x} \in X : A\mathbf{x} = \mathbf{b}} \frac{\phi(\mathbf{x})}{\alpha(\mathbf{x})}, \qquad \text{where} \qquad \alpha(\mathbf{x}) := \frac{\sqrt{1 + \langle \mathbf{x}, P_{\mathbf{x}}\, \mathbf{x} \rangle}}{(1 + \|\mathbf{x}\|^2)^{(d+1)/2}} \, \frac{\Gamma\left(\frac{d+1}{2}\right)}{\sqrt{\pi}^{d+1}},$$

and $P_{\mathbf{x}}$ is the orthogonal projection onto the normal space $N_{\mathbf{x}} X$. As before, $d = \dim X$ is the dimension of X. The additional factor α is related to the change of variables when embedding $\mathbb{R}^n$ into the n-dimensional real projective space.

Theorem 15.25 *Let $d := \dim X$ and $c := n - d = \operatorname{codim} X$. Let $\varphi(A, \mathbf{b})$ be the probability density for which the entries of $(A, \mathbf{b}) \in \mathbb{R}^{d \times n} \times \mathbb{R}^d$ are i.i.d. standard Gaussian. Denote*

$$\psi(A, \mathbf{b}) := \frac{\varphi(A, \mathbf{b}) \cdot \overline{\phi}(A, \mathbf{b})}{\mathbb{E}_{(A,\mathbf{b}) \sim \varphi}\, \overline{\phi}(A, \mathbf{b})}.$$

Then, ψ is a probability density and the random linear space $L := \{\mathbf{x} \in \mathbb{R}^n \mid A\mathbf{x} = \mathbf{b}\} \in \mathrm{Gr}(c, \mathbb{R}^n)$ for $(A, b) \sim \psi$ has the properties:

1. *$X \cap L$ is finite with probability one.*
2. *If we choose one of the finitely many points in $\mathbf{x} \in X \cap L$ with probability*

$$\mathrm{Prob}\{\mathbf{x}\} := \frac{\phi(\mathbf{x})}{\alpha(\mathbf{x}) \cdot \overline{\phi}(A, \mathbf{b})},$$

the random point $\mathbf{x}$ is distributed according to the density ϕ.

Proof See [23, Theorem 1.1]. □

We review another algorithm from the literature. The algorithm in [124] is similar to the Metropolis-Hastings algorithm. The basic idea is as follows. Suppose we want to sample from a target density $\phi(\mathbf{y})$. Write this as $\phi(\mathbf{y}) = \exp(-V(\mathbf{y}))$ and assume that $V(\mathbf{y})$ is smooth. The function V is called a *potential function*. Given a point $\mathbf{x} \in X$, we create a proposal by sampling first in a random tangent direction $\mathbf{v} \in T_{\mathbf{x}}X$ and then computing the intersection of X with the random linear space

$$L = \mathbf{x} + \mathbf{v} + N_{\mathbf{x}}X \in \mathrm{Gr}(c, \mathbb{R}^n).$$

This creates a Markov chain on X, but as we have discussed before, it is not clear how to compute the density for this random proposal. Instead, the authors in [124] prove directly reversibility of their Markov chain, so that they can apply Lemma 15.19. Algorithm 7 shows a (simplified version) of their algorithm.

Algorithm 7: The algorithm from [124].

1 **Input:** A probability measure π on X with a density $\exp(-V(\mathbf{y}))$, where V is smooth. A variance parameter $\sigma^2 > 0$. A fixed starting point $\mathbf{x} \in X$.
2 **Output:** A Markov chain on X with stationary distribution π.
3 Set $\mathbf{x}_0 = \mathbf{x}$.
4 **for** $k = 0, 1, 2, \ldots$ **do**
5 Randomly draw $\mathbf{v} \in T_{\mathbf{x}_k}X$ by sampling $\mathbf{v}$ from the multivariate normal distribution on $T_{\mathbf{x}_k}X$ with mean $\mathbf{0}$ and covariance matrix $\sigma^2 \cdot I$.
6 Set $L = \mathbf{x}_k + \mathbf{v} + N_{\mathbf{x}_k}X$.
7 Sample a point $\mathbf{y} \in X \cap L$ uniformly.
8 Compute $\mathbf{w} \in T_{\mathbf{y}}X$ such that $\mathbf{x}_k \in K := \mathbf{y} + \mathbf{w} + N_{\mathbf{y}}X$.
9 Compute $w(\mathbf{x}_k, \mathbf{y}) = \min\left\{1,\ \frac{|X \cap L|}{|X \cap K|} \cdot \exp\big(-(V(\mathbf{y}) - V(\mathbf{x}))\big) \cdot \exp\big(-\frac{1}{2\sigma^2}\,(\|\mathbf{w}\|^2 - \|\mathbf{v}\|^2)\big)\right\}$.
10 Sample a Bernoulli random variable $\beta \in \{0, 1\}$ with $\mathrm{Prob}\{\beta = 1\} = w(\mathbf{x}_k, \mathbf{y})$.
11 **if** $\beta = 1$ **then**
12 Set $\mathbf{x}_{k+1} := \mathbf{y}$.
13 **else**
14 Return to line 5.
15 **end**
16 **end**

Remark 15.26 The sampling of the random tangent vector $\mathbf{v}$ in line 5 of Algorithm 7 can be achieved as follows. Let $U \in \mathbb{R}^{n \times d}$ be a matrix whose columns form an orthonormal basis of $T_{\mathbf{x}}X$. Such a matrix can be computed by using the Gram-Schmidt algorithm. Sample $\mathbf{u} \in \mathbb{R}^d$ with i.i.d. $N(0, \sigma^2)$-entries. Then $\mathbf{v} = U\mathbf{u}$.

The following theorem asserts that Algorithm 7 works correctly.

Theorem 15.27 *Algorithm 7 produces a Markov chain that is reversible with respect to π. In particular, by Lemma 15.19, the Markov chain has π as stationary distribution.*

Proof See [124, Theorem 1]. □

References

1. H. Abo, A. Seigal, and B. Sturmfels. *Eigenconfigurations of tensors*, pages 1–25. 01 2017.
2. Daniele Agostini, Taylor Brysiewicz, Claudia Fevola, Lukas Kühne, Bernd Sturmfels, and Simon Telen. Likelihood degenerations. *Adv. Math.*, 414:Paper No. 108863, 39, 2023. With an appendix by Thomas Lam.
3. Yulia Alexandr and Alexander Heaton. Logarithmic Voronoi cells. *Algebr. Stat.*, 12(1):75–95, 2021.
4. Carlos Améndola, Lukas Gustafsson, Kathlén Kohn, Orlando Marigliano, and Anna Seigal. The maximum likelihood degree of linear spaces of symmetric matrices. *Matematiche (Catania)*, 76(2):535–557, 2021.
5. Raman Arora, Amitabh Basu, Poorya Mianjy, and Anirbit Mukherjee. Understanding deep neural networks with rectified linear units. In *International Conference on Learning Representations*, 2018.
6. Sanjeev Arora, Nadav Cohen, and Elad Hazan. On the optimization of deep networks: Implicit acceleration by overparameterization. In *International Conference on Machine Learning*, pages 244–253. PMLR, 2018.
7. S. Asmussen and P. W. Glynn. *Stochastic Simulation: Algorithms and Analysis*. Springer, 2007.
8. Pierre Baldi and Kurt Hornik. Neural networks and principal component analysis: Learning from examples without local minima. *Neural networks*, 2(1):53–58, 1989.
9. Jiakang Bao, Yang-Hui He, Edward Hirst, Johannes Hofscheier, Alexander Kasprzyk, and Suvajit Majumder. Hilbert series, machine learning, and applications to physics. *Physics Letters B*, 827:136966, 2022.
10. Alfred Barnard Basset. *An elementary treatise on cubic and quartic curves*. Cambridge, Deighton, Bell, 1901.
11. S. Basu and A. Lerario. Hausdorff approximations and volume of tubes of singular algebraic sets. *arXiv:2104.05053*, 2021.
12. D. J. Bates, P. Breiding, T. Chen, J. D. Hauenstein, A. Leykin, and F. Sottile. Numerical nonlinear algebra. *arXiv:2302.08585*, 2023.
13. Daniel Bates, Jonathan Hauenstein, Andrew Sommese, and Charles Wampler. *Numerically solving polynomial systems with Bertini*, volume 25 of *Software, Environments, and Tools*. Society for Industrial and Applied Mathematics (SIAM), Philadelphia, PA, 2013.
14. Adrian Becedas, Kathlén Kohn, and Lorenzo Venturello. Voronoi diagrams of algebraic varieties under polyhedral norms. arXiv:2209.11463.
15. Edgar A Bernal, Jonathan D Hauenstein, Dhagash Mehta, Margaret H Regan, and Tingting Tang. Machine learning the real discriminant locus. *Journal of Symbolic Computation*, 115:409–426, 2023.
16. D. N. Bernstein. The number of roots of a system of equations. *Funkcional. Anal. i Priložen.*, 9(3):1–4, 1975.
17. D. N. Bernstein, A. G. Kušnirenko, and A. G. Hovanskiĭ. Newton polyhedra. *Uspehi Mat. Nauk*, 31(3(189)):201–202, 1976.
18. J. Bezanson, A. Edelman, S. Karpinski, and V. Shah. Julia: A fresh approach to numerical computing. *SIAM Review*, 59(1):65–98, 2017.
19. L. Blum, F. Cucker, M. Shub, and S. Smale. *Complexity and real computation*. Springer-Verlag, New York, 1998.
20. Tobias Boege, Jane Coons, Chris Eur, Aida Maraj, and Frank Röttger. Reciprocal maximum likelihood degrees of Brownian motion tree models. *Matematiche (Catania)*, 76(2):383–398, 2021.
21. Viktoriia Borovik and Paul Breiding. A short proof for the parameter continuation theorem. *arXiv:2302.14697*, 2023.
22. Madeline Brandt and Madeleine Weinstein. Voronoi cells in metric algebraic geometry of plane curves. arXiv:1906.11337.
23. P. Breiding and O. Marigliano. Random points on an algebraic manifold. *SIAM Journal on Mathematics of Data Science*, 2(3):683–704, 2020.
24. P. Breiding, K. Ranestad, and M. Weinstein. Enumerative geometry of curvature of algebraic hypersurfaces. *arXiv:2206.09130*, 2022.

25. P. Breiding, K. Rose, and S. Timme. Certifying zeros of polynomial systems using interval arithmetic. *ACM Trans. Math. Softw.*, 49(1), mar 2023.
26. P. Breiding and S. Timme. HomotopyContinuation.jl: A Package for Homotopy Continuation in Julia. In *Mathematical Software – ICMS 2018*, pages 458–465, Cham, 2018. Springer International Publishing.
27. P. Breiding and N. Vannieuwenhoven. The condition number of Riemannian approximation problems. *SIAM Journal on Optimization*, 31(1):1049–1077, 2021.
28. Paul Breiding, Sara Kališnik, Bernd Sturmfels, and Madeleine Weinstein. Learning algebraic varieties from samples. *Rev. Mat. Complut.*, 31(3):545–593, 2018.
29. Paul Breiding, Julia Lindberg, Wern Juin Gabriel Ong, and Linus Sommer. Real circles tangent to 3 conics. *arXiv:2211.06876*, 2022.
30. Paul Breiding, Kemal Rose, and Sascha Timme. Certifying zeros of polynomial systems using interval arithmetic. *ACM Trans. Math. Software*, 49(1):Art. 11, 14, 2023.
31. Paul Breiding and Sascha Timme. Homotopycontinuation.jl: A package for homotopy continuation in julia. *Math. Software – ICMS 2018, 458–465, Springer*, 2018.
32. Joan Bruna, Kathlén Kohn, and Matthew Trager. Pure and spurious critical points: a geometric study of linear networks. *Internat. Conf. on Learning Representations*, 2020.
33. P. Bürgisser and F. Cucker. *Condition: The Geometry of Numerical Algorithms*, volume 349 of *Grundlehren der mathematischen Wissenschaften*. Springer, Heidelberg, 2013.
34. P. Bürgisser, F. Cucker, and M. Lotz. The probability that a slightly perturbed numerical analysis problem is difficult. *Math. Comput.*, 77:1559–1583, 09 2008.
35. Peter Bürgisser. Condition of intersecting a projective variety with a varying linear subspace. *SIAM Journal on Applied Algebra and Geometry*, 1(1):111–125, 2017.
36. Freddy Cachazo, Nick Early, Alfredo Guevara, and Sebastian Mizera. Scattering equations: from projective spaces to tropical Grassmannians. *J. High Energy Phys.*, (6):039, 32, 2019.
37. Freddy Cachazo, Bruno Umbert, and Yong Zhang. Singular solutions in soft limits. *J. High Energy Phys.*, (5):148, 32, 2020.
38. D. Cartwright and B. Sturmfels. The number of eigenvalues of a tensor. *Linear Algebra and its Applications*, 438(2):942–952, 2013. Tensors and Multilinear Algebra.
39. Jean-Dominique Cassini. *De l'Origine et du progrès de l'astronomie et de son usage dans la géographie et dans la navigation*. L'Imprimerie Royale, 1693.
40. Fabrizio Catanese, Serkan Hoşten, Amit Khetan, and Bernd Sturmfels. The maximum likelihood degree. *Amer. J. Math.*, 128(3):671–697, 2006.
41. Türkü Özlüm Çelik, Asgar Jamneshan, Guido Montúfar, Bernd Sturmfels, and Lorenzo Venturello. Optimal transport to a variety. In *Mathematical aspects of computer and information sciences*, volume 11989 of *Lecture Notes in Comput. Sci.*, pages 364–381. Springer, Cham, 2020.
42. Türkü Özlüm Çelik, Asgar Jamneshan, Guido Montúfar, Bernd Sturmfels, and Lorenzo Venturello. Wasserstein distance to independence models. *J. Symbolic Comput.*, 104:855–873, 2021.
43. Michel Chasles. *Aperçu historique sur l'origine et le développement des méthodes en géométrie: particulièrement de celles qui se rapportent à la géometrie moderne, suivi d'un mémoire de géométrie sur deux principes généreaux de la science, la dualité et l'homographie*. M. Hayez, 1837.
44. F. Chazal and A. Lieutier. The "λ-medial axis". *Graphical Models*, 67(4):304–331, 2005.
45. Heng-Yu Chen, Yang-Hui He, Shailesh Lal, and Suvajit Majumder. Machine learning lie structures & applications to physics. *Physics Letters B*, 817:136297, 2021.
46. L. Chiantini, G. Ottaviani, and N. Vannieuwenhoven. An algorithm for generic and low-rank specific identifiability of complex tensors. *SIAM J. Matrix Anal. Appl.*, 35(4):1265–1287, 2014.
47. Diego Cifuentes, Corey Harris, and Bernd Sturmfels. The geometry of SDP-exactness in quadratic optimization. *Math. Program.*, 182(1-2, Ser. A):399–428, 2020.
48. Diego Cifuentes, Kristian Ranestad, Bernd Sturmfels, and Madeleine Weinstein. Voronoi cells of varieties. *J. Symbolic Comput.*, 109:351–366, 2022.
49. Roger Cotes. *Harmonia mensurarum*. Robert Smith, 1722.
50. David Cox, John Little, and Donal O'Shea. *Ideals, Varieties, and Algorithms: An introduction to computational algebraic geometry and commutative algebra*. Undergraduate Texts in Math. Springer, Cham, fourth edition, 2015.
51. L. De Lathauwer. Blind Separation of Exponential Polynomials and the Decomposition of a Tensor in Rank-$(L_r, L_r, 1)$ Terms. *SIAM J. Matrix Anal. Appl.*, 32(4):1451–1474, 2011.
52. V. de Silva and L.-H. Lim. Tensor rank and the ill-posedness of the best low-rank approximation problem. *SIAM Journal on Matrix Analysis and Applications*, 30(3):1084–1127, 2008.
53. Michel Demazure. Sur deux problemes de reconstruction. Technical Report 882, INRIA, 1988.
54. J. W. Demmel. On condition numbers and the distance to the nearest ill-posed problem. *Numer. Math.*, 51(3):251–289, 1987.

55. S. Di Rocco, D. Eklund, and M. Weinstein. The bottleneck degree of algebraic varieties. *SIAM Journal on Applied Algebra and Geometry*, 4(1):227–253, 2020.
56. Sandra Di Rocco, David Eklund, and Madeleine Weinstein. The bottleneck degree of algebraic varieties. *SIAM J. Appl. Algebra Geom.*, 4(1):227–253, 2020.
57. M. do Carmo. *Riemannian Geometry*. Birkhäuser, 1993.
58. I. Domanov and L. Lathauwer. On Uniqueness and Computation of the Decomposition of a Tensor into Multilinear Rank-$(1, L_r, L_r)$ Terms. *SIAM J. Matrix Anal. Appl.*, 41(2):747–803, 2020.
59. Michael Douglas, Subramanian Lakshminarasimhan, and Yidi Qi. Numerical calabi-yau metrics from holomorphic networks. In *Mathematical and Scientific Machine Learning*, pages 223–252. PMLR, 2022.
60. Jan Draisma, Emil Horobeţ, Giorgio Ottaviani, Bernd Sturmfels, and Rekha R. Thomas. The Euclidean distance degree of an algebraic variety. *Found. Comput. Math.*, 16(1):99–149, 2016.
61. Jan Draisma and Jose Rodriguez. Maximum likelihood duality for determinantal varieties. *Int. Math. Res. Not. IMRN*, (20):5648–5666, 2014.
62. Simon S Du, Wei Hu, and Jason D Lee. Algorithmic regularization in learning deep homogeneous models: Layers are automatically balanced. *Advances in neural information processing systems*, 31, 2018.
63. Eliana Duarte, Orlando Marigliano, and Bernd Sturmfels. Discrete statistical models with rational maximum likelihood estimator. *Bernoulli*, 27(1):135–154, 2021.
64. Timothy Duff, Kathlén Kohn, Anton Leykin, and Tomas Pajdla. PLMP – Point-Line Minimal Problems in Complete Multi-View Visibility. In *Proceedings of the IEEE/CVF International Conference on Computer Vision*, pages 1675–1684, 2019.
65. E. Dufresne, P. Edwards, H. Harrington, and J. Hauenstein. Sampling real algebraic varieties for topological data analysis. In *2019 18th IEEE International Conference On Machine Learning And Applications (ICMLA)*, pages 1531–1536, 2019.
66. Emily Dufresne, Parker Edwards, Heather Harrington, and Jonathan Hauenstein. Sampling real algebraic varieties for topological data analysis. *18th IEEE International Conference on Machine Learning and Applications (ICMLA)*, 2019.
67. A. Edelman and E. Kostlan. How many zeros of a random polynomial are real? *Math. Soc. Mathematical Reviews*, 32:1–37, 05 1995.
68. David Eklund. The numerical algebraic geometry of bottlenecks. *Adv. in Appl. Math.*, 142:Paper No. 102416, 20, 2023.
69. Chris Eur, Tara Fife, Jose Samper, and Tim Seynnaeve. Reciprocal maximum likelihood degrees of diagonal linear concentration models. *Matematiche (Catania)*, 76(2):447–459, 2021.
70. S. Friedland and G. Ottaviani. The number of singular vector tuples and uniqueness of best rank-one approximation of tensors. *Foundations of Computational Mathematics*, 14(6):1209–1242, 2014.
71. William Fulton. *Intersection theory*, volume 2 of *Ergebnisse der Mathematik und ihrer Grenzgebiete (3) [Results in Mathematics and Related Areas (3)]*. Springer-Verlag, Berlin, 1984.
72. William Fulton. *Intersection theory*. Springer-Verlag, Berlin, 1998.
73. William Fulton, Steven Kleiman, and Robert MacPherson. About the enumeration of contacts. *Algebraic Geometry – Open Problems*, 997:156–196, 1983.
74. Israel Gel'fand, Mikhael Kapranov, and Andrei Zelevinsky. *Discriminants, resultants, and multidimensional determinants*. Mathematics: Theory & Applications. Birkhäuser Boston, Inc., Boston, MA, 1994.
75. Israel M Gelfand, Mikhail M Kapranov, and Andrei V Zelevinsky. *Discriminants, resultants, and multidimensional determinants*. Birkhäuser, 1994.
76. A. Gray. *Tubes*. Birkhäauser Verlag, Basel, second edition, 2004.
77. Dan Grayson and Michael Stillman. Macaulay2, a software system for research in algebraic geometry. *available at* `www.math.uiuc.edu/Macaulay2/`.
78. J Elisenda Grigsby, Kathryn Lindsey, Robert Meyerhoff, and Chenxi Wu. Functional dimension of feedforward relu neural networks. *arXiv:2209.04036*, 2022.
79. Philipp Grohs and Gitta Kutyniok. *Mathematical Aspects of Deep Learning*. Cambridge University Press, 2022.
80. Richard Hartley. Projective reconstruction and invariants from multiple images. *IEEE Transactions on Pattern Analysis and Machine Intelligence*, 16(10):1036–1041, 1994.
81. Richard Hartley and Frederik Schaffalitzky. Reconstruction from projections using Grassmann tensors. *International Journal of Computer Vision*, 83(3):274–293, 2009.
82. Richard Hartley and Peter Sturm. Triangulation. *Computer vision and image understanding*, 68(2):146–157, 1997.
83. Richard Hartley and Andrew Zisserman. *Multiple View Geometry in Computer Vision*. Cambridge, 2nd edition, 2003.
84. J. D. Hauenstein and D. Kahle. Stochastic exploration of real varieties via variety distributions. *Preprint available at* `www.nd.edu/~jhauenst/preprints/khVarietyDistributions.pdf`, 2023.
85. J. D. Hauenstein and F. Sottile. Algorithm 921: alphaCertified: certifying solutions to polynomial systems. *ACM Trans. Math. Software*, 38(4):Art. 28, 20, 2012.

86. Jonathan Hauenstein, Jose Israel Rodriguez, and Bernd Sturmfels. Maximum likelihood for matrices with rank constraints. *J. Algebr. Stat.*, 5(1):18–38, 2014.
87. Kathryn Heal, Avinash Kulkarni, and Emre Can Sertöz. Deep learning Gauss–Manin connections. *Advances in Applied Clifford Algebras*, 32(2):24, 2022.
88. Didier Henrion, Jean Bernard Lasserre, and Carlo Savorgnan. Approximate volume and integration for basic semialgebraic sets. *SIAM Rev.*, 51(4):722–743, 2009.
89. Otto Hesse. Die cubische Gleichung, von welcher die Lösung des Problems der Homographie von M. Chasles abhängt. *Journal für die reine und angewandte Mathematik*, 62, 1863.
90. Anders Heyden and Kalle Åström. Algebraic properties of multilinear constraints. *Mathematical Methods in the Applied Sciences*, 20(13):1135–1162, 1997.
91. N. J. Higham. *Accuracy and stability of numerical algorithms*. Society for Industrial and Applied Mathematics, second edition, 1996.
92. Serkan Hoşten, Amit Khetan, and Bernd Sturmfels. Solving the likelihood equations. *Found. Comput. Math.*, 5(4):389–407, 2005.
93. Audun Holme. The geometric and numerical properties of duality in projective algebraic geometry. *Manuscripta mathematica*, 61:145–162, 1988.
94. Emil Horobeţ and Madeleine Weinstein. Offset hypersurfaces and persistent homology of algebraic varieties. *Comput. Aided Geom. Design*, 74:101767, 14, 2019.
95. E. Horobet and M. Weinstein. Offset hypersurfaces and persistent homology of algebraic varieties. *Computer Aided Geometric Design*, 74:101767, 2019.
96. D. Hough. *Explaining and Ameliorating the Condition of Zeros of Polynomials*. PhD Thesis, Mathematics Department, University of California, Berkeley, 1977.
97. R. Howard. The kinematic formula in Riemannian homogeneous spaces. *Mem. Amer. Math. Soc.*, 106(509):vi+69, 1993.
98. Petr Hruby, Timothy Duff, Anton Leykin, and Tomas Pajdla. Learning to solve hard minimal problems. In *Proceedings of the IEEE/CVF Conference on Computer Vision and Pattern Recognition*, pages 5532–5542, 2022.
99. Kun Huang, Robert Fossum, and Yi Ma. Generalized rank conditions in multiple view geometry with applications to dynamical scenes. In *European Conference on Computer Vision*, pages 201–216. Springer, 2002.
100. Zongyan Huang, Matthew England, David J Wilson, James Bridge, James H Davenport, and Lawrence C Paulson. Using machine learning to improve cylindrical algebraic decomposition. *Mathematics in Computer Science*, 13:461–488, 2019.
101. Birkett Huber and Bernd Sturmfels. A polyhedral method for solving sparse polynomial systems. *Math. Comp.*, 64(212):1541–1555, 1995.
102. June Huh. The maximum likelihood degree of a very affine variety. *Compos. Math.*, 149(8):1245–1266, 2013.
103. June Huh. Varieties with maximum likelihood degree one. *J. Algebr. Stat.*, 5(1):1–17, 2014.
104. June Huh and Bernd Sturmfels. Likelihood geometry. In *Combinatorial algebraic geometry*, volume 2108 of *Lecture Notes in Math.*, pages 63–117. Springer, Cham, 2014.
105. B. Hunyadi, D. Camps, L. Sorber, W. V. Paesschen, M. De Vos, S. V. Huffel, and L. D. Lathauwer. Block term decomposition for modelling epileptic seizures. *EURASIP J. Adv. Signal Process.*, (1):139, 2014.
106. Kenji Kawaguchi. Deep learning without poor local minima. *Advances in neural information processing systems*, 29, 2016.
107. Joe Kileel and Kathlén Kohn. Snapshot of algebraic vision. *arXiv:2210.11443*, 2022.
108. Joe Kileel, Matthew Trager, and Joan Bruna. On the expressive power of deep polynomial neural networks. *Advances in neural information processing systems*, 32, 2019.
109. Steven Kleiman. Tangency and duality. In *Proceedings 1984 Vancouver Conference in Algebraic Geometry*, pages 163–226. Amer. Math. Soc., 1986.
110. F. Klein. Eine neue Relation zwischen den Singularitäten einer algebraischen Curve. *Math. Ann.*, 10(2):199–209, 1876.
111. Kathlén Kohn, Thomas Merkh, Guido Montúfar, and Matthew Trager. Geometry of linear convolutional networks. *SIAM Journal on Applied Algebra and Geometry*, 6(3):368–406, 2022.
112. Kathlén Kohn, Guido Montúfar, Vahid Shahverdi, and Matthew Trager. Function space and critical points of linear convolutional networks. *arXiv:2304.05752*, 2023.
113. Eric Kostlan. On the distribution of roots of random polynomials. In *From Topology to Computation: Proceedings of the Smalefest (Berkeley, CA, 1990)*, pages 419–431. Springer, New York, 1993.
114. Eric Kostlan. On the expected number of real roots of a system of random polynomial equations. In *Foundations of computational mathematics (Hong Kong, 2000)*, pages 149–188. World Sci. Publ., River Edge, NJ, 2002.
115. Christoph Koutschan. Holonomicfunctions: A mathematica package for dealing with multivariate holonomic functions, including closure properties, summation, and integration. *available at* `www3.risc.jku.at/research/combinat/software/ergosum/RISC/HolonomicFunctions.html`.

116. Pierre Lairez. Computing periods of rational integrals. *Math. Comp.*, 85(300):1719–1752, 2016.
117. Pierre Lairez, Marc Mezzarobba, and Mohab Safey El Din. Computing the volume of compact semi-algebraic sets. In *ISSAC'19—Proceedings of the 2019 ACM International Symposium on Symbolic and Algebraic Computation*, pages 259–266. ACM, New York, 2019.
118. Jean Bernard Lasserre. *Moments, positive polynomials and their applications*, volume 1 of *Imperial College Press Optimization Series*. Imperial College Press, London, 2010.
119. L. D. Lathauwer. Decompositions of a higher-order tensor in block terms - Part II: Definitions and uniqueness. *SIAM J. Matrix Anal. Appl.*, 30:1033–1066, 2008.
120. Thomas Laurent and James Brecht. Deep linear networks with arbitrary loss: All local minima are global. In *International Conference on Machine Learning*, pages 2902–2907. PMLR, 2018.
121. J. M. Lee. *Riemannian Manifolds: Introduction to Curvature*. Springer, 1997.
122. J. M. Lee. *Introduction to Smooth Manifolds*. Springer, New York, USA, 2 edition, 2013.
123. K. Lee. Certifying approximate solutions to polynomial systems on Macaulay2. *ACM Communications in Computer Algebra*, 53(2):45–48, 2019.
124. T. Lelievre, G. Stoltz, and W. Zhang. Multiple projection mcmc algorithms on submanifolds. *IMA Journal of Numerical Analysis*, 2022.
125. Hao Li, Zheng Xu, Gavin Taylor, Christoph Studer, and Tom Goldstein. Visualizing the loss landscape of neural nets. *Advances in neural information processing systems*, 31, 2018.
126. M. Lotz. On the volume of tubular neighborhoods of real algebraic varieties. *Proceedings of the American Mathematical Society*, 143, 10 2012.
127. Laurent Manivel, Mateusz Michalek, Leonid Monin, Tim Seynnaeve, and Martin Vodička. Complete quadrics: Schubert calculus for gaussian models and semidefinite programming. *Journal of the European Mathematical Society*, 2023.
128. Laurentiu G Maxim, Jose I Rodriguez, and Botong Wang. Euclidean distance degree of the multiview variety. *SIAM Journal on Applied Algebra and Geometry*, 4(1):28–48, 2020.
129. Clerk Maxwell. On the description of oval curves, and those having a plurality of foci. *Proceedings of the Royal Society of Edinburgh*, 2, 1846.
130. Dhagash Mehta, Tianran Chen, Tingting Tang, and Jonathan D Hauenstein. The loss surface of deep linear networks viewed through the algebraic geometry lens. *IEEE Transactions on Pattern Analysis and Machine Intelligence*, 44(9):5664–5680, 2021.
131. S. P. Meyn and R. L. Tweedie. *Markov chains and stochastic stability*. Springer-Verlag, London., 1993.
132. Mateusz Michalek, Leonid Monin, and Jaroslaw Wiśniewski. Maximum likelihood degree, complete quadrics, and $\mathbb{C}^*$-action. *SIAM J. Appl. Algebra Geom.*, 5(1):60–85, 2021.
133. Mateusz Michalek and Bernd Sturmfels. *Invitation to nonlinear algebra*, volume 211 of *Graduate Studies in Mathematics*. American Mathematical Society, Providence, RI, 2021.
134. Guido Montúfar, Yue Ren, and Leon Zhang. Sharp bounds for the number of regions of maxout networks and vertices of minkowski sums. *SIAM Journal on Applied Algebra and Geometry*, 6(4):618–649, 2022.
135. A. P. Morgan and A. J. Sommese. Coefficient-parameter polynomial continuation. *Applied Mathematics and Computation*, 29(2):123–160, 1989.
136. Gabin Maxime Nguegnang, Holger Rauhut, and Ulrich Terstiege. Convergence of gradient descent for learning linear neural networks. *arXiv:2108.02040*, 2021.
137. Jiawang Nie, Pablo A Parrilo, and Bernd Sturmfels. Semidefinite representation of the k-ellipse. In *Algorithms in Algebraic Geometry*, volume 146 of *I.M.A. Volumes in Mathematics and its Applications*, pages 117–132. Springer, 2008.
138. B. O'Neill. *Elementary Differential Geometry*. Elsevier, revised second edition edition, 2001.
139. G. Ottaviani and L. Sodomaco. The distance function from a real algebraic variety. *Computer Aided Geometric Design*, 82:101927, 2020.
140. Giorgio Ottaviani and Luca Sodomaco. The distance function from a real algebraic variety. *Comput. Aided Geom. Design*, 82:101927, 20, 2020.
141. Giorgio Ottaviani, Pierre-Jean Spaenlehauer, and Bernd Sturmfels. Exact solutions in structured low-rank approximation. *SIAM J. Matrix Anal. Appl.*, 35(4):1521–1542, 2014.
142. S. Smale P. Niyogi and S. Weinberger. Finding the homology of submanifolds with high confidence from random samples. *Discrete Comput. Geometry*, (39):419–441, 2008.
143. Dylan Peifer, Michael Stillman, and Daniel Halpern-Leistner. Learning selection strategies in buchberger's algorithm. In *International Conference on Machine Learning*, pages 7575–7585. PMLR, 2020.
144. P. Petersen. *Riemannian Geometry*. Springer, second edition, 2006.
145. R. Piene, C. Riener, and B. Shapiro. Return of the plane evolute. *arXiv:2110.11691*, 2021.
146. Ragni Piene. Polar classes of singular varieties. In *Annales scientifiques de l'École Normale Supérieure*, volume 11, pages 247–276, 1978.

147. Ragni Piene. Cycles polaires et classes de chern pour les variétés projectives singulieres. *Introductiona la théorie des singularités, II*, 37:7–34, 1988.
148. Julius Plücker. *Gesammelte wissenschaftliche Abhandlungen: Im Auftrad des Kgt*, volume 2. BG Teubner, 1895.
149. Y. Qi, P. Comon, and L.-H. Lim. Semialgebraic geometry of nonnegative tensor rank. *SIAM J. Matrix Anal. Appl.*, 37:1556–1580, 11 2016.
150. Adityanarayanan Radhakrishnan, Mikhail Belkin, and Caroline Uhler. Overparameterized neural networks implement associative memory. *Proceedings of the National Academy of Sciences*, 117(44):27162–27170, 2020.
151. Christophe Raffalli. Distance to the discriminant. *arXiv:1404.7253*, 2014.
152. J. R. Rice. A theory of condition. *SIAM J. Numer. Anal*, 3:287–310, 1966.
153. Gareth O. Roberts and Jeffrey S. Rosenthal. General state space Markov chains and MCMC algorithms. *Probability Surveys*, 1:20–71, 2004.
154. S. Di Rocco, D. Eklund, and O. Gäfvert. Sampling and homology via bottlenecks. *Math. Comp.*, 91(338):2969–2995, 2022.
155. Jose Israel Rodriguez and Botong Wang. The maximum likelihood degree of mixtures of independence models. *SIAM J. Appl. Algebra Geom.*, 1(1):484–506, 2017.
156. Mutsumi Saito, Bernd Sturmfels, and Nobuki Takayama. *Gröbner deformations of hypergeometric differential equations*, volume 6 of *Algorithms and Computation in Mathematics*. Springer-Verlag, Berlin, 2000.
157. George Salmon. *A Treatise on the Higher Plane Curves*. Hodges and Smith, Dublin, 1852.
158. George Salmon. *A Treatise on the Analytic Geometry of Three Dimensions*. Hodges, Smith, and Company, 1865.
159. Muhamad Risqi U Saputra, Andrew Markham, and Niki Trigoni. Visual slam and structure from motion in dynamic environments: A survey. *ACM Computing Surveys (CSUR)*, 51(2):1–36, 2018.
160. Anna-Laura Sattelberger and Bernd Sturmfels. D-modules and holonomic functions. *to appear in: Varieties, Polyhedra and Computation, EMS Series of Congress Reports*, arxiv:1910.01395.
161. Luca Sodomaco. The distance function from the variety of partially symmetric rank-one tensors. *PhD thesis,Universitá degli Studi di Firenze*, 2020.
162. A. J. Sommese and C. W. Wampler. *The Numerical Solution of Systems of Polynomials Arising in Engineering and Science*. World Scientific, 2005.
163. M. Sorensen and L. De Lathauwer. Coupled Canonical Polyadic Decompositions and (Coupled) Decompositions in Multilinear Rank-$(L_r, n, L_r, n, 1)$ Terms—Part I: Uniqueness. *SIAM J. Matrix Anal. Appl.*, 36(2):496–522, 2015.
164. Henrik Stewénius, Frederik Schaffalitzky, and David Nistér. How hard is 3-view triangulation really? In *Proceedings of the IEEE International Conference on Computer Vision*, pages 686–693, 2005.
165. Elisabetta Strickland. On the conormal bundle of the determinantal variety. *J. Algebra*, 75(2):523–537, 1982.
166. Rud Sturm. Das Problem der Projectivität und seine Anwendung auf die Flächen zweiten Grades. *Mathematische Annalen*, 1(4):533–574, 1869.
167. Bernd Sturmfels. *Solving Systems of Polynomial Equations*. Number 97 in CBMS Regional Conferences Series. American Mathematical Society, 2002.
168. Bernd Sturmfels and Simon Telen. Likelihood equations and scattering amplitudes. *Algebr. Stat.*, 12(2):167–186, 2021.
169. Bernd Sturmfels, Sascha Timme, and Piotr Zwiernik. Estimating linear covariance models with numerical nonlinear algebra. *Algebr. Stat.*, 11(1):31–52, 2020.
170. Seth Sullivant. *Algebraic statistics*, volume 194 of *Graduate Studies in Mathematics*. American Mathematical Society, Providence, RI, 2018.
171. Gyula Sz.-Nagy. Tschirnhaus' sche eiflächen und eikurven. *Acta Mathematica Hungarica*, pages 36–45, 1950.
172. Matteo Tacchi, Jean Bernard Lasserre, and Didier Henrion. Stokes, Gibbs, and volume computation of semi-algebraic sets. *Discrete Comput. Geom.*, 69(1):260–283, 2023.
173. Matteo Tacchi, Tillmann Weisser, Jean Bernard Lasserre, and Didier Henrion. Exploiting sparsity for semi-algebraic set volume computation. *Found. Comput. Math.*, 22(1):161–209, 2022.
174. Gerald J Toomer. *Apollonius: Conics Books V to VII: The Arabic Translation of the Lost Greek Original in the Version of the Banū Mūsā*, volume 1. Springer, 1990.
175. L. N. Trefethen and D. Bau. *Numerical Linear Algebra*. SIAM, 1997.
176. A. Turing. Rounding-off errors in matrix processes. *The Quarterly Journal of Mechanics and Applied Mathematics*, 1, 1948.
177. H. Weyl. On the volume of tubes. *Amer. J. Math.*, 61(2):461–472, 1939.
178. J. H. Wilkinson. Note on matrices with a very ill-conditioned eigenproblem. *Numer. Math.*, 19:176–178, 1972.
179. Francis Williams, Matthew Trager, Daniele Panozzo, Claudio Silva, Denis Zorin, and Joan Bruna. Gradient dynamics of shallow univariate relu networks. *Advances in Neural Information Processing Systems*, 32, 2019.
180. Lior Wolf and Amnon Shashua. On projection matrices $\mathbb{P}^k \to \mathbb{P}^2$, $k = 3, \ldots, 6$, and their applications in computer vision. *International Journal of Computer Vision*, 48(1):53–67, 2002.
181. M. Yang. On partial and generic uniqueness of block term tensor decompositions. *Annali dell'universita' di Ferrara*, 60(2):465–493, 2014.

182. Doron Zeilberger. A holonomic systems approach to special functions identities. *J. Comput. Appl. Math.*, 32(3):321–368, 1990.
183. Liwen Zhang, Gregory Naitzat, and Lek-Heng Lim. Tropical geometry of deep neural networks. In *International Conference on Machine Learning*, pages 5824–5832. PMLR, 2018.
184. Qunjie Zhou, Torsten Sattler, Marc Pollefeys, and Laura Leal-Taixe. To learn or not to learn: Visual localization from essential matrices. In *2020 IEEE International Conference on Robotics and Automation (ICRA)*, pages 3319–3326. IEEE, 2020.